NOBLE GAS GEOCHEMISTRY OF ICELANDIC BASALTS

Eleanor Tamiko Dixon

Thesis submitted for the degree of Doctor of Philosophy of

The Australian National University

The Australian National University

July 2000

Statement

The results and conclusions presented in this thesis are my own, unless otherwise acknowledged in the text, figure captions or table footnotes.

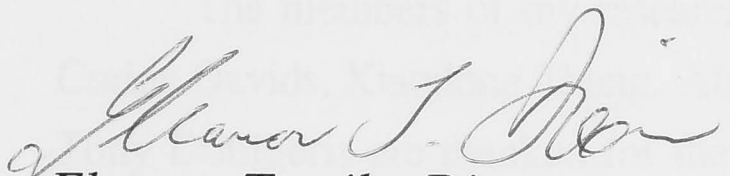

Eleanor Tamiko Dixon

ACKNOWLEGEMENTS

I would like to take this opportunity to thank the numerous people who provided support or guidance that enabled me to complete this project.

I would first like to thank my two supervisors, Masahiko Honda and Ian McDougall. Their instruction in the field of noble gas geochemistry and comments on the logic and structure of this thesis were fundamental in enabling me to develop, strengthen and express my ideas. In particular, M. Honda is acknowledged for his patient instruction on operation of the mass spectrometer. Ian McDougall is gratefully acknowledged for his persistent efforts to improve my writing. My advisor, Ian Campbell is gratefully acknowledged for listening to my ideas on many subjects and providing helpful discussions, both as a friend and a mentor. His understanding and support helped me to progress through the various challenges presented during the interpretations of my results. My former supervisors, Eric Essene and Alex Halliday are thanked for their continued support.

The members of my research group, Igor Yatsevich, Robyn Maier, Jim Dunlap, Corine Davids, Xiaodong Zhang, Alfredo Camacho, Jennifer Delhaize, Geoff Fraser and Tony Doulgeris are thanked for their companionship over the years. Igor, the former nuclear physicist from the former Soviet Union, is thanked in particular for his support and numerous helpful discussions on ideas and calculations, as well as for fixing things in the laboratory. His "devil's advocate" approach to science and life in general were important in formulating my ideas. Many thanks also to Tony, whose assistance with computer problems went well above and beyond the call of duty. Roger Willison is thanked for support, technical assistance, and for making me a personally engraved stainless steel chisel for glass samples. Shane Paxton and John Mya are thanked for help with mineral separation and for their positive attitudes and enormous smiles. Nick Ware is thanked for help with the electron microprobe. Steve Eggins gratefully acknowledged for helping with the Laser ICP-MS analyses. Dan Sinclair and Stewart Fallon were extremely helpful with formatting and computer tricks. Mark Fanning and Richard Armstrong are thanked for letting me run SHRIMP. Anne Gillard in administration is thanked for her efficiency in getting things done.

Ingvar Sigurdsson and Sigurdir Gunnarsson, Magnea Gunnarsdottir and Malfridur (Frida) Gunarsdottir are warmly remembered for their friendship and hospitality while I performed fieldwork in Iceland. I have very fond memories of my stay in Iceland, and would like to express my regrets in memory of Frida. Many thanks

to Lotte Melchior Larson, who provided samples from West Greenland. Ole Sigmondson is acknowledged for carrying several kilograms of rocks in his luggage from Iceland to Australia.

There are several other people whose efforts in reading through numerous drafts of my chapters have helped to improve their structure and style. One of these people is Sue Keay, whose efforts have been nothing short of legendary. Dave Phillips is thanked for his thorough reading of Chapter 4. Des Patterson, my academic "older brother," provided helpful and insightful comments on Chapter 7. Greg Yaxley and Juergen Streit are thanked for reading through chapters 5 and 6. Chuck Magee had the dubious honour of reading through most of my chapters, which he did good naturedly and provided useful feedback. Takuya Matsumoto, my second academic older brother, is thanked for his help in the early days of my Ph.D., and for helpful discussions and insights on a wide variety of subjects. Gwion Harfoot hunted for (and found) typos in several chapters and is acknowledged for his patient ProoFreadinkg.

I thank the following people for the fantastic times that I have had in Australia: Lucy Royle, Greg Cameron, Silke Speier, Greg Terrill, Martha Power, Pyramo Marianelli, Roz Walker, Daniella Rubbatto, Joerg Hermann, Andrew Alibone, Ulli Troizche, Jim Dunlap, Erica Hendy, Charlotte Allen, Brad and Nancy Opdyke, Kevin Fleming, Andrew Berry, Anna Chappell, Dirk Christian, Richard Wyzochanski, Stewart Fallon, Chuck Magee, Matt Wells, Jess Weir, Simon Gane, Claudine Stirling, Nat and Mick Stuckings, Amy Pierce, Stephan Klemme, Jette Neilson, Chris Heath, Linda Ayliffe, Juergen Streit, Andrew Kiss, Helen MacGregor, Steve Eggins, Torsten Juelich, and Richard Denis. These and other people contributed to the good times, great conversations and laughs that made my time here in Australia most enjoyable.

I would not have survived this PhD with my sanity intact if not for the loyal and unyielding support and friendship of certain people, who stuck through the best and the worst of times with me. These people are: Julian Ballard, a loyal friend, great jogging partner, and a faithful supporter and listener for matters personal and professional, who provided help and a source of inspiration; Sue Keay, for her legendary support, friendship, loyalty, the really good times and her fantastic sense of humour; Monica Handler, whose understanding of human nature is truly exceptional, and whose kindness, intelligence and friendship were really instrumental in helping me to persevere; Greg and Jenny Yaxley (and Kerry and Keaghan), for the great times out on the back balcony, for support and for so generously letting me rent their lovely house during their absence; Nyssa Gygory-Faul and Uli Faul, who also allowed me to housesit during one of the very busy times of my PhD; Anthea Munroe, for always being there for a good gossip session and to listen to my woes, no matter how petty; Gill Whiting, for her easy companionship, good nature, smile and friendship; Catherine Gutierrez, for always being

there for me, and helping to ease the stress of the day; Paul Danehy and Shelly Simonds (and little Tess) for being my "family" here in Australia, and for all those wonderful American dinners on Easter, Thanksgiving, Christmas, New Year's, for the camping trips and expeditions to Queensland; Pauline Treble, for listening, being honest, and providing great companionship; Bryony Wakefield, for the trolley-pushing shopping expeditions, and everything else; Margaret Bickmore, my faithful foreign correspondent; and especially Gwion Harfoot, for his kindness, care and life support, without which I would not have been able to keep smiling at the end of writing-up.

Lastly, I would like to thank my parents. The ethics and principles instilled in me by my mother kept me going during the long hours in the lab and in my office. I am very grateful to her for the things she taught me. Finally, I would like to dedicate this thesis to my father, whose interest in all aspects of science has provided me with a continued source of inspiration. His unflagging support, encouragement and enthusiasm through my many years of education, without ever once questioning my goals or sanity has helped to provide me with the motivation for pursuing this degree in science.

"Not knowing when the dawn will come, I open every door."

Emily Dickinson

ABSTRACT

Iceland is an ocean island that occurs along a spreading ridge, the Mid-Atlantic Ridge (MAR). A comprehensive noble gas investigation that included all five of the stable noble gases on samples from different volcanic centers in Iceland is needed so that the noble gas isotopic and elemental ratios can be compared with those from other ocean island basalts (OIBs) to further understand the origin and degree of mantle noble gas isotopic heterogeneity.

The noble gas elemental and isotopic ratios from 26 different samples of youthful age (<15 ka) basalts from 13 localities in Iceland are reported here; a total of 28 olivine, one pyroxene and 9 glass separates were analysed. The $^{3}He/^{4}He$ ratios in samples well-shielded from cosmic rays range from 12 ± 2 to 29 ± 3 Ra. The $^{3}He/^{4}He$ ratios from partly-shielded samples extend from values as low as 8.3 ± 0.8 Ra, close to the average mid ocean ridge basalt (MORB) ratio, to as high as 75 ± 7 Ra (total gas ratios). The neon isotopic ratios from well-shielded samples predominantly lie close to either the air-solar mixing line or the MORB trend. The maximum $^{20}Ne/^{22}Ne$ ratio is 11.98 ± 0.56. Neon isotopic ratios near the air-solar mixing line have not been described previously in mantle-derived samples and are the most significant results from this study. Neon isotopic ratios of the total gas released from partly-shielded olivine samples predominantly lie on a trend that is intermediate between the air-solar mixing line and the MORB trend. The $^{40}Ar/^{36}Ar$ ratios range from the atmospheric ratio to a maximum value of 1229 ± 150. The krypton isotopic ratios from this study are indistinguishable from the atmospheric ratios at the one sigma uncertainty level. The xenon isotopic ratios are generally indistinguishable from the atmospheric ratios at the one sigma uncertainty level in all but one sample (*ice-9g*). The maximum value of the $^{129}Xe/^{130}Xe$ (6.67 ± 0.09) and $^{136}Xe/^{130}Xe$ (2.22 ± 0.03) ratios in sample *ice-9g1* are 2% higher than the atmospheric ratio.

There are at least two possible means of preserving the near-solar neon isotopic ratios in the Icelandic plume source. One is if the near-solar neon isotopic ratios are derived from a plume source with a $[Ne_{solar}]/[U+Th]$ ratio that is at least nine times higher than that in the MORB source. This estimate assumes that the U and Th contents of the MORB and the Icelandic plume sources are similar. Owing to the highly incompatible nature of neon during mantle melting, a mantle source that has a high $[Ne_{solar}]/[U+Th]$ ratio is likely to be relatively unmelted and undegassed. A relatively unmelted region of the mantle is inferred to have a composition that is close to the

postulated primitive mantle composition. The near-solar neon isotopic component in some Icelandic basalts may therefore originate from a primitive, undegassed mantle component in the Icelandic plume source. This component is believed to comprise only a small proportion of the material sampled by the Icelandic plume so that it has little influence on the observed neodymium, strontium and lead isotopic compositions of the basalts. An alternative possibility is that the gases with near-solar neon isotopic ratios in the Icelandic plume source were derived from the Earth's core. This scenario is considered highly speculative owing to the lack of experimental evidence to show that noble gases could be stored in iron-nickel alloys under the pressure and temperature conditions that exist in the core.

To further understand the compositions of mantle sources sampled by the Icelandic plume, the trace element compositions of eight Icelandic natural glass separates from picritic and tholeiitic basalt samples were analysed by LA-ICPMS. The incompatible element ratios reveal a large range in compositions, with Nb/U from 50.9 to 104, Nb/Th from 16.2 to 34.1 and Ce/Pb from 24 to 36. The maximum observed ratios in these Icelandic basalts are well above the range observed in OIBs and MORBs, with Nb/U = 47 ± 10, Nb/Th = 15 ± 1.7 and Ce/Pb = 25 ± 5. The Nb/U, Ce/Pb and Nb/Th ratios from this study of Icelandic basalts are linearly correlated. The Th/U ratios in Icelandic basalts, OIBs and MORBs are near-constant and close to ~3, showing that fractionation of Th and U has not caused fractionation of the Nb/U and Nb/Th ratios in these Icelandic basalts.

The relatively homogenous Nb/U, Nb/Th and Ce/Pb ratios in most OIBs and MORBs have previously been used to argue that OIBs cannot be derived directly from melting of primitive mantle. Instead, following extraction of continental crust, the OIB and MORB sources are postulated to have been well-mixed to produce relatively homogeneous incompatible element ratios. In contrast, the mantle source sampled by the Icelandic plume does not appear to be homogeneous in terms of trace element ratios. The maximum Nb/U ratio measured in this study of Icelandic basalts of near 100 is close to previous estimates for the composition of the mantle following extraction of continental crust. This suggests that after extraction of the continental crust from the postulated primitive mantle composition, the mantle source of Icelandic plumes may not have been well-mixed.

Additional compositional heterogeneity may have been introduced into the Icelandic plume at shallow levels in the upper mantle beneath Iceland, where MORB material may be entrained into the Icelandic plume as it is spread laterally by the diverging lithospheric plates along the MAR. Mixing between plume and MORB end-members may produce a range of chemical compositions. The lead, strontium and neodymium isotopic ratios of Icelandic basalts from the Reykjanes Peninsula overlap

normal MORB compositions, so that on geochemical grounds, MORBs are a possible end-member that mixes with the Icelandic plume..

The near-solar neon isotopic ratios measured in some Icelandic basalts in this study are expected to be coupled with near-solar helium isotopic ratios. Contrary to expectations, the helium isotopic ratios measured in Icelandic basalts are much lower than the possible range of solar $^{3}He/^{4}He$ ratios (100 to 320 Ra). Binary mixing between MORB-derived and plume-derived noble gases, in which the He/Ne ratios in at least one of the two end-members is fractionated, is postulated to explain the apparent-decoupling of helium and neon isotopic ratios in Icelandic basalts. The range in $^{129}Xe/^{130}Xe$ and $^{136}Xe/^{130}Xe$ ratios observed in one sample from this study and in results from previous studies of Icelandic basalts may result from addition of MORB-derived xenon, with relatively radiogenic xenon isotopic ratios, to plume-derived xenon, with relatively unradiogenic xenon isotopic ratios. The proposed binary mixing model is consistent with the helium, neon, argon, and xenon isotopic ratios in Icelandic basalts.

The binary mixing model was further evaluated using noble gas elemental ratios in Icelandic basalts. The elemental ratios produced by a binary mixture of OIB and MORB end-members should lie between the ratios in these end-members. An Icelandic sample that has elemental ratios within the range of compositions observed in OIBs and MORBs is consistent with mixing between a plume and MORB component with $^{3}He/^{22}Ne_{s}$ ratios of 5 and 25, respectively. This plume $^{3}He/^{22}Ne_{s}$ ratio (5) is close to the primordial mantle ratio, and the MORB $^{3}He/^{22}Ne_{s}$ ratio (25) consistent with the range of fractionated elemental ratios observed in MORBs. The majority of Icelandic basalts from this study have elemental ratios that lie on different trends than those observed in OIBs and MORBs. Following the proposed mixing described above, the noble gas elemental ratios in these Icelandic samples may have been further fractionated by processes including preferential helium loss, solubility controlled fractionation and crystal-melt fractionation as the magma ascended through the crust via dikes to the surface. These elemental fractionation processes would not affect the noble gas isotopic ratios.

The most important finding from this study is the discovery of near-solar neon isotopic ratios in Icelandic basalts because they imply that very primitive mantle material is preserved in the Icelandic plume source.

TABLE OF CONTENTS

LIST OF FIGURES

LIST OF TABLES

CHAPTER 1: INTRODUCTION

1.1 Purpose and aim of investigation

The Earth and its atmosphere contain the noble gases, helium, neon, argon, krypton and xenon, whose elemental and isotopic ratios can be used to help understand processes that occurred during the Earth's formation, as well as subsequent melting and degassing processes. Mantle-derived noble gases can be analysed because they are commonly trapped in minerals and quenched glasses in mantle-derived lavas erupted at intraplate settings as ocean island basalts (OIBs) and along spreading ridges as mid-ocean ridge basalts (MORBs).

Analyses of noble gases from OIBs and MORBs have shown that the Earth contains components of primordial gases, i.e., those isotopes of gases that were present at the time the Earth formed and have not been augmented by radioactive decay or nucleogenic processes. Some of the primordial gases are interpreted to have been incorporated from the solar nebula during or shortly after accretion. The distribution of these solar primordial gases in the Earth's mantle is not well known. The processes of partial melting, degassing and radioactive decay cause changes in some of the isotopic ratios of the noble gases (e.g., $^{21}Ne/^{22}Ne$, $^{3}He/^{4}He$, $^{40}Ar/^{36}Ar$). Consequently, the noble gas isotopic ratios of samples that originate from different parts of the mantle can be used to elucidate the extent of processing and degassing of the various mantle sources. The noble gas isotopic ratios may thus provide insights into the degree of mantle heterogeneity, which, in turn, can provide insights into the scale of mantle convection.

In many localities where noble gas investigations have been undertaken, only the $^{3}He/^{4}He$ ratios of mantle-derived samples have been analysed. Although relatively high $^{3}He/^{4}He$ ratios in OIBs compared with MORBs have provided important evidence to support the origin of OIBs as derived from mantle plumes that have mantle source regions that are distinct from sources of MORBs, additional important information can be derived from analyses of the other noble gases, especially neon, argon and xenon.

The aim of the present project was to analyze the elemental and isotopic compositions of all five stable noble gases in mantle-derived basaltic samples erupted in Iceland for the purpose of placing additional constraints on the degree of mantle heterogeneity in the source regions of OIBs. Such constraints may help us to

understand the degree of stirring in the mantle. Previous investigations of helium isotopic ratios from Icelandic samples had revealed relatively high $^3He/^4He$ ratios compared with those observed in samples from adjacent MORBs. Similar high $^3He/^4He$ ratios have been measured in Hawaiian basalts, and are associated with relatively solar-like neon end-member isotopic ratios. The presence of such high $^3He/^4He$ ratios in Icelandic basalts suggests that the other noble gases, such as neon, may have compositions similar to those found in Hawaiian basalts. Recent investigations of Icelandic basalts have included analyses of all the noble gases on samples obtained from one locality. A comprehensive noble gas investigation of Icelandic basalts that included analyses of all the noble gases from a range of geographic localities had not yet been undertaken. This made Iceland an ideal target for a noble gas investigation.

1.2 Thesis organization

Chapter 2. Noble gas introduction and background

This chapter presents an overview of noble gas geochemistry, including basic noble gas geochemical data. In the first section, the geochemical characteristics of the noble gases are summarized. In the second section, the physical-chemical processes that cause noble gas elemental fractionation are explained, and a model for multistage solubility controlled fractionation by bubble formation is presented. In section three, the noble gas isotopic compositions in the solar system are compared with the isotopic ratios in terrestrial mantle-derived samples and the atmosphere. The general arguments for degree of degassing of the Earth's mantle and the origin of the atmosphere as derived in part from degassing the mantle are explained. Atmospheric evolution models are then summarized to show how noble gas geochemical data may be used as a tool to help to explain the degassing history of the Earth and the formation of the Earth's atmosphere. Finally, the noble gas elemental ratios in MORBs and OIBs are described.

Chapter 3. Geophysical versus geochemical perspectives on mantle convection

In this chapter, geochemical arguments for a layered mantle, comprised of an upper, relatively degassed and depleted mantle, and a lower, relatively undegassed and undepleted mantle, are compared with geophysical arguments for whole-mantle convection. The noble gas data are evaluated in the context of whole mantle convection models to understand how the geochemical evidence and geophysical models might be reconciled. One important aspect of this problem is to explain how relatively solar-like helium and neon isotopic compositions are preserved in the mantle source regions of ocean island basalts (which are believed to originate from plumes derived from the lower

mantle), compared with less solar-like helium and neon isotopic compositions in mid-ocean ridge basalts (which are thought to be derived from the upper mantle) if the entire mantle is stirred by convection.

Chapter 4. Geology, petrology and geochemistry of Icelandic basalts

This chapter provides an overview of the Icelandic regional geologic setting, and how interaction of the Icelandic plume with an active spreading center, the Mid-Atlantic ridge (MAR), causes Icelandic basalts to be largely erupted along the Neo-Volcanic Zones, the subaerial extensions of the MAR. Interaction of the Icelandic plume melts with MORB melts may influence the geochemistry of the Icelandic basalts. The major element, trace element and lead, strontium and neodymium isotopic compositions of Icelandic basalts are described and briefly evaluated to understand the possible origins of magmas that produce Icelandic basalts. Additional trace element results from this study are then provided and compared with previous trace element results from Iceland. The incompatible element ratios, including Nb/U, Nb/Th and Ce/Pb data from this study are compared with previous incompatible element studies of OIBs and MORBs to understand the possible processes that give rise to the unusual incompatible element ratios in Icelandic basalts.

Chapter 5. Previous and new noble gas results from Icelandic basalts

The data from previous noble gas investigations of Icelandic basalts are presented, followed by the new helium, neon, argon, krypton and xenon isotopic data from this study of Icelandic basalts. The results from this study are then compared with the results from previous noble gas investigations of Icelandic basalts. The noble gas results from this study are different from those obtained in previous noble gas studies of samples from the same areas. In particular, some of the neon results from this study are more solar-like than those described in any other terrestrial samples.

Chapter 6. Noble gas isotopic ratios in Icelandic basalts

The discussion of noble gas isotopic data is divided into three separate sections. First, the isotopic data from some Icelandic samples that were only partly shielded from cosmic rays are evaluated to determine whether they preserve meaningful information about mantle-derived noble gases. Second, a general explanation is given for the means by which near-solar neon isotopic ratios measured in this study may be preserved in the mantle. Finally, a model involving binary mixing between the Icelandic plume and MORB-derived noble gases is presented to explain the range of helium, neon, argon and xenon isotopic ratios in Icelandic basalts from this study and previous studies.

Chapter 7. Noble gas elemental abundance ratios in Icelandic basalts

The noble gas elemental ratios in Icelandic basalts elemental ratios are first evaluated to determine whether they are consistent with the binary mixing model presented in Chapter 6. A sequence of elemental fractionation processes that may produce the observed large range in elemental ratios in the majority of Icelandic basalts from this study is then described.

Chapter 8. Synthesis

An overview of the major findings and interpretations presented in this thesis. With the exception of this chapter, which does not include cited references, cited references are provided at the end of each chapter for the reader's convenience.

Appendix 1. Sample locations and petrographic descriptions

Appendix 2. Major and trace element analytical methods

Appendix 3. Noble gas analytical methods

CHAPTER 2: NOBLE GAS INTRODUCTION AND BACKGROUND

This general introduction to noble gas geochemistry is intended to illustrate how the noble gases may be used to help understand the formation and evolution of the Earth and its atmosphere. A brief summary of basic geochemical data is provided, including a discussion of the reactions and processes that produce the non-primordial isotopes of the noble gases. This will be followed by the identification of solar system and terrestrial noble gas reservoirs, and presentation of the isotopic and elemental noble gas ratios in terrestrial reservoirs. This information is used to evaluate the noble gas compositions of mantle-derived samples to understand the degassing history of the mantle and the formation of the atmosphere.

2.1 Geochemical characteristics of noble gases

The noble gases, helium, neon, argon, krypton and xenon, are chemically inert and do not form stable compounds with other elements under known terrestrial conditions. The isotopes of the noble gases (Table 2-1) are stable with the exception of radon, whose isotopes have very short half-lives. In the solar system, the noble gases are not necessarily "rare gases," as they are sometimes called. Helium is known to be the second most abundant element in the solar system, after hydrogen. The solar system primordial abundances of the heavy gases, argon, krypton and xenon, are believed to fit into empirical elemental abundance curves that are based on the compositions of carbonaceous (C-1) chondrites. The noble gas abundances are obtained by interpolation between the abundances of neighbouring elements. Estimates for the abundances of the lighter gases, helium and neon, are based on spectral analyses of solar flares. Although the noble gases are abundant in the solar system, they are rare in the Earth's atmosphere, with krypton and xenon constituting only 1 and 0.09 parts per million (ppm) in the atmosphere, respectively, and argon about 1% by volume of the atmosphere (Ozima and Podosek, 1983).

The noble gases have a large range in atomic masses from 3 atomic mass units (amu) (^{3}He) to 136 amu (^{136}Xe). Each noble gas has two or more isotopes (Table 2-1). The difference in mass between the isotopes of the noble gases is as high as 33%

(between ^{3}He and ^{4}He), but the maximum mass difference between most isotopes is much lower (e.g., close to 10% between ^{20}Ne and ^{22}Ne).

The isotopes of the noble gases are of two types (Table 2-1): (1) non-primordial isotopes, which are produced by radioactive decay, fission, and nucleogenic reactions, and (2) primordial isotopes, which are not produced in appreciable quantities in the Earth and are therefore interpreted to be derived from the materials that formed the Earth. For example, ^{22}Ne is regarded as a primordial isotope because, although it is produced by nucleogenic reactions involving ^{25}Mg (Table 2-2), this contribution is not significant to the total abundance of ^{22}Ne in the Earth.

Table 2-1. Isotopes of the noble gases

	He	Ne	Ar	Kr	Xe
Atomic number	2	10	18	36	54
Mean atomic mass	4.0026	20.183	39.948	83.80	131.30
Primordial isotope(s)	3	20, 22	36, 38	84	130
Radiogenic or nucleogenic isotopes	4	21	40	78, 80, 82, 83, 86	124, 126, 128, 129, 131, 132, 134, 136

Some of these radiogenic and nucleogenic isotopes (commonly denoted by an "*" with the exception of radiogenic ^{4}He) will be discussed extensively in later chapters. In particular, the production of ^{4}He from alpha decay of U and Th (Table 2-2), $^{40}Ar^{*}$ from ^{40}K via radioactive decay (Table 2-2), and production of $^{21}Ne^{*}$ by interaction of alpha particles with target nuclides such as ^{18}O via the Wetherill reactions (Wetherill, 1954) in the mantle (Table 2-3) are of great significance in relation to the isotopic and elemental ratios in mantle-derived samples. Significantly, the $^{4}He/^{21}Ne^{*}$ production ratio in the mantle and crust is nearly constant, both at present and integrated over 4.5 Ga (Table 2-3). This near-constant production ratio results in correlated $^{3}He/^{4}He$ and $^{21}Ne/^{22}Ne$ ratios in mantle derived samples, as will be discussed in more detail in later sections.

Table 2-2. Selected radiogenic, nucleogenic and spontaneous fission reactions that produce noble gas isotopes

Isotope	Radioactive Parent	Nucleogenic	Spontaneous fission	Half life, Ga	Yield, atom/atom
^{3}He		$^{6}Li(n,\alpha)^{3}H(\beta^{-})^{3}He$			
^{4}He	^{232}Th			14.010	6
^{4}He	^{238}U			4.468	8
^{20}Ne		$^{17}O(\alpha,n)^{20}Ne$			
^{21}Ne		$^{18}O(\alpha,n)^{21}Ne$			
^{22}Ne		$^{25}Mg(n,\alpha)^{22}Ne$			
^{40}Ar	^{40}K			1.251	
$^{83\text{-}86}Kr$			^{238}U	4.468	
^{129}Xe	^{129}I			0.017	1
$^{131\text{-}136}Xe$			^{238}U	4.468	$^{136}Xe = 3.5 \times 10^{-8}$
$^{131\text{-}136}Xe$			^{244}Pu	0.082	$^{136}Xe = 7 \times 10^{-5}$

From Ozima and Podosek (1984)

Table 2-3. Nucleogenic neon and radiogenic ^{4}He production over 4.5 Ga and current production rates calculated for typical mantle and crustal compositions

Isotope	Production rate over 4.5 Ga		Present production rate	
	cm^3STP/g		cm^3STP/g year	
	mantle	crust	mantle	crust
^{20}Ne	1.35×10^{-13}	1.45×10^{-11}	1.74×10^{-23}	1.86×10^{-21}
^{21}Ne	1.45×10^{-12}	1.50×10^{-10}	1.86×10^{-22}	1.92×10^{-20}
^{22}Ne	3.02×10^{-14}	4.10×10^{-11}	3.98×10^{-24}	5.23×10^{-21}
^{4}He	3.20×10^{-5}	3.20×10^{-3}	4.15×10^{-15}	4.15×10^{-13}
Production ratios, 4.5 Ga			Production ratios, present	
$^{20}Ne/^{22}Ne$	4.47	0.35	4.37	0.36
$^{21}Ne/^{22}Ne$	48	3.66	46.7	3.67
$^{4}He/^{21}Ne$	2.21×10^{7}	2.13×10^{7}	2.23×10^{7}	2.16×10^{7}
$^{4}He/^{40}Ar(a)$	1.7		5	

After Yatsevich and Honda (1998), based on an estimated U content of 20 ppb for the mantle and 2.0 ppm for the crust, with Th/U = 3.0, except for (a) which is from Honda and Patterson (1999) based on a mantle K/U ratio of 12700 (Jochum et al., 1983).

2.1.1 Cosmogenic nuclides

In addition to being produced in the mantle, isotopes of noble gases are also produced at or near the Earth's surface. Cosmic ray-induced spallation of target nuclei in the rock matrix is the predominant mechanism by which noble gases are produced at or near the Earth's surface. For example, spallation of the target atoms ^{18}O and ^{24}Mg

produce coupled ^{3}He and ^{21}Ne (Lal, 1987; Lal, 1988). The cosmogenic nuclide production rate depends on the rock composition, altitude, geomagnetic latitude, and the exposure geometry as a function of time (i.e., erosion rate). The cosmic ray flux decreases from the poles to the equator because of deflection by the geomagnetic field. The atmosphere shields the Earth from cosmic rays, resulting in higher cosmogenic production rates in rocks at high elevations than in those at sea-level. For example, for every 1000 m increase in elevation, the production rate of ^{3}He doubles relative to the rate at sea level (Yokoyama et al., 1977). Cosmic rays can penetrate rocks to depths of several metres, but the production rate of cosmogenic nuclides decreases exponentially with depth so that the most significant production is within ~1 m of the surface, depending on the density of the rock.

The expected amount of cosmogenic ^{3}He produced over the exposure history of a basaltic rock may be calculated from equation (2-1):

$$[^{3}He](cm^{3}STP/g\ year) = H \times [1.68 - (0.0637 \times CR) + (9.99 \times 10^{-4} \times CR^{2})] \qquad (2\text{-}1)$$

where $[^{3}He]$ is the production rate of ^{3}He in the sample for exposure at sea-level and H is the production rate in Hawaii at sea-level (3.7×10^{-18} $cm^{3}STP/g$ year) (Kurz et al., 1990), and CR (in gigavolts) is the vertical cutoff rigidity.

Noble gas studies of mantle-derived samples commonly focus on olivine basalts because olivine traps mantle-derived noble gases. If olivine basalts have been exposed to cosmic rays for a prolonged period of time, the possibility that cosmogenic noble gases may have contaminated the mantle-derived noble gases must be considered. The cosmogenic production ratios of $^{20}Ne/^{22}Ne$ and $^{21}Ne/^{22}Ne$ in olivine are 0.84 and 0.94, respectively (Lugmair et al., 1976). The cosmogenic $^{21}Ne/^{22}Ne$ end-member ratio is much higher than the maximum ratio typically measured in mantle-derived samples from Mid-Ocean Ridge Basalts (MORBs) (~0.075) (Sarda et al., 1988). Because ^{21}Ne is present in the lowest abundance of the three neon isotopes in mantle-derived samples, addition of cosmogenic ^{21}Ne to mantle-derived neon may cause the measured $^{21}Ne/^{22}Ne$ ratios to be significantly higher than the mantle neon ratio.

2.2 Physical-chemical processes controlling noble gas elemental ratios

2.2.1 Crystal/melt partitioning

Melting of mantle minerals, or crystallization of minerals from a magma can

fractionate elemental ratios in residual solids and magmatic liquids relative to the initial bulk composition. The relative differences in compatibilities of non-gaseous radioactive parent isotopes compared with their gaseous daughter isotopes (e.g., ^{238}U and ^{4}He, or ^{40}K and ^{40}Ar) between crystals and melt can affect the noble gas isotopic ratios in a mantle source over time. Partitioning between crystalline and melt phases is defined by the distribution coefficient, $D = C_{crystal}/C_{melt}$. The experimental data on crystal-liquid partitioning of noble gases in geologic systems shows a wide range in D-values, possibly owing to experimental difficulties (e.g., Carroll and Draper, 1994; Hiyagon, 1994; Jambon and Shelby, 1980; Jambon et al., 1986; Lux, 1987; Valbracht et al., 1994). Analyses to determine D-values in natural samples provide maximum estimates of the true values because some degassing may have occurred from the glass. The D-values obtained from coexisting glass and olivine phenocrysts in natural samples are 0.008 for He and 0.003 for Ar (Carroll and Draper, 1994). As might be expected, the D-values are commonly much less than unity for natural samples and suggest that noble gases behave as incompatible elements that partition preferentially into the melt phase over the solid phase.

2.2.2 Solubility controlled fractionation

Gas bubbles form as a result of saturation of gases in the melt. In basaltic magmas, noble gases are expected to be strongly undersaturated with respect to the concentrations that Henry's law would predict for a given ambient pressure, so that noble gases should not form gas bubbles on their own. Thus, the primary bubble-forming gases are not the noble gases, and are more likely to be those that are abundant in the melt. Magmatic volatiles, such as in the MORB popping rock, are comprised predominantly of CO_2 and H_2O, and the noble gases are present in relatively small concentrations (Javoy and Pineau, 1991; Pineau and Javoy, 1994). The solubility of CO_2 and the noble gases are low compared with H_2O, and CO_2 has a solubility that is lower than that of helium but higher than that of argon in basaltic melts (Carroll and Draper, 1994). The low solubilities of the noble gases and CO_2 mean that the noble gases will follow CO_2 and be preferentially partitioned into the early-formed vapor phase (Carroll and Draper, 1994). The solubility of CO_2 in magma is positively correlated with both temperature and pressure, so that as ambient pressure is decreased during the ascent of a magma containing dissolved CO_2, saturation is likely to be reached (Watson et al., 1982). A melt with a large initial concentration of CO_2 would reach saturation during the relatively early stages of magmatic ascent, causing the first bubbles to appear, and as the pressure decreases as magma continues to ascend, the saturation concentration of CO_2 also decreases, and more bubbles will form (Prousevitch et al., 1993).

The exsolution of CO_2 from the magma is controlled principally by nucleation of fluid bubbles and subsequent growth of these bubbles by diffusion (Watson et al., 1982). The noble gases should partition from the melt into the gaseous phase along with CO_2 in accordance with their solubilities in the melt, and may subsequently diffuse into the bubbles as the bubbles grow. When noble gases partition between melt and vapor phases, the melt becomes enriched in the lighter element because these elements are relatively compatible in the melt compared with the heavier elements; thus, it is expected that solubility controlled fractionation by bubble formation will result in higher He/Ne and Ne/Ar ratios in the residual melt phase than in the bubbles.

The degree of elemental fractionation of the noble gases in the residual melt phase depends on the total volume of bubbles that has formed, and whether the gas from the bubbles is allowed to leave the system. For small fractional volumes of bubbles (<0.01%) and single-stage fractionation in a closed system, there is no large effect on the elemental ratios in the residual melt, but for larger volumes of bubbles (~1%) the degree of elemental fractionation in the residual melt is greater. During equilibrium partitioning in a closed system, nearly all the gas is transferred from the melt into the gas phase if the volume fraction of vesicles is >10% of the total volume (Carroll and Draper, 1994). In this case, the elemental ratios in the vesicles should approximately the same as the initial ratio in the melt (Lux, 1987). The gas concentration in the residual melt following loss of bubbles is expected to be relatively low, but owing to partitioning of the relatively heavy elements into the bubbles, the elemental ratios in the residual melt will be enriched in the light element. The maximum degree of fractionation of the elemental ratio in a closed system is attained after approximately 1 - 10% vesicles have formed.

In an open system in which the gases from the vesicles escape, the elemental ratios in the residual gas in the melt may be more highly fractionated relative to the initial ratios than in the case of a closed system (Carroll and Draper, 1994). Provided that the noble gases partition rapidly into the volume provided by the CO_2 bubbles, and the flux of CO_2 bubbles into and out of the system is constant so that the total volume of the CO_2 bubbles present in the system remains near-constant, the partial pressure of noble gases in the CO_2 bubbles may be assumed to be at equilibrium with the noble gas concentration in the residual melt.

Equations describing solubility controlled fractionation

Noble gas solubilities are generally higher in more silica-rich melts, possibly owing to the higher number of interstitial sites within rings of interconnected silicate tetrahedra (Carroll and Draper, 1994, and references therein). For a given silicate melt composition, solubility decreases with increasing atomic radius of the gas, so that helium is the most soluble of all the noble gases (Fig. 2-1). In a tholeiite basalt at 1350°C, one

study estimates that the Henry's law constant (S) for noble gas solubility (in cm^3STP/g atm x 10^{-5}) are: $S_{He} = 64 \pm 8$, $S_{Ne} = 35 \pm 6$, $S_{Ar} = 8.7 \pm 0.6$, $S_{Kr} = 6.3 \pm 0.4$, $S_{Xe} = 2.7 \pm 0.4$ (Lux, 1987). Experiments using gas pressures between 1 x 10^{-3} and 1 x 10^{3} bar show that the solubility of the noble gases decreases as an approximately linear function of gas pressure within this pressure range (Henry's Law behaviour) and is almost independent of temperature (Carroll and Draper, 1994).

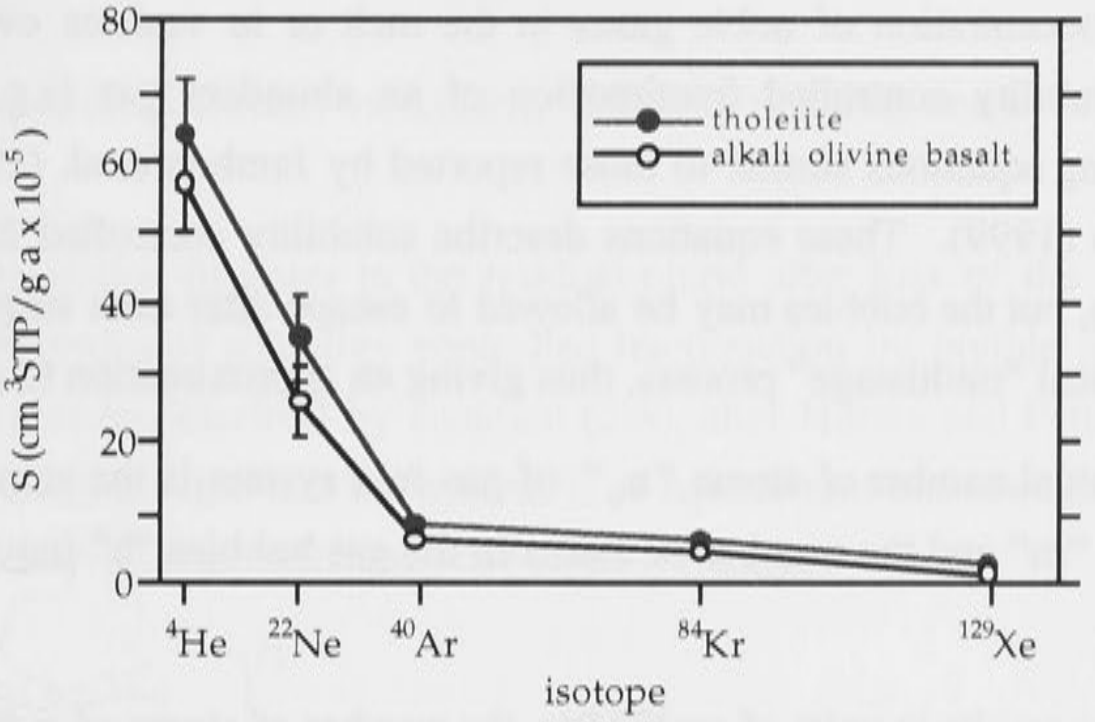

Figure 2-1. Henry's law constants (S) for noble gas solubility in two silicate liquids at 1350°C in units of cm^3STP/g atmosphere. After Lux (1987).

Because the solubilities of helium and argon in the melt phase differ by about a factor of seven, whereas those of helium and neon differ by a factor of two (Lux, 1987), the degree of helium and argon fractionation between a basaltic melt and vapour phase following bubble formation will be much greater than between helium and neon. Neon is more soluble than argon by approximately a factor of four (Lux, 1987), so the degree of fractionation between neon and argon following formation of gas bubbles from a melt will also be greater than between helium and neon. The theoretical maximum degree of fractionation that may be produced in the melt phase by solubility controlled fractionation in a closed system owing to removal of gas in a bubble phase (at equilibrium) is equal to the initial ratio in the melt multiplied by the ratio of the relative solubilities (S_i) of the two gases of interest as shown in equation (2-2) using the He/Ar ratio as an example.

$$[He]_{melt}/[Ar]_{melt} = [He]_{gas}/[Ar]_{gas}\,(S_{He}/S_{Ar}) \qquad (2\text{-}2)$$

For the Henry's law constants given above (Lux, 1987), the relative degree of fractionation of the He/Ar ratio can be estimated (equation 2-3),

$$S_{He}/S_{Ar} = 64/8.7 = 7.4 \quad (2\text{-}3)$$

In comparison, the degree of fractionation of the Ne/Ar ratio and the He/Ne ratios are smaller and equal to (35/8.7) 4.0 and (7.4 / 4.0) 1.9, respectively.

Multistage solubility controlled fractionation

The following multistage solubility controlled fractionation model will be applied in Chapter 7 to explain the noble gas elemental ratios obtained from this study. The changes in concentration of noble gases in the melt or in vesicles owing to multiple stages of solubility controlled fractionation of an abundant gas (e.g., CO_2) may be simulated using equations similar to those reported by Jambon et al. (1986) and Honda and Patterson (1999). These equations describe solubility controlled fractionation in a closed system, but the bubbles may be allowed to escape after each stage of vesiculation in a hypothetical "multistage" process, thus giving an approximation to an open system.

The initial number of atoms "n_o" of gas in a system is the sum of atoms in the residual melt "m" and the number of atoms in the gas bubbles "b" (equation 2-4)

$$n_o = n_m + n_b \quad (2\text{-}4)$$

To express the results in units of cm^3STP/g, the number of atoms of a given gas "i", or "n_i" can be related to the gas concentration, "C" (cm^3STP/g) in the magma, such that

$$n_i = \frac{N_a}{V_a}\rho_m V_m C \ (cm^3STP/g)$$

where V_a is the molar volume of 22,400 cm^3/mole, ρ_m is density of the melt in g/cm^3, V_m is the melt volume and N_a is Avogadro's number, 6.02×10^{23} atoms/mole.

From the ideal gas law, $P_a V_a = n_a \kappa T_a$, where T_a is 273 K and Pa is one atmosphere and κ is Boltzman's constant (equation 2-5)

$$n_i = \frac{P_a}{\kappa T_a}\rho_m V_m C \ (cm^3STP/g) \quad (2\text{-}5)$$

The total volume of the system is increased by the total volume of the bubbles, so that ρ_m remains the same before and after the bubbles form. Using the ideal gas law again, this time for the noble gases in the bubbles,

$$P_b V_b = n_b \kappa T_o$$

(where T_o is is the temperature of equilibration of the bubble and the melt phases, "n" is the number of atoms, V_b is the volume of bubbles, and P_b is the gas pressure in the bubbles), equation (2-5) can be transformed to equation (2-6),

$$\frac{P_a}{\kappa T_a}\rho_m V_o C_o = \frac{P_a}{\kappa T_a}\rho_m V_o C_r + \frac{P_b V_b}{\kappa T_o} \quad (2\text{-}6)$$

where C_r is the gas concentration in the residual melt (cm^3STP/g). Note that this equation assumes that the volume of the system has increased by the total volume of the bubbles, so that the density of the melt remains approximately the same.

Combining Henry's law for gas "i", $C_r = S_i P_b$, with equation (2-6) gives an expression for the fraction of gas remaining in the residual melt (equation 2-7),

$$\frac{C_r}{C_o} = \frac{1}{1+\left(\frac{V^* T_a}{T_o P_o \rho_m S_i}\right)} \tag{2-7}$$

where $V^* = V_g/V_o$ is the fractional vesicularity (cm^3/cm^3) of melt and S_i is the solubility of gas "i".

The concentration of gases in the residual phase after loss of the bubble phase following "n" episodes of solubility controlled fractionation by bubble formation at a constant volume may be described by equation (2-8), after Honda and Patterson (1999). All of these equations assume that the system is at equilibrium and remains closed until the bubbles are removed after each stage of bubble formation.

$$\frac{C_r}{C_o} = \left(\frac{\frac{S_i P_o \rho_o (1-V^*)}{V^*(T_a/T_o)}}{1+\left[\frac{S_i P_o \rho_o (1-V^*)}{V^*(T_a/T_o)}\right]}\right)^n \tag{2-8}$$

Calculated noble gas elemental ratios and gas concentrations

Approach

For the first stage of fractionation, when the initial CO_2 bubbles form, equation (2-7) above is used to calculate the gas concentrations of helium, neon and argon and elemental ratios in the melt phase. The elemental ratios and gas concentrations produced by the succeeding stages of fractionation are calculated from equation (2-8). The change in residual melt composition with each stage of vesiculation is determined by using the residual melt ratio from the previous step as the starting composition for the next increment of gas removal (Fig. 2-2). This approach is similar to that which was used by Carroll and Draper (1994).

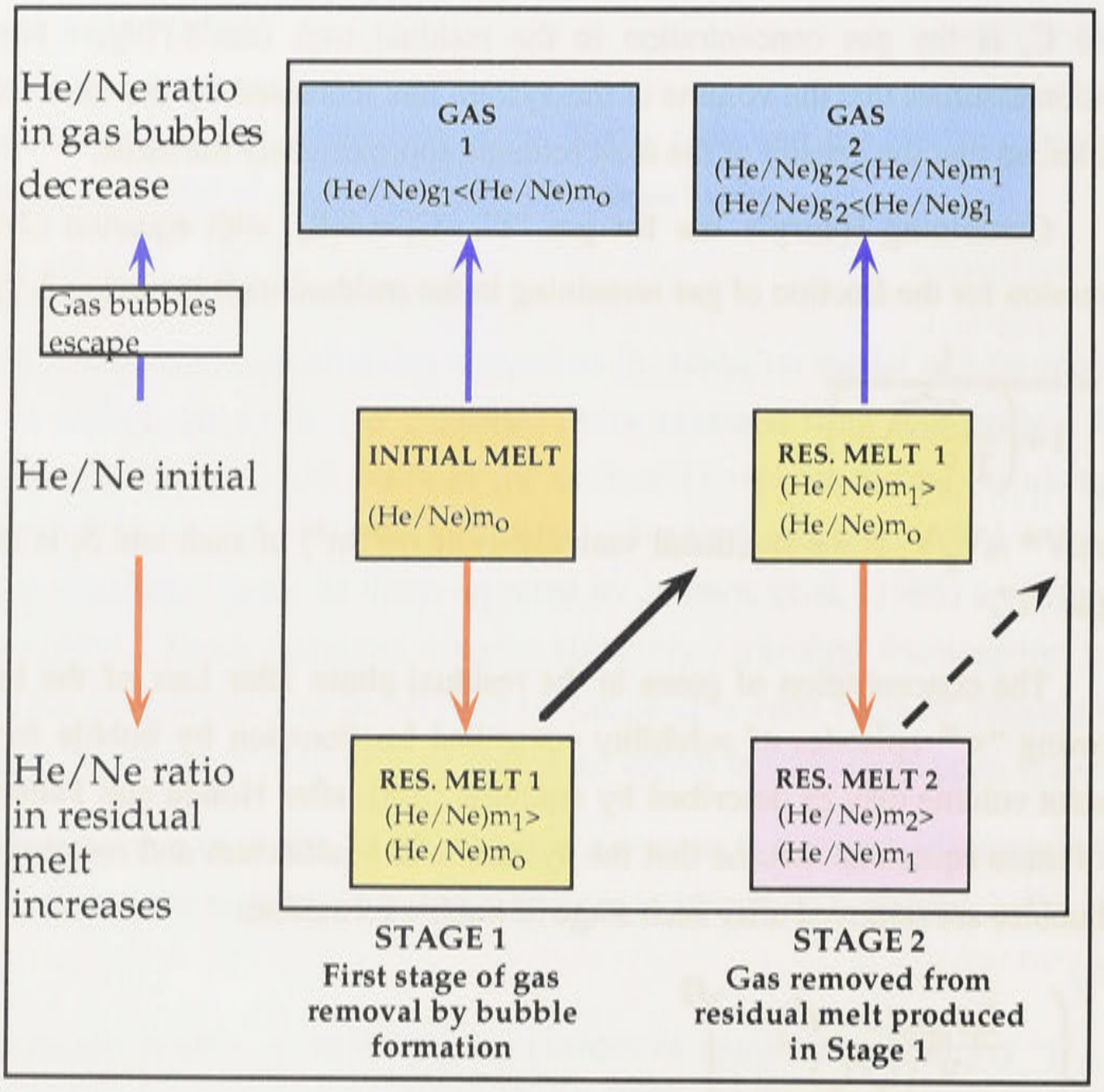

Figure 2-2. Schematic representation of stepwise solubility controlled fractionation by bubble formation. Two stages of bubble formation are shown here. For a given initial elemental ratio (e.g., the He/Ne ratio) in a melt, the elemental ratio of the escaping gas (g) is enriched in the heavy element, whereas that of the residual melt (m) is enriched in the light element relative to the initial ratio. The second stage of diffusion (Stage 2) uses the elemental ratio in the residual melt as the new "initial ratio." Bubbles forming from this melt have a lower He/Ne ratio than the residual melt, but a higher He/Ne ratio than the gas that was released in Stage 1 because the ratio in the residual melt has increased relative to the initial ratio. The residual melt produced in stage 2 has a higher He/Ne ratio than that produced in stage 1.

Initial compositions

For the purposes of this calculation, the initial gas concentrations in the melt are assigned the following values: $C^o_{^3He}$=1 x 10^{-10} cm^3STP/g, $C^o_{^4He}$ = 2.4 x 10^{-6} cm^3STP/g, $C^o_{^{21}Ne^*}$ = 1.1 x 10^{-13} cm^3STP/g, $C^o_{^{22}Ne}$ = 1.67 x 10^{-11} cm^3STP/g and $C^o_{^{40}Ar^*}$ = 4.81x 10^{-7} cm^3STP/g. These concentrations give initial elemental ratios that are equal to the mantle production ratios, $^4He/^{21}Ne^*$ = 2.2 x 10^7; $^4He/^{40}Ar^*$ = 5 and $^{21}Ne^*/^{40}Ar^*$ = 2.2 x 10^{-7}. Other parameters used in the calculations are: T_o = 1273K, T_a = 273 K, the solubility constants for helium, neon and argon from Lux (1987) that were given previously and a density of 2.7 g/cm^3. The changes in elemental ratios and gas concentrations produced in the escaping gas and in the residual melt are calculated using

different vesicle volumes (0.01%, 0.1% and 1%). Larger degrees of elemental fractionation would be produced at each stage if the vesicle volumes were larger.

Results

Elemental ratios

The mantle production ratios (e.g., $^{4}He/^{40}Ar^{*}$, $^{21}Ne^{*}/^{40}Ar^{*}$) that were shown in Table 2-3 provide a convenient reference composition for comparison with the results of calculations to determine the incremental changes in elemental ratios produced during vesicle formation in an open system (equations (2-7) and (2-8)). The results are shown in plots of $^{4}He^{*}/^{21}Ne^{*}$ versus $^{4}He/^{40}Ar^{*}$ (Fig. 2-3) and $^{21}Ne^{*}/^{40}Ar^{*}$ versus $^{4}He/^{40}Ar^{*}$ (Fig. 2-4). The degree of fractionation of the elemental ratios in the residual melt that occurs at each stage of fractionation depends on the vesicle volume. A relatively large degree of fractionation of the $^{4}He/^{40}Ar^{*}$ ratio, for example, may be produced in a single stage of bubble formation if the volume fraction of vesicles is relatively large (~1%) (Fig. 2-3). Successive stages of bubble formation cause the elemental ratios in the residual melt become progressively enriched in the light element relative to the initial elemental ratio (here assumed to be the mantle production ratio) (Figures 2-3 and 2-4). The elemental ratios produced by bubble formation over a range of V* ratios lie on the same trend (Figures 2-3 and 2-4).

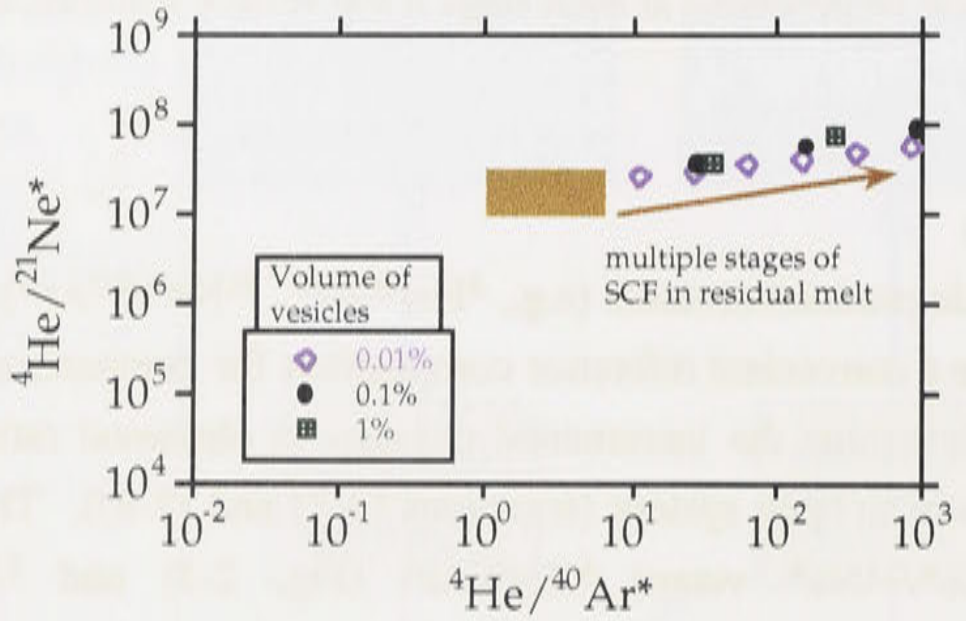

Figure 2-3. Plot of $^4He/^{21}Ne^*$ versus $^4He/^{40}Ar^*$ showing the calculated compositions in the residual melt phase that are predicted by equations (2-7 and 2-8) for different vesicle volume fractions in which gases from vesicles are lost after each stage of solubility controlled fractionation. The initial composition is shown by the orange rectangle, which also represents the range in the mantle production ratios. The $^4He/^{40}Ar^*$ ratio is more fractionated than the $^4He/^{21}Ne^*$ ratio because there is a relatively large difference in solubilities of ^4He and $^{40}Ar^*$. For small volume fractions of vesicles (0.01%), the change in the $^4He/^{40}Ar^*$ ratios of the residual melt is relatively small. At higher volume fractions of vesicles (0.1% to 1%), the degree of elemental fractionation of the $^4He/^{40}Ar^*$ ratio in the residual melt is much larger. Although the degree of fractionation differs for each of the various volume fractions of vesicles shown here, the calculated elemental ratios form trends that have similar slopes over a range of volume fractions of vesicles (0.01% to 1%). Note that the integrated vesicularity needed to produce the maximum degree of elemental fractionation shown here does not correspond to the vesicle volume that would be observed in the sample because the gases in vesicles are lost from the system. The magmas may have relatively small observed vesicle fractions, yet have highly fractionated noble gas abundances (Carroll and Draper, 1994).

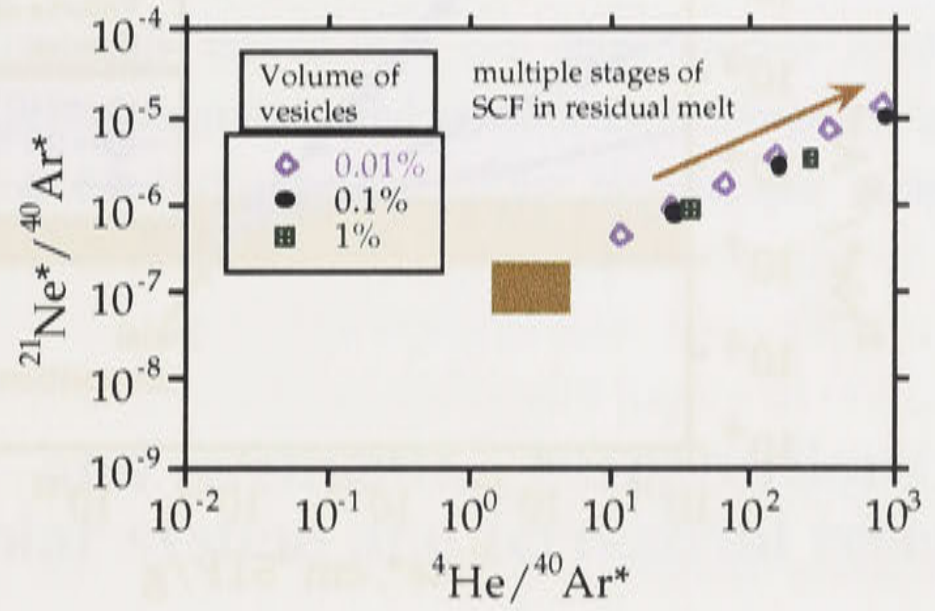

Figure 2-4. Plot of $^{21}Ne^*/^{40}Ar^*$ versus $^{4}He/^{40}Ar^*$ showing the calculated compositions that would be produced by solubility controlled fractionation (SCF) (symbols). The initial composition is represented by the orange rectangle. Incremental changes in the elemental ratios of the residual melt and escaping gas phases are shown for 0.01%, 0.1% and 1% vesicles, with the direction of increasing fractionation indicated by the orange arrow.

Gas concentrations

Figure 2-5 shows that the elemental ratios in the residual melt become enriched in the light element as the gas concentration decreases during multiple stages of solubility controlled fractionation. In other words, there is a negative correlation between the elemental ratio and the gas concentration (Honda and Patterson, 1999). The relationship between the elemental ratio and the gas concentration in the residual melt at each stage of solubility controlled fractionation depends on the volume fraction of vesicles, such that the change in the elemental ratio and the decrease in the gas concentration is largest for the highest volume fraction of vesicles (Fig. 2-5). Because the residual melt is increasingly enriched in the light element with successive stages of fractionation, bubbles forming from this melt will progressively also become enriched in the light element relative to the initial melt composition.

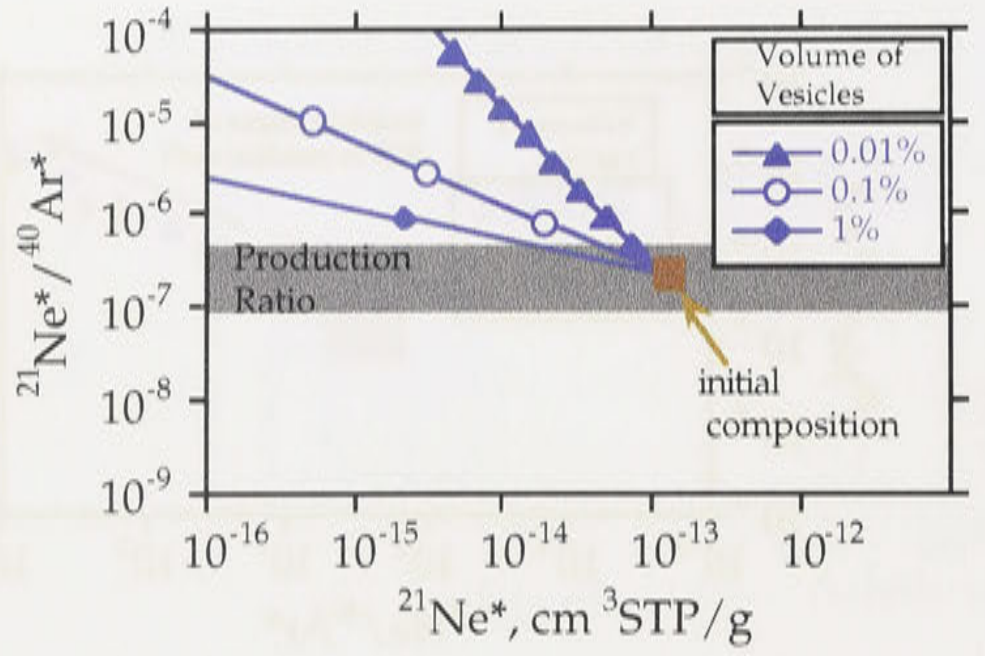

Figure 2-5. Plot of $^{21}Ne^*/^{40}Ar^*$ versus $^{21}Ne^*$ cm^3STP/g, showing the changes in the composition of the residual melt that would be produced during multistage vesicle formation and gas loss (see text). As in previous plots, the vesicle volumes at each stage of fractionation are: 0.01%, 0.1% and 1%. Different slopes are produced by fractionation of gases at different vesicle volumes, but in general, the $^{21}Ne^*/^{40}Ar^*$ ratio of the residual melt increases as the $^{21}Ne^*$ concentration decreases.

Summary

Solubility controlled fractionation by bubble formation requires that the magma becomes saturated with respect to a gas (e.g., CO_2) in order to produce bubbles. As the ambient pressure decreases during magma ascent, the noble gases may be partitioned into the bubbles along with CO_2 according to their relative solubilities in the melt. Following solubility controlled fractionation, the elemental ratio of gases in the residual melt would be enriched in the light noble gas elements compared with the initial ratio in the melt.

2.2.3 Diffusion

Diffusion of noble gases into and out of magmas, minerals and rocks is a process which alters noble gas elemental concentrations, and to a lesser extent, isotopic composition of a given element (Ozima and Podosek, 1983). The diffusive flux of a noble gas is proportional to the concentration gradient (Ozima and Podosek, 1983). The diffusion coefficient is dependent on temperature and is generally assumed to be independent of concentration. Noble gas diffusion coefficients are a function of atomic radius of the noble gases so that a gas with a small atomic radius has a larger diffusion coefficient than those with larger radii (Lux, 1987). Helium is thus the most soluble and also the most diffusive of the noble gases in melts. Helium is more diffusive than neon

by roughly a factor of two, and more diffusive than xenon by approximately a factor of 17 in a tholeiitic basalt melt at 1350°C (Lux, 1987). Diffusive loss of gases from crystalline rocks is commonly viewed as a two stage process involving "volume" diffusion from grain interiors to grain boundary surfaces, followed by "grain boundary" or "surface" diffusion for diffusion out of the macroscopic sample (Ozima and Podosek, 1983).

2.3 Isotopic and elemental compositions of noble gases in solar system and terrestrial reservoirs

The noble gas compositions in the solar system can broadly be subdivided into two major reservoirs: the solar and the meteoritic (sometimes called "planetary") reservoirs. The elemental and isotopic compositions of the solar component have been determined by analysing lunar fines (Benkert et al., 1993) and trapped gases in meteorites (Murer et al., 1997), as well as aluminium and platinum foils that were exposed to the solar wind during the Apollo missions to the Moon (Geiss et al., 1972).

The elemental and isotopic compositions of the meteoritic component were determined by analyses of noble gases in C-1 chondrites (e.g., Black and Pepin, 1969). C-1 chondrites are thought to be among the most primitive objects in the solar system. It is curious that their noble gas elemental and isotopic compositions differ from those in the solar wind. Close inspection of the noble gas isotopic ratios in different carriers or temperature fractions of carbonaceous chondrites reveal a number of different isotopic components. Some of the minor components have been interpreted to originate from supernovae or other pre-solar noble gases (Ozima and Podosek, 1983). These details, although interesting, are beyond the scope of the present discussion. What is most important is that the noble gas composition of carbonaceous chondrites is fairly uniform, implying that the meteoritic component was widespread in the early solar system.

2.3.1 Comparison of solar, atmospheric, planetary and meteoritic elemental noble gas compositions

The Earth's lost primary atmosphere

The gas planets, including Jupiter and Saturn, have primary atmospheres that were acquired by gravitational capture from the primordial solar nebula (Pollack and Bodenheimer, 1989). The Earth's primary atmosphere is widely believed to have been lost because the present-day atmosphere does not have a composition like that of the Sun. If the Earth's atmosphere was a remnant of the primary atmosphere, the degree of

depletion of volatile species should follow a mass-dependent pattern (Ozima and Podosek, 1983). Neon, which is the second most depleted element in the Earth's atmosphere (after helium) should be more abundant than all other lighter species (H_2, H_2O, CH_4), and less abundant than heavier species (e.g., Ar, CO, CO_2 and HCl) (Ozima and Podosek, 1983). The expected mass dependent abundances of volatile species in the atmosphere are not observed, suggesting that the Earth's present atmosphere was not trapped by gravitation from the solar nebula. The present day atmosphere is interpreted to be secondary and to have been derived from other sources (Brown, 1952).

Although the absolute abundances of noble gases in the atmospheres of Earth, meteorites and the other terrestrial planets (Venus, Mars) differ (Table 2-4), they have generally similar elemental abundance patterns (Fig. 2-6). In particular, the noble gas elemental abundance patterns in ^{22}Ne, ^{36}Ar and ^{84}Kr of primitive carbonaceous chondrites (meteoritic component) and those of the Earth's atmosphere are similar, with the exception of ratios involving ^{4}He and ^{130}Xe (Table 2-4). The relative abundance of He in the terrestrial and planetary atmospheres is not very informative because He is continually escaping from the gravitational fields of the terrestrial planets (Kockharts, 1973). The relative abundance of ^{130}Xe is higher in the meteoritic reservoir relative to the Earth's atmosphere, the terrestrial planets and the solar reservoir (Fig. 2-7).

Table 2-4. Noble gas elemental abundances in the solar, meteoritic and Earth's atmospheric components

	$^4He/^{20}Ne$	$^4He/^{36}Ar$	$^{20}Ne/^{36}Ar$	$^{36}Ar/^{84}Kr$	$^{84}Kr/^{130}Xe$	$^4He/^{130}Xe$
Solar wind			47 ±3 (a)			
Solar wind	600		37			
Solar (lunar soil)	253		27	1590	38	4.1×10^8
Meteoritic	220		0.28	80	8	3.9×10^4
Earth atmosphere	0.32 (b)	0.166	0.52	48	180	1.4×10^3

SW + SEP, (Murer et al., 1997); (b) (Verniani, 1966); other data from Ozima and Podosek (1983 and references therein).

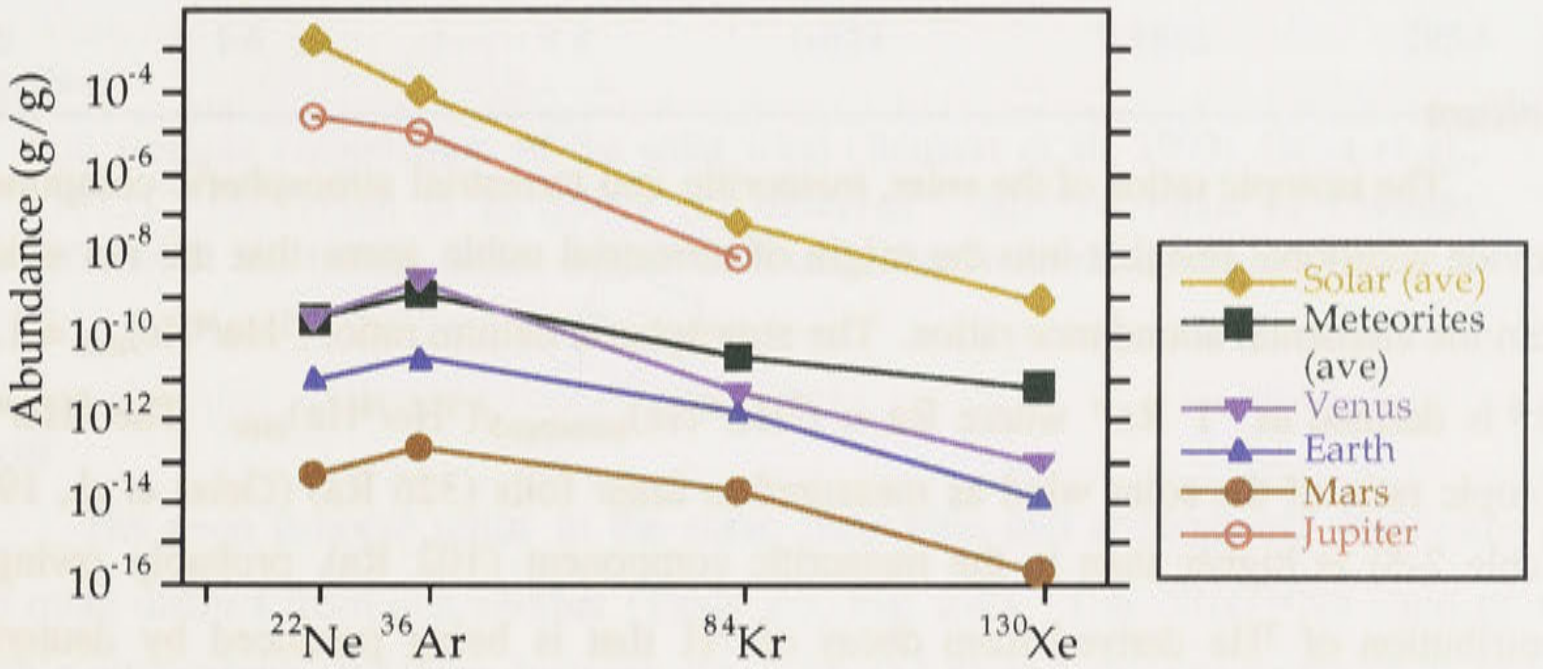

Figure 2-6. Noble gas elemental abundances in the implanted solar wind, meteorites (C-1 Chondrites), Venus, Earth, Mars and Jupiter. Data are from Pepin, (1991) except for ^4He data (Ozima and Podosek, 1983) and Jupiter data (Niemann et al., 1996).

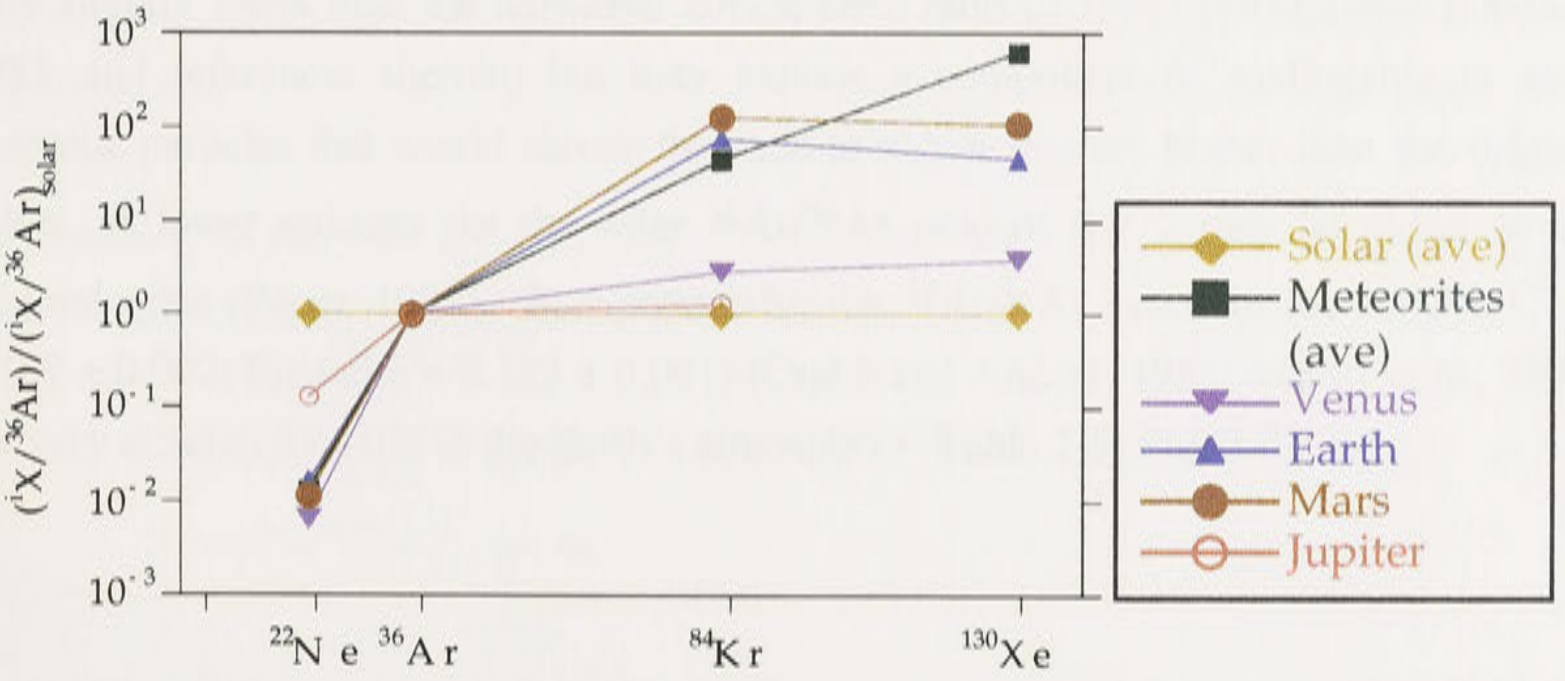

Figure 2-7. As in Figure 2-6, but relative to the solar wind and normalised to ^{36}Ar.

The higher relative abundance of xenon in the meteoritic component relative to the Earth's atmosphere has lead to the inference that the Earth's atmosphere is "missing" xenon. That is, if the Earth's atmosphere was derived from degassing of chondritic material, the elemental abundance pattern in the Earth's atmosphere should be similar to the meteoritic pattern. If the Earth did not initially have a meteoritic xenon abundance pattern, it is possible that xenon is not "missing" from the Earth. A discussion of this problem may be found elsewhere (Jephcoat, 1998; Ozima, 1998; Podosek et al., 1981; Wacker and Anders, 1984) and is beyond the scope of the present discussion.

2.3.2 *Comparison of solar, meteoritic and terrestrial atmospheric isotopic noble gas compositions*

Helium

The isotopic ratios of the solar, meteoritic and terrestrial atmospheric components provide additional insights into the origin of terrestrial noble gases that are not evident from the elemental abundance ratios. The atmospheric helium ratio, $(^3He/^4He)_{atm} = 1.4 \times 10^{-6}$ is defined as "1 Ra" where $Ra = (^3He/^4He)_{measured}/(^3He/^4He)_{atm}$. The $^3He/^4He$ isotopic ratio of the solar wind as measured in lunar foils (326 Ra) (Geiss et al., 1972) (Table 2-5) is higher than in the meteoritic component (102 Ra), probably owing to contribution of ^3He derived from decay of ^3H that is being produced by deuterium burning in the Sun (Anders and Grevesse, 1989). The solar and meteoritic $^3He/^4He$ ratios are higher than that in the Earth's atmosphere by more than two orders of magnitude. The lower $^3He/^4He$ ratio in the atmosphere results from addition of a large proportion of radiogenic ^4He produced from U and Th in the Earth and degassed to the atmosphere (e.g. Bernatowicz and Podosek, 1978) (Table 2-5, Fig. 2-8).

Table 2-5. Helium, neon and argon isotopic ratios in the solar, meteoritic and atmospheric (terrestrial) reservoirs

Composition	$^{3}He/^{4}He$ (10^{-6})	Ra	$^{20}Ne/^{22}Ne$	$^{21}Ne/^{22}Ne$	$^{38}Ar/^{36}Ar$	$^{40}Ar/^{36}Ar$
Solar (a)	457	326	13.8 ± 0.1	0.0328 ± 0.0005	0.179 ± 0.003 (ave) (b)	~$3x10^{-4}$ (c)
Solar, corrected					0.173 ±0.002 (b)	
Meteoritic (CI chondrite)	143	102	8.2	0.024	0.189 ± 0.002	~3×10^{-4}
Enstatite chondrite					0.183 ± 0.001	
Earth atmosphere	1.4	1	9.8	0.029	0.1880	295.5

(a) Isotopic composition of the solar wind (Benkert et al., 1993; Geiss et al., 1972). (b) (Pepin et al. 1999) (c) observed $^{40}Ar/^{36}Ar$ ratios in Ureilites (Göbel et al., 1978). Other data from Ozima and Podosek (1983).

Neon

The neon isotopic ratios in the solar, meteoritic and atmospheric reservoirs are also quite distinct from one another (Table 2-5, Fig. 2-8). The $^{20}Ne/^{22}Ne$ ratio of the Earth's atmosphere (9.8) lies between the solar (13.8) and the meteoritic (8.2) ratios. The $^{21}Ne/^{22}Ne$ ratio of the Earth's atmosphere (0.029) is also between the solar (0.0328) and meteoritic (0.024) ratios.

Argon

The estimated average solar $^{38}Ar/^{36}Ar$ ratio (0.179 ± 0.003) (Pepin, 1991) is only slightly lower than the terrestrial atmospheric ratio (0.1880) (Ozima and Podosek, 1983, and references therein) but may include a component of spallogenic or solar energetic particles that would elevate the ratio to values that are higher than the original value. A lower estimate for the solar $^{38}Ar/^{36}Ar$ ratio of 0.172 may be closer to the original value (Pepin, 1991). In comparison, the $^{38}Ar/^{36}Ar$ ratios in meteorites (C1 = 0.189 ± 0.002; Enstatite = 0.183 ± 0.001) (Crabb and Anders, 1982; Mazor et al., 1970) are very close to the ratio in the Earth's atmosphere (Table 2-5, Fig. 2-8).

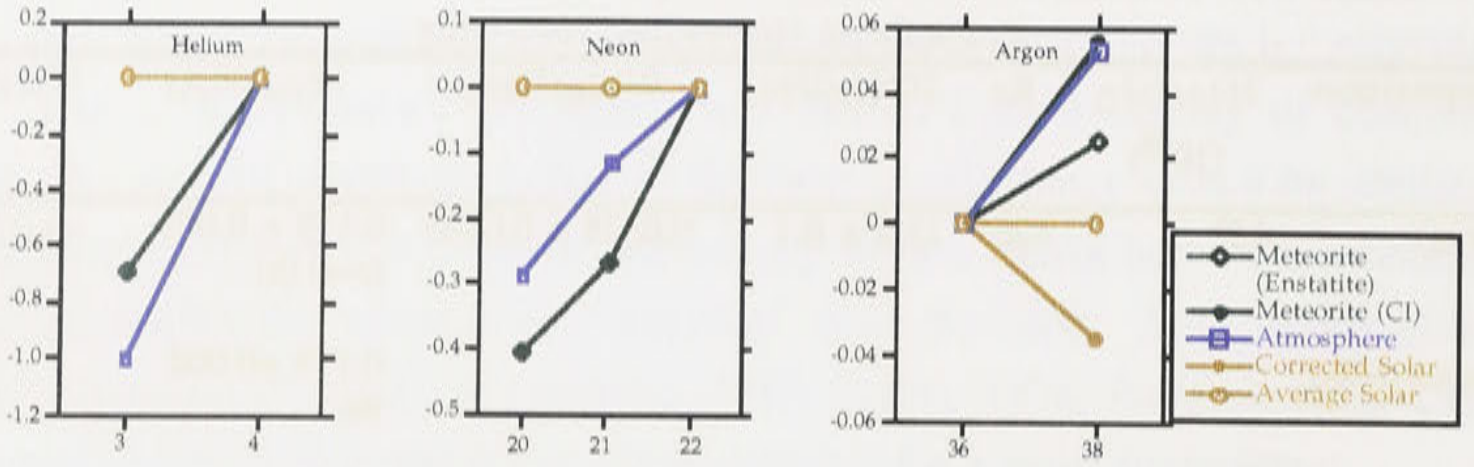

Figure 2-8. Isotopic composition of noble gases in the solar, meteoritic and atmospheric components. The isotopes for each element are shown on the x-axis (^{3}He, ^{4}He, ^{20}Ne, ^{21}Ne, ^{22}Ne, ^{36}Ar, and ^{38}Ar). The helium isotopic ratios are normalized to ^{4}He, the neon isotopic ratios normalized to ^{22}Ne, and the argon isotopic ratios normalized to ^{36}Ar. The isotopic ratios in different components are expressed as fractional deviations from the solar ratio.

The $^{40}Ar/^{36}Ar$ ratio in the Earth's atmosphere of 295.5 is greatly elevated relative to that predicted for the primordial ratio from stellar nucleosynthesis of ~3 x 10^{-4} (Göbel et al., 1978) (Table 2-5) owing to an overwhelming contribution of ^{40}Ar produced from decay of ^{40}K in the Earth.

Krypton

The isotopic ratios of krypton in the meteoritic and atmospheric reservoirs (Table 2-6) show a similar pattern relative to the solar composition, but the difference between the atmospheric composition and the solar composition is smaller than that between the meteoritic and the solar composition. The meteoritic and atmospheric $^{78}Kr/^{84}Kr$, $^{80}Kr/^{84}Kr$, $^{82}Kr/^{84}Kr$ and $^{83}Kr/^{84}Kr$ ratios are lower than the solar ratio (Fig. 2-9), but the $^{86}Kr/^{84}Kr$ ratios are higher than the solar ratio. The meteoritic and atmospheric ratios exhibit mass-dependent fractionation with heavy isotope enrichment relative to the solar ratios, but the meteoritic ratios are slightly more fractionated than the atmospheric ratios.

Table 2-6. Krypton isotopic ratios in the solar, meteoritic and atmospheric (terrestrial) reservoirs

Composition	^{78}Kr	^{80}Kr	^{82}Kr	^{83}Kr	^{84}Kr	^{86}Kr
Solar	0.6359	40.75	20.501	20.276	=100	30.115
CI Chondrite	0.596 ±0.005	3.92 ±0.03	20.15 ±0.08	20.14 ±0.08	=100	30.95 ±0.08
Earth atmosphere	0.609 ±0.002	3.960 ±0.002	20.22 ±0.02	20.14 ±0.02	=100	30.52 ±0.03

Data are normalised to ^{84}Kr. After Pepin (1991)

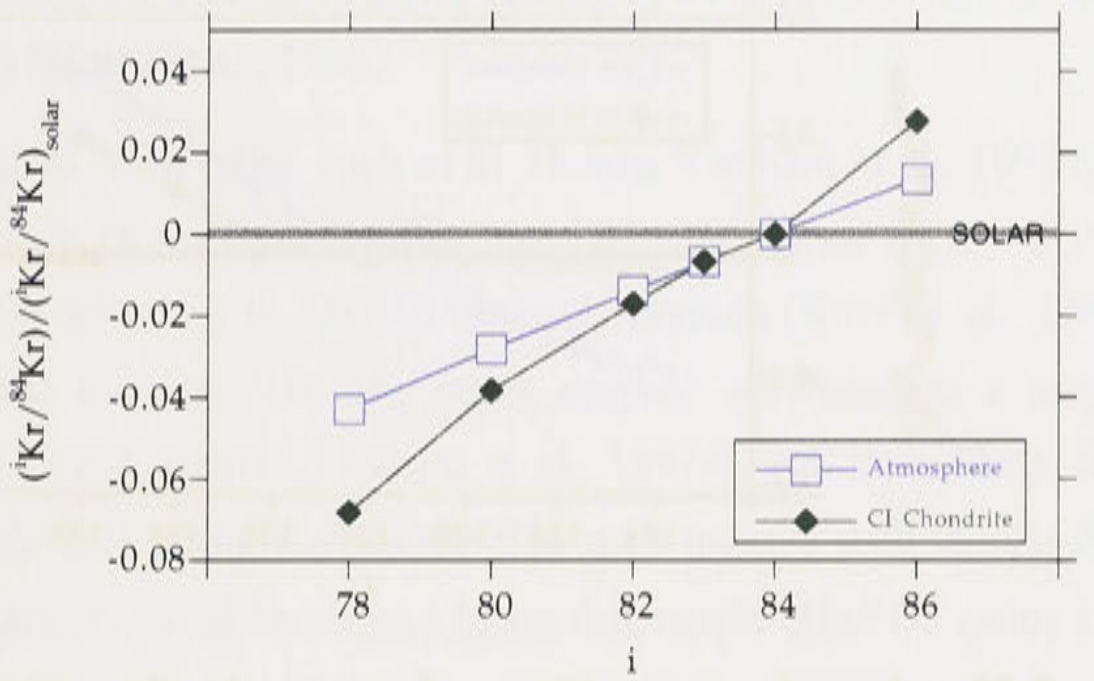

Figure 2-9. Isotopic composition of krypton in the atmospheric and meteoritic components, normalized to ^{84}Kr and the solar ratio.

Xenon

Xenon isotopic ratios are commonly normalized to ^{130}Xe because ^{130}Xe is not produced by spontaneous fission or radioactive decay in the Earth and can be considered a primordial isotope. The isotopic ratios of the lightest xenon isotopes ($^{124}Xe/^{130}Xe$, $^{126}Xe/^{130}Xe$, and $^{128}Xe/^{130}Xe$) in CI chondrites are similar to the solar composition, whereas the ratios in the atmosphere are much lower than the solar composition (Table 2-7, Fig. 2-10). The isotopic ratios of the heavier Xe isotopes (>^{130}Xe) are elevated in the atmosphere and in meteorites relative to the solar ratio. The xenon isotopic ratios in the atmospheric component are mass fractionated and enriched in the heavy isotopes relative to the solar composition. The heavy xenon isotope enrichment in the meteoritic component is believed to arise from exotic noble gas components derived from presolar grains that formed in the stellar atmospheres (Anders and Zinner, 1993). The elevated $^{129}Xe/^{130}Xe$ in the atmosphere and in some meteorites (e.g., Allende) to values higher than the solar ratio is attributed to production of ^{129}Xe from extinct ^{129}I (half life of 17 Ma, Table 2-2) (Ozima and Podosek, 1983).

Table 2-7. Xenon isotopic ratios in the solar, meteoritic, and atmospheric (terrestrial) reservoirs

Compo-sition	^{124}Xe	^{126}Xe	^{128}Xe	^{129}Xe	^{130}Xe	^{131}Xe	^{132}Xe	^{134}Xe	^{136}Xe
Solar	2.947	2.541	50.873	628.7	=100	499.58	606.79	212.88	166.34
CI Chondrite	2.85 ±0.05	2.51 ±0.04	50.7 ±0.4	635.8 to 670.8	=100	504 ±3	615 ±3	236 ±1	199 ±1
Earth atmosphere	2.337 ±0.007	2.18 ±0.01	47.15 ±0.05	649.6 ±0.6	=100	521.3 ±0.6	660.7 ±0.5	256.3 ±0.3	217.6 ±0.2

Data are normalised to ^{130}Xe. After Pepin (1991)

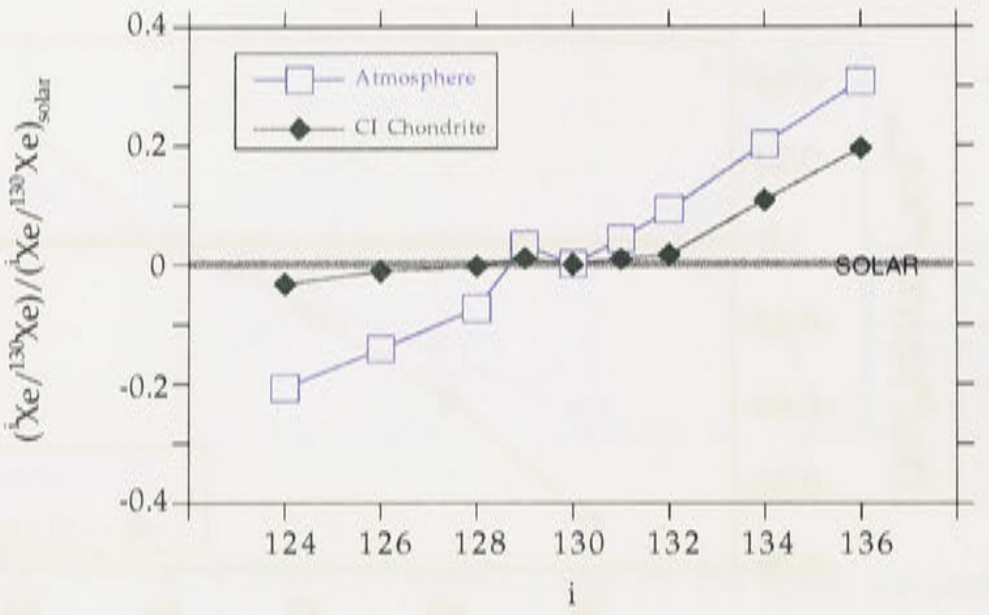

Figure 2-10. Isotopic compositions of xenon in the atmosphere and meteoritic components, normalized to ^{130}Xe and the solar composition.

2.4 Mantle noble gases

2.4.1 Part I: Isotopic ratios

Variations in the isotopic ratios of the noble gases from mantle-derived samples potentially can be used to identify source components, mixing processes between noble gas components with different isotopic compositions, or addition of isotopes produced by radioactive decay or nucleogenic reactions in the Earth.

Helium

The relatively short residence time of helium in the atmosphere of ~10^6 years results in its low atmospheric abundance (5.2 ppm) (Ozima and Podosek, 1983) and minimizes problems associated with atmospheric contamination of samples containing mantle gases. The $^3He/^4He$ ratios in glasses from mid-ocean ridges (MORs) (8.5 ± 1.4 Ra) are nearly constant and are higher than those in the atmosphere (1 Ra) (Hilton et al., 1993; Poreda et al., 1986) (Fig. 2-11). Still higher $^3He/^4He$ ratios have been found in glasses and olivines from some Ocean Island Basalts (OIBs), with values of near 30 Ra from several localities (e.g., 32 Ra (Loihi), ~25 Ra (Samoa), 37 Ra (Iceland)) (Condomines et al., 1983; Hilton et al., 1999; Honda et al., 1991; Kurz et al., 1982a; Kurz et al., 1983; Poreda and Farley, 1992; Rison and Craig, 1983; Staudacher et al., 1986) (Fig. 2-12). Helium isotopic ratios higher than the MORB values have also been found in geothermal fluids from Yellowstone (16 Ra) (Craig et al., 1978; Kennedy et al., 1985), and from Continental Flood Basalts (CFBs), including the Deccan Traps (13.9 Ra) (Basu et al., 1993), Siberian Traps (12.7 Ra) (Basu et al., 1995), West Greenland (30 Ra)

(Graham et al., 1998), the Columbia River basalts (11.4 Ra) (Dodson et al., 1997) and Ethiopia (16.9 Ra) (Marty et al., 1996).

Some samples from OIBs, such as St. Helena (Graham et al., 1992a) and Tristan da Cunha and Gough (Kurz et al., 1982a), have $^3He/^4He$ ratios of 5 - 6 R/Ra that are lower than the ratio measured in MORB-derived samples (Kurz et al., 1982a). It has been suggested that the low $^3He/^4He$ ratios may be attributed to a recycled crustal component in the plume source (Graham et al., 1992a), but it is likely that in some localities, crustal fluids bearing radiogenic ^4He may interact with mantle-derived melts and minerals at shallow crustal levels and lower the mantle $^3He/^4He$ ratios (Hilton et al., 1995).

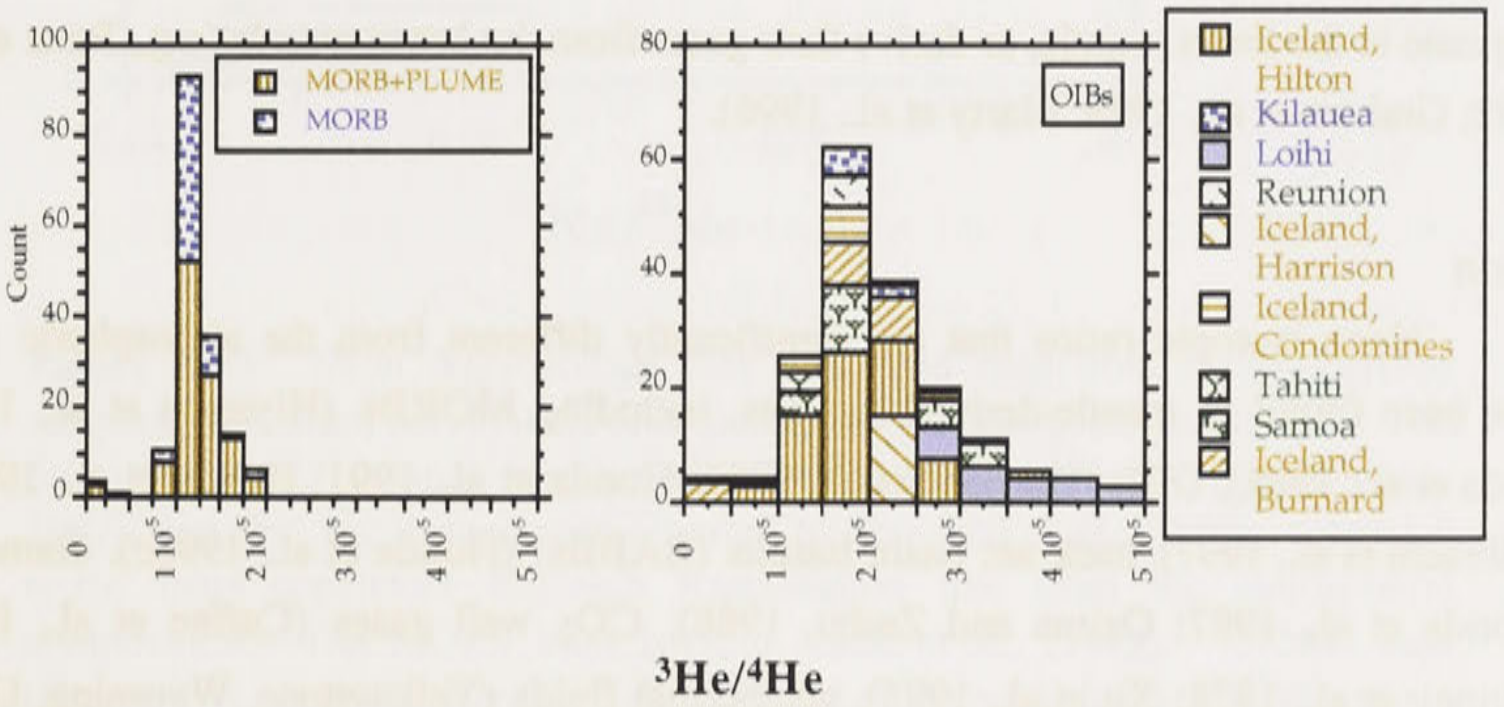

Figure 2-11, left. Histogram of $^3He/^4He$ ratios in samples from MORBs (Hiyagon et al., 1992; Kurz and Jenkins, 1981; Marty and Ozima, 1986; Ozima and Zashu, 1983; Sarda et al., 1988) and samples from spreading ridges in localities where plume-MORB interactions are thought to occur (Graham et al., 1992b; Jambon et al., 1985; Kurz et al., 1982b; Moreira et al., 1995; Niedermann et al., 1997). **Figure 2-12, right.** Histogram of $^3He/^4He$ ratios in OIBs, including Iceland (Burnard et al., 1994; Condomines et al., 1983; Harrison et al., 1999; Hilton et al., 1990), Hawaii (Hiyagon et al., 1992; Honda et al., 1991; Sarda et al., 1988; Valbracht et al., 1997), Reunion (Staudacher et al., 1990), Samoa (Farley and Craig, 1994; Poreda and Farley, 1992), and Tahiti (Staudacher and Allègre, 1989).

The remarkably uniform helium isotopic ratios in MORBs (Fig. 2-11) suggest that the MORB source reservoir is well mixed (Hiyagon et al., 1992; Kurz, 1991; Lupton, 1983; Sarda et al., 1988). In contrast, the large range in helium ratios in OIBs (Fig. 2-12) suggests that they are derived from relatively heterogeneous sources. The ^3He isotope in the mantle is considered to be primordial in origin, because there are no reactions in the mantle that produce significant amounts of ^3He. In contrast, ^4He is continually being produced from decay of U and Th (Table 2-3). The lower $^3He/^4He$

ratios for MORBs compared with most OIBs implies that the MORB source has a lower $^{3}He/[U+Th]$ ratio than that of most OIBs. Preferential degassing of primordial ^{3}He from the MORB source relative to the OIB source, followed by production of radiogenic ^{4}He, would cause the $^{3}He/^{4}He$ ratio to decrease more rapidly in the MORB source than the OIB source if it is assumed that the U and Th contents of both sources are approximately equal (Craig and Lupton, 1976; Tolstikhin, 1975). Continued mixing of the MORB source by convection, but limited mixing of the noble gases between the MORB and OIB sources, could account for the observed $^{3}He/^{4}He$ ratios. These observations provide some of the evidence for the origin of OIBs from plumes that derive their primordial gases from relatively undegassed regions in the lower mantle (e.g., Allègre et al., 1987; Allègre et al., 1983). The high observed $^{3}He/^{4}He$ ratios in CFBs are interpreted to indicate that, like OIBs, CFBs are derived from mantle plumes that originate in the lower mantle, or derive their gases from the lower mantle (e.g., Basu et al., 1993; Graham et al., 1998; Marty et al., 1996).

Neon

Neon isotopic ratios that are significantly different from the atmospheric ratio have been found in mantle-derived samples, including MORBs (Hiyagon et al., 1992; Sarda et al., 1988), OIBs (Harrison et al., 1999; Honda et al., 1991; Honda et al., 1993b; Valbracht et al., 1997), back arc basin basalts (BABBs) (Honda et al., 1993c), diamonds (Honda et al., 1987; Ozima and Zashu, 1988), CO_2 well gases (Caffee et al., 1988; Phinney et al., 1978; Xu et al., 1995), geothermal fluids (Yellowstone, Wyoming, USA) (Kennedy et al., 1985) and mantle xenoliths (Samoa, Reunion) (Poreda and Farley, 1992; Staudacher et al., 1990). The $^{20}Ne/^{22}Ne$ ratios in MORBs and OIBs range from the atmospheric ratio of 9.8 to values close to the solar ratio of 13.8, with the maximum observed $^{20}Ne/^{22}Ne$ ratio of 13.7 ± 0.3 obtained from Icelandic basalt samples (Harrison et al., 1999). The observed $^{21}Ne/^{22}Ne$ ratios range from close to the atmospheric ratio of 0.029 up to 0.064 (Fig. 2-13).

Most of the neon isotopic data obtained thus far from mantle-derived samples lie within a field defined by the Loihi line (e.g., Honda et al., 1991; Valbracht et al., 1997) and the MORB correlation line (Hiyagon et al., 1992; Sarda et al., 1988) (Fig. 2-13). These lines intersect at the isotopic composition of neon in the atmosphere. The MORB correlation line is defined by MORB samples that lie on a nearly linear array in $^{20}Ne/^{22}Ne$ vs $^{21}Ne/^{22}Ne$ space with a slope of 85 that passes through the atmospheric neon composition. This linear array has been interpreted to be a mixing line between the MORB mantle and atmospheric neon endmembers (Sarda et al., 1988). The Loihi line similarly forms a mixing line between the atmospheric and Loihi mantle neon endmembers. However, the Loihi mantle endmember is distinct from the MORB source

endmember because the Loihi line has a steeper slope of ~380 in the neon three-isotope plot (Fig. 2-13).

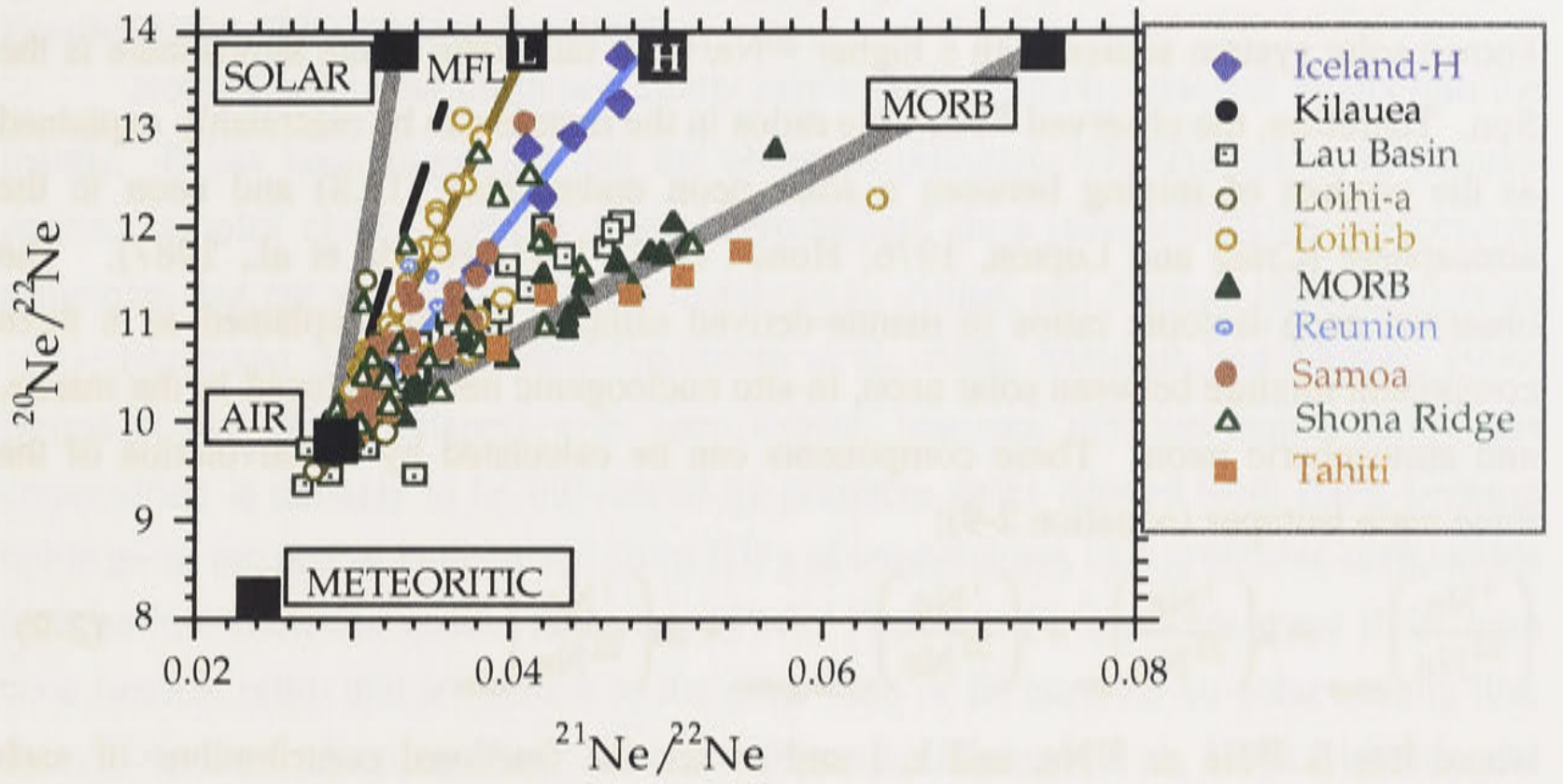

Figure 2-13. Neon three-isotope plot with neon data from mantle-derived samples. The solar, Air, MORB and meteoritic end-members are shown. The box labelled "L" stands for "Loihi" (Honda et al., 1993c; Valbracht et al., 1997), and "H" for Iceland data reported by Harrison et al. (1999). "MFL" is the mass dependent Rayleigh fractionation line from the atmospheric composition. The MORB lines is from Sarda et al., (1988). MORB data (Hiyagon et al., 1992; Sarda et al., 1988), Loihi and Kilauea (Honda et al., 1993b) (Loihi-a) (Hiyagon et al., 1992; Valbracht et al., 1997) (Loihi-b); Lau Basin (Honda et al., 1993c); Reunion (Staudacher et al., 1990); Samoa (Farley and Poreda, 1992; Poreda and Farley, 1992); Shona Ridge (Moreira et al., 1995); and Tahiti (Staudacher and Allègre, 1989). The analytical uncertainties have been omitted for clarity.

The values of the $^{21}Ne/^{22}Ne$ ratios of the Loihi and MORB endmembers of 0.041 and 0.074, respectively, are obtained by extrapolating the measured $^{20}Ne/^{22}Ne$ ratios to the solar $^{20}Ne/^{22}Ne$ ratio of 13.8. These different $^{21}Ne/^{22}Ne$ endmember ratios can be explained by different proportions of primordial solar neon ($^{21}Ne_{solar}$) relative to nucleogenic ^{21}Ne ($^{21}Ne^*$) produced in the mantle (Table 2-3), i.e., [($^{21}Ne^*$ + $^{21}Ne_{solar}$)/$^{21}Ne_{air}$]. However, the observed range in $^{20}Ne/^{22}Ne$ ratios, from the atmospheric ratio to higher values cannot be accounted for by fissiogenic or nucleogenic processes in the mantle because the $^{20}Ne/^{22}Ne$ production ratio in the mantle of 4.5 (Table 2-3) is lower than the atmospheric $^{20}Ne/^{22}Ne$ ratio of 9.8 (Table 2-5). Furthermore, mass-dependent isotopic fractionation of atmospheric neon cannot explain the observed neon isotopic ratios from Loihi and Kilauea because the slope of the Loihi

line is different from that which would be produced by mass fractionation of atmospheric neon (Hiyagon et al., 1992; Honda et al., 1991). Addition of meteoritic neon ($^{20}Ne/^{22}Ne$ of 8.2) to atmospheric neon would lower the neon isotopic ratio, and does not provide an explanation for the observed relatively high ratios in mantle-derived samples. The only known solar system source with a higher $^{20}Ne/^{22}Ne$ ratio than in the atmosphere is the Sun. Therefore, the observed $^{20}Ne/^{22}Ne$ ratios in the mantle can be reasonably explained as the product of mixing between a solar neon endmember (13.8) and neon in the atmosphere (Craig and Lupton, 1976; Honda et al., 1991; Honda et al., 1987). The observed neon isotopic ratios in mantle-derived samples can be explained as a three component mixture between solar neon, in-situ nucleogenic neon produced in the mantle, and atmospheric neon. These components can be calculated by deconvolution of the three neon isotopes (equation 2-9):

$$\left(\frac{^{i}Ne}{^{22}Ne}\right)_{meas} = k\left(\frac{^{i}Ne}{^{22}Ne}\right)_{air} + l\left(\frac{^{i}Ne}{^{22}Ne}\right)_{nucleogenic} + m\left(\frac{^{i}Ne}{^{22}Ne}\right)_{solar} \qquad (2\text{-}9)$$

where ^{i}Ne is ^{20}Ne or ^{21}Ne, and k, l and m are the fractional contributions of each endmember to the reference isotope ^{22}Ne (Honda et al., 1993a; Honda et al., 1991). The endmember compositions for the $^{21}Ne/^{22}Ne$ and $^{20}Ne/^{22}Ne$ solar and atmospheric ratios are shown in Table 2-5. The nucleogenic $^{21}Ne/^{22}Ne$ and $^{20}Ne/^{22}Ne$ endmember ratios are shown in Table 2-3.

The higher values of $^{21}Ne/^{22}Ne$ in MORBs relative to OIBs are attributed to lower $Ne_{solar}/[U + Th]$ ratios in the MORB source than the OIB source. This explanation for the observed range in mantle-endmember neon isotopic compositions is similar to that described previously for helium, with the MORB source having a lower relative $^{3}He/[U + Th]$ ratio than the OIB source. Helium and neon isotopic ratios are expected to be coupled because the production ratio of radiogenic ^{4}He and nucleogenic ^{21}Ne in the mantle ($^{4}He/^{21}Ne^{*}$) is nearly constant (~2 x 10^{7}) (Table 2-3). Samples that define a linear trend in the neon three-isotope plot should therefore have a common $^{3}He/^{4}He$ ratio. There should also be a correlation between the steepness of the slope (with respect to the slope of the air-solar mixing line) and the value of the $^{3}He/^{4}He$ ratio, so that samples lying on steeper slopes should have higher $^{3}He/^{4}He$ ratios. The observed neon and helium isotopic ratios from OIBs and MORBs are qualitatively consistent with this prediction. MORB glasses have relatively low $^{3}He/^{4}He$ ratios of 8.5 Ra and a neon mixing trend with a relatively shallow slope of ca. 85, whereas samples from Hawaii have relatively high $^{3}He/^{4}He$ ratios of up to 30 Ra associated with a neon mixing trend that has a relatively steep slope of approximately 380. Neon data that lie between the slopes defined by MORB and Hawaiian samples, such as those from Samoa and Reunion, should be associated with $^{3}He/^{4}He$ ratios intermediate between the MORB

and Hawaiian values of 8.5 Ra and 33 Ra, respectively. The $^3He/^4He$ ratios observed in samples from Samoa and Reunion are consistent with expectations and are equal to 22 Ra and 13.5 Ra, respectively.

Possible external inputs into the mantle

Noble gases in the Earth potentially may be influenced by external inputs into the mantle. It has been suggested that the observed primitive $^3He/^4He$ ratios in mantle-derived samples could originate from interplanetary dust particles (IDPs) in oceanic sediments that are subducted into the mantle (e.g., Amari and Ozima, 1988; Anderson, 1993; Esser and Turekian, 1988; Fukumoto et al., 1986; Matsuda and Murota, 1990; Ozima et al., 1984). Experiments have shown, however, that the mantle noble gas composition is unlikely to be influenced by primitive gases derived from IDPs because noble gases are probably degassed from IDPs at temperatures and pressures comparable to those in subduction zones (Hiyagon, 1994). Furthermore, although some IDPs have neon isotopic ratios that are similar to the solar ratio or lie near the air-solar mixing line, many IDPs have a large spallogenic neon component (Hiyagon et al., 1992; Matsuda and Murota, 1990) (Fig. 2-14). It would be difficult to explain the relationship between helium and neon isotopic ratios in mantle-derived samples if mantle neon originated from IDPs with a large range of isotopic compositions as seen in Figure 2-14. It appears unlikely that IDPs are the source of primitive neon in the Earth's mantle.

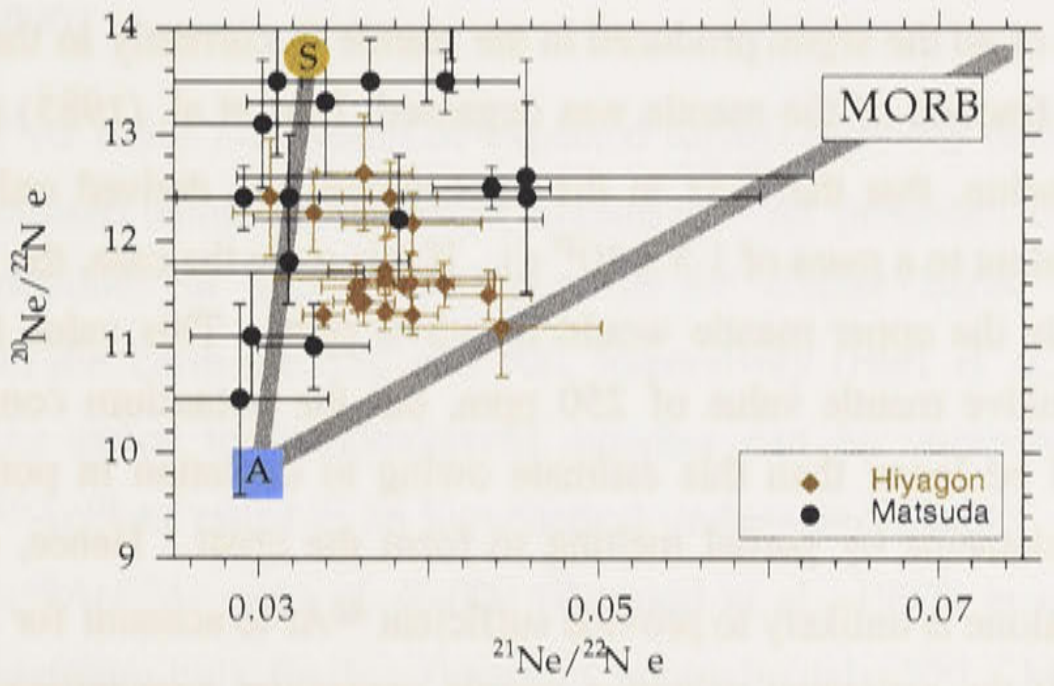

Figure 2-14. Neon three-isotope plot showing the compositions of gas released by step-heating of interplanetary dust particles (IDPs) derived from oceanic sediments. Data are from (Hiyagon, 1994; Matsuda and Murota, 1990). Although the data lie within the same field as mantle-derived samples, there is significant scatter in isotopic composition resulting from spallogenic neon that has been added to the solar neon. It appears unlikely that the observed correlations between helium and neon isotopic ratios would exist in in mantle derived samples if primordial gases were originally derived from IDPs because neon derived from IDPs has a wide range of isotopic compositions.

Argon

Degassing of mantle argon to form the atmosphere

A significant proportion of the present-day atmosphere is interpreted to be derived from degassing of the Earth's mantle by crustal formation. Nearly all (99.6%) of the argon in the atmosphere is ^{40}Ar, and this ^{40}Ar was produced almost entirely from decay of ^{40}K in the Earth ($t_{1/2} = 1.25 \times 10^9$ a) (von Weizsächer, 1937). von Weizsächer (1937) suggested that the extent of mantle degassing could be deduced from the amount of ^{40}Ar in the atmosphere. The inferred degree of mantle degassing depends critically on the estimated potassium concentration in the mantle. The potassium concentration in chondrites of 560 ppm (Anders and Grevesse, 1989) is an upper limit to the potassium concentration in the Earth because the Earth is generally thought to be depleted in potassium with respect to chondrites (Gast, 1960; Lewis and Prinn, 1984). A relatively small amount of degassing, representing 20% of all the argon produced in the mantle by decay of ^{40}K over time, is required if the mantle had a chondritic potassium concentration. This estimate can be compared with that based on a minimum estimate for the potassium content of the Earth of 135 ppm (Morgan and Anders, 1980). Such a low potassium concentration would require that ca. 90% of all ^{40}Ar produced in the mantle was degassed into the atmosphere. A more widely accepted estimate for the potassium content of the silicate Earth is 250 ppm, obtained from the estimated U abundance of 20 ppb (Zindler and Hart, 1986) and K/U ratio of 12,700 (Jochum et al., 1983). Using this estimate, 50% of all the argon produced in the mantle is currently in the atmosphere. To estimate what fraction of the mantle was degassed, Hart et al. (1985) postulated, for the sake of discussion, that the ^{40}Ar in the atmosphere was derived only from the upper mantle (equivalent to a mass of 1.3×10^{27} g). If this were the case, the minimum amount of potassium in the upper mantle would be ~370 ppm. This value is higher than the estimated primitive mantle value of 250 ppm, but the potassium content in the upper mantle should be lower than this estimate owing to depletion in potassium and other incompatible elements by partial melting to form the crust. Hence, outgassing of the upper mantle alone is unlikely to provide sufficient ^{40}Ar to account for the amount in the atmosphere. If the estimated primitive mantle potassium concentration of 250 ppm is correct, more than 1.9×10^{27} g of the total mantle mass of 4×10^{27} g, or more than 50% of the mantle mass, is required to be degassed. Thus, from this estimate, both the upper mantle and part of the lower mantle are degassed (Hart et al., 1985). The uncertainties in the exact amount of potassium in the silicate Earth preclude precise estimates for the degree of mantle degassing, but it is likely to be between 50 and 90%. The rate of degassing to form the atmosphere that would be deduced from the abundance of ^{40}Ar in the atmosphere also depends on the estimate for the initial potassium concentration in the Earth. The higher the estimated potassium concentration, the slower the estimated

degassing rate needs to be to account for the observed ^{40}Ar in the atmosphere. The degassing rate also depends on the degassing coefficient from the Earth to the atmosphere, which is not well constrained (Ozima and Podosek, 1983).

Mantle argon ratios

$^{40}Ar/^{36}Ar$ ratios

The $^{40}Ar/^{36}Ar$ ratios measured in MORB samples range from the atmospheric ratio to much higher values (Figure 2-15), with an estimated minimum ratio of 40,000 (Burnard et al., 1997; Fisher, 1997; Hiyagon et al., 1992; Jambon et al., 1985; Kyser and Rison, 1982; Moreira et al., 1998; Ozima and Zashu, 1983; Sarda et al., 1985; Staudacher et al., 1989). These ratios are much higher than the measured values in OIB samples, which are typically less than 7000 (Figure 2-16) (Hiyagon et al., 1992; Honda et al., 1991; Honda et al., 1993b; Kaneoka et al., 1983; Sarda et al., 1988; Staudacher and Allègre, 1989; Staudacher et al., 1986; Staudacher et al., 1990). The maximum observed $^{40}Ar/^{36}Ar$ ratio from Hawaiian basalts is 6300 ± 400 (Valbracht et al., 1997), which is similar to the maximum observed ratio from Icelandic glasses of 6500 ± 300 (Harrison et al., 1999). The maximum $^{40}Ar/^{36}Ar$ ratio from OIB-related samples is 11,000 ± 200, from Samoan mantle xenoliths (Farley and Poreda, 1992). These observed ratios may be minimum values for true ratios in the mantle sources because air contamination via magma-seawater interaction tends to lower the $^{40}Ar/^{36}Ar$ ratio of erupted basalts (Patterson et al., 1990).

The $^{40}Ar/^{36}Ar$ ratios that would be expected for the relatively undegassed lower mantle can be calculated using the estimated amount of ^{40}Ar produced over time. For potassium concentrations of 135 to 250 ppm in the silicate Earth, the calculated $^{40}Ar/^{36}Ar$ ratios in the Earth are 350 and 500, respectively (Hart et al., 1985). The observed $^{40}Ar/^{36}Ar$ ratios in mantle-derived samples can be compared with these estimates for the $^{40}Ar/^{36}Ar$ ratios in an hypothetical undegassed mantle. The minimum estimated MORB $^{40}Ar/^{36}Ar$ ratio of 40,000 (Burnard et al., 1997) is certainly much higher than the maximum bulk Earth estimate of approximately 500. Most $^{40}Ar/^{36}Ar$ ratios from Loihi and Iceland are less than 800, and are close to the bulk Earth estimate, but the maximum ratios near 6400 are higher than the bulk Earth estimate, suggesting that the OIB sources may be partly degassed. A heterogeneous OIB source, with partly degassed and relatively undegassed regions may account for some of the variability in $^{40}Ar/^{36}Ar$ OIB ratios and the differences between the predicted bulk Earth $^{40}Ar/^{36}Ar$ and observed ratios from OIB samples.

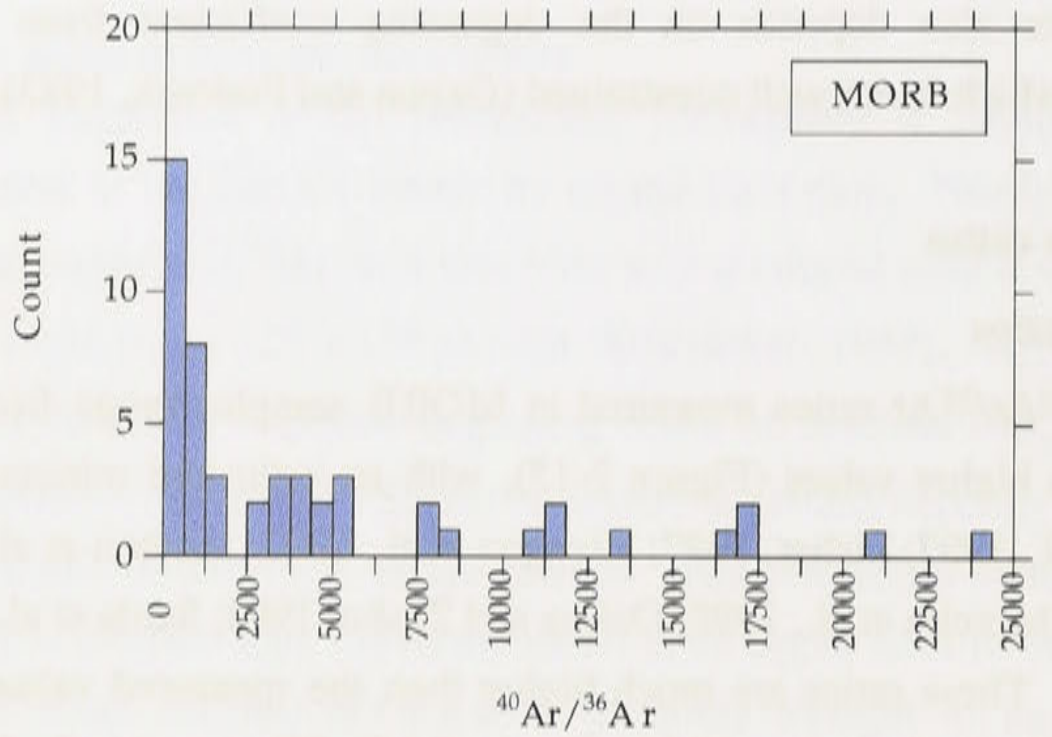

Figure 2-15. Histogram of $^{40}Ar/^{36}Ar$ ratios in MORBs (Hiyagon et al., 1992; Marty and Ozima, 1986; Ozima and Zashu, 1983; Staudacher et al., 1989).

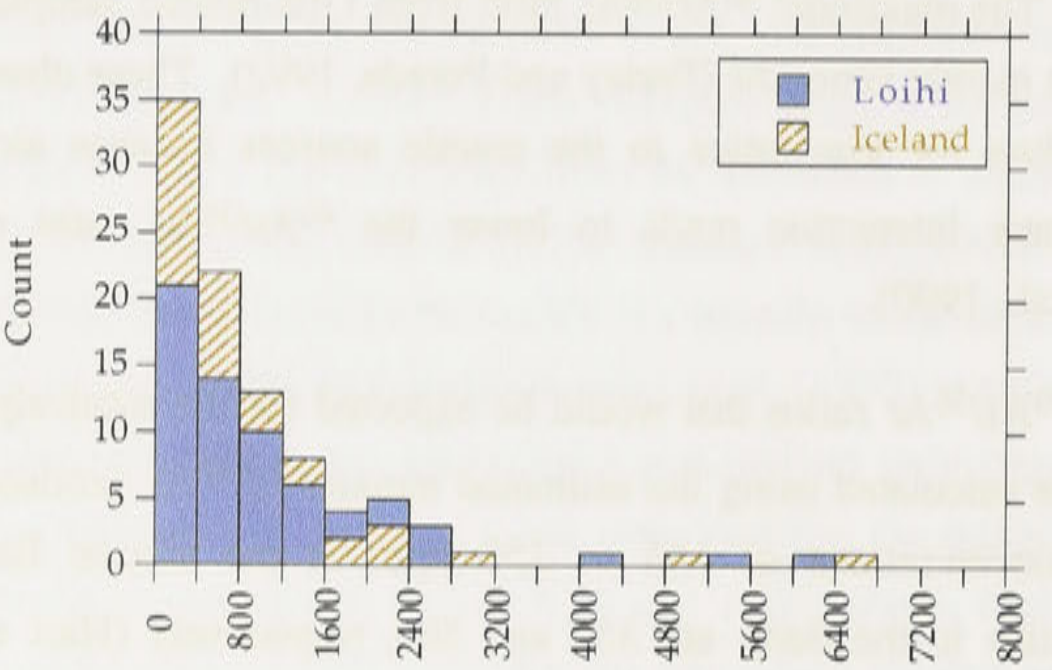

Figure 2-16. Histogram showing $^{40}Ar/^{36}Ar$ ratios in samples from Loihi and Kilauea (Hiyagon et al., 1992; Honda et al., 1993b; Sarda et al., 1988; Valbracht et al., 1997) and Iceland (Burnard et al., 1994; Harrison et al., 1999). The distribution of $^{40}Ar/^{36}Ar$ ratios from the two localities is similar, as is the maximum ratio.

The relatively high minimum estimate of the $^{40}Ar/^{36}Ar$ ratio in the MORB source ($\geq$ 40,000) (Allègre et al., 1986/87; Burnard et al., 1997; Moreira et al., 1998) that is markedly higher than the atmospheric value of 295.5 is consistent with the previous discussion on degassing of the mantle to form the atmosphere. Owing to melting and extraction of material to produce the crust, the upper mantle MORB source is relatively

depleted in large ion lithophile elements, noble gases and other incompatible elements (including K, U, Th) relative to the presumed lower mantle source of OIBs. If the upper mantle MORB source was not degassed of primordial ^{36}Ar compared with the OIB source so that the ^{36}Ar concentrations were similar in both sources, the expected higher relative degree of depletion of ^{40}K in the MORB source relative to the OIB source mantle would result in a lower predicted $^{40}K/^{36}Ar$ ratio for the MORB source than the OIB source. Over time, there would be less ^{40}Ar produced in the MORB source, and therefore, the $^{40}Ar/^{36}Ar$ ratios would be lower in MORBs than in OIBs. The MORB $^{40}Ar/^{36}Ar$ ratios are clearly higher than in OIBs. Thus, the higher $^{40}Ar/^{36}Ar$ ratios in MORBs than OIBs suggest that although ^{40}K is extracted from the MORB source during formation of the crust, primordial ^{36}Ar must have been preferentially degassed from the MORB source relative to the OIB source early in the Earth's history (Hart et al., 1985), before a significant amount of ^{40}K (half-life = 1.25×10^9 annum) had decayed to ^{40}Ar (Hart et al., 1985). Degassing of ^{36}Ar from the upper mantle and part of the lower mantle is thought to have occurred in the first 1 Ga of Earth history (Turner, 1989). Following the early massive degassing event, ^{40}Ar continued to be produced in the mantle by the decay of ^{40}K to produce the observed relatively high $^{40}Ar/^{36}Ar$ ratios in MORBs (e.g., Turner, 1989).

The higher $^{40}K/^{36}Ar$ ratios required for the MORB source compared with the OIB source is consistent with the earlier explanations for the more radiogenic $^{3}He/^{4}He$ and nucleogenic $^{21}Ne/^{22}Ne$ ratios observed in MORBs compared with OIBs. Owing to the relatively incompatible nature of the noble gases compared with K, U, and Th, during degassing of the Earth, preferential loss of ^{3}He, ^{22}Ne and ^{36}Ar from the MORB source mantle would result in lower $^{3}He/[U + Th]$, $^{22}Ne/[U + Th]$ and $^{36}Ar/^{40}K$ ratios in the MORB source than the OIB source mantle, giving rise to the observed lower $^{3}He/^{4}He$, higher $^{21}Ne/^{22}Ne$ and higher $^{40}Ar/^{36}Ar$ ratios in MORBs compared with OIBs.

$^{38}Ar/^{36}Ar$ ratios

The $^{36}Ar/^{38}Ar$ ratio of mantle-derived samples have been interpreted to suggest that there is a solar component of argon in the Earth's mantle (Pepin, 1998). However, although these primordial isotopes of argon have not been augmented by radiogenic or nucleogenic isotopes over the Earth's history, it is difficult to distinguish the solar from the atmospheric $^{38}Ar/^{36}Ar$ ratio in mantle-derived samples owing to their similar values (Table 2-5) and to relatively large analytical uncertainties (Niedermann et al., 1997; Poreda and Farley, 1992; Valbracht et al., 1997) (Fig. 2-17). Alternatively, it is possible that mantle argon has been contaminated by recycled atmospheric argon introduced into the mantle via subducted oceanic crust (Kunz, 1999). The efficiency of recycling noble

gases into the mantle at subduction zones has been debated (Staudacher and Allègre, 1988), making it difficult to evaluate this possibility further.

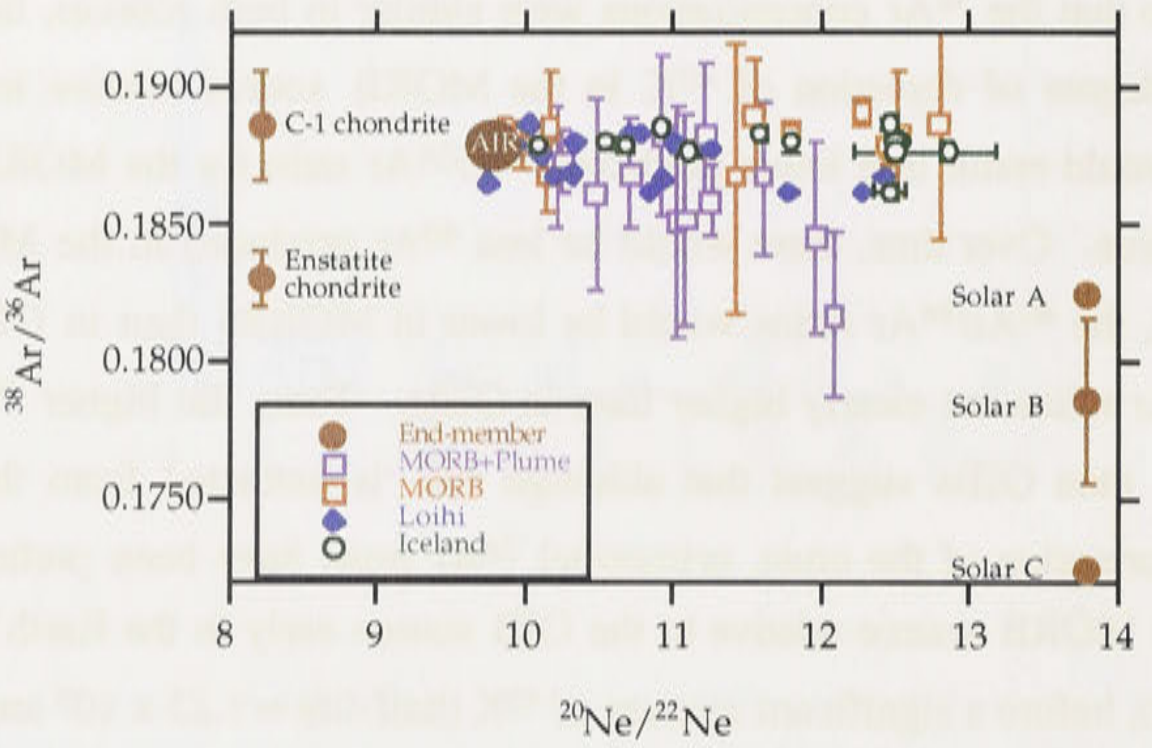

Figure 2-17. $^{38}Ar/^{36}Ar$ vs. $^{20}Ne/^{22}Ne$ diagram, after Valbracht et al. (1997). The measured $^{38}Ar/^{36}Ar$ ratios from Loihi are commonly lower than the atmospheric ratio and it has been suggested that these data support the existence of solar argon in the Earth (Pepin, 1998). Loihi data (Valbracht et al., 1997); MORB data (Hiyagon et al., 1992); MORB+Plume data (include total gas extracted only, because of large uncertainties) are from the East Pacific Rise (Niedermann et al., 1997). End-member Solar A (Benkert et al., 1993); end-member Solar B is the estimated average solar composition (Pepin, 1991; Pepin, 1998); end-member Solar C is measured from lunar regolith grains (0.173 ± 0.002) (Pepin et al., 1999). CI chondrites (Mazor et al., 1970); enstatite chondrites shown for reference, but note that the $^{20}Ne/^{22}Ne$ ratio from CI chondrites is used here (Crabb and Anders, 1982); Earth's atmosphere (AIR) (Ozima and Podosek, 1983).

Krypton

Krypton isotopic compositions in most samples, including those from MORBs, plume-derived samples and diamonds are indistinguishable from the composition in the atmosphere within experimental uncertainties (Ozima, 1994).

Xenon

Noble gas daughter isotopes that are produced from decay of parent isotopes with short half-lives may be used to place constraints on the timing of outgassing of the Earth. Several of the xenon isotopes are produced from short-lived parents, e.g., ^{129}Xe from ^{129}I (half-life of 17 Ma) and $^{131\text{-}136}Xe$ from ^{244}Pu (half-life of 82 Ma), as well as long-lived parents ^{238}U (half-life of 4468 Ma).

^{129}Xe

Relatively high $^{129}Xe/^{130}Xe$ ratios in the mantle relative to the atmosphere have been measured in samples from CO_2 well gases, including those from Harding County, New Mexico (Phinney et al., 1978) and Caroline, South Australia (Caffee et al., 1988); MORB glasses (Allègre et al., 1983; Hiyagon et al., 1992; Marty, 1989; Staudacher and Allègre, 1982) ancient diamonds from Zaire and Botswana (1.8 and 3.2 Ga, respectively) (Ozima and Zashu, 1991); basaltic glass samples from Iceland (Harrison et al., 1999; Trieloff et al., 2000) and Hawaii (Trieloff et al., 2000) and ultramafic xenoliths from Samoa (Poreda and Farley, 1992). In the Samoan xenolith samples, the relatively high $^{129}Xe/^{130}Xe$ ratios are associated with relatively primitive helium and neon isotopic ratios (Poreda and Farley, 1992). The CO_2 well gases from Colorado, New Mexico and South Australia also show excesses of $^{124\text{-}128}Xe$ correlated with excesses in ^{129}I-derived ^{129}Xe (Figs. 2-18, 2-19) and $^{20}Ne/^{22}Ne$ ratios that are higher than the atmospheric ratio (Caffee et al., 1999).

The relatively high $^{129}Xe/^{130}Xe$ ratios in mantle-derived samples and CO_2 well gases relative to the atmospheric ratios have been interpreted as suggesting that most (80% or more) degassing of the mantle to produce the atmosphere occurred before all the ^{129}I had decayed, or within the first 50 - 100 Ma of the Earth's history, and that the mantle source of ^{129}Xe has long been largely isolated from the atmosphere (Allègre et al., 1983; Staudacher and Allègre, 1982; Turner, 1989). It is also possible that the Earth formed from accreted materials that had a range of $^{129}I/Xe$ initial ratios, and that the observed samples with high $^{129}Xe/^{130}Xe$ ratios are derived from Earth-forming materials that were relatively enriched in ^{129}I (Ozima and Podosek, 1983).

^{136}Xe

Relatively high $^{136}Xe/^{130}Xe$ ratios relative to atmospheric values are sometimes found in modern MORBs and ancient diamonds, and appear to be linearly correlated with $^{129}Xe/^{130}Xe$ (see Chapter 6). It has been argued that some of the ^{136}Xe may be derived from ^{244}Pu ($t_{1/2} = 82$ Ma). Although evidence for both extinct nuclides ^{129}I and ^{244}Pu has been found in meteorites, there is considerable debate over whether the ^{136}Xe in terrestrial samples is produced predominantly from decay of ^{244}Pu or ^{238}U in terrestrial samples ($t_{1/2}$ = 4468 Ma) (e.g., Kunz et al., 1998; Podosek, 1970; Podosek and Swindle, 1988). This ambiguity arises because the trends produced by fission yield of ^{244}Pu and ^{238}U are difficult to resolve in plots of $^{131}Xe/^{130}Xe$, $^{132}Xe/^{130}Xe$ and $^{134}Xe/^{130}Xe$ versus $^{136}Xe/^{130}Xe$ (e.g., Kunz et al., 1998). Very precise Xe isotopic analyses would be required to deconvolve the contributions of fission-xenon from the two possible parent isotopes (^{244}Pu and ^{238}U).

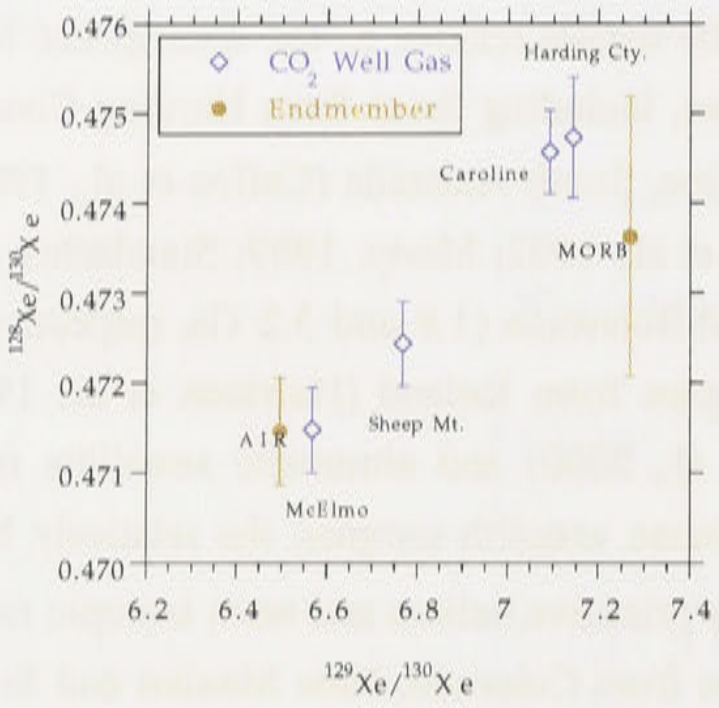

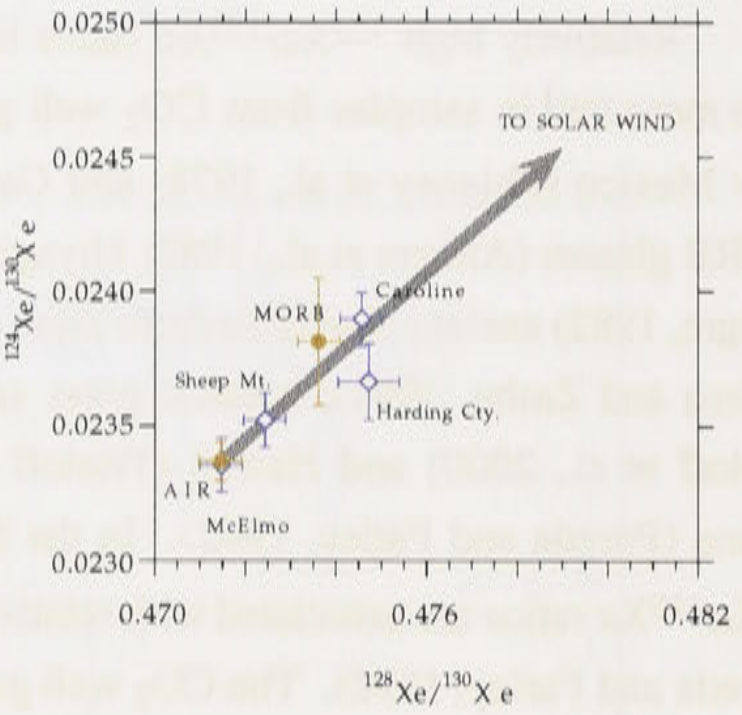

Figure 2-18, left. $^{128}Xe/^{130}Xe$ versus $^{129}Xe/^{130}Xe$ for CO_2 well gases showing a correlation between ^{128}Xe, a primordial isotope, and ^{129}Xe, a radiogenic isotope. The atmospheric and MORB compositions are shown, but the solar wind ratio (Table 2-7) is not because the production of ^{129}Xe from ^{129}I causes the ratios in the well gases to be much higher than the solar ratio. **Figure 2-19, right.** $^{124}Xe/^{130}Xe$ versus $^{128}Xe/^{130}Xe$ for CO_2 well gases showing a trend that can be interpreted as resulting from mixing between solar xenon and atmospheric xenon. One sigma uncertainties are shown. (Caffee et al., 1999).

Correlations between xenon isotopes and other noble gas isotopes

The correlations between the light xenon isotopes ($^{124\text{-}128}Xe$) and ^{129}Xe in CO_2 well gases (Figs. 2-18, 2-19) have been interpreted to indicate the presence of a mantle reservoir containing solar xenon, because solar xenon is enriched in the light isotopes of xenon relative to the Earth's atmosphere (Fig. 2-7) (Caffee et al., 1999). The MORB-like neon isotopic ratios and $^{3}He/^{4}He$ ratios of approximately 3 Ra also suggests primordial mantle-derived noble gases are present in these samples (Caffee et al., 1999) The relatively low $^{3}He/^{4}He$ ratios are attributed to addition of radiogenic ^{4}He produced in the crust. Staudacher (1987) argued that MORB-like neon isotopic ratios in the Harding County CO_2 well gases implied that the gases, including xenon, were derived from the upper mantle. As mantle neon is believed to initially have had a solar isotopic composition (see section 2.4.1, Neon), the suggestion that solar primordial xenon in CO_2 well gases is derived from the upper mantle MORB source (Staudacher, 1987) implies that all of the noble gases in the mantle, not just the light gases (helium and neon), may have originally been dominated by solar gases. However, because solar xenon has only been found in CO_2–rich well gases and has not yet been found in basaltic mantle-derived samples, further investigation is required to determine whether solar xenon is an important component in the mantle.

Enstatite chondrites are characterized by high I/Xe ratios, as well as O isotopic abundances that most closely match those of Earth (Caffee et al., 1988 and references therein). Caffee et al. (1988) suggested that the source region of CO_2 well gases contains a small amount of material derived from enstatite chondrites (see also Javoy (1995)). The correlation between the $^{129}Xe/^{130}Xe$ ratios and the ratios of the lighter isotopes of xenon is interpreted to be the result of mixing between solar Xe and ^{129}Xe produced from ^{129}I decay in enstatite chondrites in Earth-forming materials (Caffee et al., 1999).

Formation and evolution of the Earth's atmosphere

One of the main reasons for investigating the compositions of noble gases in mantle-derived samples is to assist in understanding the origin of the Earth's atmosphere. Given that the Earth's atmosphere is likely to be secondary, and to originate largely from mantle degassing (e.g., Bernatowicz and Podosek, 1978; Brown, 1952; Ozima and Podosek, 1983; Turner, 1989), one of the important objectives in noble gas geochemistry is to develop a model to reconcile the atmospheric composition with the presumed initial solar, and possibly also meteoritic, noble gas compositions that may have contributed to the terrestrial noble gas budget. There are numerous noble gas models to describe the origin of the Earth's atmosphere (e.g., Allègre et al., 1986/87; Allègre et al., 1987; Brown, 1952; Harper and Jacobsen, 1996; Hart et al., 1985; Javoy, 1998; Kamijo et al., 1998; Marty, 1989; Matsui and Abe, 1986; Pepin, 1991; Pepin, 1997; Tolstikhin and Marty, 1998; Turner, 1989; Zahnle et al., 1990; Zhang and Zindler, 1989), and only a brief and general summary of some of the models is given here. The models described below include most of the major factors involved in noble gas models to explain the degassing history of the Earth.

The Earth and other planets probably formed by accretion of planetesimals (Wetherill and Stewart, 1989) in the presence of gases from the solar nebula (Donahue and Pollack, 1983). Much of the initial gas from the accreting planetesimals is usually interpreted to have been lost from the Earth by impact erosion and hydrodynamic escape (e.g., Pepin, 1997). As a result, the gases in the Earth are generally inferred to be dominated by the solar component. The atmospheric composition differs from the solar composition, and may be a mixture of solar gases degassed from the mantle and meteoritic gases derived from a late-accreting chondritic veneer (e.g., Harper and Jacobsen, 1996; Kamijo et al., 1998). Other explanations for the composition of the atmosphere include fractionation of atmospheric gases by hydrodynamic escape during the Moon forming impact (Pepin, 1997)(Kamijo et al., 1998) or addition of cometary material (Porcelli and Wasserburg, 1995a).

In detail, the means by which the Earth's interior has degassed to form the atmosphere is complex. To evaluate the possible degassing mechanisms, most noble gas models establish a three reservoir system comprised of the undegassed mantle, the degassed mantle, and the atmosphere/crust reservoirs (e.g., Staudacher and Allègre, 1982). The mass flux of material into the upper mantle from the lower mantle, and out of the upper mantle to the atmosphere are generally assumed to be equal so that the upper mantle is in steady state. These models also assume that the Earth and its atmosphere are a closed system. This means that the atmosphere plus continental crust are complementary to the degassed mantle reservoir, so that if the atmosphere plus continental crust were re-mixed into the degassed mantle, the mixture would have a composition equivalent to that in the undegassed mantle. In other words, gases transferred from the mantle to the atmosphere are not lost from the atmosphere to space (except for helium). Some models justify the assumption of a closed system using the compositions of $^{129}Xe/^{130}Xe$ ratios in mantle-derived sampless versus in the atmosphere (e.g., Zhang and Zindler, 1989). These models postulate that loss of atmospheric gases cannot have occurred much later than a few half-lives of ^{129}I, otherwise, the $^{129}Xe/^{130}Xe$ isotopic ratios in the mantle and the atmosphere would be nearly the same. The amount of radiogenic ^{40}Ar that could be lost during a few half-lives of ^{129}I is negligible, so that the closed system assumption is considered to be well-founded for ^{40}Ar (Zhang and Zindler, 1989). However, if the assumptions based on the xenon isotopes are incorrect, then the assumption of a closed system for argon may not be valid. Argon mass balance in the atmosphere/mantle system is a fundamental part of models to describe mantle degassing because it permits estimation of the mass of degassed mantle. As explained previously, the amount of ^{40}Ar produced in the Earth is calculated using the uranium content in the bulk silicate earth of ~20 ppb (Hart and Zindler, 1986) and a K/U ratio of 1.27×10^4 (Jochum et al., 1983). From these values, the $^{40}Ar/^{36}Ar$ ratio in the mantle is estimated to be between 350 and 600 (Zhang and Zindler, 1989), and is interpreted to be between 40 and 70% degassed (Zhang and Zindler, 1989).

The assumption of steady state that is used in many of the terrestrial degassing models eliminates the requirement for time-dependent parameters for present rare gas transfers between the mantle and atmospheric reservoirs (Porcelli and Wasserburg, 1995a). The steady state models for mantle-degassing require a mass flux from the lower, relatively undepleted mantle, to the upper, more depleted mantle. This mass flux of material from the less-depleted mantle is generally postulated to be transported via plumes into the upper mantle (e.g., Allègre et al., 1986/87; Kellog and Wasserburg, 1990). Some steady state models proposed that most of the radiogenic ^4He lost at the Earth's surface originated in the lower mantle and was transferred from the lower to the upper mantle via diffusion (see Chapter 3) (Allègre et al., 1986/87; O'Nions and Oxburgh, 1983). In contrast, the heavier noble gases, argon, krypton and xenon were

believed to be trapped below a boundary layer between the upper and lower mantles owing to their relatively low diffusivities compared with that of helium (Allègre et al., 1986/87). Other, non-steady state models to describe Earth degassing have also been proposed, and though some include a mass flux of noble gases and lower mantle material into the upper mantle (Porcelli and Wasserburg, 1995a), others include only mass flow of material, without noble gases, from the lower to the upper mantle (Kamijo et al., 1998).

The time-scale and mechanisms of degassing are also important factors in models to describe degassing of the Earth to form the atmosphere. Degassing of the Earth occurs through volcanism at ridge crests and hot spots, and through hydrothermal activity. The mechanism proposed to cause degassing controls the ratios of noble gases to radioactive parent isotopes, such as [U+Th]/^{22}Ne, [U+Th]//^{3}He, ^{129}I/^{130}Xe, ^{40}K/^{36}Ar, and hence the noble gas isotopic ratios, ^{21}Ne/^{22}Ne, ^{4}He/^{3}He, ^{129}Xe/^{130}Xe and ^{40}Ar/^{36}Ar, respectively. One model postulated two-stage degassing, comprised of an initial rapid stage, and a later relatively slow stage to explain the noble gas isotopic ratios (e.g., Allègre et al., 1986/87). The early, rapid stage would have occurred when the Earth was relatively hot, i.e., during the first 50 Ma of Earth history. This early degassing is postulated to have been a massive event, and to have caused 80 to 85% of the total degassing of stable isotopes from the mantle. The relatively high ^{129}Xe/^{130}Xe isotopic ratios observed in mantle-derived samples were postulated to have been produced in the mantle during this early stage of degassing, prior to decay of all the ^{129}I. The second stage of relatively slow degassing occurs owing to processes such as seafloor spreading and is estimated to have caused 15-20% of the total degassing of the stable isotopes from the mantle (Allègre et al., 1986/87). The high relatively high ^{40}Ar/^{36}Ar ratios in MORBs would be produced during this period, owing to continuous degassing at ridge-crests.

An alternative type of model proposed that the Earth may have acquired two solar gas reservoirs: one that was occluded from the nebula on to planetary embryo materials, and the second that was co-accreted as a primary atmosphere from the degassing of impacting planetesimals during planetary growth (Pepin, 1997). Following degassing of solar gases from the Earth to the atmosphere, the atmospheric gases are postulated to have been isotopically fractionated by hydrodynamic escape caused by the thermal energy derived from the giant impact that formed the Moon (Benz and Cameron, 1990; Pepin, 1997). Subsequent degassing of some of the solar gases from the Earth's interior can account for the present-day abundances and isotopic compositions of atmospheric krypton and argon. However, the ^{20}Ne/^{22}Ne ratio is fractionated to values higher than the atmospheric ratio, and addition of solar neon from degassing of the Earth would further increase the isotopic ratio. There is no postulated addition of neon from meteorites in this model, so to produce the current atmospheric neon isotopic composition would require an episode of hydrodynamic escape driven by extreme ultraviolet solar radiation that was strong enough to entrain neon but not the heavier

gases. The $^{21}Ne/^{22}Ne$ ratio is also fractionated, but can be reconciled with the present-day atmospheric composition by addition of nucleogenic ^{21}Ne degassed from the Earth. A fractionation process driven by thermal energy from the giant impact can explain the fractionated terrestrial xenon abundances if it is assumed that xenon was partitioned into solid phases under high pressures and was never transported into the atmosphere (Pepin, 1991). Subsequently, the atmospheric composition would then be modified by addition of radiogenic and fissiogenic isotopes of xenon produced in the Earth.

In summary, these models show that the Earth's atmosphere may be understood as having been produced in part by degassing primordial gases from the Earth's mantle reservoirs, followed by relatively slow degassing of radiogenic gases produced in the mantle over time. It is unclear whether additional components derived from late-accreting material (e.g., chondrites or comets) are required to account for differences between the predicted and observed gas concentrations and noble gas isotopic ratios in the Earth's atmosphere.

2.4.2 Part II: Elemental ratios

The large range in atomic radii and masses of the noble gases causes them to each behave rather differently during melting, degassing of magmas and crystallization. Noble gas elemental abundances in mantle-derived samples are probably controlled by a number of factors that include diffusion, solubility controlled fractionation and crystal-melt fractionation (Section 2.2). The elemental ratios of noble gases in different phases or systems can potentially be used to identify such processes. Mantle noble gas elemental ratios are calculated from the isotopic ratios, rather than being obtained directly from the measured concentrations, because using isotopic ratios permits correction for atmospheric contamination of mantle-derived noble gases. The low abundance of helium in the atmosphere means that contamination of mantle-derived helium in samples is minimal; it is not usually necessary to correct the measured helium abundance for atmospheric helium contamination. However, corrections must be made for atmospheric contamination of mantle-derived neon and argon. The solar component of ^{22}Ne ($^{22}Ne_s$) and the nucleogenic component of ^{21}Ne ($^{21}Ne^*$) can be calculated using equation (2-9). The amount of radiogenic argon ($^{40}Ar^*$) in a sample can be approximated using equation (2-11) (Marty and Ozima, 1986 and references therein):

$$\left(\frac{^{40}Ar}{^{36}Ar}\right)_{meas} = \frac{^{40}Ar^* + (^{40}Ar)_{atm}}{(^{36}Ar)_{meas}}$$

$$\left(\frac{^{40}Ar}{^{36}Ar}\right)_{meas} = \frac{^{40}Ar^*}{(^{36}Ar)_{meas}} + \frac{(^{40}Ar)_{air}}{(^{36}Ar)_{mantle} + (^{36}Ar)_{air}}$$

$$\left(\frac{^{40}Ar}{^{36}Ar}\right)_{meas} \approx \frac{^{40}Ar^{*}}{(^{36}Ar)_{meas}} + \left(\frac{^{40}Ar}{^{36}Ar}\right)_{air} \quad (2\text{-}10)$$

$$^{40}Ar^{*} \approx (^{36}Ar)_{meas} \times \left[(^{40}Ar/^{36}Ar)_{meas} - (^{40}Ar/^{36}Ar)_{air}\right] \quad (2\text{-}11)$$

The calculated $^{40}Ar^{*}$ is a minimum estimate for the actual $^{40}Ar^{*}$ in the sample owing to the simplifying assumption made in equation (2-10) that ($^{36}Ar_{mantle}$ + $^{36}Ar_{AIR}$) is approximately equal to $^{36}Ar_{AIR}$. This estimate for $^{40}Ar^{*}$ is a good approximation to the true value because the concentration of atmospheric ^{36}Ar in most samples is generally high.

The theoretical mantle elemental production ratios (Table 2-8) are used as reference values for comparison with the calculated elemental abundance ratios of $^{21}Ne^{*}/^{40}Ar^{*}$, $^{4}He/^{40}Ar^{*}$, and $^{4}He/^{21}Ne^{*}$ from mantle-derived samples. The mantle production ratios are considered to lie within a range between the present-day and time-integrated (4.5 Ga) mantle ratios. The primordial ratio ($^{3}He/^{22}Ne_{s}$) is compared with the measured solar or estimated primordial ratios (Table 2-8).

Table 2-8. Elemental ratios in the Earth's mantle and solar wind

Ratio	Present production ratio	Production ratio over 4.5 Ga	Solar	MORB (mean)	OIB (mean)	Mean primordial ratio
$^{4}He/^{40}Ar^{*}$	5 (a)	1.7 (a)				
$^{21}Ne^{*}/^{40}Ar^{*}$	2.2×10^{-7}	7.7×10^{-8}				
$^{22}Ne/^{36}Ar$	N/A	N/A	3.4 ± 0.2 (c)	0.06 (d)		
$^{3}He/^{22}Ne_{s}$	N/A	N/A	3.8 (e)	10 ± 2 (f)	6 ± 1 (f)	8 ± 3 (f)

(a) (Honda and Patterson, 1999) (b) (Yatsevich and Honda, 1997) (c) (Murer et al., 1997); (d) (Moreira et al., 1998); (e) (Benkert et al., 1993) (f) (Honda and McDougall, 1998). N/A = not applicable.

A previous study by Honda and Patterson (1999) has shown that the elemental abundances of noble gases in mantle-derived samples from MORBs, OIBs and BABBs are highly variable. These ratios may potentially be used to understand the effect of melt generation on noble gas elemental ratios and hopefully to obtain information about the nature of mantle source regions.

Some of the observations and conclusions drawn by Honda and Patterson (1999) regarding elemental abundance ratios in mantle-derived samples are briefly summarized here, and will be discussed further in Chapter 7. The $^{4}He/^{40}Ar^{*}$, $^{4}He/^{21}Ne^{*}$ and $^{3}He/^{22}Ne_{s}$ ratios from MORBs, OIBs and BABBs show elemental fractionation over

several orders of magnitude relative to the primordial/production ratios (Fig. 2-20A-F). The data from MORB and BABB glasses have He/Ne and Ne/Ar elemental ratios that are generally higher than the reference ratios by up to two orders of magnitude. In contrast, data from OIB glasses and phenocrysts have elemental ratios that are less than or equal to these reference values. These elemental ratios from MORBs, OIBs and BABBs show a positive correlation with the absolute abundance of helium (Fig. 2-20A).

The enrichment of ^4He in MORBs relative to OIBs (Fig. 2-20A) appears to suggest that the MORB source is enriched in helium relative to the OIB source. If true, this would contradict the interpretation given previously in this chapter based on isotopic ratios that MORBs are derived from a relatively degassed mantle, but OIBs, such as Loihi, are derived from relatively undegassed mantle (Honda and Patterson, 1999). However, it is possible that helium is preferentially enriched in the melt phase in MORBs relative to OIBs owing to differences in the geometry or thermal structure between ridges and intraplate oceanic islands (Honda and Patterson, 1999).

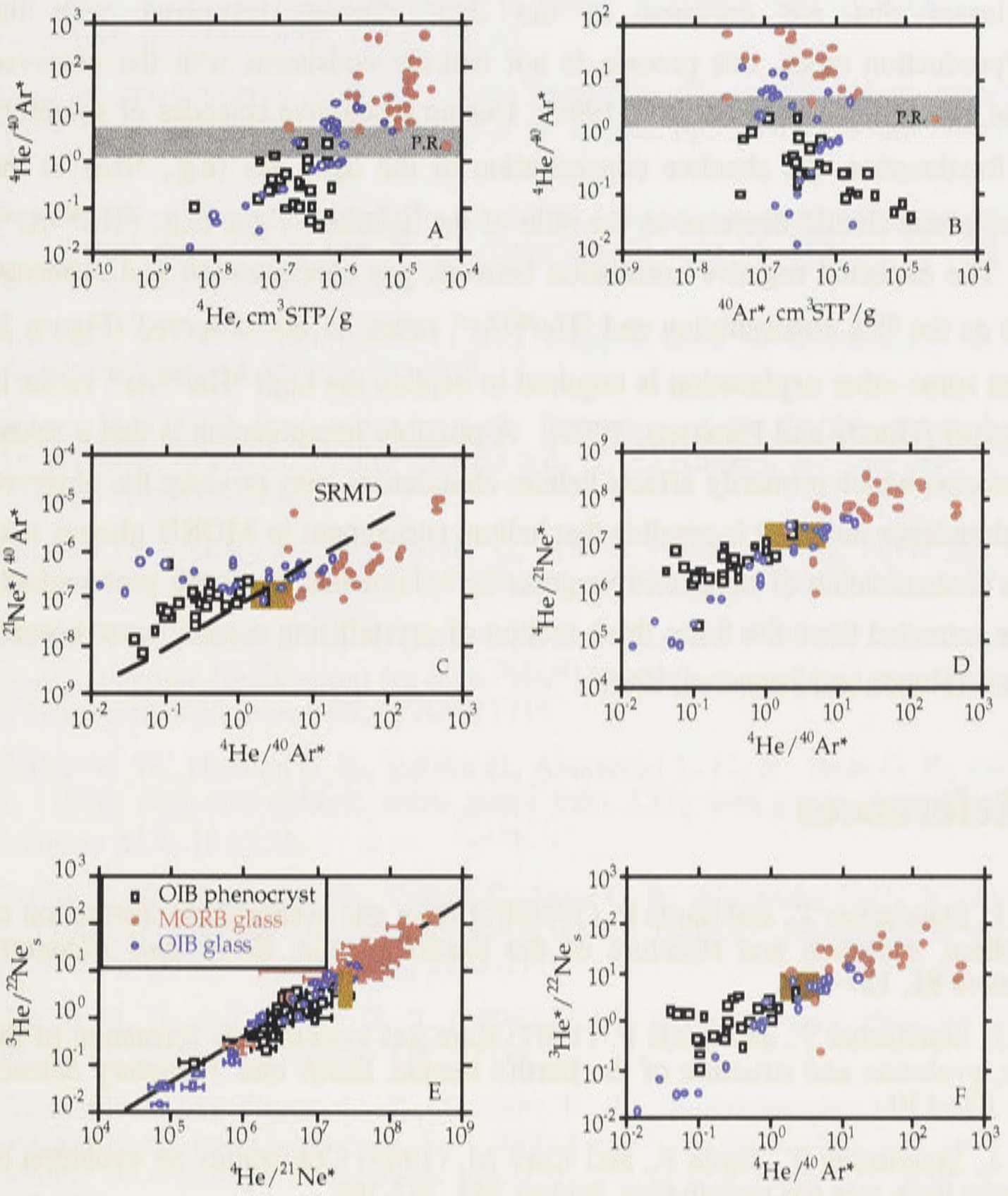

Figure 2-20A-F. Elemental abundances and abundance ratios from phenocrysts and glass separates from MORBs, BABBs and OIBs from Honda and Patterson (1999 and references therein). Note that the symbols used for MORBs and BABBs are the same because the data lie on similar trends. The solar/primordial elemental abundances and the mantle production ratios from Table 2-5 and 2-8 are shown as grey bands in Figs. A - B and as orange squares in C - F. "P.R." stands for "popping rock" or the MORB sample with very high CO_2 concentrations (Burnard et al., 1997; Moreira et al., 1998; Sarda and Graham, 1990). The diagonal lines in 2-21C shows elemental fractionation that would be produced by volume diffusion, which can be approximated by "square root of the mass difference behaviour" (SRMD) so that: $\Delta(He/Ar)=1.55\ \Delta(Ne/Ar)$ (Honda and Patterson, 1999). The data do not lie along the SRMD trend, and instead the data appear to suggest that $\Delta(He/Ar)=20\ \Delta(Ne/Ar)$. This suggests that the data may not be consistent with any mass dependent process (Honda and Patterson, 1999).

Although solubility controlled fractionation could explain the elemental ratios in MORB glasses that are enriched in the light element compared with the primordial/production ratios, this process is not entirely consistent with the observed trends in the data (Honda and Patterson, 1999). During successive episodes of solubility controlled fractionation, the absolute concentration of the light gas (e.g., ^{4}He) in the residual melt phase should decrease as the ratio of the light/heavy gas (e.g., ^{4}He/^{40}Ar*) increases. The expected negative correlation between gas concentration and elemental ratios, such as the ^{4}He concentration and ^{4}He/^{40}Ar* ratios, is not observed (Figure 2-20A) so that some other explanation is required to explain the high ^{4}He/^{40}Ar* ratios in MORB glasses (Honda and Patterson, 1999). A possible interpretation is that a mass-threshold process which primarily affects helium abundances may produce the observed elemental abundance ratios. It is possible that helium enrichment in MORB glasses may result from contamination of outgassed magmas by helium that has been preferentially excluded or extracted from the 8-km thick section of crystallising oceanic crust beneath the ridge axis (Honda and Patterson, 1999).

2.5 References

Allègre C. J., Staudacher T., and Sarda P. (1986/87) Rare gas systematics: formation of the atmosphere, evolution and structure of the Earth's mantle. *Earth and Planetary Science Letters* **81**, 127-150.

Allègre C. J., Staudacher T., and Sarda P. (1987) Rare gas systematics: formation of the atmosphere, evolution and structure of the Earth's mantle. *Earth and Planetary Science Letters* **81**, 127-150.

Allègre C. J., Staudacher T., Sarda P., and Kurz M. (1983) Constraints on evolution of Earth's mantle from rare gas systematics. *Nature* **303**, 762-766.

Amari S. and Ozima M. (1988) Extra-terrestrial noble gases in deep sea sediments. *Geochimica et Cosmochimica Acta* **52**, 1087-1095.

Anders E. and Grevesse N. (1989) Abundances of the elements: Meteoritic and solar. *Geochimica et Cosmochimica Acta* **53**, 197-214.

Anders E. and Zinner E. (1993) Interstellar grains in primitive meteorites: diamond, silicon carbide, and graphite. *Meteoritics* **28**, 490-514.

Anderson D. L. (1993) Helium-3 from the mantle: primordial signal or cosmic dust? *Science* **261**, 170-176.

Basu A. R., Poreda R. J., Renne P. R., Teichmann F., Vasiliev Y. R., Sobolev N. V., and Turrin B. D. (1995) High-^{3}He plume origin and temporal-spatial evolution of the Siberian flood basalts. *Science* **269**, 822-825.

Basu A. R., Renne P. R., DasGupta D. K., Teichmann F., and Poreda R. J. (1993) Early and late alkali igneous pulses and a high-3He plume origin for the Deccan flood basalts. *Science* **261**, 902-906.

Benkert J.-P., Baur H., Signer P., and Wieler R. (1993) He, Ne, and Ar from the solar wind and solar energetic particles in lunar ilmenites and pyroxenes. *Journal of Geophysical Research* **98**, 13147-13162.

Benz W. and Cameron A. G. W. (1990) Terrestrial effects of the giant impact. In *Origin of the Earth* (ed. H. E. Newsom and J. H. Jones), pp. 61-67. Oxford University Press. New York.

Bernatowicz T. J. and Podosek F. A. (1978) Nuclear components in the atmosphere. In *Terrestrial Rare Gases* (ed. E. C. Alexander, Jr. and M. Ozima), pp. 99-135. Japan Scientific Society Press. Tokyo.

Black D. C. and Pepin R. O. (1969) Trapped neon in meteorites - II. *Earth and Planetary Science Letters* **6**, 395-405.

Brown H. (1952) Rare gases and the formation of the Earth's atmosphere. In *The Atmospheres of the Earth and Planets* (ed. G. P. Kuiper), pp. 260-268. University of Chicago Press. Chicago.

Burnard P., Graham D., and Turner G. (1997) Vesicle-specific noble gas analyses of "popping rock": implications for primordial noble gases in Earth. *Science* **276**, 568-571.

Burnard P. G., Stuart F. M., Turner G., and Oskarsson N. (1994) Air contamination of basaltic magma: Implications for high $^{3}He/^{4}He$ mantle Ar isotopic composition. *Journal of Geophysical Research* **99**, 17709-17715.

Caffee M. W., Hudson G. B., Velsko C., Alexander E. C., Jr., Huss G. R., and Chivas A. R. (1988) Non-atmospheric noble gases from CO_2 well gases. *Lunar and Planetary Sciences* **XIX**, 154-155.

Caffee M. W., Hudson G. B., Velsko C., Huss G. R., Alexander E. C., Jr., and Chivas A. R. (1999) Primordial noble gases from Earth's mantle: identification of a primitive volatile component. *Science* **285**, 2115-2118.

Carroll M. R. and Draper D. S. (1994) Noble gases as trace elements in magmatic processes. *Chemical Geology* **117**, 37-56.

Condomines M., Gronvold K., Hooker P. J., Muehlenbachs K., O'Nions R. K., Oskarsson N., and Oxburgh E. R. (1983) Helium, oxygen, strontium and neodymium isotopic relationships in Icelandic volcanics. *Earth and Planetary Science Letters* **66**, 125-136.

Crabb J. and Anders E. (1982) Noble gases in E-chondrites. *Geochimica et Cosmochimica Acta* **45**, 2443-2464.

Craig H. and Lupton J. E. (1976) Primordial neon, helium, and hydrogen in oceanic basalts. *Earth and Planetary Science Letters* **31**, 369-385.

Craig H., Lupton J. E., Welhan J. A., and Poreda R. (1978) Helium isotope ratios in Yellowstone and Lassen Park volcanic gases. *Geophysical Research Letters* **5**, 897.

Dodson A., Kennedy B. M., and DePaolo D. J. (1997) Helium and neon isotopes in the Imnaha Basalt, Columbia River Basalt Group: evidence for a Yellowstone plume source. *Earth and Planetary Science Letters* **150**, 443-451.

Donahue T. M. and Pollack J. B. (1983) Origin and evolution of the atmosphere of Venus. In *Venus* (ed. D. Hunten, L. Colin, T. Donahue, and V. Moroz), pp. 1003-1036. University of Arizona Press. Tuscon.

Esser B. K. and Turekian K. K. (1988) Accretion rate of extraterrestrial particles determined from osmium isotope systematics of Pacific pelagic clay and manganese nodules. *Geochimica et Cosmochimica Acta* **52**, 1383-1388.

Farley K. A. and Craig H. (1994) Atmospheric argon contamination of ocean island basalt olivine phenocrysts. *Geochimica et Cosmochimica Acta* **58**, 2509-2517.

Farley K. A. and Poreda R. J. (1992) Rare gases in Samoan xenoliths. *Earth and Planetary Science Letters* **113**, 129-144.

Fisher D. E. (1997) Helium, argon, and xenon in crushed and melted MORB. *Geochimica et Cosmochimica Acta* **61**(14), 3003-3012.

Fukumoto H., Nagao K., and Matsuda J. (1986) Noble gas studies on the host phase of high $^{3}He/^{4}He$ ratios in deep-sea sediments. *Geochimica et Cosmochimica Acta* **50**, 2245-2253.

Gast P. W. (1960) Limitations on the composition of the upper mantle. *Journal of Geophysical Research* **65**, 1287-1297.

Geiss J., Buehler F., Cerutti H., Eberhardt P., and Filleaux C. H. (1972) Solar wind composition experiments. In *Apollo 16 Preliminary Scientific Report*, Vol. SP-315, pp. 14.1-14.10. NASA.

Göbel R., Ott U., and Begemann F. (1978) On trapped noble gases in ureilites. *Journal of Geophysical Research* **83**, 855-867.

Graham D. W., Humphris S. E., Jenkins W. J., and Kurz M. D. (1992a) Helium isotope geochemistry of some volcanic rocks from Saint Helena. *Earth and Planetary Science Letters* **110**, 121-132.

Graham D. W., Jenkins W. J., Schilling J.-G., Thompson G., Kurz M. D., and Humphris S. E. (1992b) Helium isotope geochemistry of mid-ocean ridge basalts from the South Atlantic. *Earth and Planetary Science Letters* **110**, 133-147.

Graham D. W., Larsen L. M., Hanan B. B., Storey M., Pedersen A. K., and Lupton J. E. (1998) Helium isotope composition of the early Iceland mantle plume inferred from the Tertiary picrites of West Greenland. *Earth and Planetary Science Letters* **160**, 241-255.

Harper C. L. and Jacobsen S. B. (1996) Noble gases and Earth accretion. *Science* **273**, 1814-1818.

Harrison D., Burnard P., and Turner G. (1999) Noble gas behaviour and composition in the mantle: constraints from the Iceland plume. *Earth and Planetary Science Letters* **171**, 199-207.

Hart R., Hogan L., and Dymond J. (1985) The closed-system approximation for evolution of argon and helium in the mantle, crust and atmosphere. *Chemical Geology (Isotope Geosciences)* **52**, 45-73.

Hart S. and Zindler A. (1986) In search of a bulk-earth composition. *Chemical Geology* **57**, 247-267.

Hilton D. R., Barling J., and Wheller G. E. (1995) Effect of shallow-level contamination on the helium isotope systematics of ocean island lavas. *Nature* **373**, 330-333.

Hilton D. R., Gronvold K., Macpherson C. G., and Castillo P. R. (1999) Extreme $^{3}He/^{4}He$ ratios in northwest Iceland: constraining the common component in mantle plumes. *Earth and Planetary Science Letters* **173**, 53-60.

Hilton D. R., Gronvold K., O'Nions R. K., and Oxburgh E. R. (1990) Regional distribution of ^{3}He anomalies in the Icelandic crust. *Chemical Geology* **88**, 53-67.

Hilton D. R., Hammerschmidt K., Loock G., and Friedrichsen H. (1993) Helium and argon isotope systematics of the central Lau Basin and Valu Fa Ridge: Evidence of crust/mantle interactions in a back-arc basin. *Geochimica et Cosmochimica Acta* **57**, 2819-2841.

Hiyagon H. (1994) Retention of solar helium and neon in IDPs in deep sea sediment. *Science* **263**, 1257-1259.

Hiyagon H., Ozima M., Marty B., Zashu S., and Sakai H. (1992) Noble gases in submarine glasses from mid-oceanic ridges and Loihi seamount: constraints on the early history of the Earth. *Geochimica et Cosmochimica Acta* **56**, 1301-1316.

Honda M. and McDougall I. (1998) Primordial helium and neon in the Earth -- a speculation on early degassing. *Geophysical Research Letters* **25**, 1951-1954.

Honda M., McDougall I., and Patterson D. B. (1993a) Solar noble gases in the Earth: the systematics of helium-neon isotopes in mantle derived samples. *Lithos* **30**, 257-265.

Honda M., McDougall I., Patterson D. B., Doulgeris A., and Clague D. A. (1991) Possible solar noble gas component in Hawaiian basalts. *Nature* **349**, 149-151.

Honda M., McDougall I., Patterson D. B., Doulgeris A., and Clague D. A. (1993b) Noble gases in submarine pillow basalt glasses from Loihi and Kilauea, Hawaii: a solar component in the Earth. *Geochimica et Cosmochimica Acta* **57**, 859-874.

Honda M. and Patterson D. B. (1999) Systematic elemental fractionation of mantle-derived helium, neon and argon in MORB glasses. *Geochimica et Cosmochimica Acta* **63**, 2863-2874.

Honda M., Patterson D. B., McDougall I., and Falloon T. J. (1993c) Noble gases in submarine pillow basalt glasses from the Lau Basin. *Earth and Planetary Science Letters* **120**, 135-148.

Honda M., Reynolds J. H., Roedder E., and Epstein S. (1987) Noble gases in diamonds: occurrences of solar-like helium and neon. *Journal of Geophysical Research* **92**, 12507-12521.

Jambon A. and Shelby J. E. (1980) Helium diffusion and solubility in obsidians and basaltic glass in the range 200-300°C. *Earth and Planetary Science Letters* **51**, 206-214.

Jambon A., Weber H., and Braun O. (1986) Solubility of He, Ne, Ar, Kr and Xe in a basalt melt in the range 1250-1600°C. Geochemical implications. *Geochimica et Cosmochimica Acta* **50**, 401-408.

Jambon A., Weber H. W., and Begemann F. (1985) Helium and argon from an Atlantic MORB glass. *Earth and Planetary Science Letters* **73**, 255-267.

Javoy M. (1995) The integral enstatite chondrite model of the Earth. *Geophysical Research Letters* **22**, 2219-2222.

Javoy M. (1998) The birth of the Earth's atmosphere: the behaviour and fate of its major elements. *Chemical Geology* **147**, 11-25.

Javoy M. and Pineau F. (1991) The volatiles record of a "popping" rock from the Mid-Atlantic Ridge at 14°N: chemical and isotopic composition of gas trapped in the vesicles. *Earth and Planetary Science Letters* **107**, 598-611.

Jephcoat A. P. (1998) Rare-gas solids in the Earth's deep interior. *Nature* **393**, 355-358.

Jochum K. P., Hofmann A. W., Ito E., Seufert H. M., and White W. M. (1983) K, U, and Th in mid-ocean ridge basalt glasses and heat production, K/U and K/Rb in the mantle. *Nature* **306**, 431-436.

Kamijo K., Hashizume K., and Matsuda J.-i. (1998) Noble gas constraints on the evolution of the atmosphere-mantle system. *Geochimica et Cosmochimica Acta* **62**, 2311-2321.

Kaneoka I., Takaoka N., and Clague D. A. (1983) Noble gas systematics for coexisting glass and olivine crystals in basalts and dunite xenoliths from Loihi Seamount. *Earth and Planetary Science Letters* **66**, 427-437.

Kellog L. H. and Wasserburg G. J. (1990) The role of plumes in mantle helium fluxes. *Earth and Planetary Science Letters* **99**, 276-289.

Kennedy B. M., Lynch M. A., Reynolds J. H., and Smith S. P. (1985) Intensive sampling of noble gases in fluids at Yellowstone: I. Early overview of the data; regional pattern. *Geochimica et Cosmochimica Acta* **49**, 1251-1261.

Kockharts L. W. (1973) Helium in the terrestrial atmosphere. *Space Science Review* **14**, 732-757.

Kunz J. (1999) Is there solar argon in the Earth's mantle? *Nature* **399**, 649-650.

Kunz J., Staudacher T., and Allegre C. J. (1998) Plutonium-fission xenon found in Earth's mantle. *Science* **280**, 877-880.

Kurz M. and Jenkins W. J. (1981) The distribution of helium in oceanic basalt glasses. *Earth and Planetary Science Letters* **53**, 41-54.

Kurz M. D. (1991) Noble gas isotopes in oceanic basalts: controversial constraints on mantle models. In *Applications of radiogenic isotope systems to problems in geology*, Vol. 19 (ed. L. Heaman and J. N. Ludden), pp. 259-286. Min. Ass. Canada Short Course Handbook.

Kurz M. D., Jenkins W. J., and Hart S. R. (1982a) Helium isotopic systematics of oceanic islands and mantle heterogeneity. *Nature* **297**, 43-46.

Kurz M. D., Jenkins W. J., Hart S. R., and Clague D. (1983) Helium isotopic variations in volcanic rocks from Loihi Seamount and the Island of Hawaii. *Earth and Planetary Science Letters* **66**, 388-406.

Kurz M. D., Jenkins W. J., Schilling J. G., and Hart S. R. (1982b) Helium isotopic variations in the mantle beneath the central North Atlantic Ocean. *Earth and Planetary Science Letters* **58**, 1-14.

Kyser T. K. and Rison W. (1982) Systematics of rare gas isotopes in basic lavas and ultramafic xenoliths. *Journal of Geophysical Research* **87**, 5611-6530.

Lal D. (1987) Production of 3He in terrestrial rocks. *Chemical Geology* **66**, 89-98.

Lal D. (1988) In situ-produced cosmogenic isotopes in terrestrial rocks. *Annual Reviews in Earth and Planetary Sciences* **16**, 355-388.

Lewis J. S. and Prinn R. J. (1984) *Planets and their atmospheres: origin and evolution.* Academic Press, New York. pp 470.

Lugmair G. W., Marti K., Kurz J. P., and Scheinin N. B. (1976) History and genesis of lunar troctolite 76535 or: how old is old? *Proceedings of the Lunar Planetary Science Conference*, 2009-2033.

Lupton J. E. (1983) Terrestrial inert gases: isotope tracer studies and clues to primordial components in the mantle. *Annual Reviews in Earth and Planetary Sciences* **11**, 371-414.

Lux G. (1987) The behaviour of noble gases in silicate liquids: Solution, diffusion, bubbles and surface effects, with applications to natural samples. *Geochimica et Cosmochimica Acta* **51**, 1549-1560.

Marty B. (1989) Neon and xenon isotopes in MORB: implications for the earth-atmosphere evolution. *Earth and Planetary Science Letters* **94**, 45-56.

Marty B. and Ozima M. (1986) Noble gas distribution in oceanic basalt glasses. *Geochimica et Cosmochimica Acta* **50**, 1093-1097.

Marty B., Pik R., and Yirgu G. (1996) Helium isotopic variations in Ethiopian plume lavas: nature of magmatic sources and limit on lower mantle contribution. *Earth and Planetary Science Letters* **144**, 223-237.

Matsuda J. and Murota M. (1990) He and Ne isotopic studies on the extraterrestrial material in deep-sea sediments. *Journal of Geophysical Research* **95**(B5), 7111-7117.

Matsui T. and Abe Y. (1986) Evolution of impact-induced atmosphere and magma ocean on the accreting Earth. *Nature* **319**, 303-305.

Mazor E., Heymann D., and Anders E. (1970) Noble gases in carbonaceous chondrites. *Geochimica et Cosmochimica Acta* **34**, 781-820.

Moreira M., Kunz J., and Allegre C. (1998) Rare gas systematics in popping rock: isotopic and elemental compositions in the upper mantle. *Science* **279**, 1178-1181.

Moreira M., Staudacher T., Sarda P., Schilling J.-G., and Allègre C. J. (1995) A primitive plume neon component in MORB: the Shona ridge-anomaly, South Atlantic (51-52°S). *Earth and Planetary Science Letters* **133**, 367-377.

Morgan J. W. and Anders E. (1980) Chemical composition of Earth, Venus and Mercury. *Proceedings of the National Academy of Sciences, USA* **77**, 6973-6977.

Murer C. A., Baur H., Signer P., and Wieler R. (1997) Helium, neon, and argon abundances in the solar wind: In vacuo etching of meteoritic iron-nickel. *Geochimica et Cosmochimica Acta* **61**, 1303-1314.

Niedermann S., Bach W., and Erzinger J. (1997) Noble gas evidence for a lower mantle component in MORBs from the southern East Pacific Rise: Decoupling of helium and neon isotope systematics. *Geochimica et Cosmochimica Acta* **61**, 2697-2715.

Niemann H. B., Atreya S. K., Carignan G. R., Donahue T. M., Haberman J. a., Harpold D. N., Hartle R. E., Hunten D. M., Kasprzak W. T., Mahaffy P. R., Owen T. C., Spencer n. W., and Hay S. H. (1996) The Galileo probe mass spectrometer: composition of Jupiter's atmosphere. *Science* **272**, 846-849.

O'Nions R. K. and Oxburgh E. R. (1983) Heat and helium in the earth. *Nature* **306**, 429-431.

Ozima M. (1994) Noble gas state in the mantle. *Reviews in Geophysics* **32**, 405-426.

Ozima M. (1998) Noble gases under pressure in the mantle. *Nature* **393**, 303-304.

Ozima M. and Podosek F. A. (1983) *Noble Gas Geochemistry*. Cambridge University Press, Cambridge. pp 367.

Ozima M., Takayanagi M., Zashu S., and Amari S. (1984) High $^{3}He/^{4}He$ ratio in ocean sediments. *Nature* **311**, 448-450.

Ozima M. and Zashu S. (1983) Noble gases in submarine pillow volcanic glasses. *Earth and Planetary Science Letters* **62**, 24-40.

Ozima M. and Zashu S. (1988) Solar-type Ne in Zaire cubic diamonds. *Geochimica et Cosmochimica Acta* **52**, 19-25.

Ozima M. and Zashu S. (1991) Noble gas state of the ancient mantle as deduced from noble gases in coated diamonds. *Earth and Planetary Science Letters* **105**, 13-27.

Patterson D. B., Honda M., and McDougall I. (1990) Atmospheric contamination: a possible source for heavy noble gases in basalts from Loihi seamount, Hawaii. *Geophysical Research Letters* **17**, 705-708.

Pepin R. O. (1991) On the origin and early evolution of terrestrial planet atmospheres and meteoritic volatiles. *Icarus* **92**, 2-79.

Pepin R. O. (1997) Evolution of Earth's noble gases: consequences of assuming hydrodynamic loss driven by giant impact. *Icarus* **126**, 148-156.

Pepin R. O. (1998) Isotopic evidence for a solar argon component in the Earth's mantle. *Nature* **394**, 664-667.

Pepin R. O., Becker R. H., and Schlutter D. J. (1999) Irradiation records in regolith materials. I: Isotopic compositions of solar-wind neon and argon in single lunar mineral grains. *Geochimica et Cosmochimica Acta* **63**, 2145-2162.

Phinney D., Tennyson J., and Frick U. (1978) Xenon in CO_2 well gas revisited. *Journal of Geophysical Research* **83**, 2313-2319.

Pineau F. and Javoy M. (1994) Strong degassing at ridge crests: The behaviour of dissolved carbon and water in basalt gasses at 14°N, Mid-Atlantic Ridge. *Earth and Planetary Science Letters* **123**, 179-198.

Podosek F. A. (1970) The abundance of ^{244}Pu in the early solar system. *Earth and Planetary Science Letters* **8**, 183-187.

Podosek F. A., Bernatowicz T. J., and Kramer F. E. (1981) Adsorption of xenon and krypton on shales. *Geochimica et Cosmochimia Acta* **45**, 2401-2415.

Podosek F. A. and Swindle T. D. (1988) Extinct Radionuclides. In *Meteorites and the Early Solar System* (ed. J. F. Kerridge and M. S. Matthews), pp. 1093-1113. The Univeristy of Arizona Press. Tuscon.

Pollack J. B. and Bodenheimer P. (1989) Theories of the origin and evolution of the giant planets. In *Origin and evolution of planetary and satellite atmospheres* (ed. S. K. Atreya, J. B. Pollack, and M. S. Matthews), pp. 881. The University of Arizona Press. Tuscon.

Porcelli D. and Wasserburg G. J. (1995a) Mass transfer of He, Ne, Ar, and Xe through a steady state upper mantle. *Geochimica et Cosmochimica Acta* **59**(23), 4921-4937.

Porcelli D. and Wasserburg G. J. (1995b) Mass transfer of xenon through a steady-state upper mantle. *Geochim. Cosmochim. Acta* **59**, 1991-2007.

Poreda R., Schilling J.-G., and Craig H. (1986) Helium and hydrogen isotopes in ocean-ridge basalts north and south of Iceland. *Earth and Planetary Science Letters* **78**, 1-17.

Poreda R. J. and Farley K. A. (1992) Rare gases in Samoan xenoliths. *Earth and Planetary Science Letters* **113**, 129-144.

Prousevitch A. A., Sahagian D. L., and Anderson A. T. (1993) Dynamics of diffusive bubble growth in magmas: isothermal case. *Journal of Geophysical Research* **98**, 22283-22307.

Rison W. and Craig H. (1983) Helium isotopes and mantle volatiles in Loihi Seamount and Hawaiian Islands basalts and xenoliths. *Earth and Planetary Science Letters* **66**, 407-426.

Sarda P. and Graham D. (1990) Mid-ocean ridge popping rocks: implications for degassing at ridge crests. *Earth and Planetary Science Letters* **97**, 268-289.

Sarda P., Staudacher T., and Allègre C. J. (1985) $^{40}Ar/^{36}Ar$ in MORB glasses: constraints on atmosphere and mantle evolution. *Earth and Planetary Science Letters* **72**, 357-375.

Sarda P., Staudacher T., and Allègre C. J. (1988) Neon isotopes in submarine basalts. *Earth and Planetary Science Letters* **91**, 73-88.

Staudacher T. (1987) Upper mantle origin for Harding County well gases. *Nature* **325**, 605-607.

Staudacher T. and Allègre C. J. (1982) Terrestrial xenology. *Earth and Planetary Science Letters* **60**, 389-406.

Staudacher T. and Allègre C. J. (1988) Recycling of oceanic crust and sediments: the noble gas subduction barrier. *Earth and Planetary Science Letters* **89**, 173-183.

Staudacher T. and Allègre C. J. (1989) Noble gases in glass samples from Tahiti: Teahitia, Rocard and Mehetia. *Earth and Planetary Science Letters* **93**, 210-222.

Staudacher T., Kurz M. D., and Allègre C. J. (1986) New noble gas data on glass samples from Loihi Seamount and Hualalai and on dunite samples from Loihi and Réunion Island. *Chemical Geology* **56**, 193-205.

Staudacher T., Sarda P., and Allègre C. J. (1990) Noble gas systematics of Réunion Island, Indian Ocean. *Chemical Geology* **89**, 1-17.

Staudacher T., Sarda P., Richardson S. H., Allègre C. J., Sagna I., and Dimitriev L. V. (1989) Noble gases in basalt glasses from a Mid-Atlantic Ridge topographic high at 14° N: geodynamic consequences. *Earth and Planetary Science Letters* **96**, 119-133.

Tolstikhin I. N. (1975) Helium isotopes in earth's interior and in the atmosphere: a degassing model for the earth. *Earth and Planetary Science Letters* **26**, 88-96.

Tolstikhin I. N. and Marty B. (1998) The evolution of terrestrial volatiles: a view from helium, neon, argon and nitrogen isotope modelling. *Chemical Geology* **147**, 27-52.

Trieloff M., Kunz J., Clague D., Harrison D., and Allegre C. (2000) The nature of pristine noble gases in mantle plumes. *Science* **288**, 1036-1038.

Turner G. (1989) The outgassing history of the Earth's atmosphere. *Journal of the Geological Society of London* **146**, 147-154.

Valbracht P. J., Honda M., Staudigel H., McDougall I., and Trost A. P. (1994) Noble gas partitioning in natural samples: results from coexisting glass and olivine phenocrysts in four Hawaiian submarine basalts. In *Noble Gas Geochemistry and Cosmochemistry* (ed. J. Matsuda), pp. 373-381. Terra Scientific Publishing Company. Tokyo.

Valbracht P. J., Staudacher T., Malahoff A., and Allègre C. J. (1997) Noble gas systematics of deep rift zones glasses from Loihi Seamount, Hawaii. *Earth and Planetary Science Letters* **150**, 399-411.

Verniani F. (1966) The total mass of the earth's atmosphere. *Journal of Geophysical Research* **71**, 385-391.

von Weizsächer C. F. (1937) Über die Möglichkeit eines dualen β^- Zerfalls von Kalium. *Physikalishe Zeitschrift.* **38**, 623-624.

Wacker J. F. and Anders E. (1984) Trapping of xenon in ice: implication for the origin of the Earth's noble gases. *Geochimica et Cosmochimica Acta* **48**, 2375-2380.

Watson E. B., Sneeringer M., A., and Ross A. (1982) Diffusion of dissolved carbonate in magmas: experimental results and applications. *Earth and Planetary Science Letters* **61**, 346-358.

Wetherill G. W. (1954) Variations in the isotopic abundances of neon and argon extracted from radioactive minerals. *Physical Science Review* **96**, 679-683.

Wetherill G. W. and Stewart G. R. (1989) Accumulation of a swarm of small planetesimals. *Icarus* **77**, 330-357.

Xu S., Nakai S.-i., Wakita H., and Wang X. (1995) Mantle-derived noble gases in natural gases from Songliao Basin, China. *Geochimica et Cosmochimica Acta* **59**(22), 4675-4683.

Yatsevich I. and Honda M. (1997) Production of nucleogenic neon in the Earth from natural radioactive decay. *Journal of Geophysical Research* **102**, 10281-10288.

Yokoyama Y., Reyss J., and Guichard F. (1977) Production of radionuclides by cosmic rays at mountain altitudes. *Earth and Planetary Science Letters* **36**, 44-50.

Zahnle K., Kasting J. F., and Pollack J. B. (1990) Mass fractionation of noble gases in diffusion-limited hydrodynamic hydrogen escape. *Icarus* **84**, 502-527.

Zhang Y. and Zindler A. (1989) Noble gas constraints on the evolution of the Earth's atmosphere. *Journal of Geophysical Research* **94**, 13719-13737.

Zindler A. and Hart S. R. (1986) Helium: problematic primordial signals. *Earth and Planetary Science Letters* **79**, 1-8.

CHAPTER 3: GEOCHEMICAL AND GEOPHYSICAL PERSPECTIVES ON MANTLE CONVECTION

3.1 Introduction

Understanding the structure and style of convection in the Earth's mantle has been approached using geochemical, seismic and geodynamic observations. Seismic and petrologic evidence indicates that the Earth's mantle consists dominantly of crystalline solids. The mantle is bounded by a cold, relatively rigid upper layer, the crust, and a relatively hot (~3500°C) lower boundary layer at the core mantle boundary. Seismic evidence has also revealed a discontinuity at 670 km depth, which is thought to result from a phase change of olivine from the spinel to perovskite structure in the mantle (Ringwood and Irifune, 1988).

The argon mass balance arguments described in Chapter 2 suggest that a mass of the mantle equivalent to about one-half to two thirds of the total mantle is likely to have been degassed of noble gases. This mass is roughly equivalent to, or somewhat greater than, the mass of the mantle above the 670 km discontinuity. The mantle is unlikely to have been uniformly degassed; the noble gas isotopic ratios (including helium, neon and argon) suggest that the upper mantle mid-ocean ridge basalt (MORB) source has been preferentially degassed relative to the ocean island basalt (OIB) source (see Chapter 2). Introduction of a large flux of outgassed upper mantle material or subducted slabs into the lower mantle and subsequent radiogenic ingrowth of ^{4}He and ^{40}Ar was considered likely to destroy the relatively primordial $^{3}He/^{4}He$ signature of lower mantle material as sampled by OIBs such as Loihi and Iceland (Albarède, 1998). This kind of evidence led to the development of a two-layered mantle model (see Chapter 2), in which the lower mantle was relatively isolated from mass input from subducted slabs or upper mantle material. In this model, plumes were believed to originate from a boundary layer at ~670 km, and to transfer geochemically unprocessed "primitive" lower mantle material across the boundary layer into the upper mantle. The geochemical cycles in the upper mantle were believed to be in steady state, so that the flux of primitive material via plumes from the lower mantle into the upper mantle was balanced by the flux of material out of the upper mantle (Kellog and Wasserburg, 1990; O'Nions and Tolstikhin, 1994; Porcelli and Wasserburg, 1995).

In contrast to the layered mantle model, the whole mantle convection model involves subduction of recycled oceanic crust into the lower mantle, rather than simple mass exchange between the upper and lower mantles (Sun and McDonough, 1989). The whole mantle convection model was developed largely in response to evidence from seismic tomographic images that showed that subducted oceanic lithosphere penetrates through the 670 km seismic discontinuity into the lower mantle to depths of at least 1500 km, where the seismic images lose their resolution (Creager and Jordan, 1984; Phipps Morgan, 1998; van der Hilst et al., 1997). These seismic images make it difficult to support preservation of primitive mantle material in the lower mantle by the existence of a permanently layered mode of convection (Albarède, 1998) because they show that the lower mantle is unlikely to have been completely isolated throughout the Earth's history. In the whole mantle convection model, plumes are believed to consist largely of material entrained from the lower mantle, and some of these plumes have relatively primitive $^{3}He/^{4}He$ ratios. If the lower mantle has not been isolated from convection, some explanation is needed for how relatively primitive $^{3}He/^{4}He$ ratios are preserved in the lower mantle.

The new geophysical evidence demands a careful reassessment of the very basic premises of the geochemical models of rare gas cycles. In particular, the requirement that a substantial fraction of the rare gas inventory appears to be stored in the lower mantle needs to be evaluated (Albarède, 1998). As will be shown in this chapter, re-evaluating the basic assumptions may relax the constraints from helium and argon that have been used to support a layered mantle model. However, the means by which primitive noble gas signatures observed in some OIBs are preserved in a whole-mantle convection regime is not well understood. One possibility is that although isolation times for chemical heterogeneities in the upper mantle may be as short as a few hundred million years, in the lower mantle they may extend to billions of years (Sun and McDonough, 1989). It is also possible that transfer across the 670 km may have been episodic (Solheim and Peltier, 1994), and/or to have evolved with time (Allègre, 1997).

In this chapter, several of the lines of evidence that have been used to understand the composition and structure of the mantle will be evaluated. These include: (1) use of strontium, neodymium and lead isotopic compositions of mantle-derived samples to identify different mantle end-members; (2) incompatible element ratios, such as Nb/U and Nb/Th ratios; (3) the primitive mantle K/U ratio and argon mass balance arguments; (4) the helium and heat fluxes from the Earth and assumptions of steady state; (5) a changing mode of convection; and (6) the effect of viscosity on the rate of mantle convection. Many of the details of how to reconcile the geochemical evidence with geophysical evidence for whole mantle convection have yet to be resolved.

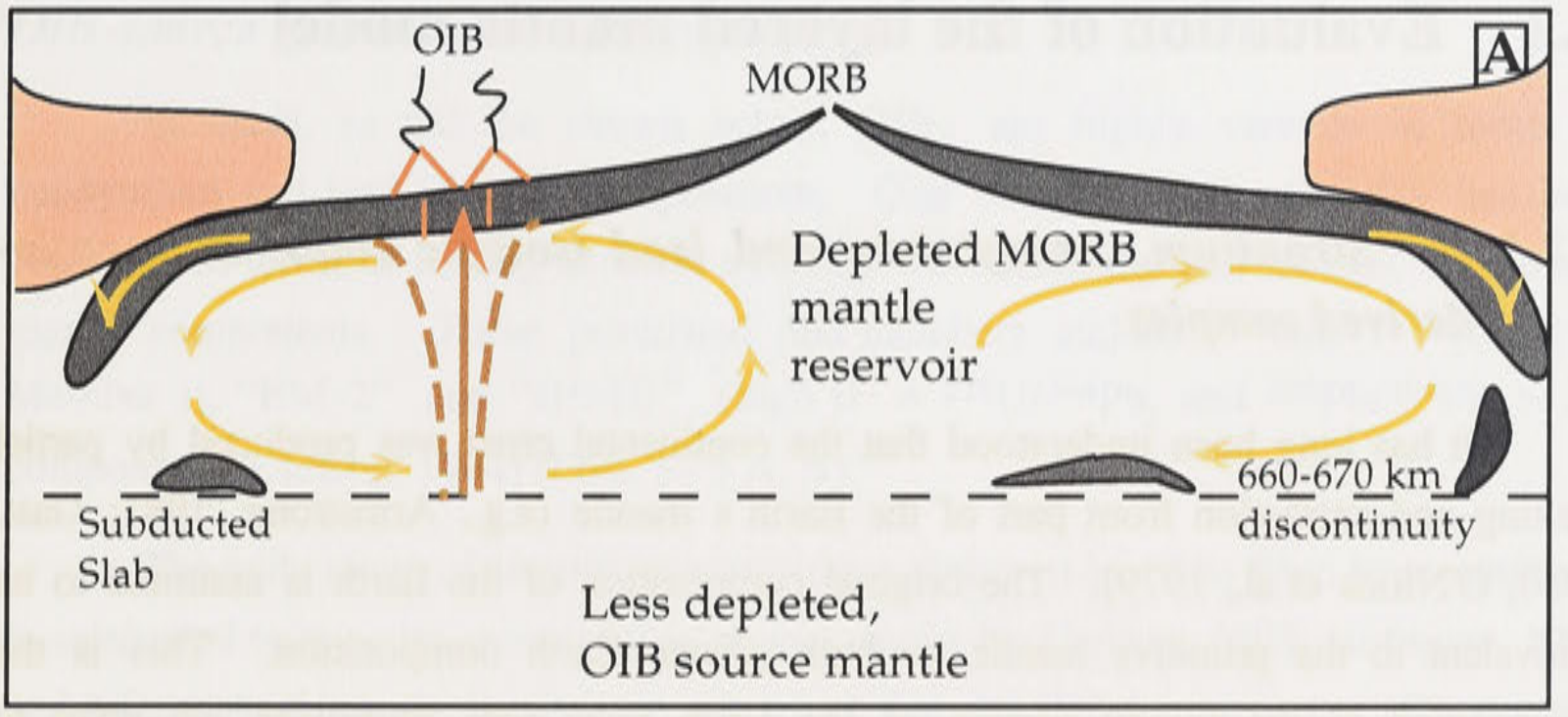

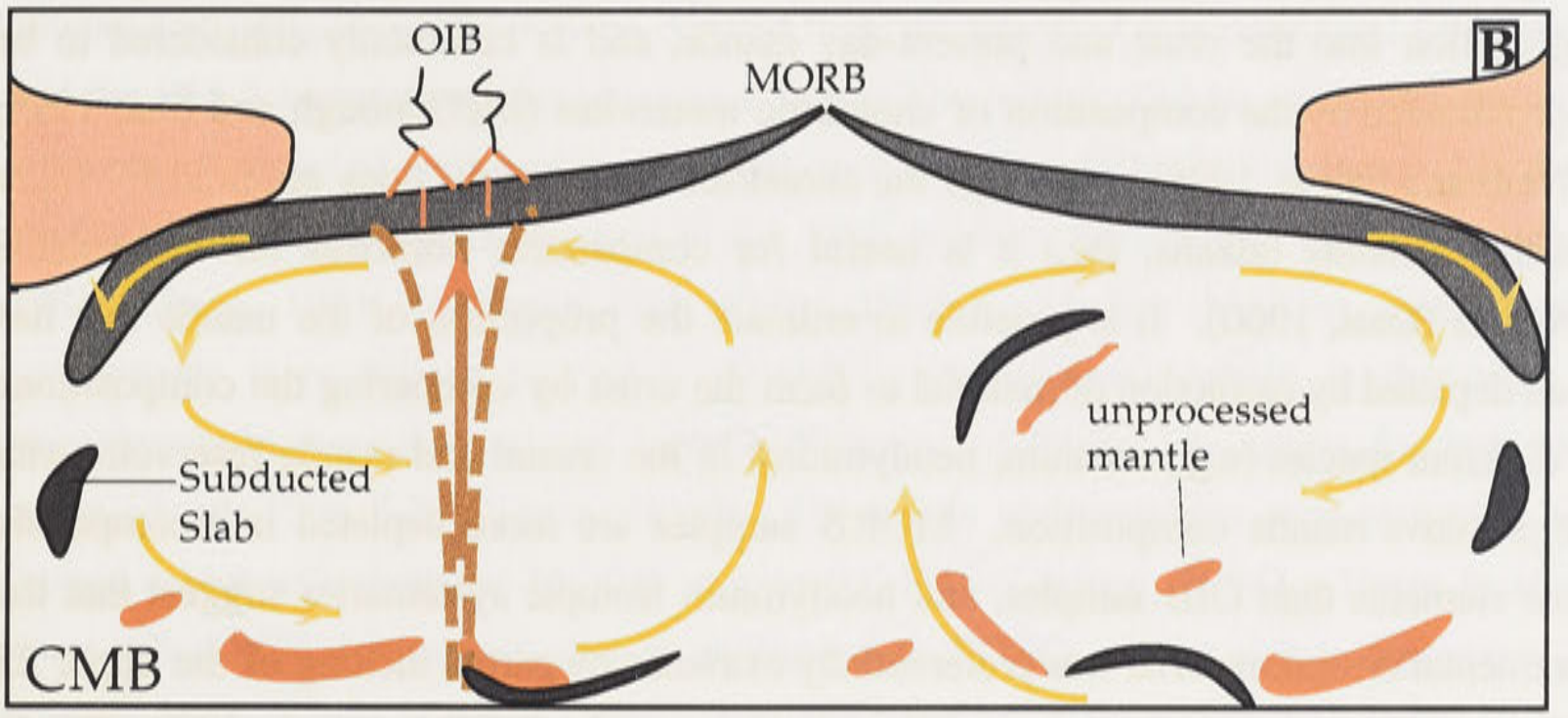

Figure 3-1A. Layered mantle convection model. The upper mantle is depleted by extraction of material to form the continental crust. Subducted slabs (gray) of oceanic crust do not penetrate through the 660-670 km discontinuity to the lower mantle OIB source. Plumes are believed to arise from the 670 km discontinuity. The lower mantle OIB source is not processed by convection and thus is relatively undepleted compared with the initial primitive mantle composition. **Figure 3-1B.** Whole mantle convection model. Subducted slabs penetrate through to the lower mantle, and nearly the entire mantle is stirred by convection. Some relatively unprocessed primitive material (red) may survive to generate the primitive $^{3}He/^{4}He$ ratios observed in some OIBs. After Phipps Morgan (1998).

3.2 Evaluation of the layered mantle model

3.2.1 Strontium, neodymium and lead isotopic ratios in mantle-derived samples

It has long been understood that the continental crust was produced by partial melting and extraction from part of the Earth's mantle (e.g., Armstrong, 1981; Gast, 1960; O'Nions et al., 1979). The original composition of the Earth is assumed to be equivalent to the primitive mantle, or bulk silicate Earth composition. This is the composition of the silicate portion of the Earth after core separation but prior to segregation into the crust and present-day mantle, and is commonly considered to be approximated by the composition of chondritic meteorites (McDonough and Sun, 1995; O'Neill and Palme, 1998). Although the chondritic Earth model does not hold for more volatile elements (alkalis, etc.) it is useful for comparative purposes for non-volatile elements (Gast, 1960). It is possible to estimate the proportion of the mantle that has been depleted by extraction of material to form the crust by comparing the compositions of different species (e.g., uranium, neodymium) in the crustal and mantle reservoirs with the primitive mantle composition. MORB samples are more depleted in incompatible trace elements than OIB samples, and neodymium isotopic systematics suggest that the continental crustal material was preferentially extracted by partial melting of the upper 25 – 30% of the volume of the originally primitive mantle (O'Nions et al., 1979; Phipps Morgan, 1998; Sun and McDonough, 1989; Wasserburg and DePaolo, 1979). Further evidence that the upper mantle MORB source may be the complementary reservoir to the continental crust is shown by $^{143}Nd/^{144}Nd$ and $^{87}Sr/^{86}Sr$ isotopic ratios. Both MORBs and OIBs lie on a trend that points to the composition of continental crust (Fig. 3-2), but MORBs have experienced a greater degree of depletion in incompatible elements than OIBs (Hofmann, 1997).

The geochemical differences between the composition of MORBs and OIBs contributed to the development of a model for a chemically layered mantle, comprised of a depleted upper mantle MORB source, and a relatively undepleted, or more primitive, lower mantle OIB source (Fig. 3-1A) (e.g., Allègre et al., 1983 and references therein). The relatively undepleted OIB source is interpreted to have a composition similar to that of the primitive mantle. The 670 km discontinuity has been inferred to be the boundary between the upper and lower mantles because the mass of the mantle above the 670 km discontinuity is approximately the same as the proportion of the mantle estimated to have been depleted by melting to form the crust.

OIB-source geochemical heterogeneity

In detail, as will be shown below, OIBs are highly variable in terms of neodymium and lead isotopic compositions. OIB compositional variability has been explained in terms of mixing between a number of chemically and isotopically distinct mantle components. These postulated end-members include: "EM-1" (i.e., End Member I), "EM-2" and "HIMU" (high $\mu = {}^{238}U/{}^{204}Pb$, and ${}^{206}Pb/{}^{204}Pb > 20$) components (Carlson, 1994) (Figs. 3 - 3 A, B).

The wide range of isotopic compositions observed in OIBs have been attributed to subducted or recycled material (see review papers by Carlson, 1995; Hofmann, 1997, and references therein). It has been proposed that the EM-1 component (Pitcairn and Tristan da Cunha hotspots) may be derived from delaminated subcontinental lithosphere, and the EM-2 component (Societies and Samoa hotspots) could be explained by small amounts of recycled sediment in the OIB source. The HIMU component has been attributed to recycled oceanic crust in the OIB source (Armstrong, 1968; Armstrong, 1981; Chase, 1981; Hofmann and White, 1982). Mixing between these mantle components is postulated to rise to "FOZO" (focal-zone), which is the point of convergence in three dimensional isotope diagrams of linear data arrays for individual ocean islands (Fig. 3-2). These various OIB mantle end-members may mix only to a limited extent with depleted MORB mantle (DMM) (Carlson, 1994). There is also a point called "C" (Common) that is analogous to FOZO, except that it represents the point of convergence of isotope arrays for data from MORBs rather than OIBs (Fig. 3-2). The compositions of FOZO and C both differ from the primitive mantle composition, but the primitive mantle composition lies within the field defined by the linear arrays formed by mantle-derived samples (represented by PRIMA in Fig. 3-2 and by the geochron in Fig. 3-3A).

The heterogeneous isotopic compositions of different OIBs conflict with the view based on the layered mantle model that the lower mantle OIB source has been isolated from convection. Although geochemical evidence is inconclusive in providing a means to evaluate the origin of isotopic heterogeneity in OIBs, the chemical variability does show that OIBs cannot have been derived solely from a chemically uniform primitive lower mantle reservoir (Hofmann, 1997). In fact, primitive mantle does not even appear to be one of the major mantle end-members (Carlson, 1994; Hofmann, 1997; Hofmann et al., 1986).

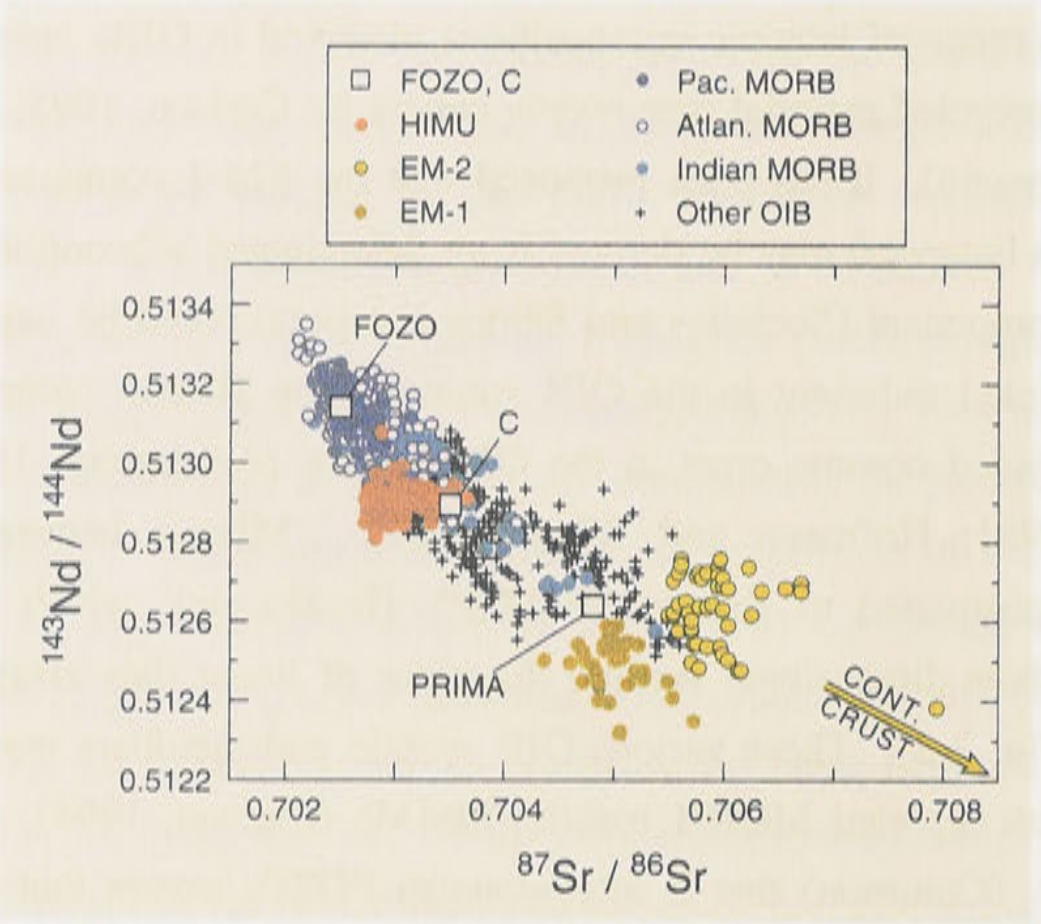

Figure 3-2. Neodymium versus strontium isotopic ratios from MORBs (including Atlantic, Pacific and Indian MORBs) and OIBs (including HIMU, EM-1, EM-2 and other OIBs). The compositions of FOZO (focus zone of OIB data), "C" ("common" composition, or the convergence of the trends formed by MORB data) and PRIMA (primitive mantle) lie in the trend defined by the isotopic ratios of oceanic basalts. This trend points to the composition of the continental crust. Figure from Hoffmann (1997).

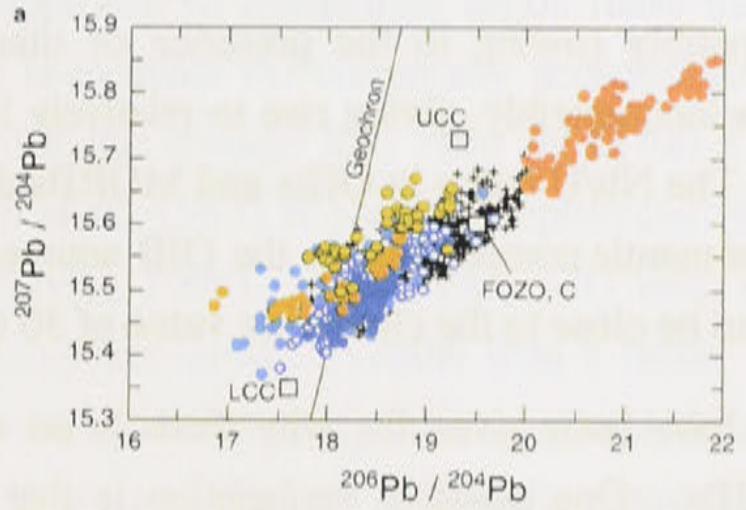

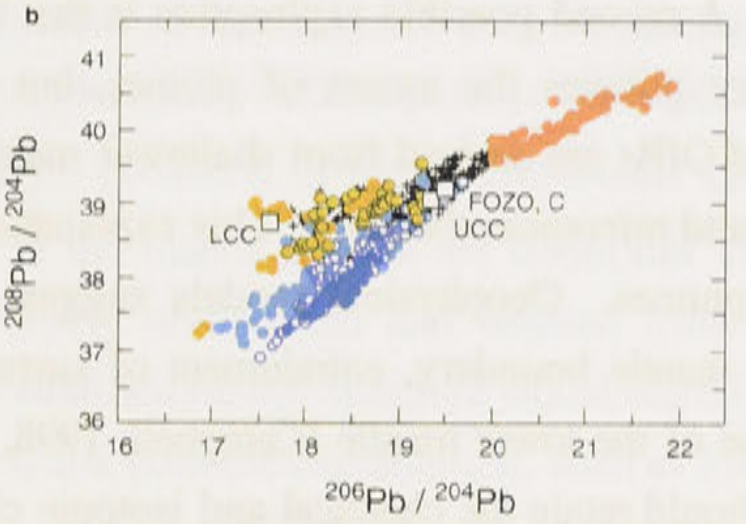

Figure 3-3a. $^{207}Pb/^{204}Pb$ versus $^{206}Pb/^{204}Pb$, showing data from the same samples as in Figure 3-2, using the same symbols and color codes. The compositions of FOZO and "C" are as described in Figure 3-2. UCC and LCC are the average compositions of the upper and lower continental crust, respectively. The locus of possible primitive mantle values assuming an overall age of the mantle of 4.50 Ga is shown by the solid line labelled "Geochron." The data lie on a trend that intersects the geochron, with some data lying to higher and lower values than the geochron. **Figure 3-3b.** $^{208}Pb/^{204}Pb$ versus $^{206}Pb/^{204}Pb$. Figures from Hoffmann (1997).

Nb/U and Nb/Th ratios

As described above, there has been considerable debate over whether the lower mantle is entirely or even substantially primitive in composition (Allègre et al., 1996; Allègre and Turcotte, 1985; Hofmann et al., 1986; Jacobsen and Wasserburg, 1979; O'Nions et al., 1979; O'Nions and Tolstikhin, 1996). The differentiation processes that produced the modern mantle from the postulated initial primitive mantle composition may be further evaluated using trace element ratios, such as Nb/U and Nb/Th.

During partial melting to produce OIBs and MORBs, uranium and niobium are believed to behave incompatibly (i.e., to partition into the melt phase) and to have similar partition coefficients, so that the Nb/U ratios in these rocks are believed to be essentially the same as in their mantle source region (Hofmann et al., 1986; Sims and DePaolo, 1997). Most OIBs (with the exception of EMI), have Nb/U ratios within the range found in MORBs (47 ± 10) (Hofmann et al., 1986). In contrast, during extraction of the

continental crust from the mantle and in arc settings/subduction zones, niobium is believed to behave compatibly (owing to the presence of titanium bearing minerals), whereas uranium behaves incompatibly, giving rise to relatively low Nb/U ratios near 10 (Hofmann et al., 1986). The Nb/U ratios in OIBs and MORBs do not appear to support a predominantly primitive mantle composition in the OIB source, as the primitive mantle Nb/U ratio is postulated to be close to the chondritic value of 30 (Hofmann et al., 1986).

Two explanations have been given for why there is no evidence for a primitive mantle component in OIBs. One possible explanation is that OIB-type sources have been well-mixed with the depleted MORB reservoir in terms of incompatible elements (Hofmann et al., 1986). A second possible explanation is that the mantle material from the core-mantle boundary initiates the ascent of plumes, but the main chemical and isotopic characteristics of OIBs are derived from shallower mantle above 1000 km (Sun and McDonough, 1989, and references therein). This explanation is not consistent with geophysical models of plumes. Geophysical models suggest that when plumes rise vertically from the core mantle boundary, entrainment of surrounding material occurs predominantly at the base of the lower mantle (Campbell, 1998, and references therein). This implies that OIBs should retain the chemical and isotopic characteristics of material derived from near the core-mantle boundary rather than from the shallower mantle above 1000 km.

The K/U ratio of the bulk silicate Earth and argon mass balance

The mantle K/U ratio is one of the fundamental parameters used in calculating the argon mass balance in the Earth (see Chapter 2). This is because the uranium content of the mantle is believed to be well determined and equal to 20 ppb, so that knowledge of the K/U ratio permits the potassium content of the mantle to be estimated. Despite the different ionic charges and radii of K and U, the K/U ratio of the mantle is observed to be nearly constant in most MORBs (12700) (Jochum et al., 1983). This near-constant ratio suggests that K and U have nearly identical effective bulk partition coefficients during the processes of depletion and partial melting to form MORBs (Jochum et al., 1983). Other similar but somewhat lower estimates for the mantle K/U ratio of 10^4 were obtained based on the K and U abundances in crustal rocks (Wasserburg et al., 1964). Some OIBs, including HIMU and EM-type OIBs, have a range of K/U ratios, and some enriched MORBs (E-MORBs) have "anomalous" K/U ratios (Table 3-1). However, the origin of these anomalous K/U ratios may be attributed to recycled components and do not necessarily provide insights into the possible value of the primitive mantle K/U ratio.

The basic inconsistency between the argon mass balance argument and the whole-mantle convection model is that if the entire mantle convects, it is likely to have been processed by mantle melting, and therefore is likely to be outgassed of much of its

radiogenic ^{40}Ar. One approach to reconciling argon mass balance with whole-mantle convection models is to re-evaluate the commonly accepted K/U ratio of the primitive mantle. It is possible that the average K/U ratio of 12700 ± 200 measured in most MORB glasses (Jochum et al., 1983) is not truly representative of the primitive mantle value (Albarède, 1998; Davies, 1999). The mantle K/U ratio may be somewhat lower than 12700, and is probably not known to better than a factor of two (Albarède, 1998; Davies, 1999). The argon mass balance arguments presented in Chapter 2 are based on the assumption that the measured K/U ratio in MORB glasses of 12700 ± 200 (Jochum et al., 1983) is equal to the primitive mantle value. If the initial mantle K/U ratio was close to 6000, the ^{40}K content of the mantle would be decreased by 50% for a given uranium abundance (Albarède, 1998). Consequently, the expected amount of radiogenic ^{40}Ar ($^{40}Ar^*$) that would be produced in the mantle would also be lowered. A lower concentration of $^{40}Ar^*$ in the mantle relaxes the constraint on the proportion of the mantle that remains relatively undegassed and isolated from melting and convection processes. A layered, or stratified mantle structure would therefore no longer be required by argon mass balance. Other possible explanations, such as loss of substantial amounts of $^{40}Ar^*$ from the Earth's atmosphere, or storing $^{40}Ar^*$ in the core, are difficult to evaluate (Davies, 1999).

Table 3-1. Average K/U ratios in MORBs and OIBs

	N-MORB	HIMU	EM-OIB	Anomalous MORB
K/U (average)	12,700 (a)	7,200 (b)	11,000 (c)	5,714 (d)

(a, d) (Jochum et al., 1983) (b, c) (Sun and McDonough, 1989)

Other assumptions in $^{40}Ar^*$ mass balance arguments

An alternative approach to resolving the apparent inconsistency between the argon mass balance argument and the whole mantle convection model is to evaluate the effects of a relatively slow rate of mantle convection. If the mantle convects slowly, a relatively small amount of the mantle will be melted over a given time period, which would in turn lead to relatively slow rates of $^{40}Ar^*$ degassing from the mantle. Hence, the $^{40}Ar^*$ mass balance arguments may not place constraints on the style of mantle convection if parts of the mantle convect slowly relative to the half-life of ^{40}K (Phipps Morgan, 1998). The $^{40}Ar^*$ mass balance arguments (see Chapter 2) are based on the total amount of ^{40}K and $^{40}Ar^*$, and not on the spatial distribution of ^{40}K-$^{40}Ar^*$ in the mantle. Although $^{40}Ar^*$ is produced in relatively large quantities within the mantle, it may be contained in a part of the mantle that has not been processed by melting and degassing since the $^{40}Ar^*$ was produced (Phipps Morgan, 1998).

How often the lower mantle has been processed (melted and degassed) by convection (overturn, differentiation and recycling) is not known. It has been suggested that higher heat flow from radioactive decay in the early Earth's history may have driven convection that was up to 20 times faster in the past than at present (Phipps Morgan, 1998). The time needed for one mantle overturn at the *current* mantle temperature is estimated to be very long, from 5.7 to 9.5 Ga, owing to cooling of the mantle over time. This means that a significant amount of $^{40}Ar^*$ produced during the most recent 3 Ga of mantle evolution may still be retained in the mantle. For a mantle K/U ratio of 12700, and using the past and present-day rates of mantle overturn described above, between 25 and 60% of the $^{40}Ar^*$ produced in the mantle can be retained, respectively (Phipps Morgan, 1998). Previous estimates based on argon mass balance arguments suggest that more than 50% of the mantle mass is degassed (Chapter 2). It may alternatively be possible that owing to relatively slow mantle convection and overturn, only 50% of the mantle mass has been degassed since the $^{40}Ar^*$ was produced within it (Phipps Morgan, 1998). This means that a layered mantle is not necessarily required to explain the $^{40}Ar^*$ mass balance.

3.2.2 Helium and heat fluxes

The observed fluxes of ^4He and heat from oceanic areas are 4×10^9 atoms/m^2s^2 (Craig et al., 1975) and 100 mW/m^2, respectively (Oxburgh and O'Nions, 1987). Decay of uranium and thorium should account for about 75% of the radiogenic heat produced at present; decay of ^{40}K produces much of the remaining 25% radiogenic heat (O'Nions and Oxburgh, 1983). The uranium and thorium required to support the radiogenic ^4He flux from the mantle, combined with the amount of potassium estimated from the K/U ratio of ~ 1×10^4, would generate only a small amount of the observed heat flux (Oxburgh and O'Nions, 1987). The observed ^4He/heat ratio is 4×10^{10} atoms/Joule, but the expected production ratio is much higher, on the order of 10^{12} atoms/Joule (Oxburgh and O'Nions, 1987).

Another way of expressing the discrepancy between helium and heat flux is that the uranium required to produce the measured ^4He flux from the mantle would account for only 5% of the heat flow. Although the distribution of uranium and thorium in the mantle that produce the radiogenic ^4He is not constrained, if it is assumed that all ^4He is produced by uranium decay only in the upper mantle, the upper mantle uranium content would be 5 ppb (with equivalent thorium) (O'Nions and Oxburgh, 1983; Oxburgh and O'Nions, 1987). This value is consistent with other estimates for the uranium content of the depleted mantle (O'Nions and Oxburgh, 1983, and references therein). This means

that the observed radiogenic ^4He flux can be accounted for by decay of 5 ppb uranium in the upper mantle, but the observed heat flow cannot.

To further understand the reasons for the differences in expected versus observed helium and heat fluxes, Oxburgh and O'Nions (1987) showed that the radiogenic helium flux from the mantle is lower than would be predicted based on the estimated bulk Earth uranium content of 20 ppb. Oxburgh and O'Nions (1987) calculated that the observed helium flux is only 10% of that which would be predicted from this uranium content. In contrast to the lower than expected helium flux, the measured heat flow is higher than that supported by present day, whole-Earth radioactive decay.

From these observations, there are two questions that need to be answered: first, in what part of the Earth might the helium remain trapped while radiogenic heat is readily transferred to the surface? And second, why is the expected heat flow based on present day, whole-Earth radioactivity much lower than observed heat flow? A possible answer to the first question is that because the amount of heat flux is much higher than the helium flux, radiogenic heat is postulated to be able to pass through the 670 km discontinuity between the lower and upper mantles and reach the Earth's surface by conduction (McKenzie and Richter, 1981) much more readily than radiogenic helium. The radiogenic helium may remain preferentially trapped in the lower mantle (O'Nions and Oxburgh, 1983). With regard to the second question, the higher than expected heat flow may be reconciled with the expected present day, whole Earth radioactivity if there is a thermal time constraint on heat loss. In other words, although the diffusivity of heat through the boundary layer may be higher than that of helium, the boundary layer is postulated to impose a thermal time constant of about 2×10^9 years on heat loss from the Earth (Oxburgh and O'Nions, 1987) so that the present day heat flux is actually derived in part from radiogenic heat produced in the past. The differences in heat and helium fluxes from the Earth suggest that the lower mantle is convectively isolated from the upper mantle (Oxburgh and O'Nions, 1987).

Calculated fluxes based on the assumption of steady state

Elements that are at steady state have input and output fluxes that are necessarily equal. Calculations based on a layered mantle model use the assumption of steady state to determine the heat, mass and geochemical fluxes into and out of the MORB source (e.g., Galer and O'Nions, 1985; White, 1993) (see Chapter 2). The helium and heat argument described above assumes that the flux of helium from the lower mantle to the upper mantle is equal to the flux from the upper mantle to mid ocean ridges (MORs). The mechanism of mass transfer from the lower to the upper mantle is postulated to be bulk entrainment from plumes (Kellog and Wasserburg, 1990), which means that the

$^{238}U/^{3}He$ ratios of the plume source and MORB source should be similar (O'Nions and Tolstikhin, 1994).

It is possible to evaluate the assumption of steady state by comparing geochemical and geophysical observations. The calculated $^{238}U/^{3}He$ ratios in the plume source may be used to estimate the plume flux into the upper mantle that is required to account for the ^{3}He loss through MORs (note that the above discussion of helium/heat fluxes could have used ^{3}He instead of ^{4}He). For a primitive mantle U content of 20 ppb and a calculated $^{238}U/^{3}He$ ratio of 0.98×10^{3}, the lower mantle ^{3}He concentration is 8.6×10^{-14} mol/g, equivalent to a total ^{3}He content of 2.6×10^{14} mol in the lower mantle (O'Nions and Tolstikhin, 1994). Entrainment of only 1% of the lower mantle mass per billion years into the upper mantle is required to account for the current rate of ^{3}He loss through MORs ($>> 1.2 \times 10^{12}$ mol/Ga, Craig et al., (1975)) (O'Nions and Tolstikhin, 1994).

This estimate of the mass flux from the lower mantle into the upper mantle (1% of lower mantle mass per billion year) may be compared with other estimates based on geophysical observations. Estimates from hot spot swells (Davies, 1988; Sleep, 1990) suggest that the mass flux from the lower mantle is an order of magnitude higher than the geochemical steady-state estimate (van Keken and Ballentine, 1999). In other words, there is a discrepancy between the lower mantle mass flux into the MORB source that is required to explain the observed helium flux from spreading ridges, and the estimated mass flux from mantle plumes based on oceanic hotspot topography. One possible means to reconcile the high estimated mass flux based on geophysical observations (White, 1993) and the helium/heat budget (O'Nions and Tolstikhin, 1994) is to assume that most of the helium transported from the lower mantle via plumes is efficiently degassed to the atmosphere rather than into the MORB source reservoir (Kellog and Wasserburg, 1990; Porcelli and Wasserburg, 1995). That is, plumes are required to account for: (1) a proportion of helium loss from the mantle that is about one order of magnitude greater than the amount degassing at MORs, but (2) only 10% of the mantle heat flow (Jochum et al., 1983). If this is the case, the low helium to heat flow ratio observed at MORs may be balanced by the high helium to heat flow ratio at plumes. The main difficulty with this explanation is that the high predicted helium flux from plumes is not observed. The hotspot helium degassing flux is not considered to be a significant source of mantle degassing compared with MORs, and is estimated to account for less than 1% of the MOR flux (Torgersen, 1989; van Keken and Ballentine, 1999). This discrepancy between geophysical and geochemical observations may imply that the assumption of steady-state requires further evaluation.

Albarède (1998) has argued that the steady-state mode of exchange for noble gas parent and daughter isotopes between the continental crust, atmosphere, upper and lower

mantle reservoirs is physically inconsistent and leads to erroneous results. Systems that can be described by equations that are explicitly dependent on time (such as those that involve radioactive isotopes or radiogenic isotopes) are not amenable to steady-state because they do not achieve steady-state until all the radioactive isotopes have decayed away (Albarède, 1998). It is possible to reproduce the observed $^{3}He/^{4}He$ ratios and explain the $^{40}Ar^{*}$ mass balance in the atmospheric and mantle reservoirs using models that are based on time-dependent equations in a whole-mantle convection regime, rather than on the steady-state assumption (Albarède, 1998). Albarède (1998) postulated that in a whole mantle convection regime, recycling of outgassed lithosphere into the lower mantle may help preserve the primitive isotopic signature of the noble gases in the lower mantle because the slabs are assumed to be depleted in U, Th, and K relative to the primitive mantle composition (Albarède, 1998; Carlson, 1995; Graham et al., 1992; see also Sun and McDonough, 1989).

3.3 Possible alternatives to the layered mantle model

3.3.1 A changing mode of convection

Although the re-evaluation of the argon mass balance problem relaxes the constraints on the style of mantle convection, the question of how primitive noble gas isotopic ratios are preserved in the lower mantle has yet to be resolved. A changing mode of convection has been proposed as one means by which to preserve observed primitive noble gas isotopic ratios in the mantle. Primitive noble gas isotopic ratios are more likely to be preserved in the lower mantle OIB-source if mantle convection was initially layered, but has subsequently evolved to whole mantle convection (Allègre, 1997). The transition from layered to whole mantle convection is postulated to have been caused by a decrease in the terrestrial heat budget over time because the amount of heat produced by radioactive decay was much larger in the past than at present. Heat generated by accretion of the Earth, and by core formation, also contributed to the higher heat flow in the past. This higher heat budget may have caused the ancient mantle to have a higher Rayleigh number (the ratio of (a) the driving force, which is due to thermal buoyancy and influenced by diffusion of heat, to (b) the retarding force, due to diffusion of momentum by viscous stresses, Griffiths (1998)). Relatively high Rayleigh numbers tend to produce multilayered convection rather than single cell convection (Allègre, 1997, and references therein). Following cooling, the Rayleigh number is expected to have decreased to a lower value so that the pattern of convection changed from multilayered to single cell convection. The transition to single cell convection is thought to have occurred relatively

recently, within the last 500 Ma. This model proposes that the diversity of $^{3}He/^{4}He$ ratios in OIBs can be explained if plumes originate at the 670 km discontinuity, but only some plumes entrain primitive helium and material from the lower mantle. The observed Nb/U ratios that suggest that hotspots originate from the same depleted reservoir as MORBs could also be explained if most plumes originate at the 670 km discontinuity (Allègre, 1997).

3.3.2 *Viscosity-dependent convection*

Viscosity-dependent convection has also been proposed as a means to preserve primitive $^{3}He/^{4}He$ ratios in a relatively viscous lower mantle, which is the source of plumes, while permitting more vigorous stirring in the less viscous MORB-source mantle (van Keken and Ballentine, 1998). Viscosity models based on plate reconstructions and geoid inversions, post-glacial rebound and the Earth's precession constant, plate reconstructions using lower mantle seismic tomography, and geoid-topography above subduction zones have all been interpreted to suggest that the lower mantle is more viscous than the mantle above 670 km (van Keken and Ballentine, 1998 and references therein). The viscosity of the lower mantle is estimated to be higher than that in the upper mantle by about a factor of 30 (Gurnis and Davies, 1986a). Numerical modelling shows that a lower viscosity in the upper mantle leads to higher upper mantle velocities, which in turn translate into a higher rate of degassing because the mantle is processed relatively rapidly at the spreading ridges. However, numerical modelling has so far been unsuccessful in showing how the observed primitive $^{3}He/^{4}He$ ratios are preserved in some OIBs (van Keken and Ballentine, 1999). Even if the model input includes a large range of values for the viscosity of the lower mantle regime that are from 30 to 100 times greater than that in the upper mantle, the $^{3}He/^{4}He$ ratio of the lower mantle decreases to values (approximately 20 Ra) that are lower than the maximum observed ratios in OIBs (~30 Ra) (van Keken and Ballentine, 1998).

A possible explanation proposed by van Keken and Ballentine (1998) for the discrepancy between the model $^{3}He/^{4}He$ ratios and the observed ratios is that the model does not consider extraction of U and Th from the mantle to the crust. They propose that decreasing the U and Th concentration in the mantle could decrease the amount of radiogenic ^{4}He that would be produced over time in the depleted mantle and potentially help to preserve primitive $^{3}He/^{4}He$ ratios.

3.4 Summary and conclusions

The existing noble gas isotopic compositions of mantle-derived samples are presently not completely explained within the context of either the layered or the whole mantle convection models. The layered mantle model, in which material from subducted slabs and the upper mantle is not input into the lower mantle, is unlikely to accurately describe convection processes in the mantle for two reasons. First, seismic tomographic evidence suggests that convection is likely to take place on the scale of the entire mantle, and second, the lower mantle as sampled by OIBs is not entirely comprised of primitive mantle, and is instead chemically heterogeneous. However, explanations to reconcile geochemical with geophysical observations, such as changing modes of convection and non-steady state fluxes in the upper mantle, either do not fully explain the geochemical observations, or require reliance on processes for which there is little evidence. It may nevertheless be possible that viscosity differences in the upper and lower mantle regimes cause the upper portion of the mantle to be stirred on a shorter time-scale than the lower mantle. The relatively slow convection rates in the lower mantle may permit preservation of geochemical heterogeneities on time scales of several billion years.

3.5 References

Albarède F. (1998) Time-dependent models of U-Th-He and K-Ar evolution and the layering of mantle convection. *Chemical Geology* **145**, 413-429.

Allègre C. J. (1997) Limitation on the mass exchange between the upper and lower mantle: the evolving convection regime of the Earth. *Earth and Planetary Science Letters* **150**, 1-6.

Allègre C. J., Hart S. R., and Minster J.-F. (1983) Chemical structure and evolution of the mantle and continents determined by inversin of Nd and Sr isotopic data, II. Numerical experiments and discussion. *Earth and Planetary Science Letters* **66**, 191-213.

Allègre C. J., Hofmann A., and O'Nions K. (1996) The argon constraints on mantle structure. *Geophysical Research Letters* **23**, 3555-3557.

Allègre C. J. and Turcotte D. L. (1985) Geodynamic mixing in the mesosphere boundary layer and the origin of oceanic islands. *Geophysical Research Letters* **12**, 207-210.

Armstrong R. L. (1968) A model for the evolution of strontium and lead isotopes in a dynamic Earth. *Reviews of Geophysics* **6**, 175-199.

Armstrong R. L. (1981) Radiogenic isotopes: the case for crustal recycling on a near-steady-state no-continental growth Earth. *Philosophical Transactions of the Royal Society of London* **301**, 433-472.

Campbell I. H. (1998) The mantle's chemical structure: insights from the melting products of mantle plumes. In *The Earth's Mantle: composition, structure, and evolution* (ed. I. Jackson), pp. 566. Cambridge University Press, Melbourne

Carlson R. W. (1994) Mechanisms of Earth differentiation: Consequences for the chemical structure of the mantle. *Reviews in Geophysics* **32**(4), 337-361.

Carlson R. W. (1995) Isotopic inferences on the chemical structure of the mantle. *Journal of Geodynamics* **20**, 365-386.

Chase C. G. (1981) Ocean island Pb: two-stage histories and mantle evolution. *Earth and Planetary Science Letters* **52**, 277-284.

Craig H., Clarke W. B., and Beg M. A. (1975) Excess ^{3}He in deep water on the East Pacific Rise. *Earth and Planetary Science Letters* **26**, 125-132.

Creager K. C. and Jordan T. H. (1984) Slab penetration in the lower mantle. *Journal of Geophysical Research* **89**, 3031-3049.

Davies G. F. (1988) Ocean bathymetry and mantle convection, large scale flow and hotspots. *Journal of Geophysical Research* **93**, 10,467-10,480.

Davies G. F. (1999) Geophysically constrained mantle mass flows and the ^{40}Ar budget: a degassed lower mantle? *Earth and Planetary Science Letters* **166**, 149-162.

Galer S. J. G. and O'Nions R. K. (1985) Residence time of thorium, uranium and lead in the mantle with implications for mantle convection. *Nature* **316**, 778-782.

Gast P. W. (1960) Limitations on the composition of the upper mantle. *Journal of Geophysical Research* **65**, 1287-1297.

Graham D. W., Humphris S. E., Jenkins W. J., and Kurz M. D. (1992) Helium isotope geochemistry of some volcanic rocks from Saint Helena. *Earth and Planetary Science Letters* **110**, 121-132.

Griffiths R. W. and Turner J. S. (1998) Understanding mantle dynamics through mathematical models and laboratory experiments. In *The Earth's Mantle: composition, structure and evolution* (ed. I. Jackson), pp. 566. Cambridge University Press, Melbourne

Gurnis M. and Davies G. F. (1986) The effect of depth-dependent viscosity on convective mixing in the mantle and the possible survival of primitive mantle. *Geophysical Research Letters* **13**, 541-544.

Hofmann A. and White W. M. (1982) Mantle plumes from ancient oceanic crust. *Earth and Planetary Science Letters* **57**, 421-436.

Hofmann A. W. (1997) Mantle geochemistry: the message from ocean volcanism. *Nature* **385**, 219-229.

Hofmann A. W., Jochum K. P., Seufert M., and White W. M. (1986) Nb and Pb in oceanic basalts: new constraints on mantle evolution. *Earth and Planetary Science Letters* **79**, 33-55.

Jacobsen S. B. and Wasserburg G. J. (1979) The mean age of mantle and crustal reservoirs. *Journal of Geophysical Research* **84**, 7411-7445.

Jochum K. P., Hofmann A. W., Ito E., Seufert H. M., and White W. M. (1983) K, U, and Th in mid-ocean ridge basalt glasses and heat production, K/U and K/Rb in the mantle. *Nature* **306**, 431-436.

Kellog L. H. and Wasserburg G. J. (1990) The role of plumes in mantle helium fluxes. *Earth and Planetary Science Letters* **99**, 276-289.

McDonough W. F. and Sun S.-s. (1995) The composition of the Earth. *Chemical Geology* **120**, 223-253.

McKenzie D. and Richter F. M. (1981) Parameterized thermal convection in a layered region and the thermal history of the Earth. *Journal of Geophysical Research* **86**, 11667-11680.

O'Neill H. S. C. and Palme H. (1998) Composition of the silicate Earth: implications for accretion and core formation. In *The Earth's Mantle: composition, structure and evolution* (ed. I. Jackson), pp. 566. Cambridge University Press, Melbourne

O'Nions R. K., Evensen N. M., and Hamilton P. J. (1979) Geochemical modeling of mantle differentiation and crustal growth. *Journal of Geophysical Research* **84**, 6091-6101.

O'Nions R. K. and Oxburgh E. R. (1983) Heat and helium in the Earth. *Nature* **306**, 429-431.

O'Nions R. K. and Tolstikhin I. N. (1994) Behaviour and residence times of lithophile and rare gas tracers in the upper mantle. *Earth and Planetary Science Letters* **124**, 131-138.

O'Nions R. K. and Tolstikhin I. N. (1996) Limits on the mass flux between the lower and upper mantle and stability of layering. *Earth and Planetary Science Letters* **139**, 213-222.

Oxburgh E. R. and O'Nions R. K. (1987) Helium loss, tectonics and the terrestrial heat budget. *Science* **237**, 1583-1588.

Phipps Morgan J. (1998) Thermal and rare gas evolution of the mantle. *Chemical Geology* **145**, 431-445.

Porcelli D. and Wasserburg G. J. (1995) A unified model for terrestrial rare gases. In *Volatiles in the Earth and Solar system* (ed. K. A. Farley), pp. 56-69. American Institute of Physics, New York

Ringwood A. E. and Irifune T. (1988) Nature of the 650-km seismic discontinuity: implications for mantle dynamics and differentiation. *Nature* **331**, 131-136.

Sims K. W. W. and DePaolo D. J. (1997) Inferences about mantle magma sources from incompatible element concentration ratios in oceanic basalts. *Geochimica et Cosmochimica Acta* **61**(4), 765-784.

Sleep N. H. (1990) Hotspots and mantle plumes: some phenomenology. *Journal of Geophysical Research* **95**, 6715-6736.

Solheim L. P. and Peltier W. R. (1994) Avalanche effects in phase transition modulated thermal convection. A model of the Earth's mantle. *Journal of Geophysical Research* **99**, 6997-7018.

Sun S.-s. and McDonough W. F. (1989) Chemical and isotopic systematics of oceanic basalts: implications for mantle composition and processes. In *Magmatism in ocean basins*, Vol. 42 (ed. A. D. Saunders and M. J. Norry), pp. 313-345, London

Torgersen T. (1989) Terrestrial helium degassing fluxes and the atmospheric helium budget: implications with respect to the degassing processes of continental crust. *Chemical Geology* **79**, 1-14.

van der Hilst R. D., Widiyantoro S., and Engdahl E. R. (1997) Evidence for deep mantle circulation from global tomography. *Nature* **386**, 584-587.

van Keken P. E. and Ballentine C. J. (1998) Whole-mantle versus layered mantle convection and the role of a high-viscosity lower mantle in terrestrial volatile evolution. *Earth and Planetary Science Letters* **156**, 19-32.

van Keken P. E. and Ballentine C. J. (1999) Dynamical models of mantle volatile evolution and the role of phase transitions and temperature-dependent rheology. *Journal of Geophysical Research* **104**, 7137-7151.

Wasserburg G. J. and DePaolo D. J. (1979) Models of earth structure inferred from neodymium and strontium isotopic abundances. *Proceedings of the National Academy of Science* **76**, 3594-3598.

Wasserburg G. J., MacDonald G. J. F., Hoyle F., and Fowler W. A. (1964) Relative contributions of uranium, thorium, and potassium to heat production in the Earth. *Science* **143**, 465-467.

White W. M. (1993) $^{238}U/^{204}Pb$ in MORB and open system evolution of the depleted mantle. *Earth and Planetary Science Letters* **115**, 211-226.

CHAPTER 4: GEOLOGY, PETROGRAPHY AND GEOCHEMISTRY OF ICELANDIC BASALTS

4.1 Introduction

4.1.1 Geologic setting

Iceland is situated along a segment of the Mid-Atlantic Ridge (MAR) associated with high basaltic magma production (Fig. 4-1) (Schilling, 1973). The volcanic activity is more voluminous than that generally associated with MAR spreading (Smallwood et al., 1995) and causes Iceland to have a much higher elevation and greater crustal thickness (8-25 km) than normal oceanic crust (7-10 km) (Hemond et al., 1993; White et al., 1995). The high magma production is thought to be the result of anomalously hot mantle (200 – 250°C hotter than ambient mantle) that is related to a mantle plume beneath Iceland (McKenzie and Bickle, 1988; McKenzie, 1984; Schilling, 1973). The distinctive geochemistry of Icelandic volcanism (e.g., Hart et al., 1973; Sun and Jahn, 1975), including the higher $^{3}He/^{4}He$ ratios, relative to adjacent mid-ocean ridge basalts (MORBs) (Schilling, 1973), is consistent with a mantle plume origin for much of the enhanced Icelandic volcanism. Additional evidence from recent seismic tomography studies support a plume origin for Iceland (Bijwaard, 1999; Helmberger et al., 1998; Shen et al., 1998) and suggest that it may originate from as deep as the core-mantle boundary (Griffiths and Campbell, 1990; Helmberger et al., 1998).

Iceland grows primarily by crustal accretion from tholeiitic volcanic systems associated with the Neo-Volcanic Zones (NVZs). The NVZs on Iceland (Fig. 4-1) are tectonically active zones of recent volcanism and rifting that are the subaerial manifestations of the Mid-Atlantic Ridge. The western NVZ is the on-land extension of the Reykjanes Ridge, and extends through the Reykjanes Peninsula to central Iceland to become the Mid-Icelandic Belt (MIB), which may be considered a "leaky' transform fault (Hardarson and Fitton, 1997). The rift continues from central Iceland through northern Iceland (the northern NVZ). There are two off-axis rift zones, the Snaefellsnes and the eastern volcanic zones (SVZ and ENVZ, respectively). The ENVZ is a new spreading axis, where erupted basalts are chemically distinct from those in the western

and northern NVZs and the MIB (Jakobsson et al., 1978). It is thought that the focus of extension will eventually transfer from the WNVZ to the ENVZ (Oskarsson et al., 1985).

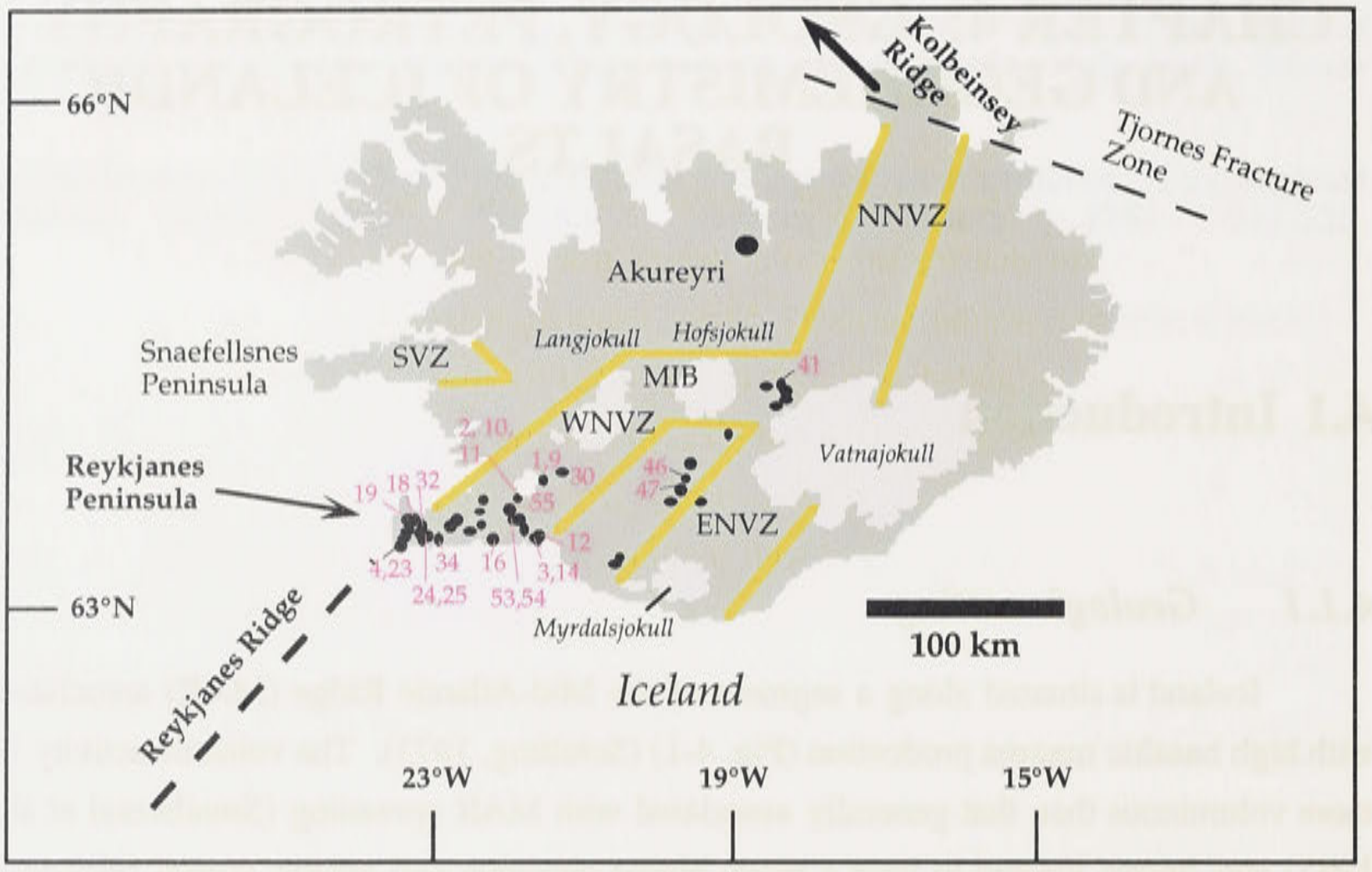

Figure 4-1. Map of Iceland showing the Neo-Volcanic Zones (NVZ) and the off-axis volcanic zones (VZ). MIB is the Mid-Iceland Belt. The glaciers (jokulls) are shown for reference. The white area on the Reykjanes Peninsula is Lake Thingvallavatn. Sample locations are shown for all samples collected for this study (Appendix 1), but only the samples analysed for noble gases or trace elements are numbered.

The age of Icelandic rocks increases with distance from the MAR/NVZ from ~east to west because it is an active spreading centre, so that the oldest rocks in Iceland (~16 Ma) (McDougall et al., 1976; Saemundsson, 1978) are in northwest and eastern Iceland at the greatest distance from the NVZ (McDougall et al., 1984; Moorbath et al., 1968; Risku-Norja, 1985). Pliocene-Pleistocene basalts (0.7 to about 3.1 Ma) and the older Tertiary basalts (older than about 3.1 Ma) (Hardarson and Fitton, 1997) are adjacent to the NVZ and form a roughly symmetrical pattern about the NVZ (Risku-Norja, 1985). Those within the NVZ, such as picritic and tholeiitic lavas along the Reykjanes Peninsula, are very young (0.7 Ma to present) (Tronnes, 1990, and references therein) and predominantly postglacial (< 13 ka). Some of the volcanism along the Reykjanes Peninsula is comprised of subaquatic and subglacial hyaloclastites in the form of pillow lavas, pillow breccias and tuffs (Tronnes, 1990). Marine deposits are found more than 100 m above the present sea level in southern Iceland, and more than 50 km from the present coast. These marine deposits originate from the Weicheselian glaciation and date from 9000 – 12700 BP (radiocarbon dates of marine shells). Prior to 13 ka,

most of Iceland is interpreted to have been covered by an ice-cap which may have depressed its surface. Subsequently, relative sea-level drop may have occurred owing to isostatic rebound of the Icelandic crust (Jull and McKenzie, 1996; Sigmundsson, 1991).

Icelandic volcanism

The Icelandic crust is thought to be intruded by magma chambers, with radii in the range of 1 – 5 km, that are situated at depths from a few kilometers to a few tens of kilometers below the ground surface. Many magma chambers are open systems into which magma may be added or removed by dikes (Figure 4-2), and are commonly envisaged as complex bodies of sills and dikes (Fridleiffson, 1977; Gudmundsson, 1998 and references therein). There are two basic types of dike swarms in Iceland: local swarms of inclined sheets associated with shallow crustal magma chambers, and regional swarms of subvertical dikes associated with relatively large, deep-seated magma reservoirs (Figure 4-2) (Gudmundsson, 1998 and references therein). The basaltic dikes in Iceland range in thickness from a few centimeters to 60 meters, but the majority of dikes in the Quaternary rocks of southwest Iceland are between 0.5 and 2 m wide (Fridleiffson, 1977; Gudmundsson, 1998).

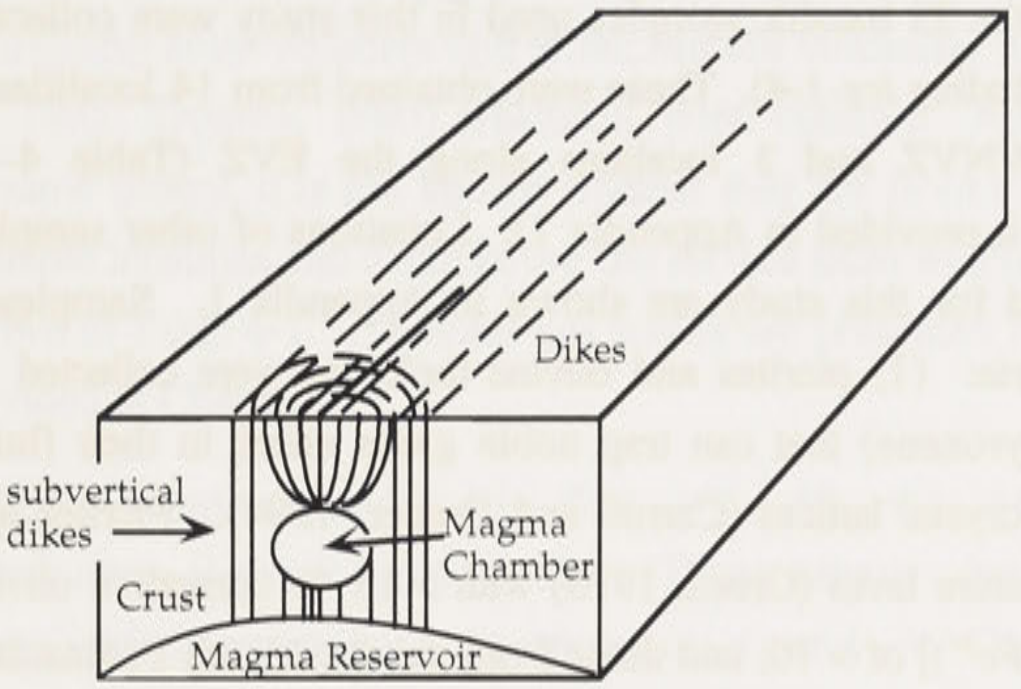

Figure 4-2. Simplified illustration of the two basic types of dike swarms in Iceland: local swarms of inclined sheets associated with shallow crustal magma chambers, and regional swarms of subvertical dikes associated with large, deep seated magma reservoirs. After Gudmundsson (1998).

The most abundant rocks in Iceland are olivine tholeiites, which erupt along the rift zones. Picrites are largely restricted to peripheral regions such as the Reykjanes Peninsula. More differentiated rocks, including quartz tholeiite to rhyolite, are generally restricted to the volcanic centers (Hemond et al., 1993). Alkali volcanics occur in off-axis rift areas including the SVZ (Hemond et al., 1993). Tholeiitic volcanism along the Reykjanes Peninsula in the western NVZ initially occurred along fissure swarms that have evolved over time to form central volcanoes. The volcanic activity along the Reykjanes Peninsula from the period starting from 0.7 Ma to the present has been

divided into three stages (Tronnes, 1990): (1) small picritic lava shields; (2) relatively large olivine tholeiite shields; and (3) lava flows erupted from fissure swarms. The small dykes and shield volcanoes are grouped into volcanic systems. From southwest to northeast along the Reykjanes Peninsula, these are the Reykjanes, Grindavik, Krisuvik, Blafjoll and Hengill volcanic systems (Jakobsson et al., 1978). The Hengill volcanic system erupts through thicker Icelandic crust than the volcanic systems to the west, where there is a transition to the thinner oceanic crust along the submarine Reykjanes Ridge (Tronnes, 1990).

4.2 Samples

4.2.1 Sample localities and sampling strategy

Samples for this investigation were collected to characterize the possible range in noble gas isotopic compositions of Icelandic basalts from the volcanic zones. The majority of the 28 basaltic samples used in this study were collected by the author (all samples excluding *ice-1-4*). These were obtained from 14 localities along the Reykjanes Peninsula WNVZ and 3 localities along the EVZ (Table 4-1) (detailed location information is provided in Appendix 1). Locations of other samples that were collected but not used for this study are shown in Appendix 1. Samples were selected using several criteria: (1) picrites and olivine tholeiites were collected because they contain olivine (± pyroxene) that can trap noble gases either in their fluid/glass inclusions or within their crystal lattices (Carroll and Draper, 1994). Picrites are typically primitive, high temperature lavas (Green, 1970) with > 15 % normative olivine and Mg numbers [$Mg/(Mg + Fe^{2+})$] of > 70, and those from the Reykjanes Peninsula are among the most primitive known in Iceland (Hansteen, 1991; Tronnes, 1990). Olivine tholeiites have normative olivine between 8 and 15%, Mg# between 50 and 75% and are less primitive than picrites. (2) Basalts that were erupted beneath glaciers or water commonly form pillow basalts with quenched, glassy rims. Such quenched glasses were also sampled as they contain relatively high concentrations of noble gases. Glasses that have relatively low percentages of vesicles were targeted because those with relatively high percentages of vesicles (>50%) (having a "frothy" appearance) are easily crushed during sampling and contaminated by atmospheric gases. (3) Samples were collected from quarries, under in-situ boulders in outcrops, or from actively eroding cliff-faces, wherever possible, to reduce potential interferences from cosmogenic isotopes (see Chapter 2). In some localities, several samples were collected from a range of depths below the surface. This was to evaluate the relative decrease in production of cosmogenic ^{3}He and ^{21}Ne with

depth owing to the increase in the degree of shielding of the rock from cosmic rays (see Chapter 2, cosmogenic nuclides). Note that four samples (*ice-1-4*) were collected by Ingvar Sigurdsson of the University of Iceland, Reykjavik. For these samples, the original depth of the sample from the surface is unknown. (4) Finally, great care was taken to collect fresh samples. Samples were only collected where no altered olivine or glass was visible, as alteration tends to increase the likelihood of atmospheric contamination of the mantle noble gases.

On the basis of size and abundance of olivine (and/or clinopyroxene) phenocrysts and the quality and freshness of the glass samples, a subset of the samples was selected for noble gas analyses. The picrites and olivine tholeiites used for noble gas analyses are from the volcanic systems along the Reykjanes Peninsula, including: the Reykjanes (*ice-4, -18, -19, -23*), Grindavik (*ice- 24, 25, 32*), Blafjoll (*ice-16*) and Hengill volcanic systems (*ice-1, 2, 3, 9, 10, 12, 14, 30, 54* and *55*) (Table 4-1). Note that samples *ice-1* and *ice-9; ice-2* and *ice-11; and ice-3;* and *ice-14* and *ice-4 and ice-23* are from the same localities, but samples *ice-1, -2, -3*, and *-4* were collected by I. Sigurdsson (Table 4-1). A sample from one locality in the EVZ (*ice-47*) was also analysed for noble gases (Fig. 4-1). Sample *ice-9* (olivine and glass) and the samples of Harrison et al. (1999) are both from a quarry at the southern end of the Midfell volcanoes in the Hengill swarm (Risku-Norja, 1985; Tronnes, 1990) (Harrison, pers. comm.). Although these samples are from the same quarry, it is not known whether they are from the same flow unit. Details of the sample localities and depth below the surface from which the samples were collected are shown in Table 4-1. The noble gas results are presented in Chapter 5. Age estimates are provided in Chapter 6.

Eight natural glass samples (*ice-9, -18, -32.2, -41, -46, -47, -54, -55*) were analysed for major and trace element compositions. These samples have also been analysed for noble gases with the exceptions of samples *ice-41* and *-46*. These samples were analysed for trace elements in part to determine their Nb/U and Nb/Th ratios, for reasons that were explained in Chapter 3. The glass samples were chosen to cover a wide geographic distribution. Samples *ice-41, -46, and -47* are from the EVZ and the remaining five samples are from the WVZ. The samples from the WVZ are derived from two different volcanic systems: the Reykjanes (*ice-18, -19, -32*) and Hengill systems (*ice-9, -54, 55*). Not all samples were analysed for major and trace element compositions because natural glasses were not available in all cases.

4.2.2 Sample descriptions and general petrography

The petrography and mineralogy of Reykjanes Peninsula samples (including the Midfell volcanoes in the Hengill system) have been presented in a number of studies (e.g., Hansteen, 1991; Jakobsson et al., 1978; Risku-Norja, 1985; Sigurdsson, 1994;

Tronnes, 1990). As found in previous studies, the phenocryst phases in the picrite and olivine tholeiite samples from this study are olivine, Cr-spinel ± plagioclase ± clinopyroxene. The olivines used in this study are euhedral to subhedral, < 8 mm in length. Olivine may contain abundant spinel inclusions, typically very few fluid inclusions, and variable amounts of glass inclusions (Hansteen, 1991). Plagioclase occurs as phenocrysts only in samples *ice-9* and *–19,* and as xenocrysts in *ice-24.* The groundmass in most samples is comprised of intergrowths of plagioclase microlites in a finer grained glassy matrix. The sample collected at Midfell (*ice-9*) is unusual in that it is from a locality where gabbroic nodules are incorporated in picritic basalts. The gabbroic nodules are composed of plagioclase, Al-Cr diopside and olivine (Risku-Norja, 1985; Tronnes, 1990). The host rock is comprised of olivine, plagioclase, clinopyroxene and spinel phenocrysts. The compositions of the minerals in the nodules are virtually identical in composition to those in the phenocrysts (Risku-Norja, 1985). Petrographic descriptions of individual samples from this study can be found in Appendix 1.

Table 4-1. Icelandic samples

Locality	Sample No.	rep-licates	analysis type	mater-ial	weight, g	rock type	size fraction	% vesicles	Descrip-tion	Depth, vertical, cm, shielding	Elev., m
Midfell	*ice-1*	a	step-heat	olivine	5.029	picrite	420µm<x <1mm			quarry, collected by I. Sigurdsson	
		b	step-heat	olivine	5.638		420µm<x <1mm				
Sandfell/ Hengill	*ice-2.1*	a	step-heat	olivine	4.309	picrite	420µm<x <1mm			surface, collected by I. Sigurdsson	
	-2.2	a	step-heat	olivine	6.162		420µm<x <1mm				
	-2.2	b	step-heat	olivine	6.190		1mm<x <2.36mm				
Burfell i olfusi	*ice-3*	a	step-heat	olivine	3.384	picrite	420µm<x <1mm			quarry, collected by I. Sigurdsson	
		b	step-heat	olivine	2.786		420µm<x <1mm				
Haleyjarbunga	*ice-4*	a	step-heat	olivine	3.181	picrite	420µm<x <1mm			surface, collected by I. Sigurdsson	
Midfell	*ice-9*	a	step-heat	olivine	5.162	picrite	420µm<x <1mm		minor px	quarry	300
		b	step-heat	olivine	5.160		420µm<x <1mm				
		c	step-heat	olivine	5.176						
		d	crush	olivine	0.702						
		g1	step-heat	glass	2.026		1mm<x <2.36mm	shards from vesicle walls			
		g2	crush	glass	0.585		420µm<x <1mm	5-10%			
		g3	crush	glass	0.720		420µm<x <1mm	<5%	different split from ice-9g1		
Maelifell	*ice-10.1*	a	step-heat	olivine	4.660	picrite	420µm<x <1mm			surface	
Maelifell	*ice-10.2*	a	step-heat	olivine	5.904	picrite	420µm<x <1mm		abundant px	100	344

Locality	Sample No.	rep-licates	analysis type	mater-ial	weight, g	rock type	size fraction	% vesicles	Descrip-tion	Depth, vertical, cm, shielding	Elev., m
Sandfell/ Hengill	*ice-11.1*	a	step-heat	olivine	3.759	picrite	420µm<x <2.36mm			surface	
Sandfell/ Hengill	*ice-11.2*	a	step-heat	olivine	5.535	picrite	420µm<x <2.36mm			30	244
Asar	*ice-12.1*	a	step-heat	olivine	3.061	picrite	420µm<x <850µm			40	
Asar	*ice-12.2*	a	step-heat	olivine	5.103	picrite	420µm<x <850µm			surface	50
Burfell i olfusi	*ice-14*	a	step-heat	olivine	3.087	picrite	420µm<x <1mm			old quarry	150
Eldborg	*ice-16*	a	step-heat	olivine	5.388	olivine tholeiite	420µm<x <1mm		2-3% px	50	100
Stapafell	*ice-18*									active quarry	60
		b	step-heat	olivine	3.649	olivine tholeiite	420µm<x <1mm				
		g2	step-heat	glass	3.704		420µm<x <1mm	<30%			
		g3	crush	glass	0.983		1mm<x <2.36mm	~30%			
Sulur	*ice-19*	a	step-heat	olivine	5.341	olivine tholeiite	420µm<x <1mm		from pillow margin	active quarry	50
Sulur	*ice-19*	b			5.153		420µm<x <1mm				
Haleyarbunga	*ice-23a*	a	step-heat	olivine	5.060	picrite	420µm<x <1mm			Cliff face, recent exposure	300
Hraunsvik/ Hrolfsvik	*ice-24*	a	step-heat	olivine	2.847	plagioclase-olivine xenolith	420µm<x <1mm			Cliff face, recent exposure	sea level
Bleikholl	*ice-25*	a	step-heat	olivine	4.912	olivine tholeiite				60	160
near Landamnna-hellir	*ice-30*	a	step-heat	olivine	5.071	olivine tholeiite	420µm<x <1mm		from pillow basalt	Cliff face, recent exposure	100

Locality	Sample No.	rep-licates	analysis type	mater-ial	weight, g	rock type	size fraction	% vesicles	Descrip-tion	Depth, vertical, cm, shielding	Elev., m
near Svartsen-gisfell	*ice-32.1*	a	step-heat	olivine	5.054	olivine tholeiite	420µm<x <1mm	<5%	dyke in hyaloclastite	Cliff face, recent exposure	sea-level
	ice-32.2	g1	crush	glass	3.056	olivine tholeiite	1mm<x <2.36mm	<5%	pillow in hyaloclastite		sea-level
		g2	crush	glass	1.040		1mm<x <2.36mm	<5%	non-vesicular hyaloclastite		
SW of Skala-Maelifell	*ice-34*	a	step-heat	olivine	3.556	olivine/pyroxene tholeiite	420µm<x <1mm		abundant px	400	100
SW of Skala-Maelifell	*ice-34*	PX	step-heat	Pyrox-ene	0.705	olivine/pyroxene tholeiite	420µm<x <1mm		abundant px	400	100
Sigalda	*ice-47*	g	crush	glass	0.921	tholeiite	1mm<x <2.36mm	~1%	pillow basalt glasses, aphyric	Cliff face, recent exposure	500
Lambafell	*ice-54*	g	crush	glass	0.843	olivine tholeiite	420µm<x <1mm	<5%	pilllow basalt glasses	quarry	300
Kongsgil	*ice-55*	g	crush	glass	0.818	olivine-plagioclase tholeiite	90µm<x <1mm	<5%	glasses from pillow basalts	graded ski slope	300

4.3 Major and trace element studies of samples from the Reykjanes Peninsula, Iceland

4.3.1 Previous work

Major elements

The major element compositions of Icelandic basalts from the Reykjanes Peninsula have been analysed previously (e.g., Hemond et al., 1993; Jakobsson et al., 1978; Risku-Norja, 1985; Sigurdsson, 1994; Tronnes, 1990). The MgO content is generally the most sensitive indicator of chemical variation in Icelandic basaltic suites (Tronnes, 1990). Icelandic picrites and tholeiites generally show covariations in major element oxide composition when plotted against MgO. The samples from the Hengill system, Reykjanes and Grindavik swarms show negative correlations for most data in the plots of SiO_2, TiO_2, Al_2O_3, FeO, MnO, Na_2O, K_2O and P_2O_5 versus MgO (Fig. 4-3) (Hemond et al., 1993; Jakobsson et al., 1978). Positive correlations are seen for some data in plots of Al_2O_3 and CaO versus MgO (Fig. 4-3). In the study by Sigurdsson (1994) of picrites and tholeiites from throughout the Reykjanes Peninsula, similar trends are apparent, except that samples with greater than 8 wt.% MgO show positive correlations with Al_2O_3 and CaO, whereas in samples with less than 8% wt.% MgO, the correlations are negative. The change in the slope of the trends is interpreted to indicate olivine control down to 11% MgO, until plagioclase, then clinopyroxene, join the liquidus (Sigurdsson, 1994).

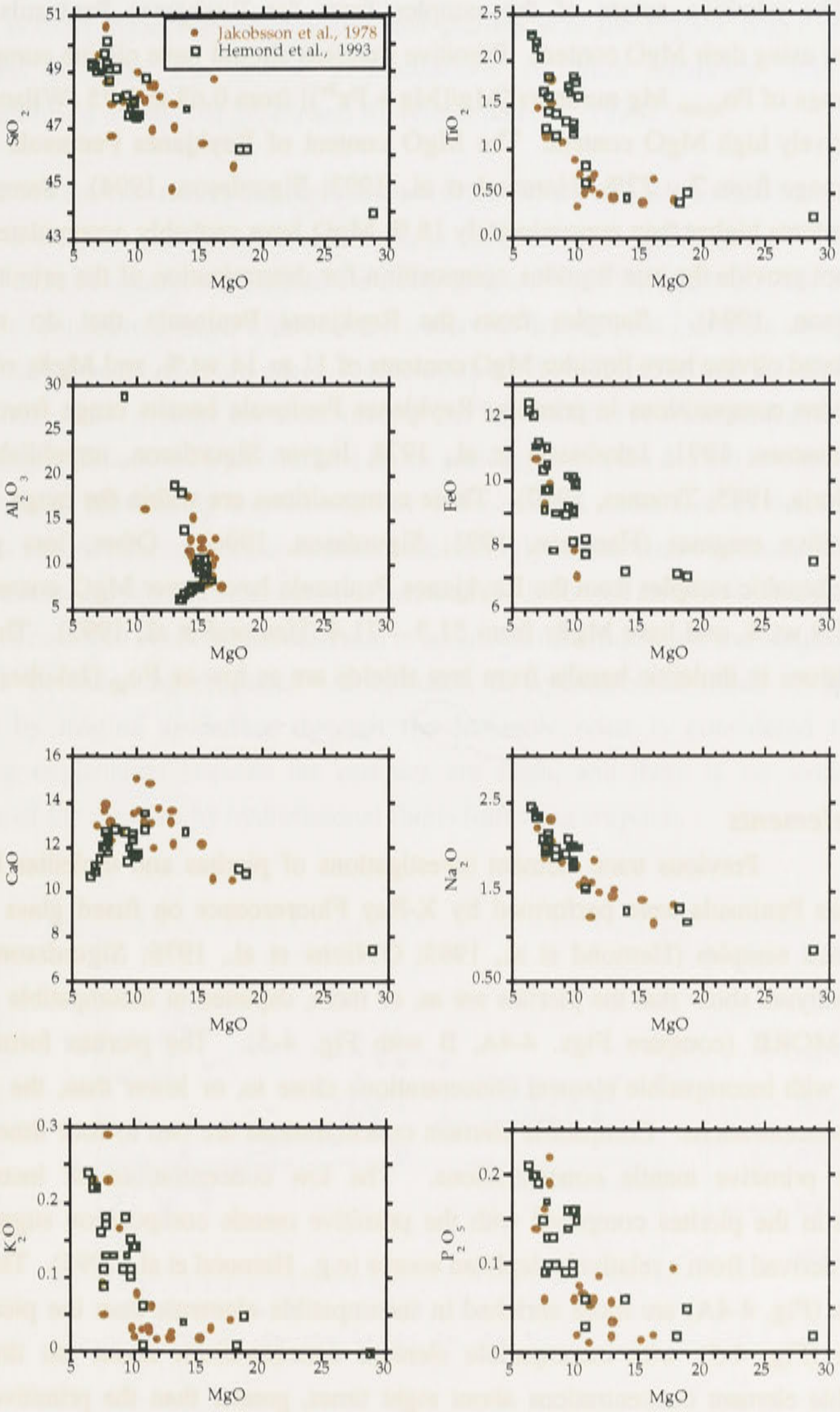

Figure 4-3. Major element compositions (weight percent oxides) in picrites and tholeiitic basalts from the Reykjanes Peninsula, Iceland. Samples from Jakobsson et al, (1978) are from the Reykjanes and Grindavik fissure swarms and include picritic basalts, olivine tholeiites, and tholeiites.

Primitive basalt compositions

The primitive nature of the samples from the Reykjanes Peninsula can be evaluated using their MgO content. Primitive magmas should have olivine compositions in the range of Fo_{86-90}, Mg numbers [$Mg/(Mg + Fe^{2+})$] from 0.68 to 0.75 (Wilson, 1989) and relatively high MgO content. The MgO content of Reykjanes Peninsula tholeiitic basalts range from 7 – 22% (Hemond et al., 1993; Sigurdsson, 1994). Samples with MgO contents higher than approximately 18 % MgO have probably accumulated olivine and do not provide the true liquidus composition for determination of the primitive Mg# (Sigurdsson, 1994). Samples from the Reykjanes Peninsula that do not have accumulated olivine have liquidus MgO contents of 11 to 14 wt.%, and Mg#s of 69.5 to 75. Olivine compositions in primitive Reykjanes Peninsula basalts range from Fo_{86} to Fo_{93} (Hansteen, 1991; Jakobsson et al., 1978, Ingvar Sigurdsson, unpublished data; Risku-Norja, 1985; Tronnes, 1990). These compositions are within the range expected for primitive magmas (Hansteen, 1991; Sigurdsson, 1994). Other, less primitive, tholeiitic basaltic samples from the Reykjanes Peninsula have lower MgO contents from 6.9 – 11.9 wt.%, and have Mg#s from 51.3 – 71.4 (Hemond et al., 1993). The olivine compositions in tholeiitic basalts from lava shields are as low as Fo_{80} (Jakobsson et al., 1978).

Trace elements

Previous trace element investigations of picrites and tholeiites from the Reykjanes Peninsula were performed by X-Ray Fluorescence on fused glass discs of whole rock samples (Hemond et al., 1993; O'Nions et al., 1976; Sigurdsson, 1994). These analyses show that the picrites are as, or more, depleted in incompatible elements than N-MORB (compare Figs. 4-4A, B with Fig. 4-5). The picrites form convex patterns with incompatible element concentrations close to, or lower than, the primitive mantle concentrations. Compatible element concentrations are two to four times greater than the primitive mantle concentrations. The low concentrations of incompatible elements in the picrites compared with the primitive mantle composition suggests that they are derived from a relatively depleted source (e.g., Hemond et al., 1993). The olivine tholeiites (Fig. 4-4A) are more enriched in incompatible elements than the picrites and MORBs (Fig. 4-5), with incompatible element concentrations about ten times, and compatible element concentrations about eight times, greater than the primitive mantle concentrations, respectively. In general, the shape of the trace element patterns formed by the tholeiitic basalts indicates melting from a source that is less differentiated and less depleted than that of the picrites.

In detail, the picrites have distinct positive anomalies in Nb, Sr, Ba and Rb. In contrast, in the tholeiites, positive anomalies in Ba, Sr, and Rb are small or absent. The positive anomalies in Sr, Ba and Rb in picrites have been attributed to addition of material

to the magma or its source (Hemond et al., 1993), as is described further below. Such addition is most evident in the tholeiites and picrites with the highest MgO content as they tend to have the lowest concentrations of trace elements with similar incompatibilities to those of Sr, Ba and Rb (Hemond et al., 1993).

There are two main possible sources of the Sr, Ba and Rb anomalies. The first, recycled oceanic or continental crustal rock, is considered an unlikely source for these elements as such sources would also be likely to have $^{87}Sr/^{86}Sr$ ratios that are similar to seawater or continental crust, which are not observed. Instead, the Icelandic samples with large Sr-Ba-Rb anomalies are characterized by low $^{87}Sr/^{86}Sr$ ratios that are close to the composition of the average Icelandic crust ($^{87}Sr/^{86}Sr$ = 0.7031) (Hemond et al., 1993). Incorporation of meteoric hydrothermal fluids enriched in Sr, Ba and Rb into the basalt is considered the most likely explanation for the observed anomalies in the Reykjanes Peninsula samples because these elements are strongly concentrated in fluids in thermal brines from the Reykjanes Peninsula (Hemond et al., 1993 and references therein). Such incorporation could occur by introduction of hydrothermal fluids into the magma, or into the basalt or following eruption. Assimilation of hydrothermal fluids or secondary minerals by magma ascending through the Icelandic crust is considered the most promising explanation because the samples are fresh, and there is no evidence for alteration of the samples by hydrothermal fluids following eruption.

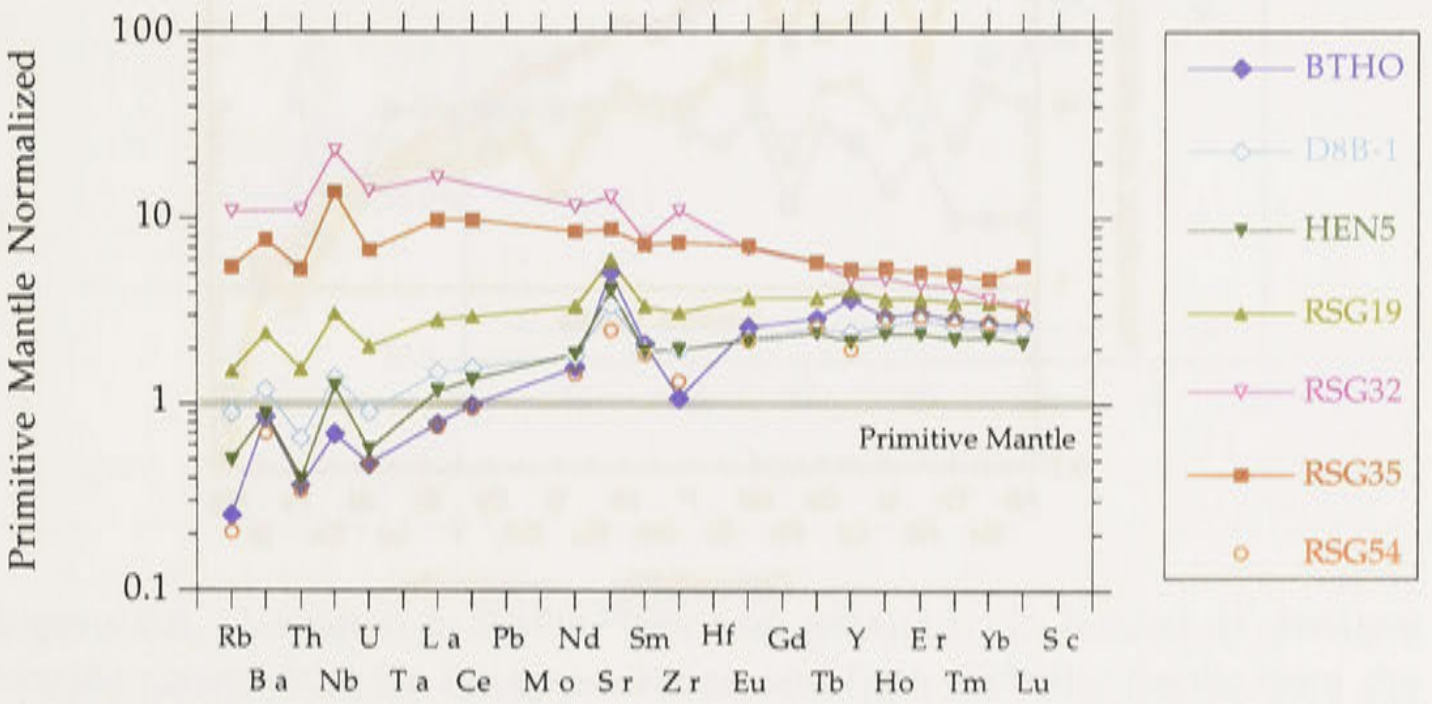

Figure 4-4A. Trace element data from Reykjanes Peninsula picrites and tholeiites (Hemond et al., 1993), normalized to the primitive mantle composition of Sun and McDonough (1989).

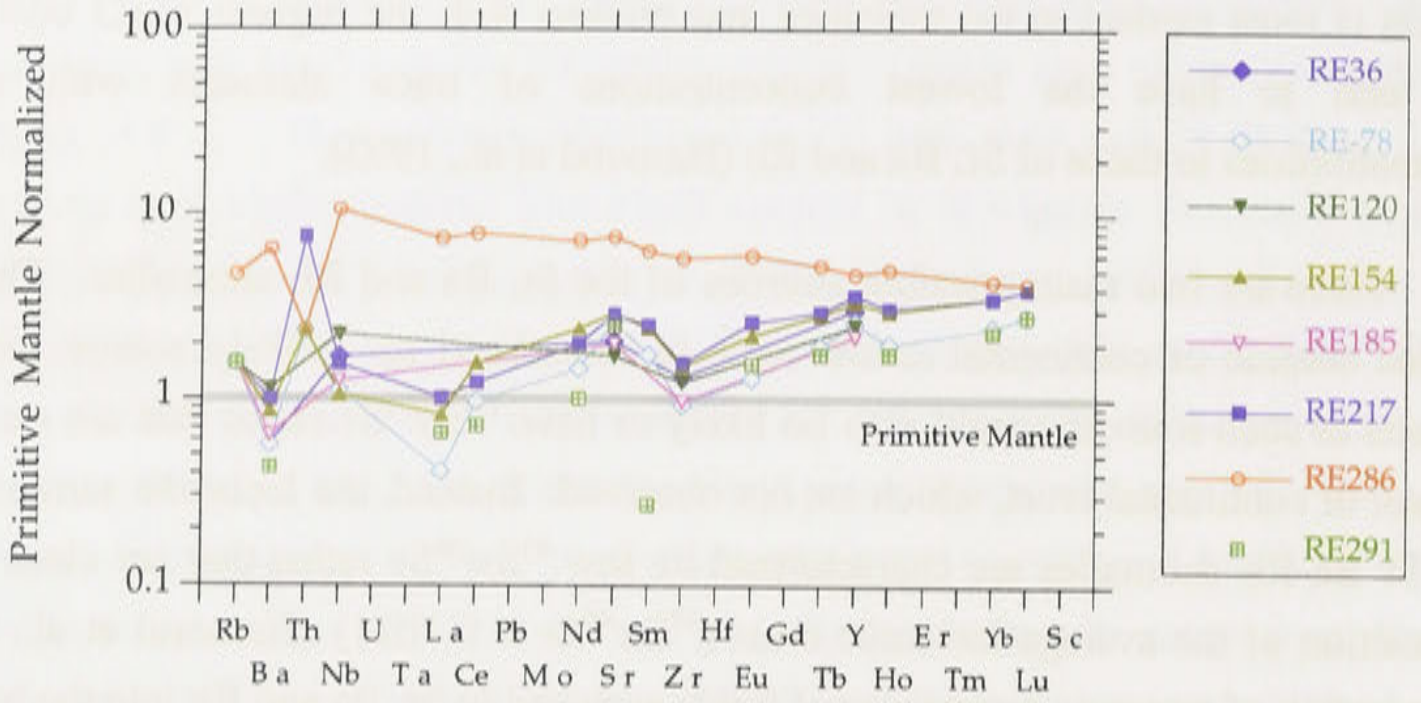

Figure 4-4B. Trace element compositions of primitive picrites from the Reykjanes Peninsula, Iceland. Data from (Sigurdsson, 1994).

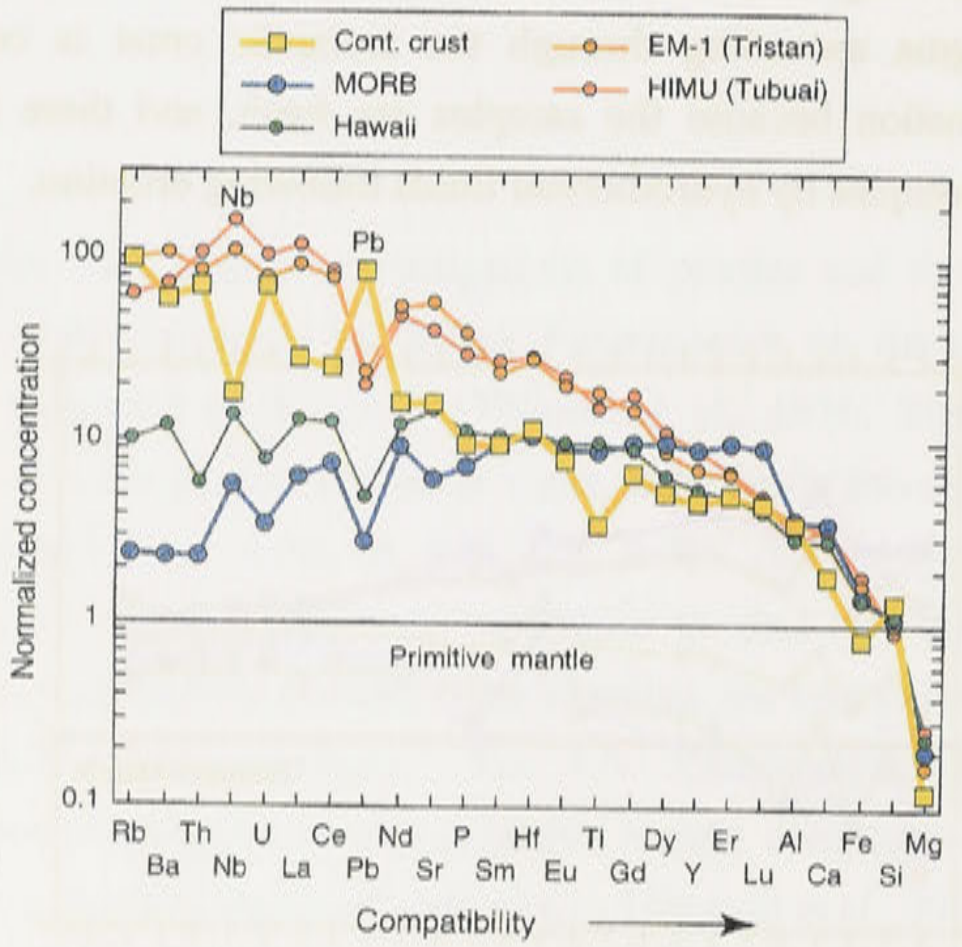

Figure 4-5. Trace element compositions in the average continental crust, Hawaii, MORBs, EM-1 type OIB and HIMU OIB (see Chapter 3). The direction of increasing compatibility of the trace element in the melt is shown. Data are normalized to the composition of the primitive mantle. Figure from Hoffmann (1997).

Pb, Sr and Nd Isotopes

Evaluation of lead, strontium and neodymium isotope geochemistry is important to understand the possible origins of the mantle components that contribute to Icelandic volcanism. This discussion will focus on geochemical results from previous investigations of samples from along the Reykjanes Peninsula (Iceland) and the adjacent Reykjanes Ridge (MORB) because most of the samples from the present investigation were obtained from the Reykjanes Peninsula region (Fig. 4-1).

Reykjanes Ridge MORB samples

Approaching Iceland from the south along the Reykjanes Ridge, MORB samples from 52.8°N to 63.4°N latitude show there is a regular increase in $^{206}Pb/^{204}Pb$ ratios from relatively low values of 18.289 to higher values of 18.680 (Fig. 4-6). The $^{207}Pb/^{204}Pb$ and the $^{208}Pb/^{204}Pb$ ratios of the same samples also increase, from 15.445 to 15.495, and 37.778 to 38.284, respectively. On Iceland itself, basaltic samples from the Reykjanes Peninsula have $^{206}Pb/^{204}Pb$ isotopic ratios near 18.777, similar to, but slightly higher than, the ratio measured in a MORB sample directly offshore along the Reykjanes Ridge (Sun and Jahn, 1975) (Fig. 4-6).

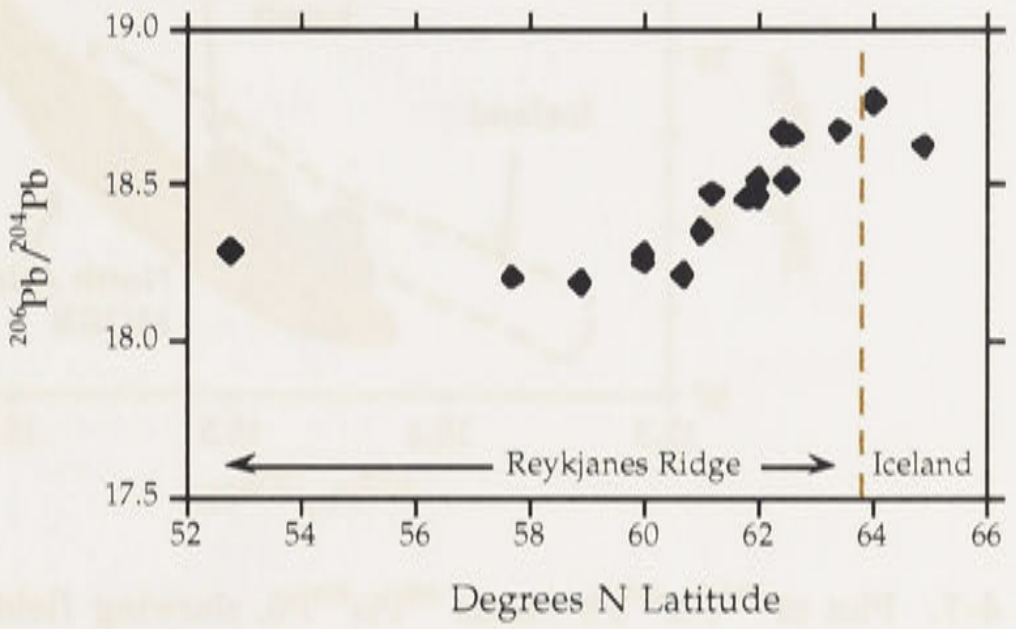

Figure 4-6. Variation in $^{206}Pb/^{204}Pb$ with proximity to Iceland in dredged basaltic glasses from the Reykjanes Ridge, and from tholeiitic basalts from the Reykjanes Peninsula, Iceland (Sun and Jahn, 1975).

The lead isotopic compositions of Reykjanes Ridge samples may be generated by two component mixing between: (1) a depleted MORB source and (2) an intermediate Icelandic source composition represented by basalts on the Reykjanes Peninsula. Binary mixing is suggested by the MORB samples from the Reykjanes Ridge because the data lie on linear trends in plots of $^{206}Pb/^{204}Pb$, $^{207}Pb/^{204}Pb$ and $^{208}Pb/^{204}Pb$ versus 1/Pb (Langmuir et al., 1978; Sun and Jahn, 1975).

Reykjanes Peninsula Icelandic samples

Previously, the available data from Icelandic picrites and N-MORBs (n = 50 samples) (North Atlantic plume-free MORB) appeared to define distinct, parallel fields in plots of $^{208}Pb/^{204}Pb$ versus $^{207}Pb/^{204}Pb$ (Fig. 4-7). The absence of overlap between the lead isotopic compositions from Icelandic basalts and MORBs made it unclear whether a MORB-source component contributed to the Icelandic plume (Elliott et al., 1991; Hards et al., 1995; Kerr et al., 1995; Langmuir et al., 1978; O'Nions et al., 1976; Schilling, 1973; Thirwall, 1995). Thus, two main models were developed for the observed Pb, Nd and Sr isotopic ratios in Icelandic basalts. One is that, like the Reykjanes Ridge MORB sample compositions, the isotopic compositions of Reykjanes Peninsula Icelandic samples may be generated by binary mixing between an incompatible element-enriched Icelandic plume component and a depleted MORB source (Elliott et al., 1991; Schilling, 1973; Schilling et al., 1982; Schilling et al., 1983; Sun et al., 1975). The second model is that MORB source material has not been entrained into the Icelandic plume. Instead, there may be three components: (1) a Reykjanes Peninsula source; (2) an alkali basalt source; and (3) a depleted source of different chemistry than that of the MORBs to the south of Iceland (Langmuir et al., 1978).

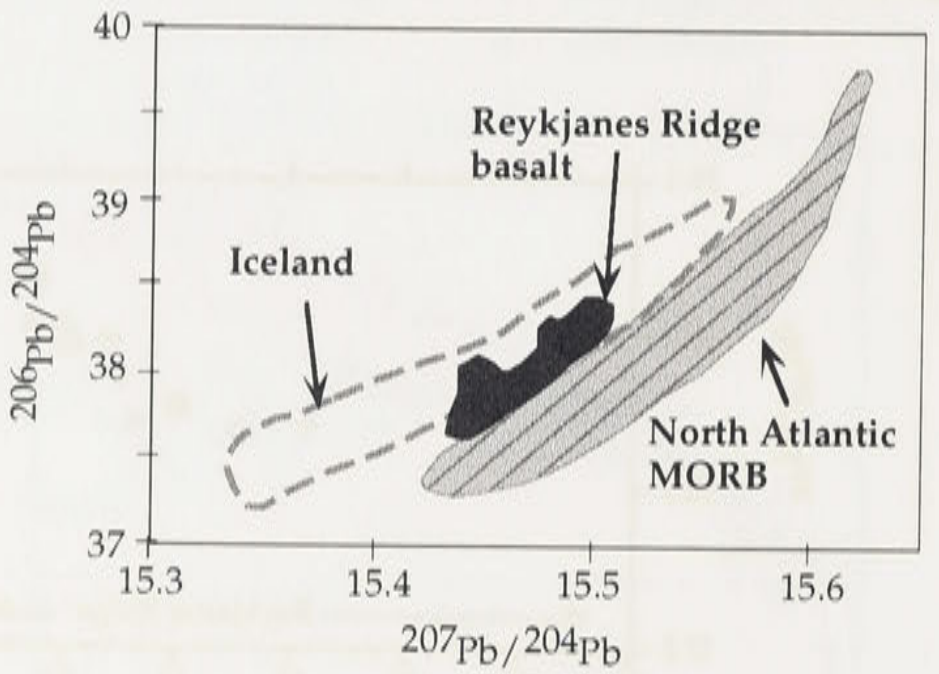

Figure 4-7. Plot of $^{207}Pb/^{204}Pb$ versus $^{208}Pb/^{204}Pb$, showing fields for Icelandic volcanic rocks and North Atlantic normal (N-type) MORB away from known mantle plumes and transform faults. This plot is based on data available as of 1995. There is no overlap between the lead isotopic compositions of Iceland and North Atlantic MORB, suggesting that Icelandic and MORB melts have not mixed. Sources for Reykjanes Ridge data: Sun et al., (1975), Hards et al., (1995) and references therein. After Kerr et al., (1995).

A recent study with a larger database (n = 180 N-MORB samples) has shown that there is significant overlap between the lead isotopic compositions of MORBs (0° to 53°N latitude, well south of the Icelandic plume) (Merz and Haase, 1997), and those of Icelandic basalts, including basalts from the Reykjanes Peninsula (Fig. 4-8A-3). The compositions of MORBs on the Reykjanes Ridge close to Iceland show even more overlap with the compositions of basalts from the Reykjanes Peninsula, Iceland, than do normal MORB. Similar overlaps between MORB and Icelandic compositions can also be seen in plots of $^{208}Pb/^{204}Pb$ and $^{207}Pb/^{204}Pb$ versus $^{206}Pb/^{204}Pb$ (Fig. 4-8A, 1-3), as well as $^{143}Nd/^{144}Nd$ versus $^{87}Sr/^{86}Sr$ (Merz and Haase, 1997) (Fig. 4-8B).

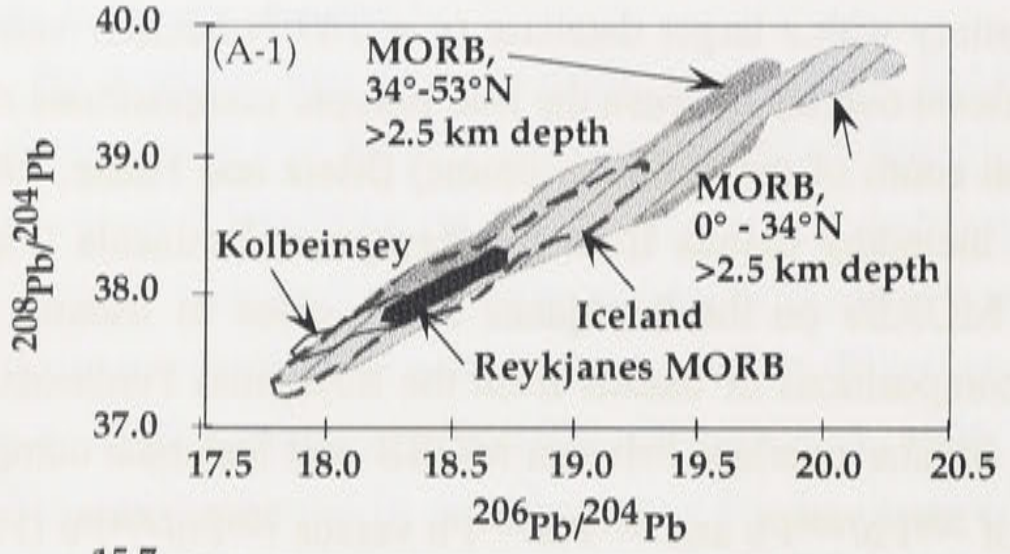

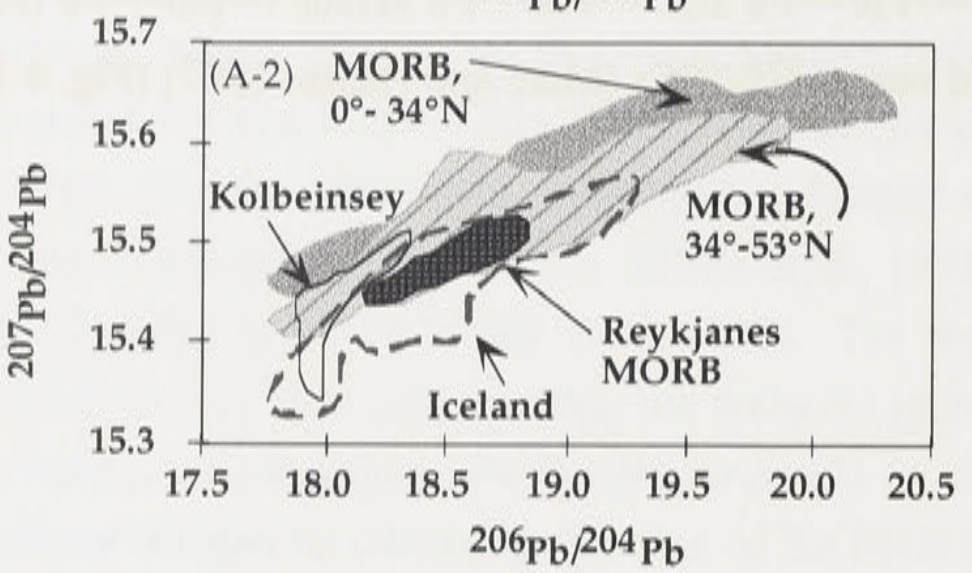

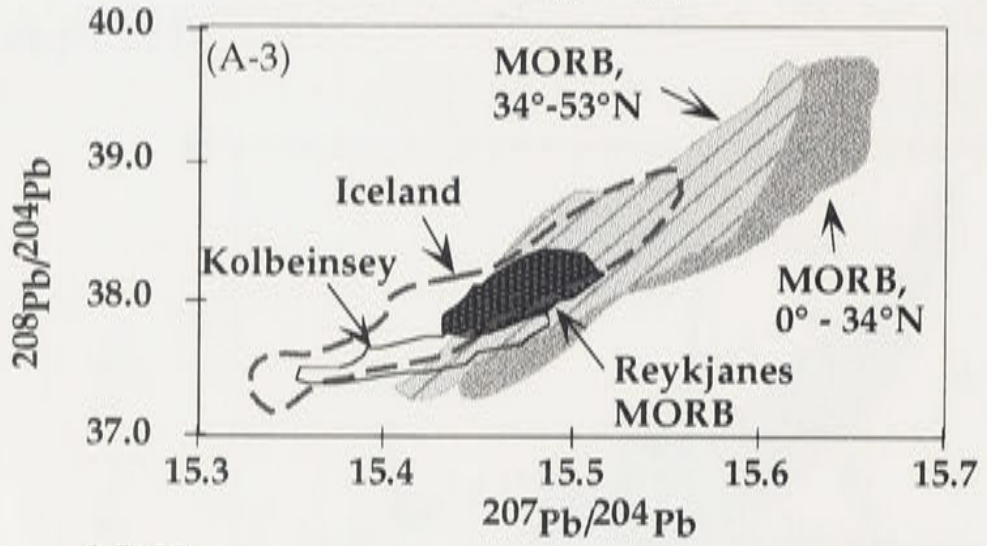

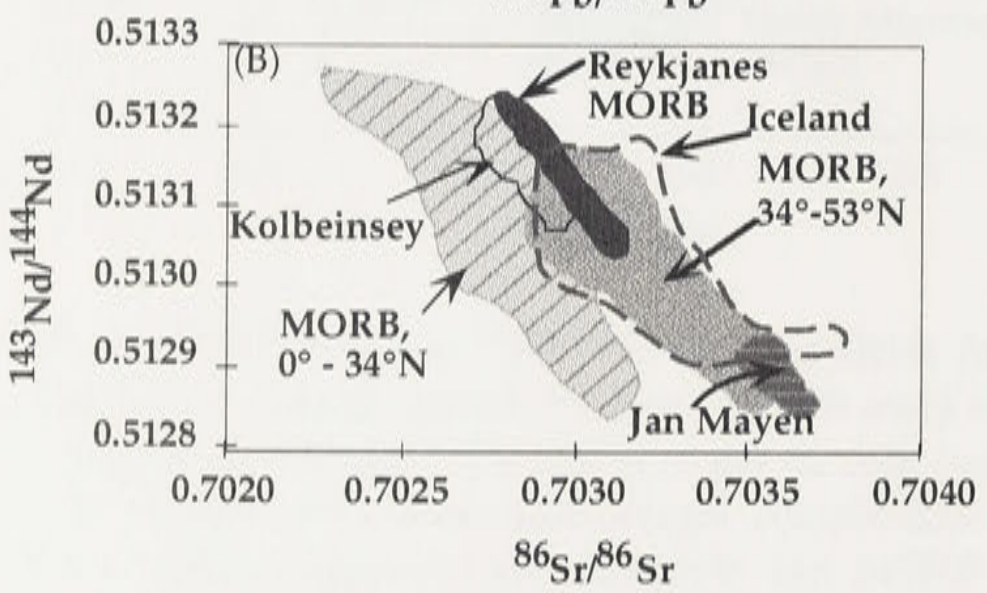

Figure 4-8A. (1) $^{208}Pb/^{204}Pb$ versus $^{206}Pb/^{204}Pb$. (2) $^{207}Pb/^{204}Pb$ versus $^{206}Pb/^{204}Pb$ (3) $^{208}Pb/^{204}Pb$ versus $^{207}Pb/^{204}Pb$. Pb isotope variations for North Atlantic lavas between the equator and 86° N latitude. **Figure 4-8B.** $^{143}Nd/^{144}Nd$ versus $^{87}Sr/^{86}Sr$ for lavas in the North Atlantic between the equator and 86°N latitude (Merz and Haase, 1997 and references therein). These plots show substantial overlap between the Pb, Sr, and Nd isotopic compositions of Icelandic basalts and MORBs (from a variety of locations, including Kolbeinsey, Jan Mayen, and other locations indicated by latititude).

Possible evidence for MORB-source involvement in the source of Icelandic basalts may be indicated by the overlap of MORB and Icelandic compositions in plots of Pb, Sr, and Nd isotopic compositions in the more recent, larger dataset (Merz and Haase, 1997) (Figs. 4-8A, B). There may be a third component in addition to the enriched plume component and the MORB component because the Icelandic data do not form linear trends in plots of $^{206}Pb/^{204}Pb$, $^{207}Pb/^{204}Pb$ and $^{208}Pb/^{204}Pb$ vs. 1/Pb (Langmuir et al., 1978). Irrespective of whether mixing occurs between two or three components, contribution of MORB-source material to Icelandic basalts cannot be excluded on the basis of Pb, Sr or Nd isotope plots (Merz and Haase, 1997). This conclusion is relevant to the discussion of noble gas results in subsequent chapters because it means that a MORB-type noble gas component may be regarded as a possible endmember that contributes to the noble gas signatures in Icelandic basalts.

4.3.2 Analytical results for samples from the present study

Trace element compositions of selected Icelandic samples

Eight Icelandic natural glass samples from picrites and tholeiite samples were analysed by LA-ICPMS to determine their Nb/U, Nb/Th, Ce/Pb (see Chapter 3) and other trace element composition. The details of analytical methods are shown in Appendix 2. Note that natural glasses may contain some olivine microphenocrysts that retain trace elements, and these phases have not been homogenized by melting the whole rock. This may create trace element anomalies that are not present in results of whole-rock analyses. The results of the analyses are shown in Table 4-2.

Table 4-2. Trace element compositions in Icelandic natural basaltic glasses

in ppm	Rb	Sr	Y	Zr	Nb	Cs	Ba	La	Ce	Nd	Sm	Eu	Gd	Ho	Yb	Hf	Ta	Pb	Th	U
ice-9	n.a.	n.a.	n.a.	n.a.	0.8	n.a.	n.a.	n.a.	n.a.	n.a.	n.a.	n.a.	n.a.	n.a.	n.a.	n.a.	0.05	0.23	0.0356	0.0117
– (N=5)					0.1												0.00	0.04	0.0005	0.0003
ice-9	0.34	121.1	13.7	18.0	0.86	0.0038	6.3	0.89	2.79	2.98	1.24	0.55	1.77	0.472	1.32	0.63	0.053	0.08	0.0359	0.012
– (N=3)	0.01	0.9	0.2	0.4	0.04	0.0007	0.1	0.03	0.07	0.06	0.02	0.01	0.03	0.004	0.02	0.02	0.002	0.06	0.0002	0.001
ice-18	6.96	215	24.9	103.2	17.3	0.077	82.0	10.46	24.8	15.2	3.96	1.39	4.32	0.861	2.257	2.58	0.991	0.70	0.68	0.211
– (N=3)	0.01	1	0.2	0.6	0.1	0.002	0.8	0.07	0.2	0.1	0.05	0.02	0.05	0.010	0.010	0.02	0.002	0.02	0.01	0.002
ice-32.2	4.7	237	26.2	108	17.1	0.051	69	10.1	24.5	15.6	4.17	1.51	4.60	0.91	2.33	2.70	0.98	0.56	0.50	0.164
– (N=3)	0.1	2	0.8	3	0.6	0.004	2	0.3	0.7	0.5	0.14	0.05	0.10	0.03	0.09	0.09	0.03	0.05	0.02	0.005
ice-41	5.3	153	39.1	117	10.9	0.057	46.9	8.2	20.6	14.6	4.56	1.61	5.7	1.36	3.77	3.15	0.67	0.86	0.68	0.211
– (N=3)	0.1	2	0.7	2	0.2	0.003	0.9	0.2	0.4	0.4	0.07	0.05	0.1	0.03	0.08	0.06	0.02	0.03	0.03	0.005
ice-46	4.61	169	28.5	94	9.3	0.045	42.8	7.00	17.5	12.1	3.63	1.33	4.433	1.00	2.711	2.50	0.565	0.67	0.570	0.1808
– (N=3)	0.08	2	0.3	1	0.1	0.004	0.5	0.07	0.2	0.1	0.04	0.01	0.009	0.02	0.005	0.04	0.005	0.02	0.006	0.0009
ice-47	4.51	169	28.8	94.6	9.30	0.044	43.1	7.08	17.6	12.2	3.69	1.34	4.47	1.011	2.74	2.524	0.583	0.62	0.573	0.182
– (N=3)	0.09	2	0.2	0.6	0.07	0.001	0.3	0.06	0.2	0.1	0.02	0.02	0.05	0.008	0.03	0.009	0.008	0.01	0.009	0.003
ice-54	11.8	262	24.6	115	21.7	0.136	141	15.2	34.1	19.0	4.5	1.50	4.56	0.86	2.22	2.81	1.26	1.26	1.26	0.39
– (N=3)	0.3	2	0.6	3	0.5	0.004	4	0.3	0.9	0.5	0.1	0.04	0.09	0.01	0.04	0.07	0.03	0.04	0.03	0.01
ice-55	5.43	209.1	24.9	89.2	13.72	0.058	72.7	9.04	21.51	13.82	3.74	1.35	4.24	0.88	2.30	2.34	0.82	0.831	0.590	0.187
– (N=3)	0.01	0.7	0.2	0.7	0.02	0.002	0.1	0.02	0.03	0.09	0.04	0.01	0.04	0.01	0.02	0.04	0.01	0.005	0.010	0.002

n.a. = not analysed

A primitive mantle-normalised trace element diagram shows the range in incompatible element compositions from this study (Fig. 4-9). Most olivine tholeiite samples from this study have relatively flat trace element patterns that are similar to those found in previous studies of Icelandic tholeiitic basalts described above. These samples are enriched in incompatible elements relative to N-MORB (Fig. 4-5). Sample *ice-9g* is the only picritic sample analysed for trace elements from this study, and is depleted in incompatible elements compared with N-MORB. Its composition is similar to compositions found previously for other primitive lavas from the Reykjanes Peninsula (Hemond et al., 1993; Sigurdsson, 1994) (Figs. 4-4A, B). As seen in the primitive samples from Hemond et al. (1993) (Fig. 4-4A), *ice-9g* has positive anomalies in Ba, Nb and Sr (and possibly Pb in the analysis with longer count times, but this anomaly is not seen in previous trace element analyses of Icelandic basalts and requires authentication). In addition, there are also negative anomalies in Zr and Hf in *ice-9g*. In comparison, other, more enriched samples from this study have positive anomalies in Nb and Ta, but little or no anomalies in Ba, Sr, Zr, or Hf.

The observed positive anomalies in Ba and Sr in the most incompatible element depleted sample from this study (*ice-9g*) may be caused by assimilation of hydrothermal water bearing these elements into the magma, as described previously (Hemond et al., 1993). The negative anomalies in Zr and Hf could result from substitution of these elements into Cr-spinel that was not homogenized into the glass. Zirconium and Hf are known to also substitute for Ti in titanite and rutile (Wilson, 1989). Niobium also behaves compatibly in Ti-bearing phases, as seen in arc-settings (see Chapter 3). However, in the Icelandic samples, there is no negative Nb anomaly, suggesting that Ti-bearing phases are not responsible for the observed Zr and Hf anomalies.

Positive anomalies in Nb and Ta are seen in transitional-type MORBs and some N-type MORBs with light rare earth element (REE)-depleted to slightly enriched patterns (Sun and McDonough, 1989). Such anomalies have been interpreted to result from recycling and resorption of former oceanic crust into the oceanic mantle source of MORBs. In the tholeiitic samples from this study, there are pronounced Nb and Ta anomalies, but there does not appear to be a Ta anomaly in the picritic sample. Although the Ta anomaly is potentially important and interesting, because it is not observed in other tholeiitic samples from Iceland, such as in Hemond et al. (1993) (Fig. 4-4A) it should be treated with a certain degree of caution until it can be authenticated.

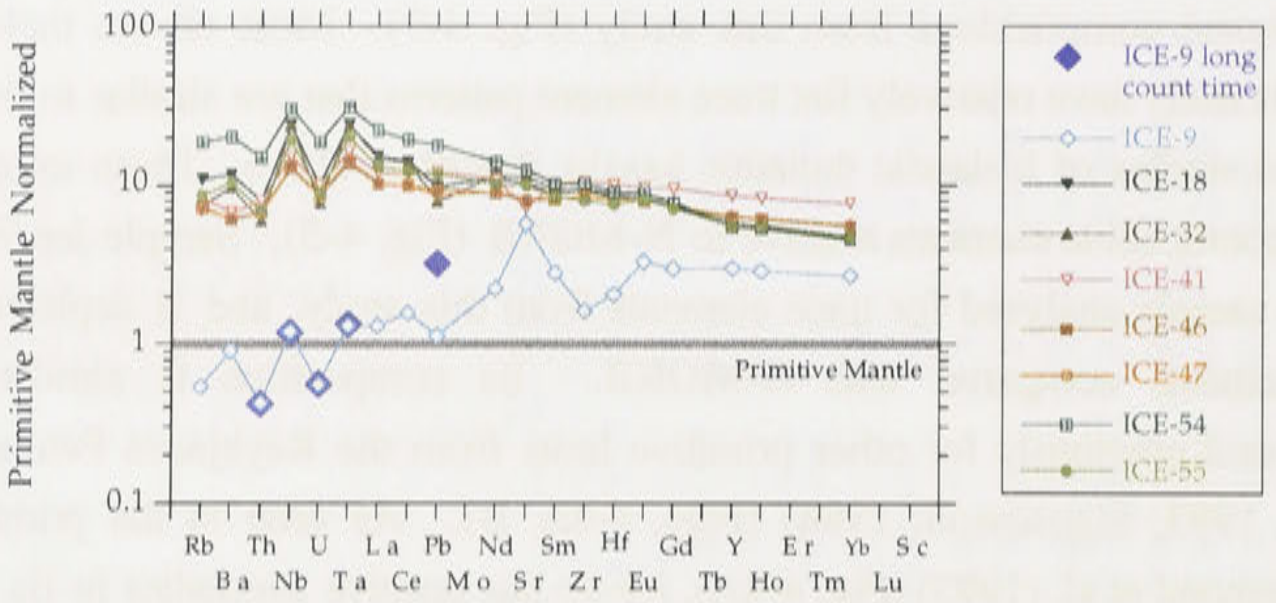

Figure 4-9. Trace element variation in Icelandic basalts, normalized to the primitive mantle composition (McDonough and Sun, 1995) (similar to primitive mantle of (Sun and McDonough, 1989)). Most of the samples from this study (excluding *ice-9g*) have trace element abundance patterns that are similar to that of Hawaiian tholeiitic basalts in Figure 4-5. These samples are enriched in incompatible elements compared with the primitive mantle and N-MORBs. Sample *ice-9g* is the most incompatible element-depleted sample from this study, but is similar to primitive samples from previous studies (Hemond et al., 1993; Sigurdsson, 1994). This sample has positive anomalies in Nb, Sr and Ba, and negative anomalies in Hf and Zr. The other samples from this study have positive Nb and Ta anomalies, but less pronounced Ba anomalies, and no Sr, Hf and Zr anomalies. The Pb anomaly in sample *ice-9g* (long count time) is not seen in previous trace element results from Reykjanes Peninsula basalts and requires further authentication.

Incompatible element ratios

There is a wide range of values in the incompatible element ratios, Nb/U, Nb/Th and Ce/Pb, in the eight Icelandic basalts from this study. A similar range was also reported, but not discussed, in a previous study of Icelandic basalts by Hemond et al. (1993). The Nb/U and Nb/Th ratios from this study are linearly correlated over a large range, from Nb/U of 51 to 104 (Table 4-2), and Nb/Th from 16 to 34 (Fig. 4-10). The Nb/U ratios are also linearly correlated with Ce/Pb, which ranges from 24 to 36 (Fig. 4-11). The niobium, uranium and thorium data reported by Hemond et al. (1993) were determined using XRD analyses of fused glasses from whole rock samples. These data lie on the same trend, and have similar maximum ratios, as the data from this study (Fig. 4-10). In comparison, the Nb/U, Nb/Th and Ce/Pb ratios in OIBs and MORBs are generally fairly constant (Nb/U = 47 ± 10, Nb/Th = 15 ± 2, Ce/Pb = 25 ± 5) (Hofmann et al., 1986; Jochum et al., 1983) (see Chapter 3). The Th/U ratios of MORBs and OIBs are also generally similar, and have average values of 2.55 and 3.33, respectively (Sun and McDonough, 1989).

The large range in Nb/U, Nb/Th and Ce/Pb ratios observed in Icelandic basalts (Figs. 4-10 and 4-11) is unexpected for oceanic basalts (Hofmann et al., 1986). The linear correlation in Nb/U versus Nb/Th ratios (Figure 4-10) arises in part from the nearly constant Th/U ratios, which only range between 3.05 to 3.23 for the data from this study. These Th/U ratios are between the average values from MORBs (2.55) and OIBs (3.33) (Sun and McDonough, 1989). Despite their near-constant Th/U ratios, most MORBs and OIBs do not have a large range in Nb/U and Nb/Th (or Ce/Pb) ratios, suggesting that additional processes may be involved to produce the observed range in ratios in Icelandic basalts.

Hofmann et al. (1986) suggested that the relatively homogeneous Nb/U, Nb/Th and Ce/Pb ratios in OIBs and MORBs may be explained if the differentiated parts of the mantle, that were chemically depleted after formation of the continental crust, were subsequently internally rehomogenized. This relatively depleted, but chemically homogeneous, mantle was then differentiated into MORB and OIB source regions by formation and subduction of oceanic crust. The primary (continental crust-mantle) differentiation is postulated to have fractionated the Nb/U and Ce/Pb ratios. This is because during the primary differentiation, U is thought to have been more incompatible than Nb, and Pb more incompatible than Ce (Hofmann et al., 1986). In contrast, during the secondary (MORB source-OIB source) differentiation, the bulk parition coefficients of U and Pb are believed to have been similar to those of Nb and Ce, respectively (Hofmann et al., 1986) (see Chapter 3). Hoffmann et al. (1986) concluded on the basis of the homogeneous incompatible element ratios in OIBs and MORBs that OIBs cannot be derived from a primitive portion of the mantle, from mixtures of primitive and depleted mantle, or from recycled continental crust.

The large range in Nb/U, Nb/Th and Ce/Pb ratios suggests that the mantle sampled by the Icelandic plume is heterogeneous in terms of incompatible element ratios. In contrast to the interpretation by Hoffmann et al. (1986), the heterogeneous Nb/U, Nb/Th and Ce/Pb ratios in Icelandic basalts may suggest that some parts of the mantle sampled by Icelandic plume have not been completely homogenized following crustal extraction. The calculated theoretical Nb/U ratio for the upper mantle following crustal extraction is 152 (Sun and McDonough, 1989). The maximum Nb/U ratio from Icelandic basalts near 100 (Fig. 4-10) is intermediate between this calculated value and the average observed ratio in most oceanic basalts (approximately 50). The large range in Nb/U, Nb/Th, and Ce/Pb ratios may suggest that the mantle sampled by the Icelandic plume has not been well-stirred into the ambient mantle (MORB or OIB source material with Nb/U = ~50) following crustal extraction.

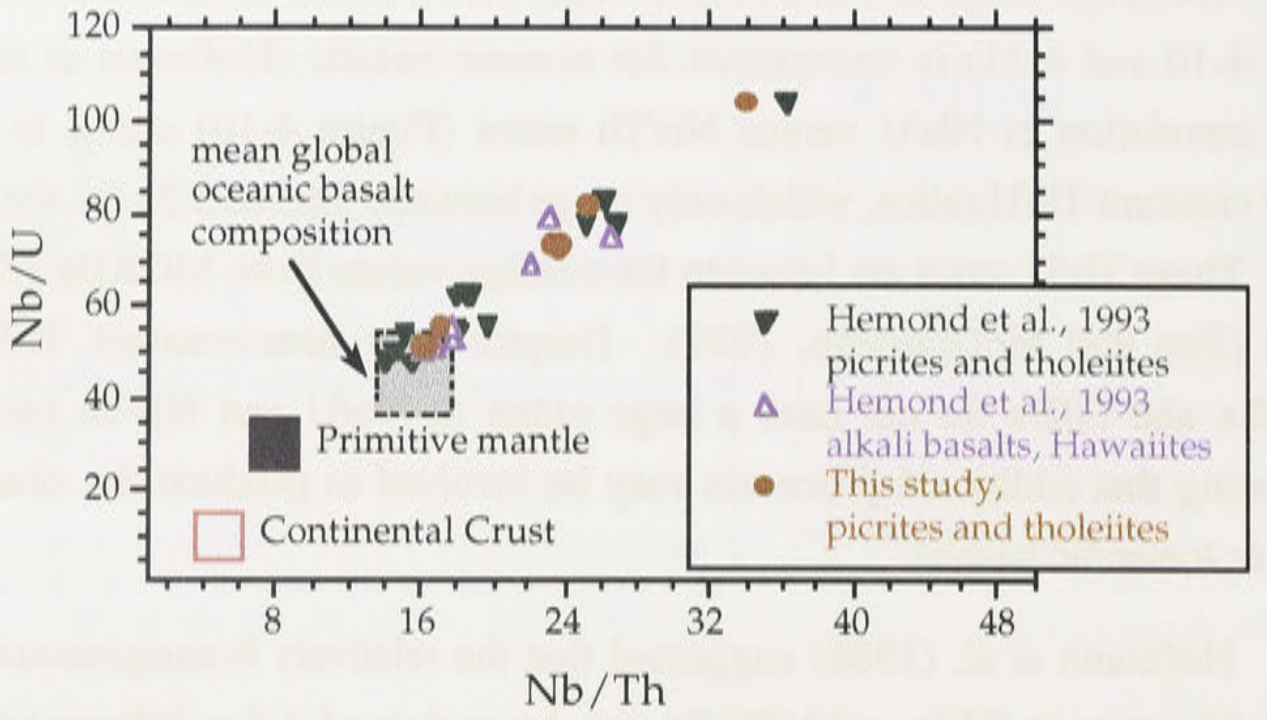

Figure 4-10. Nb/U versus Nb/Th ratios of Icelandic picrites and tholeiites from this study and that of Hemond et al.(1993). The Nb/U data from both studies extend from typical mantle basalt values of 47 ± 10 (Hofmann et al., 1986) to maximum values near 100, and the Nb/U ratios from 14 to 36. The compositions of OIBs, primitive mantle, and continental crust are shown for reference. The source of Icelandic basalts is evidently heterogeneous in terms of incompatible element ratios.

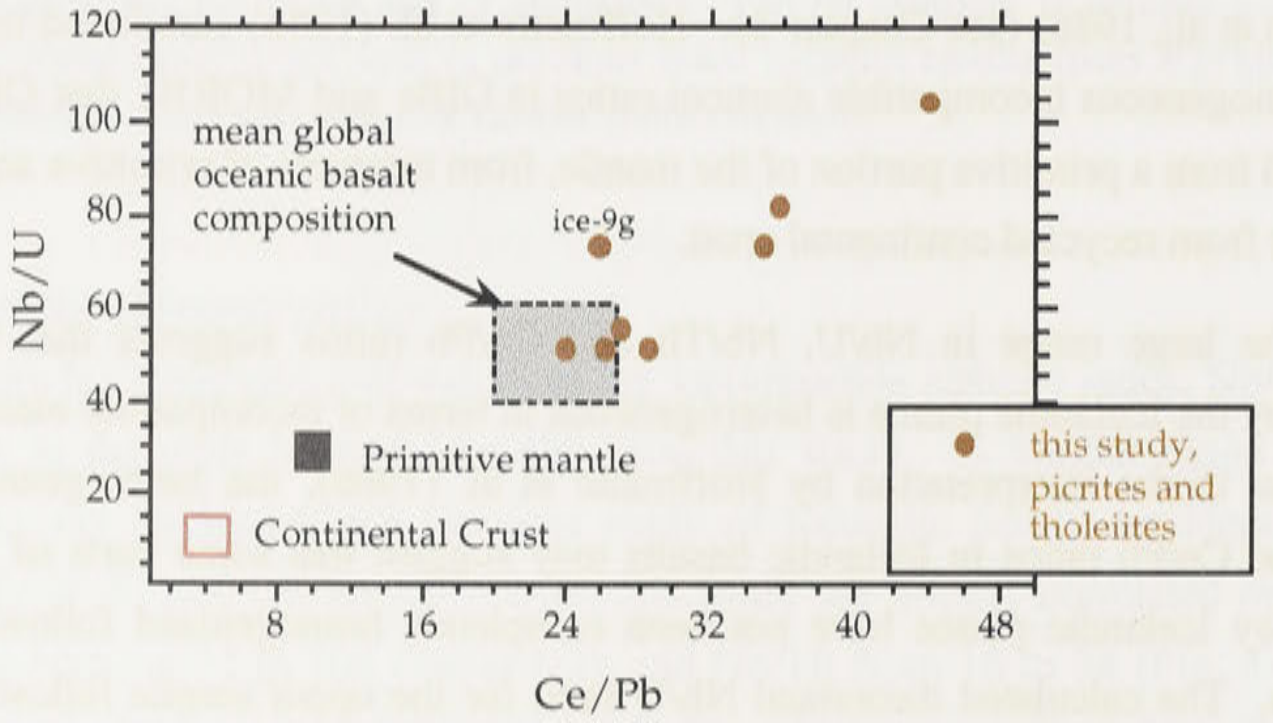

Figure 4-11. Plot of Nb/U versus Ce/Pb, showing the data from this study. The compositions of mean global oceanic basalt, the postulated primitive mantle, and the continental crust are also shown (Hofmann et al., 1986). The composition of sample *ice-9g* lies off the main trend formed by the other Icelandic data. This is because this sample is very depleted in incompatible elements compared with the other Icelandic samples, but unlike Nb and U, Ce and Pb were not counted for long time-periods. The Nb/U ratio is likely to be accurate, but the Ce/Pb ratio may not be.

The relationship between the noble gas isotopic compositions and incompatible elements may depend on the their behaviour under different pressure and temperature conditions during mantle melting. The noble gas isotopic ratio would not necessarily be expected to co-vary linearly (i.e., to be coupled with) with the Nb/U, Nb/Th or Ce/Pb ratios for two reasons: (1) the elemental ratio of the gaseous to the non-gaseous species may vary (e.g., [Ne]/[Nb], [He]/[U]) owing to partial melting, diffusion or solubility controlled fractionation during magmatic ascent (see Chapter 2); (2) there may be more than one mantle end-member present (e.g., MORB and OIB), so that the [noble gas]/[trace element] ratio in the mixture varies. Additional complexity may be introduced by the presence of more than two mantle components in the mixture.

4.4 Summary

Icelandic basalts have lead, strontium and neodymium isotopic ratios that overlap the compositions of MORBs that are free from the influence of plume melts. Thus, it is possible that addition of a MORB-derived component to the Icelandic plume may contribute to the observed heterogeneity in the isotopic ratios of Icelandic basalts. The Icelandic tholeiites and picrites are heterogeneous in terms of Nb/U, Ce/Pb and Nb/Th ratios. This may imply that, in contrast to previous interpretations based on OIBs and MORB data, the mantle that is sampled by the Icelandic plume has not been completely re-homogenized following continental crust extraction. These factors may influence the noble gas isotopic compositions in Icelandic basalts. However, owing to the differences in behaviour of noble gases compared with other elements during melting, crystallization, and bubble formation, incompatible element ratios and Pb, Sr and Nd isotopic ratios are unlikely to be linearly correlated with noble gas isotopic ratios.

4.5 References

Bijwaard H. (1999) Tomographic evidence for a narrow whole mantle plume below Iceland. *Earth and Planetary Science Letters* **166**, 121-126.

Carroll M. R. and Draper D. S. (1994) Noble gases as trace elements in magmatic processes. *Chemical Geology* **117**, 37-56.

Elliott T. R., Hawkesworth C. J., and Gronvold K. (1991) Dynamic melting of the Iceland plume. *Nature* **351**, 201-206.

Fridleiffson I. B. (1977) Distribution of large basaltic intrusions in the Icelandic crust and the nature of the layer 2-layer 3 boundary. *Geological Society of America Bulletin* **88**, 1689-1693.

Green D. H. (1970) The origin of basaltic and nephelenitic lavas. *Transactions of the Leiscester Literary and Philosophical Society* **64**, 28-54.

Griffiths R. W. and Campbell I. H. (1990) Stirring and structure in mantle starting plumes. *Earth and Planetary Science Letters* **99**, 66-78.

Gudmundsson A. (1998) Magma chambers modeled as cavities explain the formation of rift zone central volcanoes and their eruption and intrusion statistics. *Journal of Geophysical Research* **103**(B4), 7401-7412.

Hansteen T. H. (1991) Multi-stage evolution of the picritic Maelifell rocks, SW Iceland: constraints from mineralogy and inclusions of glass and fluid in olivine. *Contributions to Mineralogy and Petrology* **109**, 225-239.

Hardarson B. S. and Fitton J. G. (1997) Mechanisms of crustal accretion in Iceland. *Geology* **25**, 1043-1046.

Hards V. L., Kempton P. D., and Thompson R. N. (1995) The heterogeneous Iceland plume: new insights from the alkaline basalts of the Snaefell volcanic centre. *Journal of the Geological Society, London* **152**, 1003-1009.

Harrison D., Burnard P., and Turner G. (1999) Noble gas behaviour and composition in the mantle: constraints from the Iceland plume. *Earth and Planetary Science Letters* **171**, 199-207.

Hart S. R., Schilling J.-G., and Powell J. L. (1973) Basalts from Iceland and along the Reykjanes Ridge: Sr isotope geochemistry. *Nature* **246**, 104-107.

Helmberger D. V., Wen L., and Ding X. (1998) Seismic evidence that the source of the Iceland hotspot lies at the core-mantle boundary. *Nature* **396**, 251-255.

Hemond C., Arndt N. T., Lichtenstein U., and Hofmann A. (1993) The heterogeneous Iceland Plume: Nd-Sr-O isotopes and trace element constraints. *Journal of Geophysical Research* **98**, 16833-15850.

Hofmann A. W., Jochum K. P., Seufert M., and White W. M. (1986) Nb and Pb in oceanic basalts: new constraints on mantle evolution. *Earth and Planetary Science Letters* **79**, 33-55.

Jakobsson S. P., Jonsson J., and Shido F. (1978) Petrology of the Western Reykjanes Peninsula, Iceland. *Journal of Petrology* **19**(4), 669-705.

Jochum K. P., Hofmann A. W., Ito E., Seufert H. M., and White W. M. (1983) K, U, and Th in mid-ocean ridge basalt glasses and heat production, K/U and K/Rb in the mantle. *Nature* **306**, 431-436.

Jull M. and McKenzie D. (1996) The effect of deglaciation on mantle melting beneath Iceland. *Journal of Geophysical Research* **101**, 21,815-21,828.

Kerr A. C., Saunders A. D., Tarney J., Berry N. H., and Hards V. L. (1995) Depleted mantle-plume geochemical signatures: no paradox for plume theories. *Geology* **23**, 843-846.

Langmuir C. H., Jr. R. D. V., Hanson G. N., and Hart S. R. (1978) A general mixing equation with applications to Icelandic basalts. *Earth and Planetary Science Letters* **37**, 380-392.

McDonough W. F. and Sun S.-s. (1995) The composition of the Earth. *Chemical Geology* **120**, 223-253.

McDougall I., Kristjansson L., and Saemundsson K. (1984) Magnetostratigraphy and geochronology of northwest Iceland. *Journal of Geophysical Research* **89**, 7029-7060.

McDougall I., Watkins N. D., Walker G. P. L., and Kristjansson L. (1976) Potassium-argon and paleomagnetic analysis of Icelandic lava flows: limits on the age of Anomaly 5. *Journal of Geophysical Research* **81**, 1505-1512.

McKenzie D. and Bickle M. J. (1988) The volume and composition of melt generated by extension of the lithosphere. *Journal of Petrology* **29**, 625-679.

McKenzie D. P. (1984) The generation and compaction of partial molten rock. *Journal of Petrology* **25**, 713-765.

Merz D. F. and Haase K. M. (1997) The radiogenic isotope composition of the high-latitude North Atlantic mantle. *Geology* **25**, 411-414.

Moorbath S., Sigurdsson H., and Goodwin R. (1968) K-Ar ages of the oldest exposed rocks in Iceland. *Earth and Planetary Science Letters* **4**, 197-205.

O'Nions R. K., Pankhurst R. J., and Gronvold K. (1976) Nature and development of basalt magma sources beneath Iceland and the Reykjanes Ridge. *Journal of Petrology* **17**, 315-338.

Oskarsson N., Steinthorsson S., and Sigvaldason G. E. (1985) Iceland geochemical anomaly: origin, volcanotectonics, chemical fractionation and isotope evolution of the crust. *Journal of Geophysical Research* **90**, 10011 - 10025.

Risku-Norja H. (1985) Gabbro nodules from a picritic pillow basalt, Midfell, SW Iceland. *Nordic Volcanological Institute Professional Paper* **8501**.

Saemundsson K. (1978) Fissure swarms and Central volcanoes of the neovolcanic zones of Iceland. In *Crustal evolution in northwestern Britain and adjacent regions*, Vol. 10 (ed. D. R. Bowes and B. E. Leake), pp. 415-432. Geological Journal Special Issue.

Schilling J.-G. (1973) Iceland mantle plume: geochemical evidence along Reykjanes Ridge. *Nature* **242**, 565-571.

Schilling J.-G., Meyer P. S., and Kingsley R. H. (1982) Evolution of the Iceland hotspot. *Nature* **296**, 313-320.

Schilling J. G., Zajac M., Evans R., Johnston T., White W., Devine J. D., and Kingsley R. (1983) Petrologic and geochemical variations along the Mid-Atlantic Ridge from 29 N to 73N. *American Journal of Science* **283**, 510-586.

Shen Y., Solomon S. C., Bjarnason I. T., and Wolfe C. J. (1998) Seismic evidence for a lower-mantle origin of the Iceland plume. *Nature* **395**, 62-65.

Sigmundsson F. (1991) Post-glacial rebound and asthenosphere viscosity in Iceland. *Geophysical Research Letters* **18**, 1131-1134.

Sigurdsson I. A. (1994) Primitive magmas in convergent margins and at oceanic spreading ridges: evidence from early formed phenocryst phases and their melt inclusions. Ph.D. dissertation, University of Tasmania, 243 pages.

Smallwood J. R., White R. S., and Minshull T. A. (1995) Sea-floor spreading in the presence of the Iceland plume: the structure of the Reykjanes Ridge at 61°40'N. *Journal of the Geological Society, London* **152**, 1023-1029.

Sun S.-s. and Jahn B.-m. (1975) Lead and strontium isotopes in post-glacial basalts from Iceland. *Nature* **255**, 527-530.

Sun S.-s. and McDonough W. F. (1989) Chemical and isotopic systematics of oceanic basalts: implications for mantle composition and processes. In *Magmatism in ocean basins*, Vol. 42 (ed. A. D. Saunders and M. J. Norry), pp. 313-345, London.

Sun S.-s., Tatsumoto M., and Schilling J.-G. (1975) Mantle plume mixing along the Reykjanes Ridge axis: lead isotopic evidence. *Science* **190**, 143-147.

Thirwall M. F. (1995) Generation of the Pb isotopic characteristics of the Iceland plume. *Journal of the Geological Society, London* **152**, 991-996.

Tronnes R. G. (1990) Basaltic melt evolution of the Hengill volcanic system, SW Iceland, and evidence for clinopyroxene assimilation in primitive tholeiitic magmas. *Journal of Geophysical Research* **95**, 15,893-15,910.

White R. S., Bown J. W., and Smallwood J. R. (1995) The temperature of the Iceland plume and origin of outward-propagating V-shaped ridges. *Journal of the Geological Society, London* **152**, 1039-1045.

Wilson M. (1989) *Igneous Petrogenesis*. Chapman & Hall Australia. Melbourne. pp 466.

CHAPTER 5: PREVIOUS AND NEW NOBLE GAS RESULTS FROM ICELANDIC BASALTS

5.1 Introduction

Previous studies of Icelandic basalts revealed high $^{3}He/^{4}He$ ratios of up to 37 ± 2 Ra (Hilton et al., 1999) that exceed the maximum ratios measured in Hawaiian basalts (ca. 30 Ra). The relatively high $^{3}He/^{4}He$ ratios in Icelandic samples, together with other geochemical factors, suggest Icelandic basalts originated from a plume rather than a mid-ocean ridge basalt (MORB) source (Schilling, 1973). The characteristically primitive neon isotopic ratios found in Hawaiian basalts are expected owing to the coupling of helium and neon isotope systematics in the mantle (Honda et al., 1993b). For this reason, relatively primitive neon isotopic ratios are also expected in Icelandic basalts. The degree of noble gas isotopic heterogeneity recorded at geographically distinct localities such as Iceland, Hawaii, Reunion, and Samoa may help us to understand the extent of mantle degassing and stirring over the course of the Earth's history. Thus, one of the primary aims of this study was to determine whether Icelandic basalts have primitive neon isotopic ratios.

This chapter presents the helium, neon, argon, krypton and xenon isotopic ratios determined on gas extracted from olivine and glass separates from young and relatively primitive Icelandic picrites and tholeiitic basalts. As will be shown in this chapter, the neon isotopic ratios from some Icelandic samples are more solar-like than those found in Hawaiian basalts.

5.1.1 Previous noble gas investigations in Iceland and adjacent Mid-Atlantic Ridge

Helium

The $^{3}He/^{4}He$ ratios of basaltic samples from along the Mid-Atlantic Ridge (MAR) to the north (Kolbeinsey Ridge) and south (Reykjanes Ridge) of Iceland increase with proximity to Iceland (Poreda et al., 1986). In the south, they increase from values of about 9.3 Ra that are close to typical MORB ratios (8.5 Ra) at 53°N to a maximum of 16

Ra just south of the Reykjanes Peninsula, and suggest that close to Iceland, a higher proportion of plume derived He, with high $^3He/^4He$ ratios, has mixed with MORB-derived He (Poreda et al., 1986).

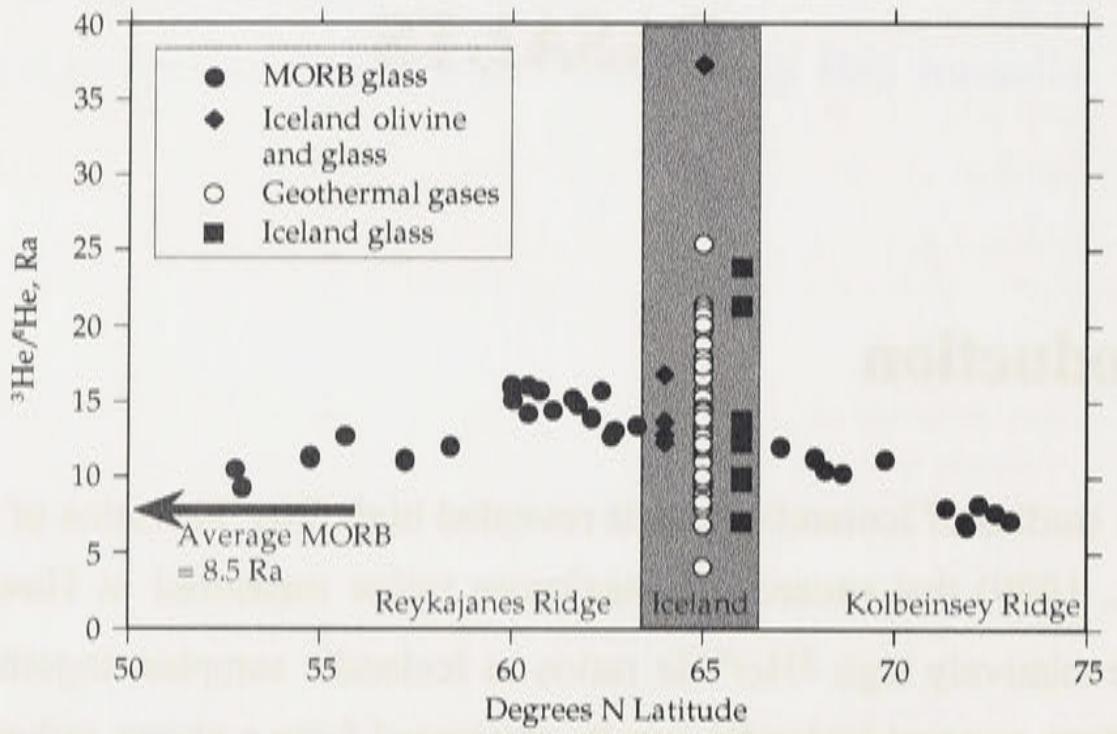

Figure 5-1. Published $^3He/^4He$ ratios from Iceland and the adjacent Mid-Atlantic Ridges to the south (Reykjanes Ridge) and north (Kolbeinsey Ridge) of Iceland (Burnard et al., 1994; Hilton et al., 1999; Hilton et al., 1990; Hilton et al., 1998; Poreda et al., 1986).

Helium studies of basaltic and geothermal Icelandic samples from the Reykjanes Peninsula (western neo-volcanic zone, NVZ), the eastern NVZ and northern NVZ (see Chapter 4) (Burnard et al., 1994; Condomines et al., 1983; Harrison et al., 1999; Hilton et al., 1990; Kurz et al., 1985; Sano et al., 1985; Trieloff et al., 2000) showed a large range in $^3He/^4He$ ratios ($2 < Ra < 30$). Most samples from the Reykjanes Peninsula, where the majority of the samples from the present study were collected, have $^3He/^4He$ ratios that are similar to the maximum value (17 Ra) from MORB samples obtained along the Reykjanes Ridge closest to Iceland (Fig. 5-1). The maximum $^3He/^4He$ ratio of 37 ± 2 Ra reported so far for Iceland (Fig. 5-2) is from crushed olivine separates from samples obtained from the north-west peninsula (Vestfidir area) of Iceland (Hilton et al., 1999). High $^3He/^4He$ ratios of near 30 Rc/Ra (Rc = air-corrected) have been measured in hydrothermal water from the Vestfidir Peninsula area in northwest Iceland (Hilton et al., 1998). The most active volcanism in Iceland is occurring beneath Vatnajokull (see Fig. 4-1) at Grimsvötn, where $^3He/^4He$ ratios are ~19 Rc/Ra (Hilton et al., 1990). Evidently, from comparison of the $^3He/^4He$ ratios from the Vestfidir region with those from Grimsvötn, the maximum measured $^3He/^4He$ ratios are not necessarily focused at the location of greatest volcanic activity. Lower $^3He/^4He$ ratios of near 5 Ra have been measured in geothermal samples and intermediate and silicic volcanic glasses. These low $^3He/^4He$ ratios have been interpreted to result from release of radiogenic ^4He from the

uppermost basaltic crust into the water or magma (Condomines et al., 1983; Hilton et al., 1998). Whether crustal contamination is the main factor responsible for the heterogeneous $^3He/^4He$ ratios has been debated; such variations in the $^3He/^4He$ ratios may alternatively be regarded as reflecting heterogeneities in the mantle beneath Iceland (Kurz et al., 1985). The lowest $^3He/^4He$ ratios measured in Icelandic samples of near 1 to 4 Ra are from melted olivine powders residual from crushing experiments (Hilton et al., 1999). The helium in the olivine matrix was interpreted to be predominantly radiogenic ^4He, but its origin was not explained (Hilton et al., 1999).

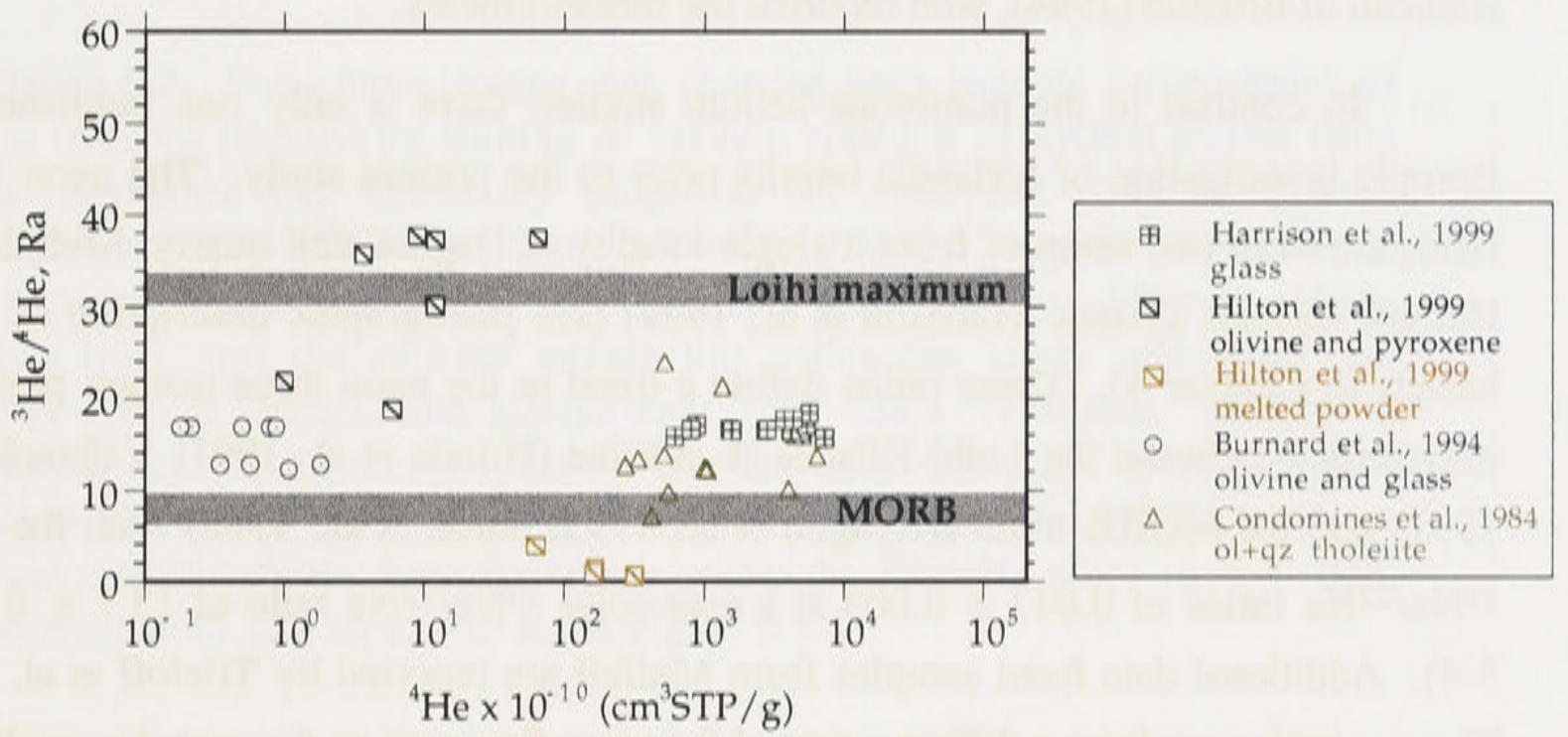

Figure 5-2. Published $^3He/^4He$ versus ^4He concentrations in Icelandic phenocryst and glass samples. The $^3He/^4He$ ratios from geothermal gases and water samples in Fig. 5-1 are not shown here. A crushed olivine sample from the Vestfidir Peninsula has the highest $^3He/^4He$ ratio measured from a mantle plume of 37 ± 2 (Hilton et al., 1999). The powder residual from crushing the phenocrysts has ratios that are lower than the MORB ratio, from 1.0 ± 0.3 to 3.9 ± 0.3 Ra. The lower $^3He/^4He$ ratios from the powders have been interpreted to result from a radiogenic component of ^4He in the crystal lattice (Hilton et al., 1999). Samples from the Reykjanes Peninsula (Burnard et al., 1994; Harrison et al., 1999) have $^3He/^4He$ ratios between 10 and 20 Ra. Samples from the Reykjanes Peninsula analysed by Condomines et al. (1983) are between 12 to 24 Ra, and extend to lower values (7 Ra) in basaltic samples from the northern NVZ (ol = olivine, qz = quartz).

Neon

Owing in part to atmospheric contamination, neon analyses of MORB glasses from the Reykjanes and Kolbeinsey Ridges do not display the systematic variation with proximity to Iceland that is seen in the $^{3}He/^{4}He$ ratios. Most of the neon isotopic ratios from 60 to 62.7°N latitude scatter about the MORB correlation line (Fig. 5-3). Two MORB glass samples from 57°14 N and 58°25 N latitude have neon isotopic ratios that lie within one sigma of the air-solar mixing line and are distinct from the atmospheric composition by more than two sigma. The significance of these data having compositions on or near the air-solar mixing line was not discussed by Poreda and Radicati di Brozolo (1984), who reported the measurements.

In contrast to the numerous helium studies, there is only one published neon isotopic investigation of Icelandic basalts prior to the present study. The neon isotopic ratios are from two samples from a single locality at Dagmalafell quarry, Midfell, in the Hengill volcanic system (Harrison et al., 1999) (see petrographic description of Midfell basalts in Chapter 4). These ratios define a trend in the neon three-isotope plot that is intermediate between the Loihi-Kilauea (L-K) line (Honda et al., 1991; Valbracht et al., 1997) and the MORB trend (Hiyagon et al., 1992; Sarda et al., 1988) with the highest $^{21}Ne/^{22}Ne$ ratios of 0.047 ± 0.005 at a near-solar $^{20}Ne/^{22}Ne$ ratio of 13.7 ± 0.3 (Fig. 5-4). Additional data from samples from Midfell are reported by Trieloff et al. (2000). These samples are from a different part of the same flow unit as the samples analysed by Harrison et al. (1999). The neon data reported by Trieloff et al. (2000) have an end-member $^{21}Ne/^{22}Ne$ ratio of near 0.038 at an extrapolated $^{20}Ne/^{22}Ne$ ratio of 13.8 (solar ratio). The maximum measured $^{20}Ne/^{22}Ne$ ratio analysed by Trieloff et al. (2000) is 12.85 ± 0.31, which is slightly lower than the maximum value measured by Harrison et al. (1999). The different neon end-member isotopic compositions reported by Harrison et al. (1999) and Trieloff et al. (2000) in different glass samples from the same flow unit suggest significant local heterogeneity in the noble gas composition of erupted lavas.

Coupled production of ^{4}He and $^{21}Ne^{*}$ permits the $^{3}He/^{4}He$ ratio to be predicted based on the slope of the trend defined by the neon data in the neon 3-isotope plot (Honda et al., 1993a). The predicted $^{3}He/^{4}He$ ratio of approximately 14 Ra from Harrison et al. (1999) is calculated from the $^{21}Ne/^{22}Ne$ end-member ratio of 0.042 – 0.052 that is intermediate between the solar (0.0328) and the MORB (0.074) endmembers (see Chapter 2). The measured $^{3}He/^{4}He$ ratios of 15 – 19 Ra are only slightly higher than the predicted ratio. In contrast, the neon data in Fig. 5-3 that lie on the air-solar mixing line are expected to be coupled with relatively high, solar-like $^{3}He/^{4}He$ ratios (100 – 320 Ra, see Chapter 2), but are instead associated with $^{3}He/^{4}He$ ratios near 12 Ra.

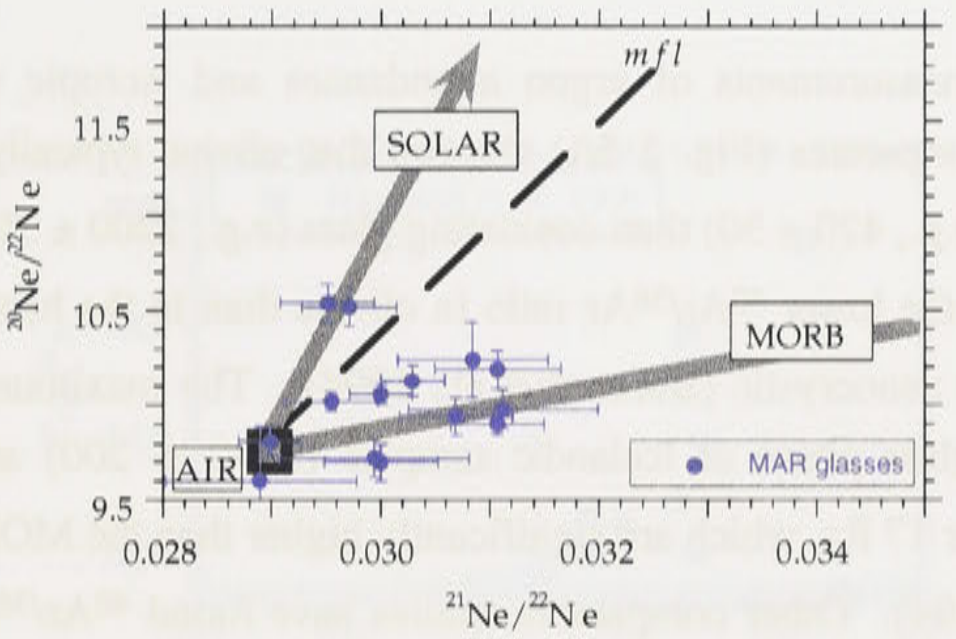

Figure 5-3. Neon three isotope plot, showing neon isotopic compositions of gas fractions released by melting or vacuum crushing of MORB glasses from the Reykjanes and Kolbeinsey Ridges to the south and north of Iceland, respectively (Poreda and Radicati di Brozolo, 1984). There is no systematic difference between the neon isotopic ratios from the two different ridges. Data lying near the air-solar mixing line within one sigma uncertainty are from samples furthest from Iceland near 57.2 – 58.4 °N latitude. Samples at this latitude in Figure 5-1 have $^{3}He/^{4}He$ near 12 Ra. Neon isotopic compositions from Reykjanes Ridge samples that lie near the MORB trend are from > 60°N latitude, from the region where the $^{3}He/^{4}He$ ratios show a slight decrease from ~17 Ra to ~13 Ra in Figure 5-1.

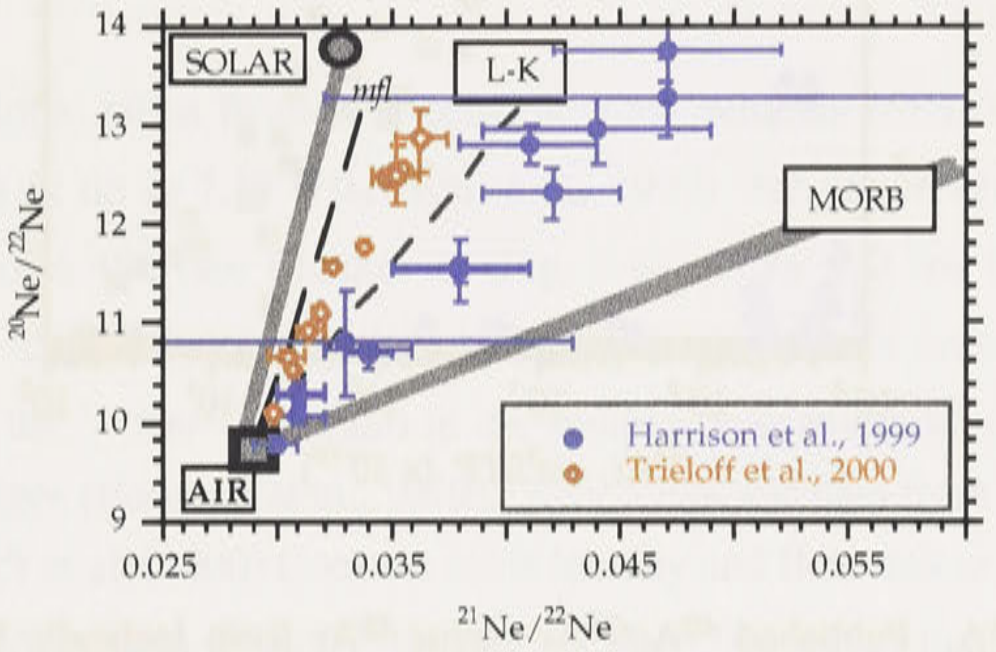

Figure 5-4. Neon three isotope plot, showing results from Icelandic samples reported by Harrison et al. (1999) and Trieloff et al. (2000). Gas was released from glass separates by in-vacuo sequential crushing. The maximum $^{20}Ne/^{22}Ne$ ratio is within one sigma uncertainty of the solar ratio. Neon isotopic ratios lie between the L-K line (Honda et al., 1993b) and the MORB trend with a $^{21}Ne/^{22}Ne$ end-member ratio of 0.047 ± 0.005. Data from Trieloff et al. (2000) have a $^{21}Ne/^{22}Ne$ end-member ratio of near 0.038 at an extrapolated $^{20}Ne/^{22}Ne$ ratio of 13.8 (solar ratio). The maximum measured $^{20}Ne/^{22}Ne$ ratio reported by Trieloff et al. (2000) is 12.85 ± 0.31.

Argon

Previous measurements of argon abundances and isotopic ratios in Icelandic olivine and glass separates (Fig. 5-5A) showed that olivine typically has much lower $^{40}Ar/^{36}Ar$ ratios (e.g., 420 ± 30) than coexisting glass (e.g., 2200 ± 200) (Burnard et al., 1994). Owing to the lower $^{40}Ar/^{36}Ar$ ratio in olivine than in the host glass, the olivine was inferred to be xenocrystic (Burnard et al., 1994). The maximum $^{40}Ar/^{36}Ar$ ratios measured in the glass phase of Icelandic samples (2200 ± 200) are associated with $^{3}He/^{4}He$ ratios near 17 Ra, which are significantly higher than the MORB ratio of 8.5 Ra (Burnard et al., 1994). Other comparable studies have found $^{40}Ar/^{36}Ar$ ratios of gases released from crushed glass samples have an even higher maximum ratio of 6501 ± 311 (Harrison et al., 1999) (Fig. 5-5A, B) that are associated with $^{3}He/^{4}He$ ratios of 15 – 18 Ra. The data from Trieloff et al. (2000) on samples from the same locality as studied by Harrison et al. (1999) have somewhat lower maximum $^{40}Ar/^{36}Ar$ ratios of 4350 ± 90 that are associated with $^{3}He/^{4}He$ ratios of 17 ± 1.

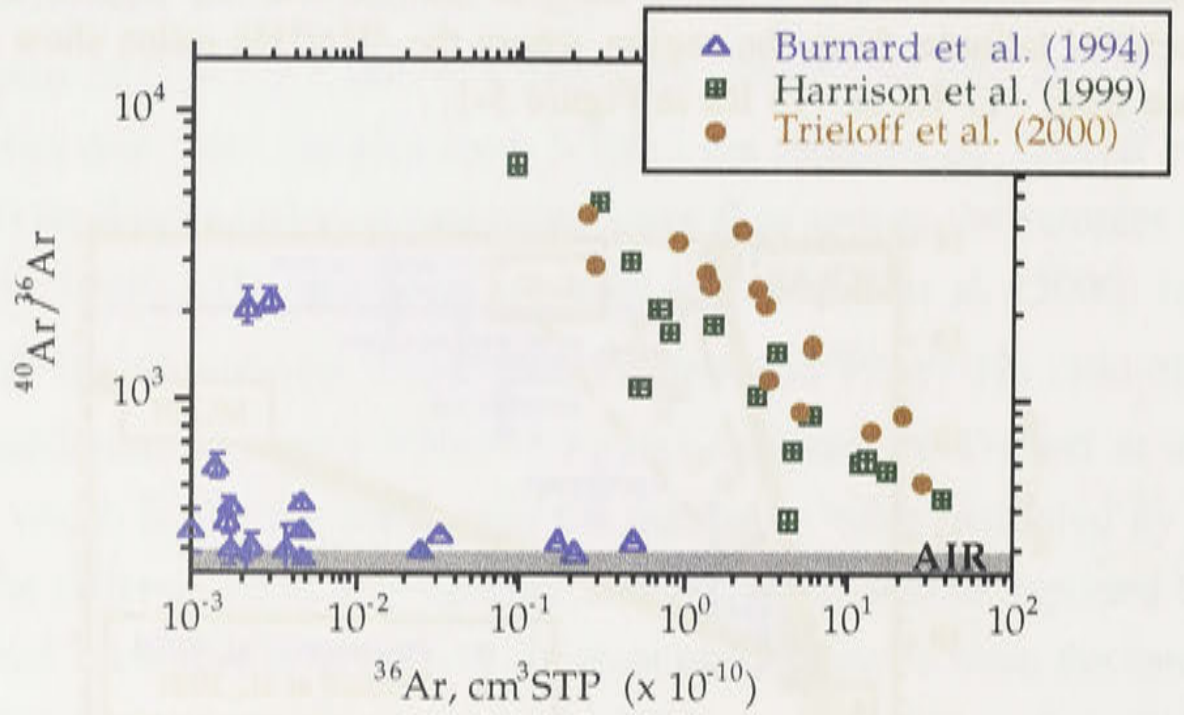

Figure 5-5A. Published $^{40}Ar/^{36}Ar$ versus ^{36}Ar from Icelandic basalts. The maximum $^{40}Ar/^{36}Ar$ ratios are in the gas fractions with the lowest ^{36}Ar concentrations, probably owing to the smaller amount of atmospheric argon in these fractions. The maximum $^{40}Ar/^{36}Ar$ ratio from Burnard et al. (1994) is 2200 ± 200, and the maximum from Harrison et al. (1999) is 6500 ± 310. The maximum $^{40}Ar/^{36}Ar$ ratios from Trieloff et al. (2000) is lower and equal to 4350 ± 90, but lies on the same trend as the data reported by Harrison et al. (1999). Such near-linear trends may be attributed to binary mixing between mantle-derived and atmospheric argon.

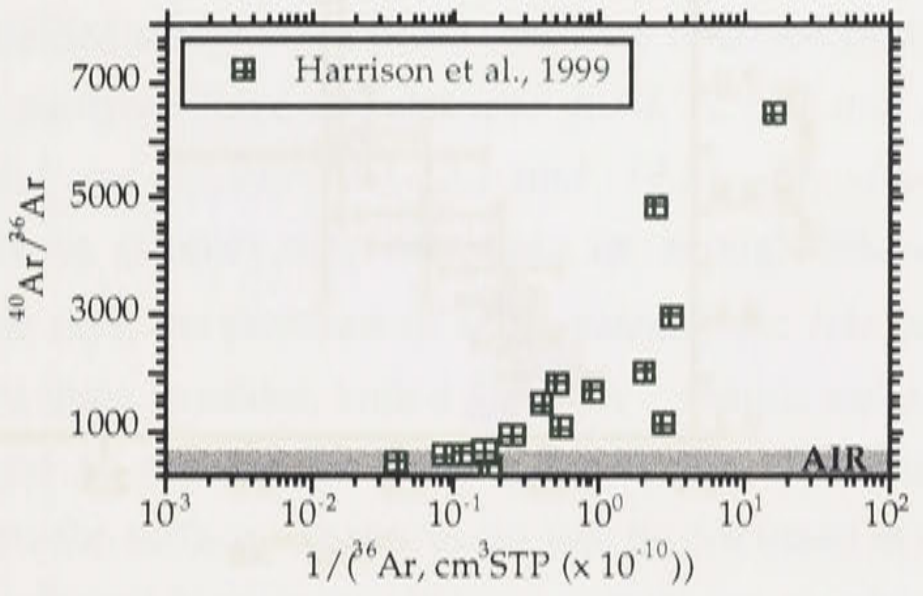

Figure 5-5B. $^{40}Ar/^{36}Ar$ versus $1/^{36}Ar$ for individual gas fractions released from two samples from the same locality reported by Harrison et al., (1999).

Krypton

No isotopic analyses of krypton have yet been reported for Icelandic samples, probably owing to the similarity between the measured ratios in basaltic samples and the krypton isotopic ratios in the atmosphere.

Xenon

Xenon isotopic ratios from two Icelandic glass samples from one locality show $^{129}Xe/^{130}Xe$ ratios of up to 7.37 (Harrison et al., 1999) that are much higher than the atmospheric ratio of 6.496 (see Chapter 2) (Fig. 5-6). Note that for these data, ^{130}Xe was not measured, and ^{132}Xe was used as the reference isotope. In order to re-normalize the data to ^{130}Xe, the $^{130}Xe/^{132}Xe$ ratio in the samples was assumed to be the same as that in the atmosphere (Harrison et al., 1999). Xenon isotopic data from Icelandic basalts obtained by Trieloff et al. (2000) from the same locality and flow unit as that described in Harrison et al. (1999) have $^{129}Xe/^{130}Xe$ and $^{136}Xe/^{130}Xe$ ratios that are significantly higher than their respective ratios in the atmosphere. The $^{129}Xe/^{130}Xe$ ratios are as high as 6.97 ± 0.20, and $^{136}Xe/^{130}Xe$ are up to 2.35 ± 0.11 (Trieloff et al., 2000). In plots of $^{129}Xe/^{130}Xe$ versus $^{136}Xe/^{130}Xe$, the Icelandic data fall on the same trend as that defined by the MORB popping rock data of Moriera et al., (1998). This is consistent with observations, as all other mantle-derived samples that have non-atmospheric $^{129}Xe/^{130}Xe$ and $^{136}Xe/^{130}Xe$ ratios lie along the same trend as the MORB data (Farley and Neroda, 1998).

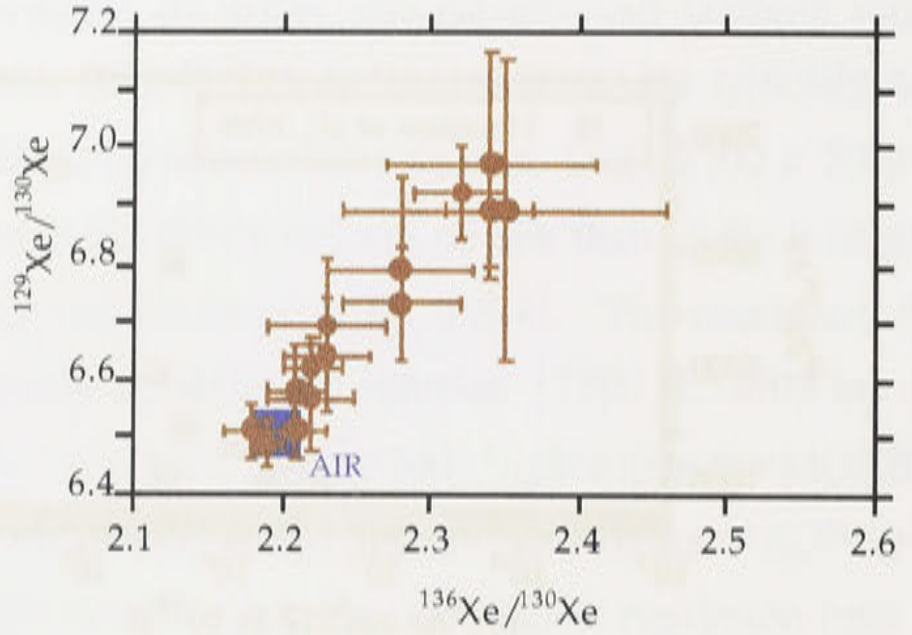

Figure 5-6. Plot of $^{129}Xe/^{130}Xe$ and $^{136}Xe/^{130}Xe$ data from Icelandic basalts reported by Trieloff et al. (2000). These data are among the few to show high $^{129}Xe/^{130}Xe$ and $^{136}Xe/^{130}Xe$ ratios relative to the atmospheric ratio in samples derived from an ocean island basalt (OIB)-type locality (see Chapter 2). The data lie along the same trend as the $^{129}Xe/^{130}Xe$ and $^{136}Xe/^{130}Xe$ data from MORBs. See chapter 6 for further explanations.

The measured $^{129}Xe/^{130}Xe$ and $^{136}Xe/^{130}Xe$ ratios in Icelandic basalts, that are higher than their respective ratios in the atmosphere, could be interpreted in a variety of ways, as described in Chapter 2. The relatively high $^{129}Xe/^{130}Xe$ and $^{136}Xe/^{130}Xe$ ratios may originate from material in the Icelandic plume source, but alternatively may result from entrainment of MORB source material that has high $^{129}Xe/^{130}Xe$ and $^{136}Xe/^{130}Xe$ ratios into the Icelandic plume. These possibilities will be discussed in more detail in Chapter 6.

5.2 Analytical results: this study

The noble gas elemental and isotopic ratios from 26 different samples from 13 localities in Iceland are reported here. A total of 28 olivine, one pyroxene and 9 glass separates were analysed. In two samples, both olivine and host glass were analysed (note: *ice-32.1, olivine,* and *32.2, glass*, are from the same locality but are different samples). In one sample (*ice-34*), both olivine and pyroxene phenocrysts were analysed, but the amount of gas released from pyroxene was generally below the blank level. Seven separates were analysed in duplicate, and two separates were analysed in triplicate.

The samples from this study will be divided into "well-shielded" and "partly-shielded" samples in plots showing isotopic and elemental abundance ratios (but not in plots of elemental abundances relative to the atmosphere). Well-shielded samples are

those that were obtained from quarries or from several meters below the surface on rapidly eroding cliff-faces and are very unlikely to have cosmogenic components of ^{3}He and ^{21}Ne. Partly-shielded samples are those that were obtained from within two meters of the surface. The partly-shielded samples are: *ice-1, -2 (2.1 and 2.2), -4, -10 (-10.1 and -10.2), -11 (-11.1 and -11.2), -12 (-12.1 and -12.2), -14, -16, -23, -24 and -25.* Although some of these samples may have been far enough below the surface to be shielded from cosmic rays, the presence of some cosmogenic ^{3}He and ^{21}Ne cannot be entirely ruled out. At three localities, both a "surface" sample and a "partly shielded" sample were analysed to evaluate the relative production of cosmogenic isotopes at different depths below the surface. These results will be discussed in detail in Chapter 6.

Gases were released from most olivine separates by step-heating, whereas they were released from glasses by step-heating and/or crushing. The weight of the sample analysed, and an explanation of the sample labelling system, are found in Table 4-1. Details of the methods used to obtain the noble gas results are found in Appendix 3.

5.2.1 Relative noble gas abundance ratios

The noble gas concentrations are reported as relative abundance ratios of a given isotope in the sample normalized to ^{36}Ar, compared with the abundance of the same ratio in air, or:

$$F(X) = (X/^{36}Ar)_{SAMPLE}/(X/^{36}Ar)_{AIR},$$

where X = ^{3}He, ^{20}Ne, ^{36}Ar, ^{84}Kr, or ^{130}Xe

The F(X) values for some MORBs (Hiyagon et al., 1992) and Hawaiian OIBs (Honda et al., 1993c) are shown in (Figs. 5-7A, B) to demonstrate the range in F(X) values in some mantle-derived samples for comparison with those in Icelandic basalts. There is a large range in relative noble gas concentrations in Icelandic basalts, and most of the olivine and glass separates have F(X) values that are within the range of values reported in other mantle-derived samples, and will not be discussed further.

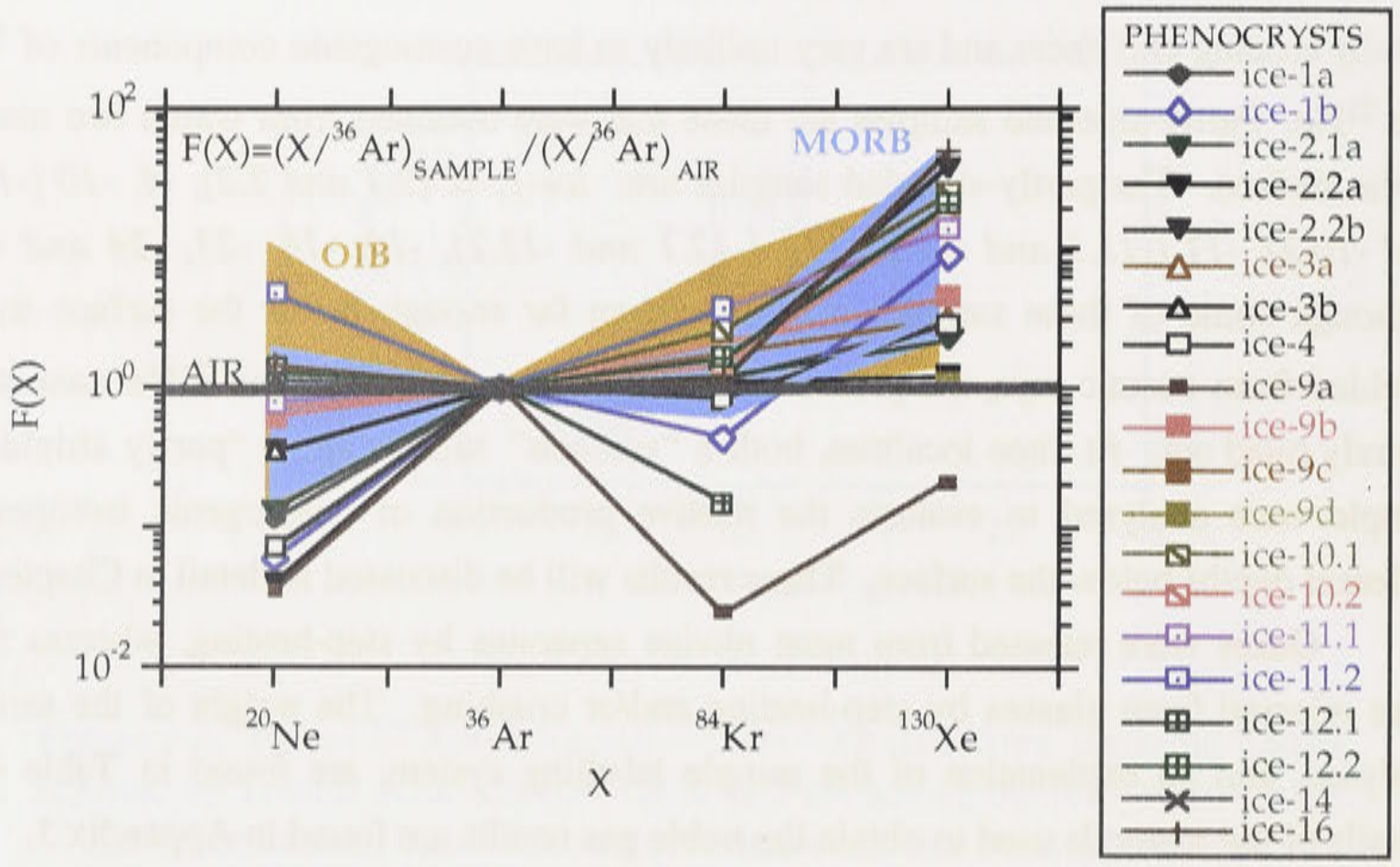

A

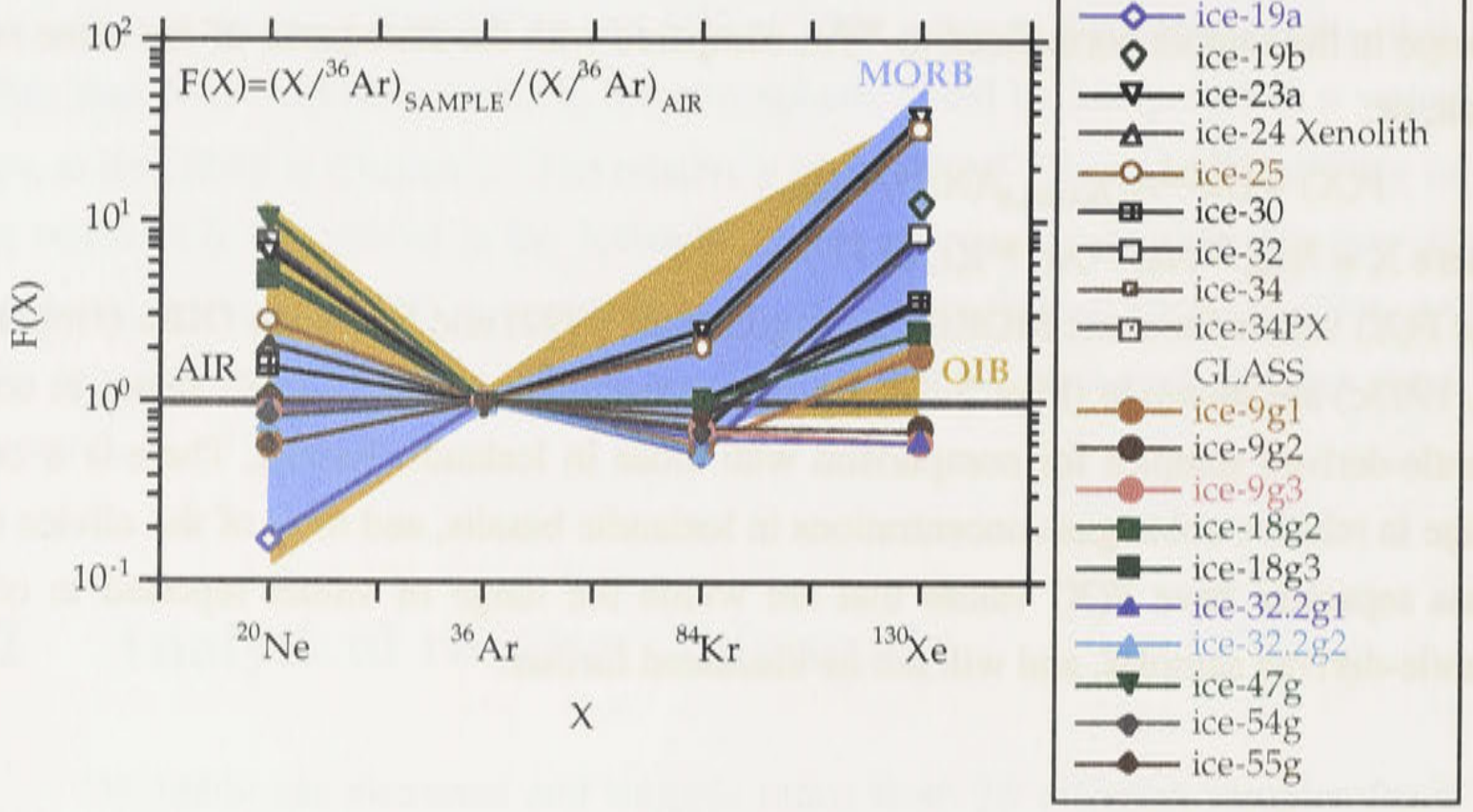

B

Figure 5-7A, B. Relative elemental abundance patterns of noble gases from Icelandic phenocryst and glass separates (this study). Note the different y-axis scales in 5-7A and 5-7B. The results from Icelandic samples show a large range in relative abundance ratios comparable to the range reported in MORBs and Hawaiian OIB (shaded regions; OIB = orange, MORB = blue). All glass separates are shown in 5-7B, the lower plot, as filled symbols, and the remaining analyses are all of olivine separates except *ice-34PX* (pyroxene). The MORBs compositions are from data reported by Hiyagon et al. (1992) and OIB compositions are from Honda et al. (1993b).

5.2.2 Noble gas concentrations and isotopic ratios

Helium

The ^{4}He abundances in Icelandic samples from this study range from 5 x 10^{-10} to 2 x 10^{-8} cm^{3}STP/g in olivine and from 2 x 10^{-8} to 6 x 10^{-6} cm^{3}STP/g in the glass separates (Table 5-1, Fig. 5-8). The minimum and maximum measured total gas ^{3}He/^{4}He ratios are 8.3 ± 0.8 Ra (*ice-2.2b*) and 75 ± 7 Ra (*ice-2.1a*) (Table 5-1). The majority of analyses of olivine and glass from step-heated and crushed samples yielded ^{3}He/^{4}He ratios between 12 and 20 Ra (Table 5-1 and Fig. 5-8). The helium isotopic compositions of the partly-shielded samples will be evaluated in Chapter 6 to determine whether they have a component of cosmogenic ^{3}He. Most total gas isotopic ratios (obtained by combining the gas released from incremental step-heating) have a similar range to those involving step-heating/crushing (Table 5-1).

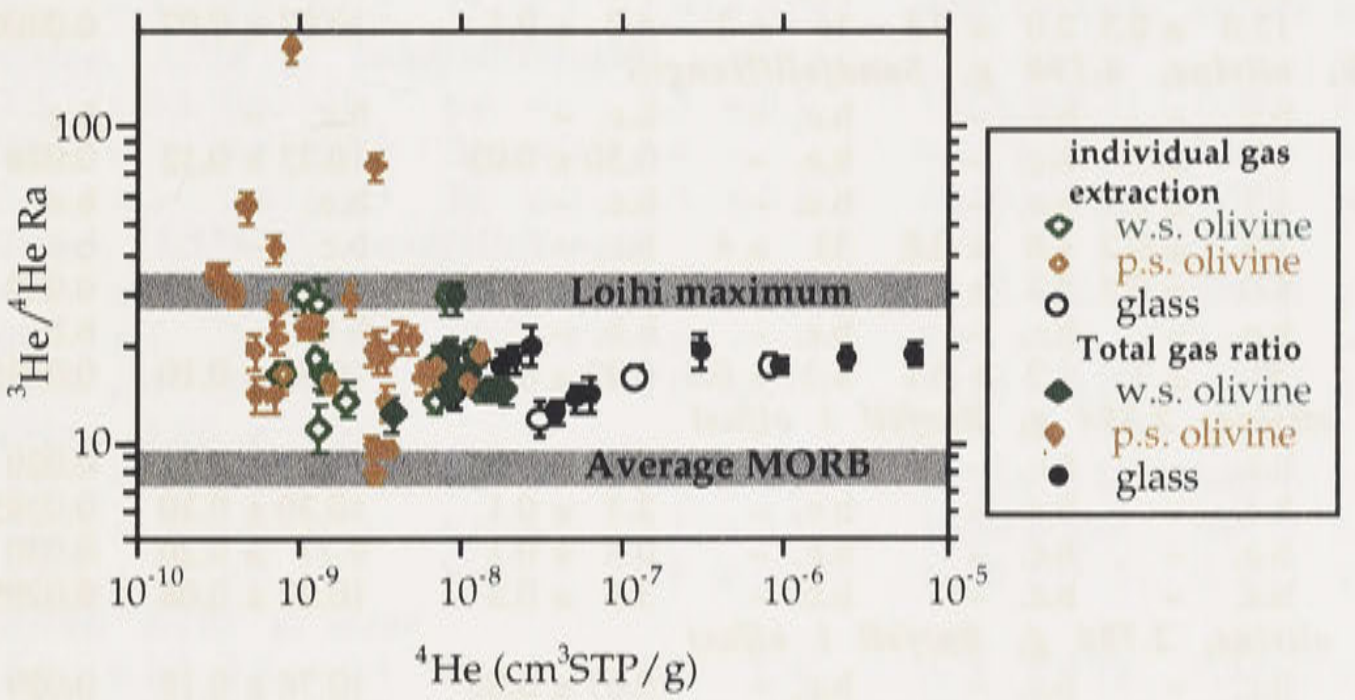

Figure 5-8. Helium results from analyses of Icelandic olivine and glass separates. Individual step-heats are shown as open symbols, whereas the sum of the total gas released is shown as filled symbols. Samples are further divided into those that were well-shielded from cosmic rays, and those that were partly shielded. The sample that has the highest ^{3}He/^{4}He ratio (individual gas extraction) of 181 ± 21 Ra is *ice-2.1a*, a partly shielded (p.s.) sample. Most ^{3}He/^{4}He ratios lie between the grey bands labelled "Loihi maximum" and "MORB." The maximum ^{3}He/^{4}He ratios from well-shielded (w.s.) Icelandic samples are similar to those from Loihi samples. The minimum ratios are close to the average MORB ratio of 8.5 Ra. The isotopic compositions of the total gas released from the olivine and glass separates are similar to those of individual gas fractions in most cases.

Table 5-1. Helium and neon data from Icelandic basalts

sample	^{4}He cm^3STP/g (1×10^{-10})	$^3He/^4He$ $(1x10^{-5})$	$^3He/^4He$ Ra	^{22}Ne cm^3STP/g (1×10^{-12})	$^{20}Ne/^{22}Ne$	$^{21}Ne/^{22}Ne$
ice-1a, olivine, 5.029 g, Midfell						
900	7.6 ± 0.4	b.c. –	b.c. –	1.06 ± 0.06	10.16 ± 0.11	0.0289 ± 0.0007
1800	29 ± 2	1.38 ± 0.10	9.8 ± 0.7	b.c. –	b.c. –	b.c. –
Total	37 ± 2	1.34 0.08	9.6 ± 0.6	1.06 ± 0.06	10.16 ± 0.11	0.0289 ± 0.0007
ice-1b, olivine, 5.638 g, Midfell						
900	7.3 ± 0.4	3.0 ± 0.4	22 ± 3	0.82 ± 0.04	10.16 ± 0.10	0.0309 ± 0.0007
1800	43 ± 2	3.0 ± 0.3	21 ± 2	0.63 ± 0.03	10.89 ± 0.10	0.0334 ± 0.0006
1850	b.c. –	b.c. –	b.c. –	b.c. –	b.c. –	b.c. –
Total	50 ± 3	3.0 ± 0.3	21 ± 2	1.45 ± 0.05	10.47 ± 0.07	0.0320 ± 0.0005
ice-2.1a, olivine, 4.309 g, Sandfell/Hengill						
900	9.1 ± 0.5	25 ± 3	181 ± 21	3.5 ± 0.2	10.91 ± 0.09	0.0296 ± 0.0006
1800	21 ± 1	4.0 ± 0.5	29 ± 3	0.88 ± 0.05	11.43 ± 0.14	0.0376 ± 0.0009
1850	b.c. –	b.c. –	b.c. –	b.b. –	b.b. –	b.b. –
Total	30 ± 1	11 ± 1	75 ± 7	4.4 ± 0.2	11.01 ± 0.08	0.0312 ± 0.0005
ice-2.2a, olivine, 6.162 g, Sandfell/Hengill						
400	b.c. –	b.c. –	b.c. –	b.c. –	b.c. –	b.c. –
700	5.5 ± 0.3	2.0 ± 0.3	14 ± 2	2.3 ± 0.1	9.98 ± 0.11	0.0278 ± 0.0005
900	b.c. –	b.c. –	b.c. –	0.34 ± 0.03	10.16 ± 0.19	0.035 ± 0.002
1350	3.0 ± 0.2	b.c. –	b.c. –	0.61 ± 0.04	10.30 ± 0.16	0.036 ± 0.001
1800	7.0 ± 0.4	2.0 ± 0.3	14 ± 2	0.97 ± 0.05	10.13 ± 0.12	0.0327 ± 0.0008
1850	b.c. –	b.c. –	b.c. –	b.c. –	b.c. –	b.c. –
1900	b.c. –	b.c. –	b.c. –	b.c. –	b.c. –	b.c. –
Total	15.6 ± 0.5	2.0 ± 0.3	14 ± 2	4.2 ± 0.1	10.07 ± 0.07	0.0306 ± 0.0004
ice-2.2b, olivine, 6.190 g, Sandfell/Hengill						
400	b.c. –	b.c. –	b.c. –	b.c. –	b.c. –	b.c. –
800	17 ± 1	b.c. –	b.c. –	0.50 ± 0.03	10.23 ± 0.12	0.028 ± 0.001
870	1.7 ± 0.1	b.c. –	b.c. –	b.c. –	b.c. –	b.c. –
1280	3.5 ± 0.2	4.6 ± 0.6	33 ± 4	b.c. –	b.c. –	b.c. –
1800	8.0 ± 0.5	2.3 ± 0.3	16 ± 2	0.42 ± 0.02	10.82 ± 0.17	0.040 ± 0.001
1850	b.c. –	b.c. –	b.c. –	b.b. –	b.b. –	b.b. –
Total	30 ± 1	1.2 ± 0.1	8.3 ± 0.8	0.92 ± 0.04	10.50 ± 0.10	0.0335 ± 0.0008
ice-3a, olivine, 3.384 g, Burfell i olfusi						
900	b.c. –	b.c. –	b.c. –	0.32 ± 0.04	11.21 ± 0.24	0.029 ± 0.003
1800	b.c. –	b.c. –	b.c. –	2.5 ± 0.1	10.30 ± 0.10	0.0295 ± 0.0005
1850	b.c. –	b.c. –	b.c. –	0.8 ± 0.1	9.77 ± 0.20	0.030 ± 0.003
Total	b.c. –	b.c. –	b.c. –	3.6 ± 0.2	10.27 ± 0.08	0.0295 ± 0.0008
ice-3b, olivine, 2.786 g, Burfell i olfusi						
900	b.c. –	b.c. –	b.c. –	0.67 ± 0.05	10.76 ± 0.18	0.029 ± 0.001
1800	b.c. –	b.c. –	b.c. –	0.61 ± 0.05	10.87 ± 0.17	0.032 ± 0.002
1850	b.c. –	b.c. –	b.c. –	b.c. –	b.c. –	b.c. –
Total	b.c. –	b.c. –	b.c. –	1.3 ± 0.1	10.81 ± 0.13	0.030 ± 0.001
ice-4, olivine, 3.181 g, Halejarbunga						
900	b.c. –	b.c. –	b.c. –	0.95 ± 0.06	10.25 ± 0.11	0.0302 ± 0.0008
1800	4.7 ± 0.3	7.8 ± 0.9	56 ± 7	0.82 ± 0.06	10.54 ± 0.16	0.054 ± 0.002
1850	b.c. –	b.c. –	b.c. –	b.b. –	b.b. –	b.b. –
Total	4.7 0.3	7.8 ± 0.9	56 ± 7	1.77 ± 0.08	10.38 ± 0.10	0.041 ± 0.001
ice-9a, olivine, 5.162 g, Midfell						
900	13.3 ± 0.8	3.9 ± 0.8	28 ± 5	n.a. –	n.a. –	n.a. –
1800	72 ± 4	2.5 ± 0.3	18 ± 2	2.0 ± 0.1	11.96 ± 0.36	0.0308 ± 0.0007
Total	85 ± 4	2.7 ± 0.3	20 ± 2	2.0 ± 0.1	11.96 ± 0.36	0.0308 ± 0.0007
ice-9b, olivine, 5.160 g, Midfell						
900	10.6 ± 0.6	4.1 ± 0.5	29 ± 3	0.34 ± 0.07	13.3 ± 1.1	0.034 ± 0.003
1800	82 ± 5	4.1 ± 0.5	29 ± 3	b.b. –	b.b. –	b.b. –
1850	b.c. –	b.c. –	b.c. –	0.49 ± 0.07	11.10 ± 0.46	0.031 ± 0.002
Total	93 ± 5	4.1 ± 0.4	29 ± 3	0.8 ± 0.1	11.98 ± 0.56	0.032 ± 0.002

sample	^{4}He cm^{3}STP/g (1×10^{-10})	^{3}He/^{4}He (1×10^{-5})	^{3}He/^{4}He Ra	^{22}Ne cm^{3}STP/g (1×10^{-12})	^{20}Ne/^{22}Ne	^{21}Ne/^{22}Ne
ice-9c, olivine, 5.176 g, Midfell						
900	13.1 ± 0.8	2.6 ± 0.2	19 ± 1	b.c. –	b.c. –	b.c. –
1800	66 ± 4	2.4 ± 0.2	17 ± 1	b.c. –	b.c. –	b.c. –
Total	79 ± 4	2.4 ± 0.1	17 ± 1	b.c. –	b.c. –	b.c. –
ice-9d, olivine, 0.702 g, Midfell						
crush	b.c. –	b.c. –	b.c. –	b.c. –	b.c. –	b.c. –
ice-9g1, glass, 2.026 g, Midfell						
700	1206 ± 70	2.3 ± 0.2	16 ± 1	11.1 ± 0.5	10.07 ± 0.14	0.0300 ± 0.0005
1600	8122 ± 471	2.5 ± 0.2	18 ± 1	23 ± 1	10.81 ± 0.14	0.0301 ± 0.0006
Total	9327 ± 476	2.4 ± 0.2	17 ± 1	34 ± 1	10.57 ± 0.10	0.0301 ± 0.0004
ice-9g2, glass, 0.585 g, Midfell						
crush	62375 ±361	2.7 ± 0.2	19 ± 1	181 ± 9	10.74 ± 0.13	0.0304 ± 0.0005
ice-9g3, glass, 0.720 g, Midfell						
crush	23772 ±137	2.6 ± 0.2	19 ± 2	339 ± 15	9.94 ± 0.08	0.0295 ± 0.0003
ice-10.1, olivine, 4.66 g, Maelifell						
900	2.9 ± 0.2	b.c. –	b.c. –	2.3 ± 0.1	9.95 ± 0.16	0.0300 ± 0.0006
1800	31 ± 2	2.8 ± 0.3	20 ± 2			
Total	34 ± 2	2.6 ± 0.3	18 ± 2	2.3 ± 0.1	9.95 ± 0.16	0.0300 ± 0.0006
ice-10.2, olivine, 5.904 g, Maelifell						
900	3.0 ± 0.2	4.8 ± 0.4	34 ± 3	1.90 ± 0.09	9.88 ± 0.10	0.0294 ± 0.0005
1800	58 ± 3	2.2 ± 0.2	16 ± 1	b.c. –	b.c. –	b.c. –
Total	61 ± 3	2.4 ± 0.2	17 ± 1	1.90 ± 0.09	9.88 ± 0.10	0.0294 ± 0.0005
ice-11.1, olivine, 3.758 g, Sandfell/Hengill						
900	2.2 ± 0.1	b.c. –	b.c. –	1.5 ± 0.1	10.56 ± 0.30	0.033 ± 0.001
1800	29 ± 2	2.8 ± 0.3	20 ± 2	b.c. –	b.c. –	b.c. –
Total	31 ± 2	2.6 ± 0.3	19 ± 2	1.5 ± 0.1	10.56 ± 0.30	0.033 ± 0.001
ice-11.2, olivine, 5.535 g, Sandfell/Hengill						
900	4.0 ± 0.2	4.1 ± 0.4	30 ± 3	1.09 ± 0.05	10.10 ± 0.12	0.0301 ± 0.0005
1800	69 ± 4	2.3 ± 0.2	17 ± 1	b.c. –	b.c. –	b.c. –
Total	73 ± 4	2.4 ± 0.2	17 ± 1	1.09 ± 0.05	10.10 ± 0.12	0.0301 ± 0.0005
ice-12.1, olivine, 3.06 g, Asar						
900	b.c. –	b.c. –	b.c. –	5.8 ± 0.3	10.25 ± 0.14	0.0308 ± 0.0005
1800	b.c. –	b.c. –	b.c. –	2.7 ± 0.2	10.30 ± 0.20	0.0319 ± 0.0008
Total	b.c. –	b.c. –	b.c. –	8.4 ± 0.3	10.26 ± 0.12	0.0311 ± 0.0004
ice-12.2, olivine, 5.103 g, Asar						
900	5.3 ± 0.3	2.8 ± 0.4	20 ± 3	8.8 ± 0.4	9.78 ± 0.08	0.0295 ± 0.0003
1800	7.4 ± 0.4	3.8 ± 0.5	27 ± 3	1.12 ± 0.06	10.08 ± 0.12	0.0343 ± 0.0007
Total	12.7 ± 0.5	3.3 ± 0.3	24 ± 2	9.9 ± 0.4	9.81 ± 0.08	0.0301 ± 0.0003
ice-14, olivine, 3.087 g, Burfell i olfusi						
900	b.c. –	b.c. –	b.c. –	b.c. –	b.c. –	b.c. –
1800	10.9 ± 0.6	3.3 ± 0.3	23 ± 2	3.4 ± 0.2	10.15 ± 0.17	0.0320 ± 0.0007
Total	10.9 ± 0.6	3.3 ± 0.3	23 ± 2	3.4 ± 0.2	10.15 ± 0.17	0.0320 ± 0.0007
ice-16, olivine, 5.388 g, Eldborg						
900	7.1 ± 0.4	5.8 ± 0.5	41 ± 4	3.1 ± 0.1	10.23 ± 0.10	0.0302 ± 0.0005
1600	123 ± 7	2.5 ± 0.2	18 ± 2	0.86 ± 0.06	10.97 ± 0.19	0.039 ± 0.001
Total	130 ± 7	2.7 ± 0.2	19 ± 2	4.0 ± 0.2	10.39 ± 0.09	0.0321 ± 0.0004
ice-18b, olivine, 3.649 g, Stapafell						
900	14.1 ± 0.8	2.4 ± 0.3	17 ± 2	17.9 ± 0.8	9.94 ± 0.08	0.0298 ± 0.0003
1800	83 ± 5	2.3 ± 0.3	16 ± 2	0.64 ± 0.04	9.64 ± 0.25	0.029 ± 0.001
Total	97 ± 5	2.3 ± 0.2	16 ± 2	18.5 ± 0.8	9.93 ± 0.08	0.0298 ± 0.0003
ice-18g2, glass, 3.704 g, Stapafell						
700	408 ± 24	1.8 ± 0.2	13 ± 2	55 ± 2	9.75 ± 0.08	0.0317 ± 0.0003
1500	112 ± 7	2.5 ± 0.3	18 ± 2	36 ± 2	9.86 ± 0.08	0.0296 ± 0.0003
Total	520 ± 25	1.9 ± 0.2	14 ± 1	90 ± 3	9.79 ± 0.06	0.0309 ± 0.0002

sample	^{4}He cm^3STP/g (1×10^{-10})	$^3He/^4He$ $(1x10^{-5})$	$^3He/^4He$ Ra	^{22}Ne cm^3STP/g (1×10^{-12})	$^{20}Ne/^{22}Ne$	$^{21}Ne/^{22}Ne$
ice-18g3, glass, 0.983 g, Stapafell						
crush	619 ± 36	2.0 ± 0.2	14 ± 2	74 ± 3	10.01 ± 0.09	0.0299 ± 0.0003
ice-19a, olivine, 5.341 g, Sulur						
900	20 ± 1	1.9 ± 0.2	14 ± 2	12.7 ± 0.6	9.87 ± 0.08	0.0299 ± 0.0003
1800	90 ± 5	2.5 ± 0.3	18 ± 2	0.58 ± 0.05	10.79 ± 0.25	0.029 ± 0.002
Total	110 ± 5	2.4 ± 0.2	17 ± 2	13.3 ± 0.6	9.91 ± 0.08	0.0298 ± 0.0003
ice-19b, olivine, 5.1531 g, Sulur						
900	14.5 ± 0.8	2.2 ± 0.2	16 ± 1	1.29 ± 0.06	9.82 ± 0.09	0.0291 ± 0.0003
1800	131 ± 8	2.0 ± 0.2	15 ± 1	0.53 ± 0.04	10.46 ± 0.17	0.030 ± 0.001
Total	145 ± 8	2.1 ± 0.2	15 ± 1	1.81 ± 0.07	10.01 ± 0.08	0.0294 ± 0.0004
ice23a, olivine, 5.06 g, Haleyjarbunga						
900	b.c. –	b.c. –	b.c. –	1.41 ± 0.08	10.07 ± 0.11	0.0286 ± 0.0005
1800	b.c. –	b.c. –	b.c. –	1.36 ± 0.08	9.84 ± 0.11	0.0293 ± 0.0006
Total	b.c. –	b.c. –	b.c. –	2.8 ± 0.1	9.96 ± 0.08	0.0289 ± 0.0004
ice-24, olivine, 2.847 g, Hraunsvik/Hrolfsvik						
900	b.c. –	b.c. –	b.c. –	b.c. –	b.c. –	b.c. –
1800	b.c. –	b.c. –	b.c. –	b.c. –	b.c. –	b.c. –
Total	b.c. –	b.c. –	b.c. –	b.c. –	b.c. –	b.c. –
ice-25, olivine, 4.912 g, Bleikholl						
900	1.04 ±	b.c. –	b.c. –	5.1 ± 0.2	9.88 ± 0.13	0.0300 ± 0.0005
1800	112 ± 7	2.2 ± 0.2	16 ± 1	0.92 ± 0.05	10.48 ± 0.18	0.0384 ± 0.0009
Total	113 ± 7	2.2 ± 0.2	16 ± 1	6.0 ± 0.2	9.97 ± 0.11	0.0312 ± 0.0004
ice-30, olivine, 5.071 g, near Landamnahellir						
900	8.4 ± 0.5	2.3 ± 0.2	17 ± 1	3.2 ± 0.2	10.19 ± 0.14	0.0300 ± 0.0005
1800	68 ± 4	1.9 ± 0.1	14 ± 1	0.31 ± 0.03	11.72 ± 0.43	0.0299 ± 0.0016
1850	7.7 ± 0.4	2.3 ± 0.2	17 ± 1	0.29 ± 0.03	11.85 ± 0.52	0.0345 ± 0.0019
Total	85 ± 4	2.0 ± 0.1	14.2 ± 0.8	3.8 ± 0.2	10.44 ± 0.13	0.0303 ± 0.0005
ice-32.1a, olivine, 5.054 g, near Svartsengisfell						
900	13.7 ± 0.8	1.6 ± 0.3	11 ± 2	15.4 ± 0.7	9.95 ± 0.08	0.0295 ± 0.0003
1800	173 ± 10	2.1 ± 0.3	15 ± 2	3.5 ± 0.2	10.28 ± 0.10	0.0302 ± 0.0005
Total	187 ± 10	2.1 ± 0.2	15 ± 2	18.9 ± 0.7	10.01 ± 0.07	0.0296 ± 0.0003
ice32.2g1, glass, 3.056 g, near Svartsengisfell						
700	300 ± 17	1.7 ± 0.2	12 ± 1	65 ± 3	9.92 ± 0.08	0.0296 ± 0.0003
1500	91 ± 5	2.0 ± 0.3	15 ± 2	14.1 ± 0.6	9.97 ± 0.09	0.0301 ± 0.0003
Total	391 ± 18	1.8 ± 0.2	13 ± 1	79 ± 3	9.93 ± 0.07	0.0297 ± 0.0003
ice-32.2g2, glass, 1.040 g, near Svartsengisfell						
crush	173 ± 10	2.5 0.3	18 ± 2	35 ± 2	9.82 ± 0.08	0.0297 ± 0.0003
ice-34a, olivine, 3.556 g, SW of Skala-Maelifell						
900	3.3 ± 0.2	b.c. –	b.c. –	3.0 ± 0.2	10.16 ± 0.12	0.0300 ± 0.0005
1800	35 ± 2	1.9 ± 0.2	14 ± 2	0.31 ± 0.06	10.52 ± 0.51	0.026 ± 0.002
Total	39 ± 2	1.7 ± 0.2	12 ± 2	3.3 ± 0.2	10.20 ± 0.12	0.0296 ± 0.0005
ice-34PX, pyroxene, 0.70516 g, SW of Skala-Maelifell						
crush	b.c. –	b.c. –	b.c. –	b.c. –	b.c. –	b.c. –
ice-47g, glass, 0.921 g, Sigalda						
crush	2928 ± 170	2.7 ± 0.3	20 ± 2	72 ± 3	9.84 ± 0.08	0.0300 ± 0.0003
ice-54g, glass, 0.8426 g, Lambafell						
crush	214 ± 12	2.6 ± 0.2	19 ± 2	30 ± 1	9.92 ± 0.09	0.0311 ± 0.0006
ice-55g, glass, 0.8184g, Kongsgil						
crush	270 ± 26	2.8 ± 0.4	20 ± 3	20 ± 1	10.01 ± 0.09	0.0319 ± 0.0006

b.c. is below cut-off (see Appendix 3), b.b. is below blank, n.a.. is not analysed.

Comparison with previous analyses of $^3He/^4He$ ratios in Icelandic basalts

Most of the $^3He/^4He$ ratios from this study are similar to those found in previous studies on samples from nearby localities. For example, samples from Sigalda (*ice-47*, $^3He/^4He = 20 \pm 2$ Ra) and Stapafell (*ice-18g*, 14 ± 2 Ra) have $^3He/^4He$ ratios similar to those from the same localities reported by Kurz et al. (1985) (20.8 Ra) and Condomines et al. (1983) (13.8 ± 0.1 Ra), respectively. In contrast, the glass and olivine from a sample from Midfell (*ice-9*) have maximum $^3He/^4He$ ratios that are distinct from those measured in a different Midfell sample (*MIDgl, -ol, -cr1, -cr2*) by Burnard et al. (1994). The olivine sample from this study has $^3He/^4He$ ratios of near 29 ± 3 Ra in *ice-9a,-b*, but lower ratios of 17 ± 1 in *ice-9c* (step-heated) and 20 ± 1 in *ice-9d* (crushed). The olivine (separates *ice-9a, -9b, -9c, -9d*) is hosted by glass (*ice-9g-1, -g2*) with $^3He/^4He$ ratios of 17 ± 1 Ra (step-heat) to 19 ± 1 Ra (crush) that are similar to the values in *ice-9c* and *–9d*. Compared with the results from this study, Burnard et al. (1994) obtained significantly lower $^3He/^4He$ ratios (13.7 Ra) from crushed olivine, but the ratios from crushed glass (16.8 ± 0.2 Ra) are similar to those from this study. A contribution from a cosmogenic component of ^3He in *ice-9a* and *-9b* to explain the relatively high $^3He/^4He$ ratios is considered unlikely because sample *ice-9* was obtained from a cliff face in an active quarry and is likely to have been well shielded. These results, together with those reported by Burnard et al. (1994), emphasize the variability of the helium isotopic compositions at this locality.

The $^3He/^4He$ ratios measured in well-shielded samples from the present study have a much greater compositional range, from 12 to 30 Ra, than those reported in Harrison et al. (1999), Trieloff et al. (2000) and Burnard et al. (1994) (15 to 19 Ra). However, the maximum ratio from well-shielded samples measured from this study of 30 Ra is not the highest measured ratio for Icelandic basalts. The maximum ratio of 37.7 Ra was measured by Hilton et al. (1999) from olivine separates from basaltic samples in north-western Iceland. The large variation in measured $^3He/^4He$ ratios throughout Iceland show that the helium isotopic ratios in the magmatic sources of Icelandic basalts are heterogeneous.

Neon

The ^{22}Ne concentrations in olivine separates from this study range from 1×10^{-12} to 2×10^{-11} cm^3STP/g, and those in glass range from 2×10^{-11} to 3×10^{-10} cm^3STP/g (Table 5-1). In Figure 5-9, most of the neon isotopic ratios lie within the triangular region defined by the air-solar mixing line and the MORB correlation line.

Individual gas fractions

i) Well-shielded olivine separates and glass separates

Six samples, not including replicates, have gas fractions released by step-heating or crushing with isotopic compositions that lie on an air-solar mixing trend within one sigma uncertainty (n = 13 gas fractions) or within two sigma uncertainty (n = 3 gas fractions). These data are also distinct from the neon isotopic composition in the atmosphere ($^{21}Ne/^{22}Ne = 0.029$; $^{20}Ne/^{22}Ne = 9.8$) by more than two sigma uncertainty. These samples (Fig. 5-9) include both olivine and glass separates from the replicates of sample *ice-9*. Also included are the results from analyses of olivine separates *ice-3a, -3b, -19a, -19b, -30, -32.1a* and *-34* (Table 5-1). The neon isotopic compositions lying on the air-solar mixing line in mantle-derived samples has not been found previously and are the most significant results of this study.

Neon isotopic ratios of gases released by crushing or step-heating from a few Icelandic samples lie near the MORB trend. Although many of the neon isotopic ratios are quite close to the atmospheric composition, several of these analyses have very small uncertainties and suggest a MORB-like noble gas component may be present. Glass separates from three samples have neon isotopic ratios from individual step-heating or crushing extractions that lie near the MORB trend in the neon three-isotope plot, with compositions that are distinct from the neon composition in the atmosphere by at least two sigma uncertainty (Fig. 5-9). These are: *ice-18b (900°C)* , *ice-18g2* (700°C), *-19a* (900°C), and *-32.2g1* (1500°C). The remaining gas fractions released by step-heating or crushing (n = 6) of well-shielded samples are within two sigma of the atmospheric ratios. These near-atmospheric isotopic ratios probably reflect exchange of atmospheric neon with mantle-derived neon in the magma prior to or during eruption.

ii) Partly shielded samples

The eleven partly-shielded olivine samples are: *ice-1, 2, 4, 10, 11, 12, 14, 16, 23, 24 and 25.* Of a total of 46 individual gas fractions, 28 gas fractions have gas concentrations that are above the blank and detection limits. Three gas fractions from *ice-1a, -1b* and *–2.1a* lie on the air-solar mixing line within one sigma uncertainty. About one third of the gas fractions (n = 8 fractions) from the partly-shielded olivine samples lie near the MORB correlation line (Fig. 5-9). Gas fractions from one sample *(ice-4)* lies well below the MORB trend. Three gas fractions have neon isotopic compositions that lie on a trend that is intermediate between the L-K and the MORB trend. The remaining gas fractions (n = 13 fractions) are close to the atmospheric neon composition.

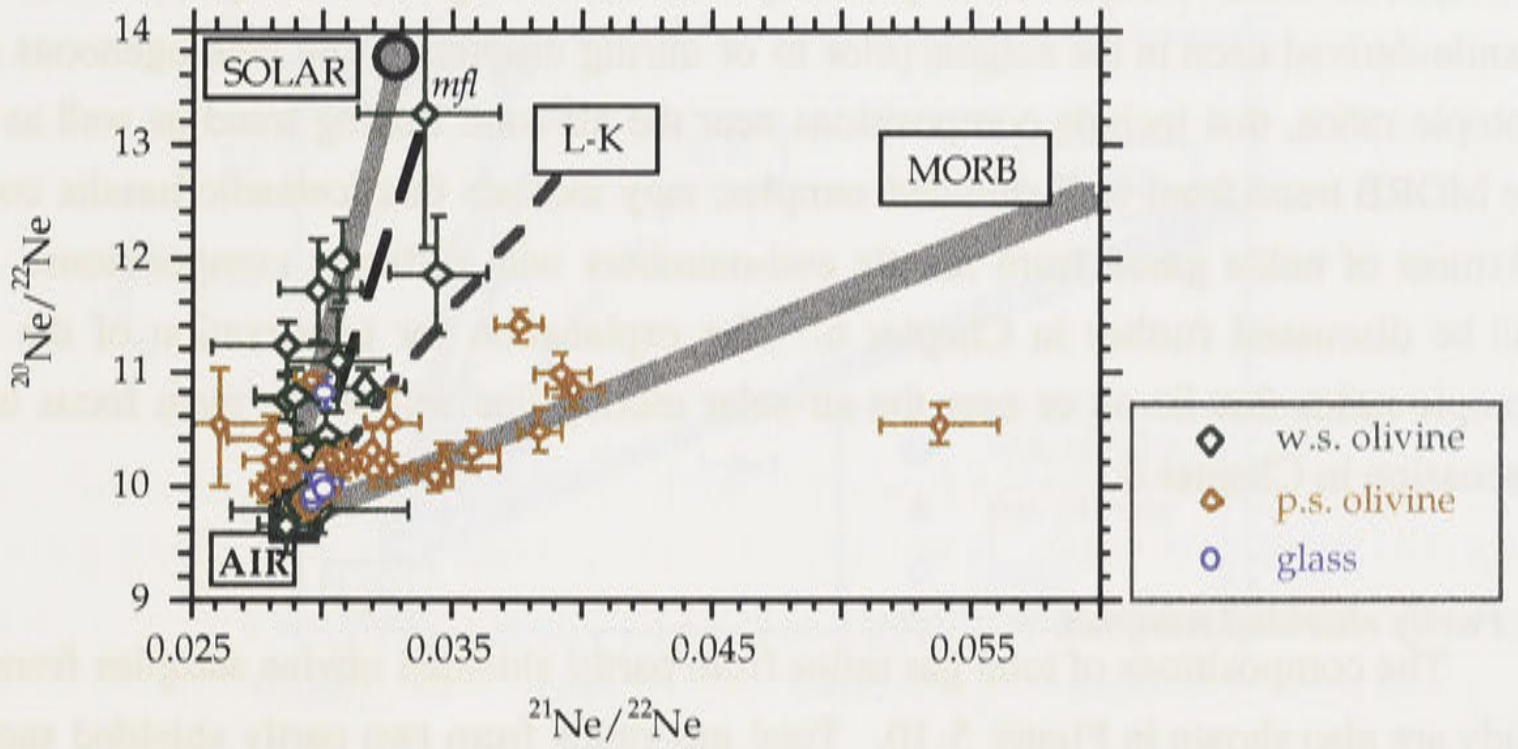

Figure 5-9. Neon three isotope plot, showing isotopic compositions of individual gas fractions from samples measured in this study. No total gas ratios are shown. The isotopic compositions of most of the well-shielded olivine samples lie close to the air-solar mixing line. The neon isotopic composition of eight gas fractions from partly-shielded olivine samples lie near the MORB correlation line. One partly-shielded sample has neon isotopic ratios below the MORB trend (*ice-4*). This sample is interpreted to have a relatively large component of cosmogenic ^{21}Ne in addition to mantle-derived neon. Gas fractions released from glass separates lie within one sigma uncertainty of the MORB trend or the atmospheric ratio for all samples except for *ice-9g*, whose composition lies within one sigma uncertainty of the air-solar mixing line.

Total gas ratios

i) Well-shielded samples

As might be expected from the neon isotopic compositions in individual gas fractions described above, the neon isotopic compositions of the total gas released from each sample also show near-solar and MORB-like compositions (Fig. 5-10). The total gas ratios from five samples (*ice-3 (-a, -b), -9 (-a, -b, -g1, -g2), -19 (-b), -30,* and *-34*) lie close to the air-solar mixing trend within one sigma uncertainty, on a slope that is steeper than the L-K line and have $^{20}Ne/^{22}Ne$ ratios that are greater than the atmospheric ratio of 9.8 by more than two sigma uncertainty. This indicates that the Icelandic plume has a higher proportion of solar to nucleogenic neon than the Hawaiian plume. Total gas ratios from five samples, including glass separates from four samples (*ice-18g2, (-g3), 32.2g1, (-g2), -47, -54g* and *–55g*) and olivine separates from two samples (*ice-18b, -19a*) lie near the MORB trend and have $^{21}Ne/^{22}Ne$ ratios that differ from the

atmospheric ratio by more than one sigma uncertainty (Fig. 5-10). The remaining gas fractions are close to the neon isotopic composition in the atmosphere. These near-atmospheric neon isotopic ratios probably reflect exchange of atmospheric neon with mantle-derived neon in the magma prior to or during eruption. The heterogeneous neon isotopic ratios, that include compositions near the air-solar mixing trend as well as near the MORB trend from well-shielded samples, may indicate that Icelandic basalts contain mixtures of noble gases from mantle end-members with different compositions. This will be discussed further in Chapter 6. The explanation for preservation of the neon isotopic ratios that lie on or near the air-solar mixing line will be the main focus of the discussion in Chapter 6.

ii) Partly shielded samples

The compositions of total gas ratios from partly shielded olivine samples from this study are also shown in Figure 5-10. Total gas ratios from two partly shielded samples lie on, or within one sigma uncertainty of the MORB correlation line (*ice-10* and *-14*). Eight olivine separates from seven samples have compositions distinct from the atmospheric ratio and the MORB trend by more than one sigma uncertainty and lie within the triangular region bounded by the air-solar mixing line and the MORB trend (*ice-1b, 2.1a, 2.2a, (-2.2b), -11.1, -11.2 -12.1 and -16*) (Fig. 5-10). The total gas ratio from one sample (*ice-4*) lies below the MORB trend. The neon composition of this sample is distinct from the MORB trend within one sigma uncertainty. The remaining three partly-shielded samples have total gas ratios that are close to the atmospheric composition.

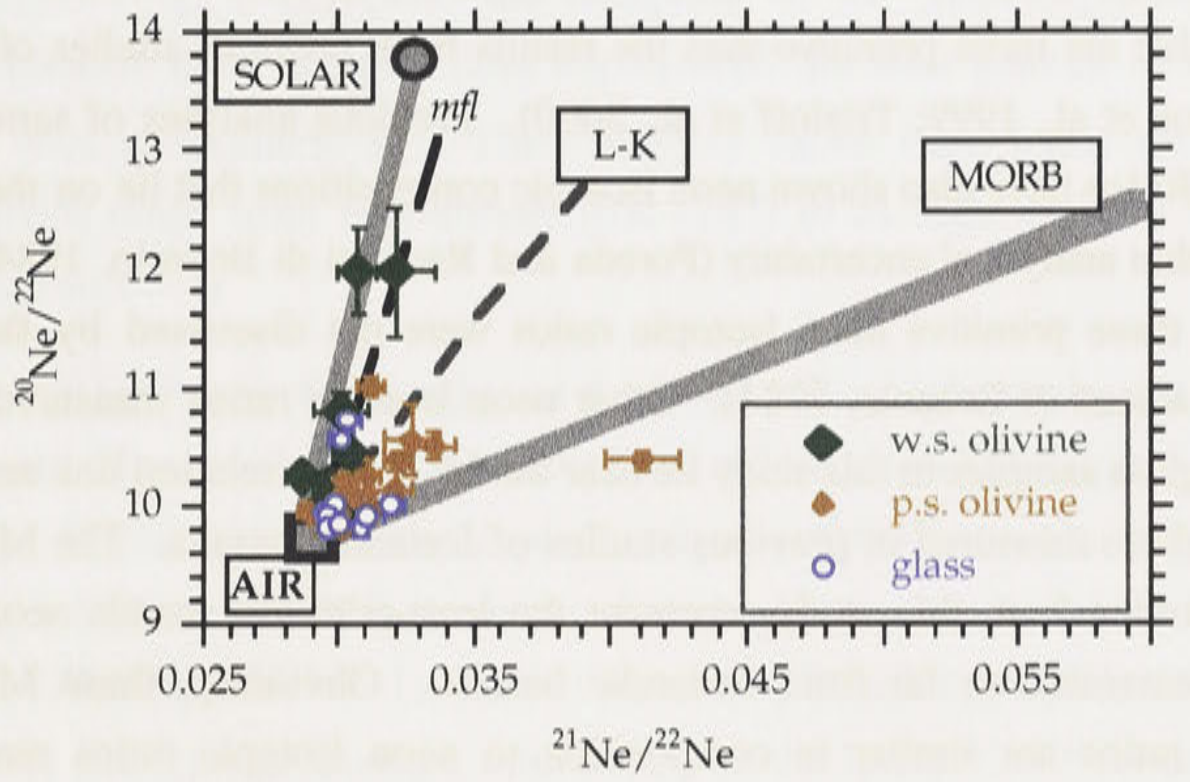

Figure 5-10. Neon isotopic compositions of the total gas released from Icelandic olivine and glass separates from this study. Five samples (*ice-3 (-a, -b), -9 (-a, -b, -g1, -g2), -19 (-b), -30,* and *-34*) have neon isotopic ratios that are within one sigma uncertainty of the air-solar mixing trend. Total gas ratios from five samples, including glass separates from four samples (*ice-18g2, (-g3), 32.2g1, (-g2), -47, -54g* and *–55g*) and olivine separates from two samples (*ice-18b, -19a*) lie near the MORB trend and have $^{21}Ne/^{22}Ne$ ratios that differ from the atmospheric ratio by more than one sigma uncertainty.

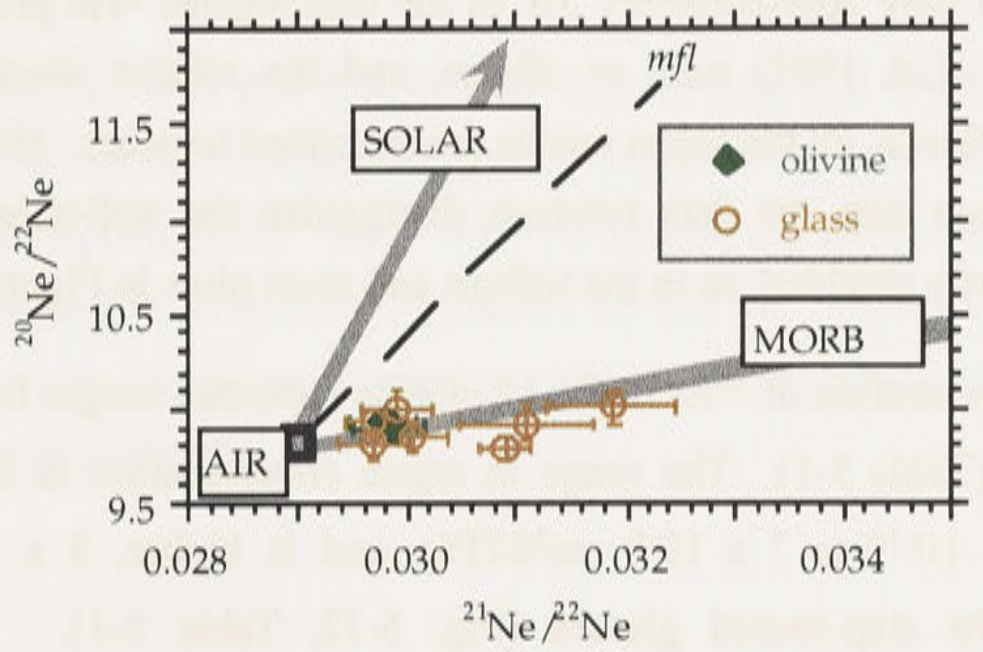

Figure 5-11. Blow-up of Fig. 5-10, showing total gas ratios of neon released from olivine (open diamonds) and glass (filled circles) from this study. There are glass separates from four samples (*ice-18g2, (-g3), 32.2g1, (-g2), -47, -54g* and *–55g*) and olivine separates from two samples (*ice-18b, -19a*) that lie near the MORB trend have neon isotopic ratios that are within one sigma uncertainty of the MORB correlation line and are distinct from the atmospheric ratio by more than one sigma uncertainty.

Comparison of neon results with previous neon measurements from Icelandic basalts

The neon isotopic ratios from this study that lie near the air-solar mixing line have end-member compositions close to the solar ratio (data extrapolated to a solar $^{20}Ne/^{22}Ne$ ratio of 13.8) that are more primitive than the results from previous studies of Icelandic basalts (Harrison et al., 1999; Trieloff et al., 2000). Previous analyses of samples from the Reykjanes Ridge have also shown neon isotopic compositions that lie on the air-solar mixing line within analytical uncertainty (Poreda and Radicati di Brozolo, 1984) (Fig. 5-3). However, these primitive neon isotopic ratios were not discussed by the authors (Poreda and Radicati di Brozolo, 1984). Other neon isotopic ratios measured in gases released from glass samples in this study lie near the MORB correlation line and are less primitive than those measured in previous studies of Icelandic basalts. The MORB-like neon isotopic ratios from this study represent the least-primitive mantle neon isotopic compositions measured so far from Icelandic basalts. Obviously, these MORB-like neon isotopic ratios are similar in composition to neon isotopic ratios measured in MORB samples from the Reykjanes Ridge to the south of Iceland (Poreda and Radicati di Brozolo, 1984), and are not unexpected considering the MORB-like $^{3}He/^{4}He$ ratios (8.5 Ra) measured in previous studies along the neovolcanic zones in Iceland (Sano et al., 1985).

Argon

In the previous sections, the helium and neon results from this study were divided into those from well-shielded and partly shielded samples. Contamination of mantle argon by cosmogenic argon can be neglected because the production rate of cosmogenic ^{36}Ar and ^{38}Ar is only approximately 5% of the cosmogenic ^{3}He production rate in Fe-bearing samples (Lal, 1991) such as olivine, and the relative abundance of argon to helium is high. Hence, all the argon results are described together. However, in the plots showing the argon data, the data symbols distinguish the well-shielded samples from those that are partly shielded, as in the helium and neon plots in Figures 5-8 to 5-10.

The concentration of ^{36}Ar in the 17 olivine separates ranges from 4×10^{-12} to 2×10^{-9} cm^3STP/g (Table 5-1). The range in argon concentration in the 6 crushed glass separates is 1×10^{-10} to 7×10^{-9} cm^3STP/g, and is higher, 3×10^{-9} to 11×10^{-9} cm^3STP/g, in the step-heated glasses (Fig. 5-12, Table 5-1). The highest ^{36}Ar concentration from the Icelandic glasses (*ice-9g*) is 1×10^{-8} cm^3STP/g. This sample also contains a higher concentration of ^{3}He (up to 1.6×10^{-10} cm^3STP/g) than the other Icelandic samples from this study (Table 5-1).

$^{40}Ar/^{36}Ar$ ratios

The highest $^{40}Ar/^{36}Ar$ ratios are typically found in samples with the lowest ^{36}Ar concentrations (Fig. 5-12) (with the exception of the glass separates from *ice-9*), probably because these samples have experienced the least amount of addition of, or exchange with, atmospheric Ar. The $^{40}Ar/^{36}Ar$ ratios from gases released by step-heating olivine range from near-atmospheric (295) to as high as 1239 ± 150 (*ice-2c*) (Fig. 5-12, Table 5-1).

The $^{40}Ar/^{36}Ar$ isotopic ratios of the gases released from glass samples by step-heating or crushing are close to the atmospheric ratio in most cases (*ice-18g, -32g, -47g, -54g, -55g*) (Table 5-1). In one sample, *ice-9g*, the $^{40}Ar/^{36}Ar$ ratio of gas released by crushing (*ice-9g2* = 942 ± 3) is about two times higher than that released by step-heating (*ice-9g1* = 478 ± 11) (Table 5-1). However, a second crushing experiment on a different glass aliquot (*ice-9g3*) produced a ratio similar to the lower $^{40}Ar/^{36}Ar$ ratio (452 ± 1). The $^{20}Ne/^{22}Ne$ ratios of samples *ice-9g1* and *-9g2*, are higher than in *ice-9g3* (Table 5-1), suggesting that the former two separates have lower relative concentrations of atmospheric neon, and that the range in $^{40}Ar/^{36}Ar$ ratios is caused by variable degrees of atmospheric contamination of the sample. The maximum $^{40}Ar/^{36}Ar$ ratio (1044 ± 268) in the olivine from the same sample (*ice-9b*) is similar to the maximum ratio in the host glass (942 ± 3). The $^{40}Ar/^{36}Ar$ ratios of the total gas released from the samples (Fig. 5-12) have a similar but slightly lower range than the gas released by individual crushing or step-heating extractions.

$^{38}Ar/^{36}Ar$ ratios

The $^{38}Ar/^{36}Ar$ ratios of gas released by step-heating and crushing of Icelandic glass and olivine separates in this study have been analysed on both the Daly Multiplier and the Faraday (see Appendix 3). The $^{38}Ar/^{36}Ar$ results are not presented here owing to large uncertainties and interferences on masses 36 and 38. However, the majority of the $^{38}Ar/^{36}Ar$ ratios are within two sigma uncertainty of the atmospheric ratio. The results are presented in Appendix 3.

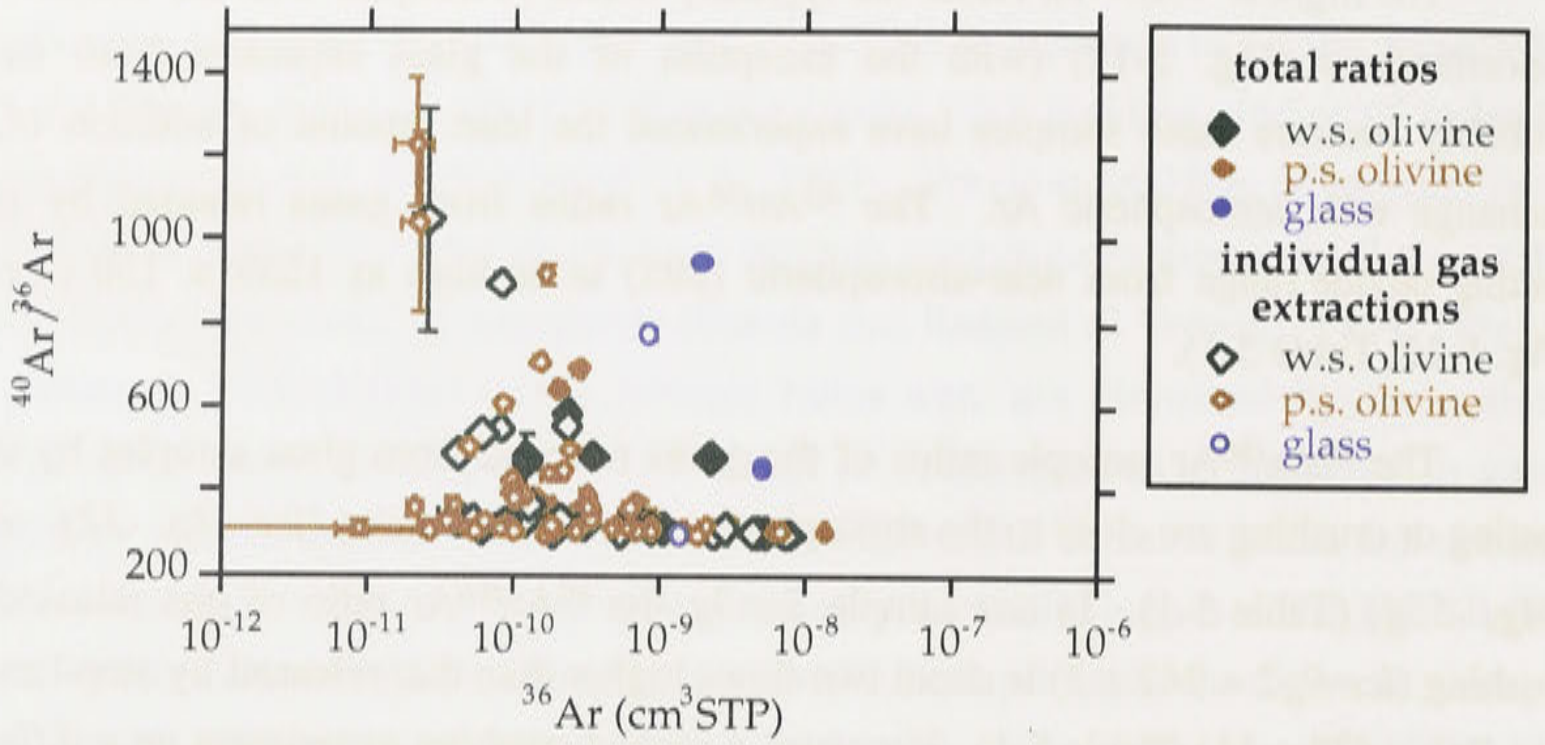

Figure 5-12. $^{40}Ar/^{36}Ar$ versus ^{36}Ar (cm^3STP) for: (1) individual gas fractions released by step-heating (open symbols) and (2) the total gas released (solid symbols) in this study. The maximum $^{40}Ar/^{36}Ar$ ratio (1229 ± 150) is from a gas fraction released from a sample that also has the lowest ^{36}Ar concentration. The glass separates from sample *ice-9* have both high ^{36}Ar contents and relatively high $^{40}Ar/^{36}Ar$ ratios compared with other glass separates. Different degrees of atmospheric contamination may account for the variability in the observed $^{40}Ar/^{36}Ar$ ratios in *ice-9g* and other Icelandic samples.

Table 5-2. Iceland argon and krypton data

T, °C	^{36}Ar cm^3STP/g (1×10^{-10})	$^{40}Ar/^{36}Ar$	^{84}Kr cm^3STP/g (1×10^{-12})	$^{78}Kr/^{84}Kr$	$^{80}Kr/^{84}Kr$	$^{82}Kr/^{84}Kr$	$^{83}Kr/^{84}Kr$	$^{86}Kr/^{84}Kr$
ice-1a, olivine, 5.029g, Midfell								
900	1.4 ± 0.1	302 ± 1	4.3 ± 0.4	0.0058 ± 0.0002	0.0386 ± 0.0005	0.200 ± 0.001	0.2003 ± 0.0009	0.306 ± 0.001
1800	0.45 ± 0.04	443 ± 3	b.c. --	b.c. --	b.c. --	b.c. --	b.c. --	b.c. --
Total	1.8 ± 0.1	337 ± 4	4.3 ± 0.4	0.0058 ± 0.0002	0.0386 ± 0.0005	0.200 ± 0.001	0.2003 ± 0.0009	0.306 ± 0.001
ice-1b, olivine, 6.638 g, Midfell								
900	3.2 ± 0.3	315.1 ± 1	3.9 ± 0.4	0.0056 ± 0.0002	0.0387 ± 0.0005	0.200 ± 0.001	0.200 ± 0.001	0.304 ± 0.003
1800	1 ± 0.1	360.4 ± 1	b.c. --	b.c. --	b.c. --	b.c. --	b.c. --	b.c. --
1850	0.25 ± 0.02	291 ± 0.9	b.c. --	b.c. --	b.c. --	b.c. --	b.c. --	b.c. --
Total	4.5 ± 0.3	324.2 ± 1.3	3.9 ± 0.4	0.0056 ± 0.0002	0.0387 ± 0.0005	0.200 ± 0.001	0.200 ± 0.001	0.304 ± 0.003
ice-2.1a, olivine, 4.309 g, Sa ndfell (Hengill)								
900	4.3 ± 0.4	292.7 ± 0.7	16 ± 1	0.0058 ± 0.0003	0.0389 ± 0.0005	0.200 ± 0.001	0.2008 ± 0.0007	0.306 ± 0.001
1800	2.1 ± 0.2	314.5 ± 0.8	b.c. --	b.c. --	b.c. --	b.c. --	b.c. --	b.c. --
1850	b.c. --	b.c. --	b.c. --	b.c. --	b.c. --	b.c. --	b.c. --	b.c. --
Total	6.4 ± 0.5	299.9 ± 0.9	16 ± 1	0.0058 ± 0.0003	0.0389 ± 0.0005	0.200 ± 0.001	0.2008 ± 0.0007	0.306 ± 0.001
ice-2.2a, olivine, 6.162 g, Sandfell (Hengill)								
400	0.015 ± 0	310 ± 13	b.c. --	b.c. --	b.c. --	b.c. --	b.c. --	b.c. --
700	10 ± 1	298.4 ± 0.7	20 ± 2	0.0059 ± 0.0002	0.0393 ± 0.0005	0.201 ± 0.001	0.2009 ± 0.0007	0.306 ± 0.001
900	1 ± 0.1	305.6 ± 0.8	b.c. --	b.c. --	b.c. --	b.c. --	b.c. --	b.c. --
1350	11 ± 1	300.9 ± 0.7	b.c. --	b.c. --	b.c. --	b.c. --	b.c. --	b.c. --
1800	0.56 ± 0.09	330.6 ± 5.3	1.3 ± 0.1	0.0059 ± 0.0002	0.0392 ± 0.0005	0.202 ± 0.001	0.202 ± 0.002	0.304 ± 0.003
1850	0.08 ± 0.08	309 ± 15	b.c. --	b.c. --	b.c. --	b.c. --	b.c. --	b.c. --
1900	0.09 ± 0.08	303 ± 7	b.b. --	b.b. --	b.b. --	b.b. --	b.b. --	b.b. --
Total	22.8 ± 1.5	300.7 ± 0.5	21 ± 2	0.0059 ± 0.0002	0.0393 ± 0.0004	0.201 ± 0.0006	0.2009 ± 0.0007	0.306 ± 0.001
ice-2.2b, olivine, 6.190 g, Sandfell (Hengill)								
400	b.b. --	b.b. --	b.b. --	b.b. --	b.b. --	0.196 ± 0.008	0.203 ± 0.005	0.32 ± 0.01
800	0.31 ± 0.03	303.8 ± 1.5	1.5 ± 0.1	0.0050 ± 0.0004	0.0394 ± 0.0005	0.199 ± 0.001	0.2015 ± 0.0009	0.315 ± 0.003
870	b.b. --	b.b. --	b.b. --	b.b. --	b.b. --	b.b. --	b.b. --	b.b. --
1280	0.034 ± 0.01	1229 ± 153	b.c. --	b.c. --	b.c. --	b.c. --	b.c. --	b.c. --
1800	0.18 ± 0.02	374 ± 3	b.c. --	b.c. --	b.c. --	b.c. --	b.c. --	b.c. --
1850	b.b. --	b.b. --	b.c. --	b.b. --	b.b. --	b.b. --	b.b. --	b.b. --
Total	0.53 ± 0.04	387 ± 14	1.5 ± 0.1	0.0050 ± 0.0004	0.0394 ± 0.0005	0.199 ± 0.001	0.2021 ± 0.0008	0.316 ± 0.002

T, °C	^{36}Ar cm^3STP/g (1×10^{-10})	$^{40}Ar/^{36}Ar$	^{84}Kr cm^3STP/g (1×10^{-12})	$^{78}Kr/^{84}Kr$	$^{80}Kr/^{84}Kr$	$^{82}Kr/^{84}Kr$	$^{83}Kr/^{84}Kr$	$^{86}Kr/^{84}Kr$
ice-3a, olivine, 3.384 g, Burfell i olfusi								
900	0.8 ± 0.1	299 ± 1	b.b. --	b.b. --	b.b. --	b.b. --	b.b. --	b.b. --
1800	1 ± 0.1	381 ± 5	b.b. --	b.b. --	b.b. --	b.b. --	b.b. --	b.b. --
1850	0.12 ± 0.05	325 ± 17	b.b. --	b.b. --	b.b. --	b.b. --	b.b. --	b.b. --
Total	2 ± 0.2	343 ± 4	b.b. --	b.b. --	b.b. --	b.b. --	b.b. --	b.b. --
ice-3b, olivine, 2.786 g, Burfell i olfusi								
900	0.33 ± 0.03	317 ± 2	b.b. --	b.b. --	b.b. --	b.b. --	b.b. --	b.b. --
1800	0.31 ± 0.03	607 ± 11	b.b. --	b.b. --	b.b. --	b.b. --	b.b. --	b.b. --
1850	0.1 ± 0.01	300 ± 4	b.b. --	b.b. --	b.b. --	b.b. --	b.b. --	b.b. --
Total	0.73 ± 0.05	436 ± 10	b.b. --	b.b. --	b.b. --	b.b. --	b.b. --	b.b. --
ice-4, olivine, 3.181 g, Halejarbunga								
900	2.8 ± 0.3	299.3 ± 0.8	8.0 ± 0.8	0.0059 ± 0.0002	0.0391 ± 0.0005	0.202 ± 0.001	0.2002 ± 0.0009	0.309 ± 0.001
1800	1.6 ± 0.2	315 ± 2	b.c. --	b.c. --	b.c. --	b.c. --	b.c. --	b.c. --
1850	0.2 ± 0.1	321 ± 16	b.c. --	b.c. --	b.c. --	b.c. --	b.c. --	b.c. --
Total	4.6 ± 0.4	306 ± 1	8.0 ± 0.8	0.0059 ± 0.0002	0.0390 ± 0.0005	0.202 ± 0.001	0.2003 ± 0.0008	0.308 ± 0.001
ice-9a, olivine, 5.162 g, Midfell								
900	4.6 ± 0.3	296.8 ± 0.7	b.b. --	b.b. --	b.b. --	b.b. --	b.b. --	b.b. --
1800	5.7 ± 0.4	311.9 ± 0.7	b.b. --	b.b. --	b.b. --	b.b. --	b.b. --	b.b. --
Total	10.3 ± 0.5	305.1 ± 0.6	b.b. --	b.b. --	b.b. --	b.b. --	b.b. --	b.b. --
ice-9b, olivine, 5.160 g, Midfell								
900	0.08 ± 0.02	337 ± 10	b.b. --	b.b. --	b.b. --	b.b. --	b.b. --	b.b. --
1800	0.05 ± 0.01	1044 ± 268	b.b. --	b.b. --	b.b. --	b.b. --	b.b. --	b.b. --
1850	0.12 ± 0.02	309 ± 3	b.b. --	b.b. --	b.b. --	b.b. --	b.b. --	b.b. --
Total	0.25 ± 0.03	468 ± 66	b.b. --	b.b. --	b.b. --	b.b. --	b.b. --	b.b. --
ice-9c, olivine, 5.176 g, Midfell								
900	0.08 ± 0.01	330 ± 8	b.b. --	b.b. --	b.b. --	b.b. --	b.b. --	b.b. --
1800	0.16 ± 0.01	545 ± 15	b.b. --	b.b. --	b.b. --	b.b. --	b.b. --	b.b. --
Total	0.24 ± 0.02	472 ± 12	b.b. --	b.b. --	b.b. --	b.b. --	b.b. --	b.b. --
ice-9d, olivine, 0.70163 g, Midfell								
crush	0.72 ± 0.05	326 ± 2	b.c. --	b.c. --	b.c. --	b.c. --	b.c. --	b.c. --
ice-9g1, glass, 2.026 g, Midfell								
700	6.9 ± 0.5	298.2 ± 0.7	7.6 ± 0.2	0.059 ± 0.002	0.0390 ± 0.0005	0.197 ± 0.001	0.1996 ± 0.0008	b.b. --
1600	4.3 ± 0.3	769 ± 6	5.8 ± 0.2	0.0221 ± 0.0009	0.0386 ± 0.0003	0.200 ± 0.001	0.201 ± 0.001	0.303 ± 0.001
Total	11.2 ± 0.5	478 ± 11	13.4 ± 0.3	0.043 ± 0.001	0.0388 ± 0.0003	0.199 ± 0.001	0.2004 ± 0.0007	0.303 ± 0.001

T, °C	^{36}Ar cm^{3}STP/g (1 x 10^{-10})	$^{40}Ar/^{36}Ar$	^{84}Kr cm^{3}STP/g (1 x 10^{-12})	$^{78}Kr/^{84}Kr$	$^{80}Kr/^{84}Kr$	$^{82}Kr/^{84}Kr$	$^{83}Kr/^{84}Kr$	$^{86}Kr/^{84}Kr$
ice-9g2, glass, 0.585 g, Midfell								
crush	33 ± 2	942 ± 3	52 ± 2	0.0064 ± 0.0003	0.0397 ± 0.0005	0.2029 ± 0.0007	0.2028 ±0.0007	0.305 ±0.001
ice-9g3, glass, 0.720 g, Midfell								
crush	72 ± 5	452 ± 1	108 ± 3	0.015 ± 0.001	0.0396 ± 0.0005	0.2011 ± 0.0007	0.201 ±0.001	0.3059 ±0.0006
ice-10.1, olivine, 4.66 g, Maelifell								
900	0.2 ± 0.02	313 ± 3	1.65 ± 0.05	6.4 ± 0.2	0.0396 ± 0.0003	0.207 ± 0.001	0.2034 ±0.0007	0.305 ±0.001
1800	0.11 ± 0.01	503 ± 17	b.c. --	b.c. --	b.c. --	b.c. --	b.c. --	b.c. --
Total	0.31 ± 0.02	379 ± 8	1.65 ± 0.05	6.4 ± 0.2	0.0396 ± 0.0003	0.207 ± 0.001	0.2034 ±0.0007	0.305 ±0.001
ice-10.2, olivine, 5.904 g, Maelifell								
900	0.31 ± 0.02	316 ± 1	1.45 ± 0.04	2.49 ± 0.03	0.0399 ± 0.0003	0.2035 ± 0.0009	0.202 ±0.001	0.304 ±0.001
1800	0.17 ± 0.01	422 ± 4	b.c. --	b.c. --	b.c. --	b.c. --	b.c. --	b.c. --
Total	0.49 ± 0.02	354 ± 3	1.45 ± 0.04	2.49 ± 0.03	0.0399 ± 0.0003	0.2035 ± 0.0009	0.202 ±0.001	0.304 ±0.001
ice-11.1, olivine, 3.758 g, Sandfell (Hengill)								
900	0.22 ± 0.02	312 ± 2	b.c. --	b.c. --	b.c. --	b.c. --	b.c. --	b.c. --
1800	0.27 ± 0.02	399 ± 3	b.c. --	b.c. --	b.c. --	b.c. --	b.c. --	b.c. --
Total	0.49 ± 0.02	361 ± 3	b.c. --	b.c. --	b.c. --	b.c. --	b.c. --	b.c. --
ice-11.2, olivine, 5.535 g, Sandfell (Hengill)								
900	b.b. --	b.b. --	b.b. --	b.b. --	b.b. --	b.b. --	b.b. --	b.b. --
1800	0.04 ± 0.01	1040 ± 214	0.33 ± 0.01	0.54 ± 0.03	0.041 ± 0.001	0.205 ± 0.002	0.205 ±0.002	0.299 ±0.003
Total	0.04 ± 0.01	1040 ± 214	0.33 ± 0.01	0.54 ± 0.03	0.041 ± 0.001	0.205 ± 0.002	0.205 ±0.002	0.299 ±0.003
ice-12.1, olivine, 3.06 g, Asar								
900	0.07 ± 0.01	358 ± 19	0.34 ± 0.01	0.69 ± 0.01	0.0394 ± 0.0002	0.203 ± 0.002	0.203 ±0.002	0.307 ±0.003
1800	1.06 ± 0.07	357 ± 1	b.c. --	b.c. --	b.c. --	b.c. --	b.c. --	b.c. --
Total	1.12 ± 0.07	357 ± 2	0.34 ± 0.01	0.69 ± 0.01	0.0394 ± 0.0002	0.203 ± 0.002	0.203 ±0.002	0.307 ±0.003
ice-12.2, olivine, 5.103 g, Asar								
900	0.94 ± 0.06	306 ± 1	3.8 ± 0.1	1.33 ± 0.02	0.0395 ± 0.0002	0.202 ± 0.001	0.2006 ±0.0006	0.305 ±0.001
1800	0.49 ± 0.03	499 ± 3	1.10 ± 0.03	0.324 ± 0.007	0.0401 ± 0.0004	0.201 ± 0.001	0.1998 ±0.0007	0.304 ±0.002
Total	1.43 ± 0.07	373 ± 4	4.9 ± 0.1	1.10 ± 0.02	0.0396 ± 0.0002	0.202 ± 0.001	0.2005 ±0.0005	0.3045 ±0.0009
ice-14, olivine, 3.087 g, Burfell i olfusi								
900	b.c. --	b.c. --	b.c. --	b.c. --	b.c. --	b.c. --	b.c. --	b.c. --
1800	0.57 ± 0.04	439 ± 5	b.c. --	b.c. --	b.c. --	b.c. --	b.c. --	b.c. --
Total	0.57 ± 0.04	439 ± 5	b.c. --	b.c. --	b.c. --	b.c. --	b.c. --	b.c. --

T, °C	^{36}Ar cm^{3}STP/g (1×10^{-10})	$^{40}Ar/^{36}Ar$	^{84}Kr cm^{3}STP/g (1×10^{-12})	$^{78}Kr/^{84}Kr$	$^{80}Kr/^{84}Kr$	$^{82}Kr/^{84}Kr$	$^{83}Kr/^{84}Kr$	$^{86}Kr/^{84}Kr$
ice-16, olivine, 5.388 g, Edlborg								
900	0.22 ± 0.02	385 ± 4	1.28 ± 0.04	0.81 ± 0.03	0.0386 ± 0.0004	0.201 ± 0.001	0.2002 ± 0.0009	0.306 ± 0.003
1800	0.31 ± 0.02	915 ± 19	b.b. --	b.b. --	b.b. --	b.b. --	b.b. --	b.b. --
Total	0.53 ± 0.03	692 ± 17	1.28 ± 0.04	0.81 ± 0.03	0.0386 ± 0.0004	0.201 ± 0.001	0.2002 ± 0.0009	0.306 ± 0.003
ice-18b, olivine, 3.649 g, Stapafell								
900	0.34 ± 0.02	320 ± 1	2.01 ± 0.06	1.29 ± 0.02	0.0399 ± 0.0003	0.202 ± 0.001	0.202 ± 0.001	0.305 ± 0.001
1800	0.113 ± 0.01	487 ± 11	b.c. --	b.c. --	b.c. --	b.c. --	b.c. --	b.c. --
Total	0.45 ± 0.02	362 ± 4	2.01 ± 0.06	1.29 ± 0.02	0.0399 ± 0.0003	0.202 ± 0.001	0.202 ± 0.001	0.305 ± 0.001
ice-18g2, glass, 3.704 g, Stapafell								
700	0.53 ± 0.04	300 ± 0.7	3.6 ± 0.1	1.14 ± 0.04	0.0396 ± 0.0004	0.2027 ± 0.0009	0.2008 ± 0.0007	0.305 ± 0.001
1500	2.5 ± 0.2	306.9 ± 0.7	3.05 ± 0.09	0.53 ± 0.02	0.0396 ± 0.0003	0.2019 ± 0.0007	0.2026 ± 0.0008	0.304 ± 0.001
Total	3 ± 0.2	305.7 ± 0.6	6.7 ± 0.1	0.86 ± 0.02	0.0396 ± 0.0002	0.2024 ± 0.0006	0.2016 ± 0.0005	0.3044 ± 0.0008
ice-18g3, glass, 0.983 g, Stapfell								
crush	2.8 ± 0.2	301.1 ± 0.9	b.c. --	b.c. --	b.c. --	b.c. --	b.c. --	b.c. --
ice-19a, olivine, 5.341 g, Sulur								
900	0.59 ± 0.04	316 ± 1	15.9 ± 0.5	0.293 ± 0.008	0.0396 ± 0.0002	0.2013 ± 0.0005	0.2010 ± 0.0005	0.305 ± 0.001
1800	14.1 ± 0.9	295 ± 1	b.c. --	0.303 ± 0.006	b.c. --	0.208 ± 0.002	0.204 ± 0.001	0.307 ± 0.001
Total	14.7 ± 0.9	296 ± 1	15.9 ± 0.5	0.293 ± 0.008	0.0396 ± 0.0002	0.2016 ± 0.0005	0.2011 ± 0.0005	0.3047 ± 0.0009
ice-19b, olivine, 5.1531 g, Sulur								
900	b.c. --	b.c. --	b.c. --	b.c. --	b.c. --	b.c. --	b.c. --	b.c. --
1800	b.c. --	b.c. --	b.c. --	b.c. --	b.c. --	b.c. --	b.c. --	b.c. --
Total	b.c. --	b.c. --	b.c. --	b.c. --	b.c. --	b.c. --	b.c. --	b.c. --
ice-23a, olivine, 5.06 g, Haleyjarbunga								
900	b.b. --	b.b. --	1.1 ± 0.04	0.104 ± 0.003	0.0388 ± 0.0005	0.200 ± 0.001	0.200 ± 0.001	0.306 ± 0.002
1800	0.21 ± 0.01	303 ± 1	b.b. --	b.b. --	b.b. --	b.b. --	b.b. --	b.b. --
Total	0.21 ± 0.01	303 ± 1	1.1 ± 0.04	0.104 ± 0.003	0.0388 ± 0.0005	0.200 ± 0.001	0.200 ± 0.001	0.306 ± 0.002
ice-24 , olivine, 2.847 g, Hraunsvik/Hrolfsvik								
900	0.13 ± 0.02	320 ± 4	b.c. --	b.c. --	b.c. --	b.c. --	b.c. --	b.c. --
1800	0.36 ± 0.03	378 ± 4	b.c. --	b.c. --	b.c. --	b.c. --	b.c. --	b.c. --
Total	0.49 ± 0.03	363 ± 3	b.c. --	b.c. --	b.c. --	b.c. --	b.c. --	b.c. --

T, °C	^{36}Ar cm^3STP/g (1×10^{-10})	$^{40}Ar/^{36}Ar$	^{84}Kr cm^3STP/g (1×10^{-12})	$^{78}Kr/^{84}Kr$	$^{80}Kr/^{84}Kr$	$^{82}Kr/^{84}Kr$	$^{83}Kr/^{84}Kr$	$^{86}Kr/^{84}Kr$
ice-25, olivine, 4.912, g, Bleikholl								
900	0.08 ± 0.01	367 ± 11	1.66 ± 0.05	0.031 ± 0.001	0.0399 ± 0.0003	0.202 ± 0.001	0.2001 ± 0.0009	0.305 ± 0.002
1800	0.32 ± 0.02	709 ± 15	b.c. --	b.c. --	b.c. --	b.c. --	b.c. --	b.c. --
Total	0.41 ± 0.02	640 ± 14	1.66 ± 0.05	0.031 ± 0.001	0.0399 ± 0.0003	0.202 ± 0.001	0.2001 ± 0.0009	0.305 ± 0.002
ice-30, olivine, 5.071 g, near Landamnahellir								
900	0.18 ± 0.01	323 ± 2	0.53 ± 0.02	0.118 ± 0.002	0.036 ± 0.001	0.201 ± 0.002	0.200 ± 0.001	b.b. --
1800	0.16 ± 0.01	896 ± 19	0.266 ± 0.009	0.126 ± 0.003	0.040 ± 0.002	0.202 ± 0.002	0.202 ± 0.002	b.b. --
1850	0.12 ± 0.01	535 ± 10	0.190 ± 0.007	0.139 ± 0.003	0.041 ± 0.002	0.207 ± 0.002	0.200 ± 0.002	b.b. --
Total	0.46 ± 0.02	580 ± 13	0.98 ± 0.02	0.124 ± 0.001	0.038 ± 0.001	0.202 ± 0.001	0.2007 ± 0.0008	b.b.
ice-32.1a, olivine, 5.054 g, near Svartsengisfell								
900	0.26 ± 0.02	366 ± 2	1.04 ± 0.03	1.25 ± 0.04	0.0396 ± 0.0007	0.202 ± 0.001	0.202 ± 0.001	0.305 ± 0.002
1800	0.46 ± 0.03	552 ± 3	b.c. --	b.c. --	b.c. --	b.c. --	b.c. --	b.c. --
Total	0.72 ± 0.04	485 ± 5	1.04 ± 0.03	1.25 ± 0.04	0.0396 ± 0.0007	0.202 ± 0.001	0.202 ± 0.001	0.305 ± 0.002
ice-32.2g1, glass, 3.056 g, near Svartsengisfell								
700	14.5 ± 1	299.7 ± 0.6	19.3 ± 0.6	0.305 ± 0.008	0.0395 ± 0.0003	0.2023 ± 0.0006	0.2019 ± 0.0006	0.304 ± 0.001
1500	1.8 ± 0.1	304.5 ± 0.8	1.8 ± 0.1	0.403 ± 0.006	0.0395 ± 0.0004	0.203 ± 0.001	0.2016 ± 0.0009	0.305 ± 0.001
Total	16.3 ± 1	300.2 ± 0.6	21.1 ± 0.6	0.314 ± 0.008	0.0395 ± 0.0003	0.2024 ± 0.0006	0.2019 ± 0.0006	0.3044 ± 0.0009
ice-32.2g2, glass, 1.040 g, near Svartsengisfell								
crush	8.4 ± 0.6	299.4 ± 0.8	9.6 ± 0.3	0.101 ± 0.003	0.0393 ± 0.0005	0.2006 ± 0.0008	0.201 ± 0.001	0.3074 ± 0.0008
ice-34a, olivine, 3.556 g, SW of Skala -Maelifell								
900	0.15 ± 0.02	329 ± 4	b.c. --	b.c. --	b.c. --	b.c. --	b.c. --	b.c. --
1800	0.62 ± 0.04	334 ± 1	b.c. --	b.c. --	b.c. --	b.c. --	b.c. --	b.c. --
Total	0.77 ± 0.05	333 ± 1	b.c. --	b.c. --	b.c. --	b.c. --	b.c. --	b.c. --
ice-34PX, pyroxene, 0.70516 g, SW of Skala -Maelifell								
crush	1.6 ± 0.1	312 ± 2	b.c. --	b.c. --	b.c. --	b.c. --	b.c. --	b.c. --
ice-47g, glass, 0.921 g, Sigalda								
crush	1.26 ± 0.09	357 ± 3	b.c. --	b.c. --	b.c. --	b.c. --	b.c. --	b.c. --
ice-54g, glass, 0.8246 g, Lambafell								
crush	6.4 ± 0.4	298.4 ± 0.9	9.0 ± 0.3	0.049 ± 0.002	0.0392 ± 0.0005	0.201 ± 0.001	0.2017 ± 0.0008	0.308 ± 0.001
ice-55g, glass, 0.8184 g, Kongsgil								
crush	6.3 ± 0.4	299.4 ± 0.9	10.8 ± 0.3	0.081 ± 0.003	0.0391 ± 0.0005	0.195 ± 0.002	0.200 ± 0.001	0.306 ± 0.002

Comparison of $^{40}Ar/^{36}Ar$ results with previous argon measurements from Icelandic basalts

The maximum $^{40}Ar/^{36}Ar$ ratios measured in this study, 1667 ± 365 in olivine (individual gas extracted by step-heating) and 942 ± 3 in glass (crushed) are lower than the maximum measured ratios in previous studies (2200 ± 200, Burnard et al. (1994) and 6501 ± 311, Harrison et al. (1999), 4350 ± 93, Trieloff et al. (2000)). These large variations in $^{40}Ar/^{36}Ar$ isotopic ratios may originate in part from heterogeneous $^{40}Ar/^{36}Ar$ ratios in the magmatic sources of Icelandic basalts. Such heterogeneity could arise from different magmatic components within the Icelandic plume, as well as from the likely addition of atmospheric argon. These possible explanations will be discussed in Chapter 6.

Krypton

Krypton abundances in glass samples range from $^{84}Kr = 7 \times 10^{-12}$ to 1×10^{-10} cm^3STP/g (Table 5-3). Krypton abundances in olivine separates range from 3×10^{-13} to 2×10^{-11} cm^3STP/g. Krypton isotopic ratios are shown in a delta (D) plot, which expresses the measured ratios in terms of fractional deviations from the atmospheric ratios, where delta is defined as $D(^iKr) = (^iKr/^{84}Kr_{MEASURED} - {}^iKr/^{84}Kr_{AIR})/(^iKr/^{84}Kr_{AIR})$ (note that "D" used here to represent delta is not to be confused with the diffusion coefficient "D" in Chapter 2). The krypton isotopic ratios from Icelandic samples measured in this study (Fig. 5-13) are within one sigma uncertainty of the atmospheric ratios (Table 5-3).

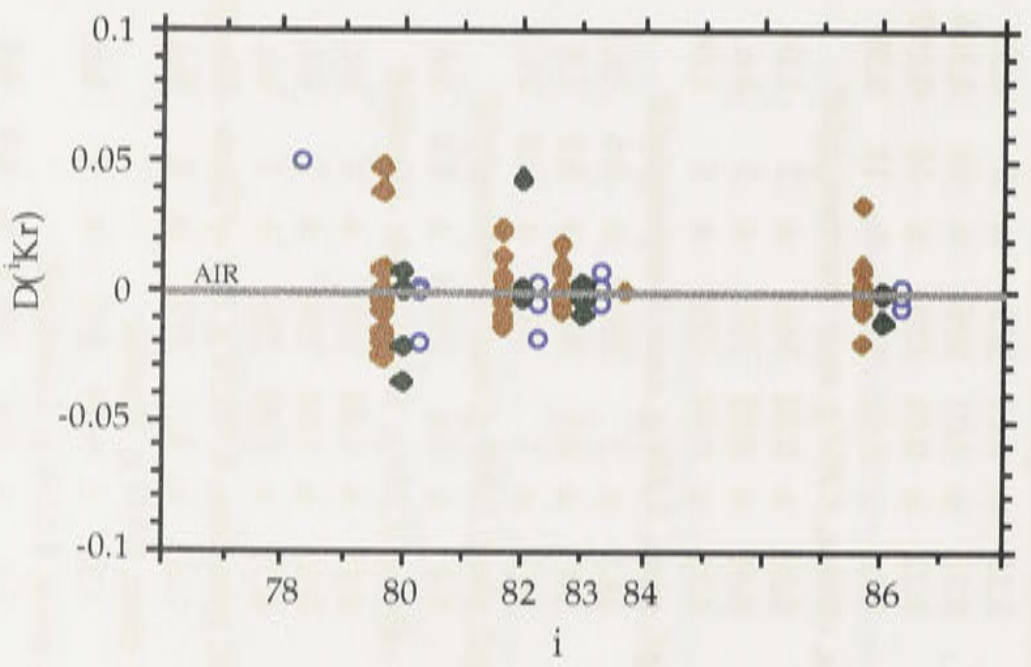

Figure 5-13. Krypton delta plot, showing measured total gas isotopic ratios from Icelandic basalts. Uncertainties have been omitted for clarity, but all isotopic ratios are within one sigma uncertainty of the krypton atmospheric ratios (green diamonds = well-shielded olivine; blue dots = glass, red diamonds = partly shielded olivine).

Xenon

Xenon concentrations in the olivine separates in this study range from ^{130}Xe = 1.3 x 10^{-14} cm^3STP/g to 45 x 10^{-14} cm^3STP/g (Table 5-3). Those in the glass separates range from 8.3 x 10^{-14} cm^3STP/g to 50 x 10^{-14} cm^3STP/g. Several olivine and glass separates (7 olivine separates and 7 glass separates) are not reported because they have absolute xenon abundances that are below the detection limit of the mass spectrometer (2 x 10^{-14} cm^3STP, see Appendix 2, methods). The reported xenon concentrations have been corrected for the xenon blank and are not below the detection limit.

Like the krypton isotopic ratios, the xenon isotopic ratios are shown as fractional deviations from the atmospheric ratio in a delta plot, where delta is here defined as:

$D(^iXe) = (^iXe/^{130}Xe_{MEASURED} - {}^iXe/^{130}Xe_{AIR})/(^iXe/^{130}Xe_{AIR})$.

The xenon isotopic ratios of most of the Icelandic samples are similar to the ratios in the atmosphere (Fig. 5-14). Only one sample (*ice-9g2*) has $^{129}Xe/^{130}Xe$ and $^{136}Xe/^{130}Xe$ ratios that are significantly different from the atmospheric ratios within one sigma uncertainty (Fig. 5-15). This sample also has neon isotopic ratios that lie on the air-solar mixing line within one sigma uncertainty. The $^{129}Xe/^{130}Xe$ and $^{136}Xe/^{130}Xe$ ratios from this study lie on the same trend as that defined by MORB samples with elevated ratios compared with the atmospheric ratio (Fig. 5-16).

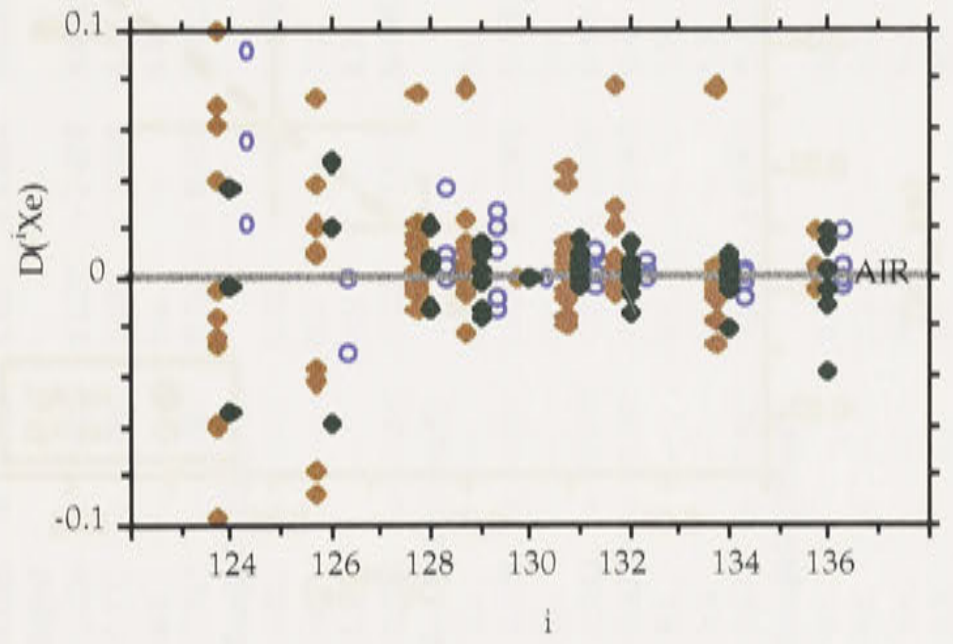

Figure 5-14. Xenon delta plot, where delta is $D(^iXe) = (^iXe/^{130}Xe_{MEASURED} - {}^iXe/^{130}Xe_{AIR})/(^iXe/^{130}Xe_{AIR})$, showing deviations of measured total gas isotopic ratios from the xenon atmospheric composition. All samples lie within one sigma uncertainty of the atmospheric ratio (uncertainties omitted for clarity) with the exception of *ice-9g*, which is shown in a separate plot below (green diamonds = well-shielded olivine; blue dots = glass, red diamonds = partly shielded olivine).

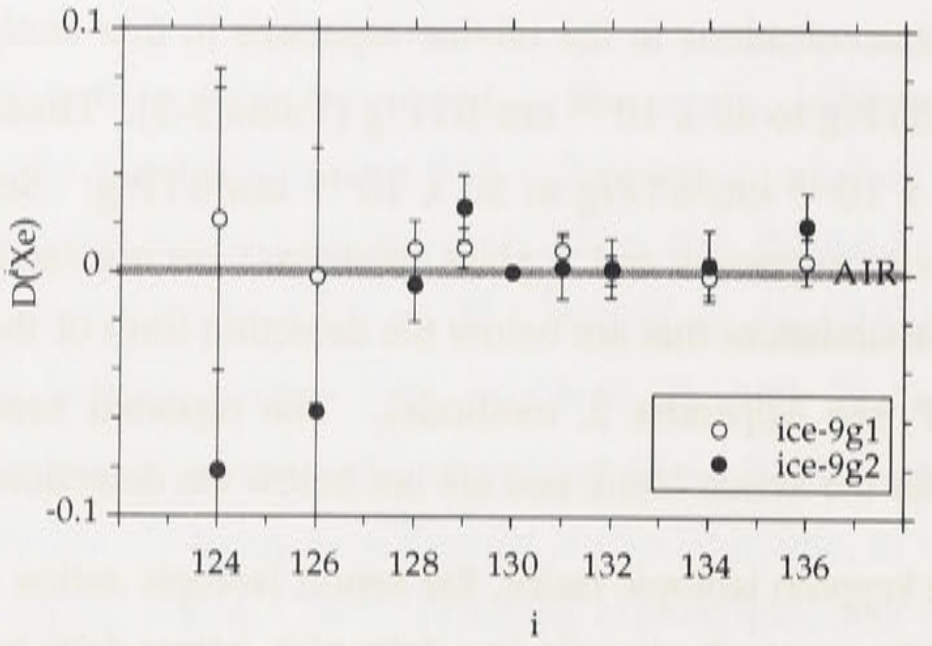

Figure 5-15. Xenon delta plot for glass separates *ice-9g1* and *–9g2*. *Ice-9g1* is the only Icelandic that has xenon isotopic ratios that are significantly different from the atmospheric ratios within one sigma uncertainty. This sample shows elevated $^{129}Xe/^{130}Xe$ and $^{136}Xe/^{130}Xe$ that are about 2% higher than the atmospheric ratios. The ratios are higher in *ice-9g1* (a step-heated glass separate) than in *ice-9g2* (crushed glass). This sample also has neon isotopic ratios that lie within one sigma uncertainty of the air-solar mixing line.

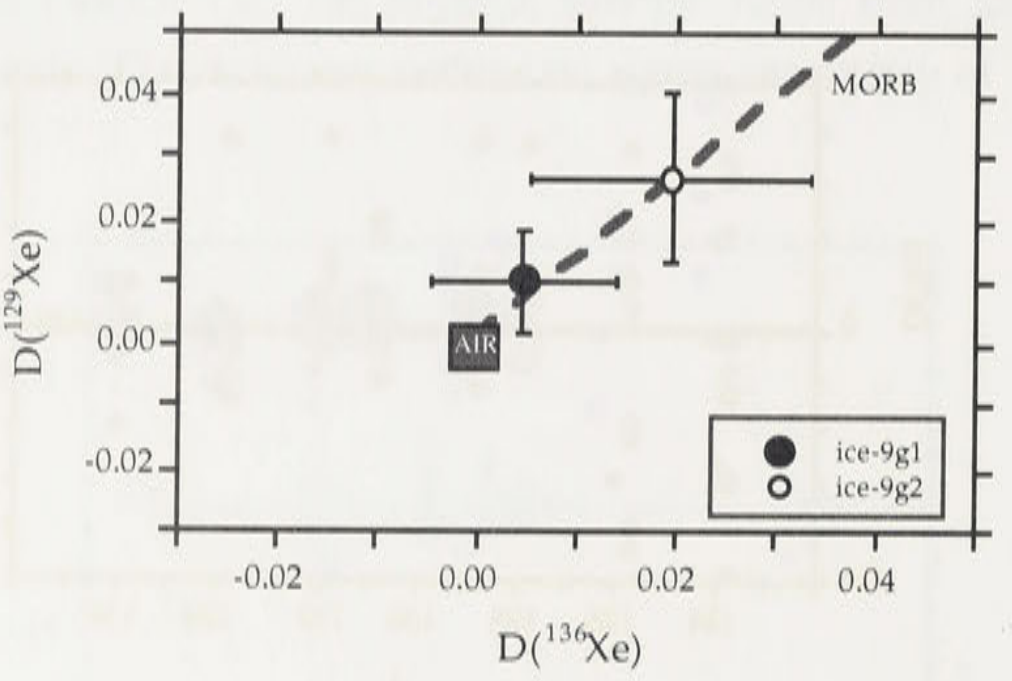

Figure 5-16. Xenon delta plot, showing $D(^{129}Xe)$ versus $D(^{136}Xe)$ plot for glass separates *ice-9g1* and *–9g2*. The xenon isotopic compositions of these glass separates have large uncertainties, but appear to lie on the same trend as xenon isotopic compositions from MORB basalts.

Table 5-3. Iceland xenon data

T, °C	^{130}Xe cm^3STP/g (1×10^{-14})	$^{124}Xe/^{130}Xe$	$^{126}Xe/^{130}Xe$	$^{128}Xe/^{130}Xe$	$^{129}Xe/^{130}Xe$	$^{131}Xe/^{130}Xe$	$^{132}Xe/^{130}Xe$	$^{134}Xe/^{130}Xe$	$^{136}Xe/^{130}Xe$
ice-1a, olivine, 5.029g, Midfell									
900	6.0 ± 0.3	0.029 ± 0.003	0.024 ± 0.003	0.470 ± 0.008	6.36 ± 0.09	5.12 ± 0.06	6.6 ± 0.1	2.52 ± 0.04	2.14 ± 0.03
1800	b.c. --	b.c. --	b.c. --	b.c. --	b.c. --	b.c. --	b.c. --	b.c. --	b.c. --
Total	6.0 ± 0.3	0.029 ± 0.003	0.024 ± 0.003	0.470 ± 0.008	6.36 ± 0.09	5.12 ± 0.06	6.6 ± 0.1	2.52 ± 0.04	2.14 ± 0.03
ice-1b, olivine, 6.638 g, Midfell									
900	43 ± 2	0.024 ± 0.001	0.022 ± 0.002	0.466 ± 0.006	6.49 ± 0.06	5.21 ± 0.05	6.63 ± 0.06	2.57 ± 0.03	2.18 ± 0.02
1800	2.4 ± 0.1	0.031 ± 0.003	0.022 ± 0.004	0.46 ± 0.02	6.49 ± 0.08	5.36 ± 0.08	6.65 ± 0.08	2.57 ± 0.04	2.26 ± 0.05
1850	b.b. --	b.b. --	b.b. --	b.b. --	b.b. --	b.b. --	b.b. --	b.b. --	b.b. --
Total	45 ± 2	0.025 ± 0.001	0.023 ± 0.010	0.465 ± 0.006	6.49 ± 0.07	5.22 ± 0.05	6.63 ± 0.06	2.57 ± 0.03	2.18 ± 0.02
ice-2.1a, olivine, 4.309 g, Sandfell (Hengill)									
900	15.9 ± 0.7	0.023 ± 0.001	0.022 ± 0.002	0.480 ± 0.008	6.58 ± 0.07	5.26 ± 0.05	6.66 ± 0.06	2.57 ± 0.03	2.17 ± 0.03
1800	b.c. --	b.c. --	b.c. --	b.c. --	b.c. --	b.c. --	b.c. --	b.c. --	b.c. --
1850	b.b. --	b.b. --	b.b. --	b.b. --	b.b. --	b.b. --	b.b. --	b.b. --	b.b. --
Total	15.9 ± 0.7	0.022 ± 0.002	0.023 ± 0.002	0.480 ± 0.008	6.58 ± 0.07	5.26 ± 0.05	6.66 ± 0.06	2.57 ± 0.03	2.17 ± 0.03
ice-2.2a, olivine, 6.162 g, Sandfell (Hengill)									
400	b.b. --	b.b. --	b.b. --	b.b. --	b.b. --	b.b. --	b.b. --	b.b. --	b.b. --
700	26 ± 1	0.024 ± 0.001	0.024 ± 0.002	0.466 ± 0.006	6.44 ± 0.07	5.17 ± 0.06	6.58 ± 0.07	2.56 ± 0.03	2.15 ± 0.02
900	b.c. --	b.c. --	b.c. --	b.c. --	b.c. --	b.c. --	b.c. --	b.c. --	b.c. --
1350	3.5 ± 0.3	0.033 ± 0.008	0.025 ± 0.003	0.49 ± 0.01	6.5 ± 0.1	5.12 ± 0.09	6.6 ± 0.1	2.56 ± 0.05	2.18 ± 0.04
1800	2.0 ± 0.2	0.027 ± 0.006	0.018 ± 0.005	0.46 ± 0.01	6.4 ± 0.2	5.2 ± 0.1	6.5 ± 0.2	2.54 ± 0.07	2.15 ± 0.06
1850	b.b. --	b.b. --	b.b. --	b.b. --	b.b. --	b.b. --	b.b. --	b.b. --	b.b. --
1900	b.b. --	b.b. --	b.b. --	b.b. --	b.b. --	b.b. --	b.b. --	b.b. --	b.b. --
Total	31 ± 1	0.026 ± 0.002	0.024 ± 0.002	0.468 ± 0.005	6.45 ± 0.06	5.16 ± 0.05	6.57 ± 0.06	2.56 ± 0.02	2.15 ± 0.02
ice-2.2b, olivine, 6.190 g, Sandfell (Hengill)									
400	b.c. --	b.c. --	b.b. --	b.c. --	b.c. --	b.c. --	b.c. --	b.c. --	b.c. --
800	b.b. --	b.b. --	b.b. --	b.b. --	b.b. --	b.b. --	b.b. --	b.b. --	b.b. --
870	b.c. --	b.c. --	b.b. --	b.c. --	b.c. --	b.c. --	b.c. --	b.c. --	b.c. --
1280	b.b. --	b.b. --	b.b. --	b.b. --	b.b. --	b.b. --	b.b. --	b.b. --	b.b. --
1800	b.b. --	b.b. --	b.b. --	b.b. --	b.b. --	b.b. --	b.b. --	b.b. --	b.b. --
1850	b.b. --	b.b. --	b.b. --	b.b. --	b.b. --	b.b. --	b.b. --	b.b. --	b.b. --
Total	b.b. --	b.b. --	b.b. --	b.b. --	b.b. --	b.b. --	b.b. --	b.b. --	b.b. --

T, °C	^{130}Xe cm^3STP/g (1×10^{-14})	$^{124}Xe/^{130}Xe$	$^{126}Xe/^{130}Xe$	$^{128}Xe/^{130}Xe$	$^{129}Xe/^{130}Xe$	$^{131}Xe/^{130}Xe$	$^{132}Xe/^{130}Xe$	$^{134}Xe/^{130}Xe$	$^{136}Xe/^{130}Xe$
ice-3a, olivine, 3.384 g, Burfell i olfusi									
900	b.c. --	b.c. --	b.c. --	b.c. --	b.c. --	b.c. --	b.c. --	b.c. --	b.c. --
1800	7.2 ± 0.3	0.026 ± 0.003	0.031 ± 0.006	0.475 ± 0.008	6.58 ± 0.09	5.21 ± 0.07	6.61 ± 0.08	2.58 ± 0.03	2.22 ± 0.03
1850	b.c. --	b.c. --	b.c. --	b.c. --	b.c. --	b.c. --	b.c. --	b.c. --	b.c. --
Total	7.2 ± 0.3	0.026 ± 0.003	0.031 ± 0.006	0.475 ± 0.008	6.58 ± 0.09	5.21 ± 0.07	6.61 ± 0.08	2.58 ± 0.03	2.22 ± 0.03
ice-3b, olivine, 2.786 g, Burfell i olfusi									
900	b.c. --	b.c. --	b.c. --	b.c. --	b.c. --	b.c. --	b.c. --	b.c. --	b.c. --
1800	b.c. --	b.c. --	b.c. --	b.c. --	b.c. --	b.c. --	b.c. --	b.c. --	b.c. --
1850	b.c. --	b.c. --	b.c. --	b.c. --	b.c. --	b.c. --	b.c. --	b.c. --	b.c. --
Total	b.c. --	b.c. --	b.c. --	b.c. --	b.c. --	b.c. --	b.c. --	b.c. --	b.c. --
ice-4, olivine, 3.181 g, Halejarbunga									
900	14.8 ± 0.7	0.024 ± 0.002	0.026 ± 0.002	0.47 ± 0.01	6.49 ± 0.07	5.19 ± 0.06	6.59 ± 0.07	2.54 ± 0.03	2.17 ± 0.02
1800	b.b. --	b.b. --	b.b. --	b.b. --	b.b. --	b.b. --	b.b. --	b.b. --	b.b. --
1850	b.b. --	b.b. --	b.b. --	b.b. --	b.b. --	b.b. --	b.b. --	b.b. --	b.b. --
Total	14.8 ± 0.7	0.024 ± 0.002	0.026 ± 0.002	0.47 ± 0.01	6.49 ± 0.07	5.19 ± 0.06	6.59 ± 0.07	2.54 ± 0.03	2.17 ± 0.02
ice-9a, olivine, 5.162 g, Midfell									
900	2.5 ± 0.2	0.026 ± 0.004	0.032 ± 0.007	0.48 ± 0.01	6.6 ± 0.1	5.26 ± 0.08	6.62 ± 0.09	2.57 ± 0.04	2.15 ± 0.04
1800	b.c. --	b.c. --	b.c. --	b.c. --	b.c. --	b.c. --	b.c. --	b.c. --	b.c. --
Total	2.5 ± 0.2	0.026 ± 0.004	0.032 ± 0.007	0.48 ± 0.01	6.6 ± 0.1	5.26 ± 0.08	6.62 ± 0.09	2.57 ± 0.04	2.15 ± 0.04
ice-9b, olivine, 5.160 g, Midfell									
900	1.3 ± 0.1	0.033 ± 0.007	b.b. --	0.47 ± 0.01	6.4 ± 0.1	5.2 ± 0.1	6.6 ± 0.1	2.55 ± 0.06	2.09 ± 0.05
1800	b.c. --	b.c. --	b.c. --	b.c. --	b.c. --	b.c. --	b.c. --	b.c. --	b.c. --
1850	b.b. --	b.b. --	b.b. --	b.b. --	b.b. --	b.b. --	b.b. --	b.b. --	b.b. --
Total	1.3 ± 0.1	0.033 ± 0.007	b.b. --	0.47 ± 0.01	6.4 ± 0.1	5.2 ± 0.1	6.6 ± 0.1	2.55 ± 0.06	2.09 ± 0.05
ice-9c, olivine, 5.176 g, Midfell									
900	b.c. --	b.c. --	b.c. --	b.c. --	b.c. --	b.c. --	b.c. --	b.c. --	b.c. --
1800	b.c. --	b.c. --	b.c. --	b.c. --	b.c. --	b.c. --	b.c. --	b.c. --	b.c. --
Total	b.c. --	b.c. --	b.c. --	b.c. --	b.c. --	b.c. --	b.c. --	b.c. --	b.c. --
ice-9d, olivine, 0.70163 g, Midfell									
crush	b.c. --	b.c. --	b.c. --	b.c. --	b.c. --	b.c. --	b.c. --	b.c. --	b.c. --
ice-9g1, glass, 2.026 g, Midfell									
700	17.3 ± 0.5	0.025 ± 0.001	0.022 ± 0.001	0.476 ± 0.007	6.55 ± 0.07	5.24 ± 0.05	6.62 ± 0.05	2.55 ± 0.02	2.18 ± 0.03
1600	6.5 ± 0.2	0.020 ± 0.004	0.021 ± 0.002	0.475 ± 0.008	6.59 ± 0.08	5.30 ± 0.06	6.60 ± 0.06	2.58 ± 0.03	2.20 ± 0.03
Total	23.7 ± 0.6	0.024 ± 0.001	0.022 ± 0.001	0.476 ± 0.005	6.56 ± 0.05	5.26 ± 0.04	6.61 ± 0.04	2.56 ± 0.02	2.19 ± 0.02

T, °C	^{130}Xe cm^3STP/g (1×10^{-14})	$^{124}Xe/^{130}Xe$	$^{126}Xe/^{130}Xe$	$^{128}Xe/^{130}Xe$	$^{129}Xe/^{130}Xe$	$^{131}Xe/^{130}Xe$	$^{132}Xe/^{130}Xe$	$^{134}Xe/^{130}Xe$	$^{136}Xe/^{130}Xe$
ice-9g2, glass, 0.585 g, Midfell									
crush	26.8 ± 0.9	0.036 ± 0.004	0.032 ± 0.008	0.49 ± 0.01	6.67 ± 0.09	5.22 ± 0.06	6.62 ± 0.08	2.57 ± 0.04	2.22 ± 0.03
ice-9g3, glass, 0.720 g, Midfell									
crush	50 ± 2	0.025 ± 0.001	0.025 ± 0.002	0.471 ± 0.005	6.63 ± 0.07	5.22 ± 0.05	6.61 ± 0.06	2.56 ± 0.03	2.17 ± 0.02
ice-10.1, olivine, 4.66 g, Maelifell									
900	8.6 ± 0.3	0.022 ± 0.002	0.020 ± 0.002	0.469 ± 0.007	6.47 ± 0.07	5.23 ± 0.04	6.62 ± 0.05	2.55 ± 0.02	2.16 ± 0.02
1800	b.c. --	b.c. --	b.c. --	b.c. --	b.c. --	b.c. --	b.c. --	b.c. --	b.c. --
Total	8.6 ± 0.3	0.022 ± 0.002	0.020 ± 0.002	0.469 ± 0.007	6.47 ± 0.07	5.23 ± 0.04	6.62 ± 0.05	2.55 ± 0.02	2.16 ± 0.02
ice-10.2, olivine, 5.904 g, Maelifell									
900	6.3 ± 0.2	0.024 ± 0.002	0.021 ± 0.001	0.468 ± 0.006	6.48 ± 0.06	5.24 ± 0.04	6.59 ± 0.04	2.55 ± 0.02	2.16 ± 0.02
1800	3.9 ± 0.1	0.021 ± 0.002	0.019 ± 0.001	0.472 ± 0.007	6.48 ± 0.06	5.19 ± 0.04	6.56 ± 0.05	2.53 ± 0.02	2.15 ± 0.02
Total	10.2 ± 0.2	0.023 ± 0.001	0.020 ± 0.001	0.469 ± 0.004	6.48 ± 0.04	5.22 ± 0.03	6.58 ± 0.03	2.54 ± 0.01	2.16 ± 0.02
ice-11.1, olivine, 3.758 g, Sandfell (Hengill)									
900	7.8 ± 0.3	0.013 ± 0.004	0.010 ± 0.005	0.48 ± 0.01	6.64 ± 0.09	5.41 ± 0.07	6.74 ± 0.08	2.57 ± 0.03	2.18 ± 0.03
1800	b.c. --	b.c. --	b.c. --	b.c. --	b.c. --	b.c. --	b.c. --	b.c. --	b.c. --
Total	8.2 ± 0.3	0.013 ± 0.004	0.010 ± 0.005	0.48 ± 0.01	6.64 ± 0.09	5.41 ± 0.07	6.74 ± 0.08	2.57 ± 0.03	2.18 ± 0.03
ice-11.2, olivine, 5.535 g, Sandfell (Hengill)									
900	b.c. --	b.c. --	b.c. --	b.c. --	b.c. --	b.c. --	b.c. --	b.c. --	b.c. --
1800	b.c. --	b.c. --	b.c. --	b.c. --	b.c. --	b.c. --	b.c. --	b.c. --	b.c. --
Total	b.c. --	b.c. --	b.c. --	b.c. --	b.c. --	b.c. --	b.c. --	b.c. --	b.c. --
ice-12.1, olivine, 3.06 g, Asar									
900	b.c. --	b.c. --	b.c. --	b.c. --	b.c. --	b.c. --	b.c. --	b.c. --	b.c. --
1800	b.c. --	b.c. --	b.c. --	b.c. --	b.c. --	b.c. --	b.c. --	b.c. --	b.c. --
Total	b.c. --	b.c. --	b.c. --	b.c. --	b.c. --	b.c. --	b.c. --	b.c. --	b.c. --
ice-12.2, olivine, 5.103 g, Asar									
900	29.7 ± 0.9	0.023 ± 0.001	0.0225 ± 0.0005	0.472 ± 0.006	6.51 ± 0.06	5.23 ± 0.04	6.64 ± 0.04	2.57 ± 0.02	2.19 ± 0.02
1800	3.8 ± 0.2	0.022 ± 0.001	0.020 ± 0.002	0.461 ± 0.010	6.52 ± 0.08	5.23 ± 0.06	6.63 ± 0.06	2.55 ± 0.03	2.15 ± 0.03
Total	33.5 ± 0.9	0.023 ± 0.001	0.0223 ± 0.0005	0.471 ± 0.005	6.51 ± 0.05	5.23 ± 0.03	6.64 ± 0.04	2.57 ± 0.02	2.18 ± 0.02
ice-14, olivine, 3.087 g, Burfell i olfusi									
900	b.b. --	b.b. --	b.b. --	b.b. --	b.b. --	b.b. --	b.b. --	b.b. --	b.b. --
1800	b.b. --	b.b. --	b.b. --	b.b. --	b.b. --	b.b. --	b.b. --	b.b. --	b.b. --
Total	b.b. --	b.b. --	b.b. --	b.b. --	b.b. --	b.b. --	b.b. --	b.b. --	b.b. --

T, °C	^{130}Xe cm^3STP/g (1×10^{-14})	$^{124}Xe/^{130}Xe$	$^{126}Xe/^{130}Xe$	$^{128}Xe/^{130}Xe$	$^{129}Xe/^{130}Xe$	$^{131}Xe/^{130}Xe$	$^{132}Xe/^{130}Xe$	$^{134}Xe/^{130}Xe$	$^{136}Xe/^{130}Xe$
ice-16, olivine, 5.388 g, Edlborg									
900	26.1 ± 0.8	0.023 ± 0.001	0.0223 ± 0.0006	0.479 ± 0.006	6.53 ± 0.06	5.25 ± 0.04	6.63 ± 0.04	2.57 ± 0.02	2.18 ± 0.02
1800	2.8 ± 0.1	0.018 ± 0.003	0.019 ± 0.003	0.470 ± 0.007	6.51 ± 0.08	5.22 ± 0.06	6.62 ± 0.06	2.57 ± 0.03	2.19 ± 0.03
Total	28.9 ± 0.8	0.023 ± 0.001	0.0220 ± 0.0006	0.478 ± 0.005	6.52 ± 0.05	5.24 ± 0.03	6.63 ± 0.04	2.57 ± 0.02	2.18 ± 0.02
ice-18b, olivine, 3.649 g, Stapafell									
900	16.0 ± 0.5	0.022 ± 0.001	0.021 ±	0.466 ± 0.006	6.49 ± 0.07	5.22 ± 0.05	6.60 ± 0.05	2.56 ± 0.02	2.17 ± 0.02
1800	0.8 ± 0.1	b.b. --	b.b. --	0.45 ± 0.02	6.4 ± 0.2	5.4 ± 0.2	6.6 ± 0.1	2.57 ± 0.09	2.13 ± 0.07
Total	16.8 ± 0.5	0.022 ± 0.001	0.021 ± 0.001	0.465 ± 0.006	6.49 ± 0.06	5.22 ± 0.04	6.60 ± 0.05	2.56 ± 0.02	2.16 ± 0.02
ice-18g2, glass, 3.704 g, Stapafell									
700	4.2 ± 0.1	0.019 ± 0.002	0.019 ± 0.003	0.476 ± 0.008	6.58 ± 0.08	5.32 ± 0.06	6.69 ± 0.06	2.58 ± 0.03	2.17 ± 0.03
1500	4.2 ± 0.1	0.022 ± 0.003	b.b.	0.466 ± 0.008	6.24 ± 0.08	5.22 ± 0.05	6.61 ± 0.06	2.55 ± 0.03	2.16 ± 0.03
Total	8.3 ± 0.2	0.021 ± 0.002	0.019 ± 0.003	0.471 ± 0.006	6.41 ± 0.06	5.27 ± 0.04	6.65 ± 0.04	2.57 ± 0.02	2.17 ± 0.02
ice-18g3, glass, 0.983 g, Stapfell									
crush	b.c. --	b.c. --	b.c. --	b.c. --	b.c. --	b.c. --	b.c. --	b.c. --	b.c. --
ice-19a, olivine, 5.341 g, Sulur									
900	72 ± 2	0.024 ± 0.001	0.0222 ± 0.0005	0.476 ± 0.006	6.55 ± 0.06	5.26 ± 0.04	6.66 ± 0.04	2.57 ± 0.02	2.18 ± 0.02
1800	59 ± 2	0.024 ± 0.001	0.0223 ± 0.0005	0.470 ± 0.005	6.48 ± 0.06	5.22 ± 0.04	6.62 ± 0.04	2.57 ± 0.02	2.19 ± 0.02
Total	130 ± 3	0.0242 ± 0.0007	0.0222 ± 0.0003	0.473 ± 0.004	6.51 ± 0.04	5.24 ± 0.03	6.64 ± 0.03	2.57 ± 0.01	2.18 ± 0.01
ice-19b, olivine, 5.1531 g, Sulur									
900	4.7 ± 0.2	b.c. --	b.c. --	b.c. --	b.c. --	b.c. --	b.c. --	b.c. --	b.c. --
1800	b.c. --	b.c. --	b.c. --	b.c. --	b.c. --	b.c. --	b.c. --	b.c. --	b.c. --
Total	4.7 ± 0.2	b.c. --	b.c. --	b.c. --	b.c. --	b.c. --	b.c. --	b.c. --	b.c. --
ice-23a, olivine, 5.06 g, Haleyjarbunga									
900	8.5 ± 0.3	0.023 ± 0.002	0.0210 ± 0.0014	0.476 ± 0.006	6.57 ± 0.065	5.28 ± 0.05	6.64 ± 0.05	2.55 ± 0.02	2.17 ± 0.03
1800	0.59 ± 0.06	b.b. --	b.b. --	b.b. --	b.b. --	b.b. --	b.b. --	b.b. --	b.b. --
Total	9.1 ± 0.3	0.023 ± 0.002	0.0210 ± 0.0014	0.476 ± 0.006	6.57 ± 0.065	5.28 ± 0.05	6.64 ± 0.05	2.55 ± 0.02	2.17 ± 0.03
ice-24 , olivine, 2.847 g, Hraunsvik/Hrolfsvik									
900	1.13 ± 0.08	b.b. --	b.b. --	0.48 ± 0.02	6.7 ± 0.3	5.0 ± 0.2	6.8 ± 0.3	2.7 ± 0.1	2.33 ± 0.10
1800	0.88 ± 0.07	b.b. --	b.b. --	0.54 ± 0.04	7.4 ± 0.5	6.0 ± 0.4	7.5 ± 0.5	2.9 ± 0.2	2.5 ± 0.2
Total	2.0 ± 0.1	b.b. --	b.b. --	0.51 ± 0.02	7.0 ± 0.3	5.4 ± 0.2	7.1 ± 0.3	2.8 ± 0.1	2.39 ± 0.09
ice-25, olivine, 4.912, g, Bleikholl									
900	13.0 ± 0.4	0.020 ± 0.001	0.021 ± 0.001	0.473 ± 0.006	6.53 ± 0.07	5.30 ± 0.05	6.66 ± 0.05	2.56 ± 0.02	2.20 ± 0.03
1800	2.17 ± 0.08	0.028 ± 0.004	0.023 ± 0.003	0.48 ± 0.01	6.42 ± 0.10	5.20 ± 0.08	6.55 ± 0.08	2.52 ± 0.04	2.13 ± 0.03
Total	15.1 ± 0.4	0.021 ± 0.001	0.021 ± 0.001	0.473 ± 0.005	6.52 ± 0.06	5.29 ± 0.04	6.64 ± 0.04	2.55 ± 0.02	2.19 ± 0.02

T, °C	^{130}Xe cm^3STP/g (1×10^{-14})	$^{124}Xe/^{130}Xe$	$^{126}Xe/^{130}Xe$	$^{128}Xe/^{130}Xe$	$^{129}Xe/^{130}Xe$	$^{131}Xe/^{130}Xe$	$^{132}Xe/^{130}Xe$	$^{134}Xe/^{130}Xe$	$^{136}Xe/^{130}Xe$
ice-16, olivine, 5.388 g, Edlborg									
900	26.1 ± 0.8	0.023 ± 0.001	0.0223 ± 0.0006	0.479 ± 0.006	6.53 ± 0.06	5.25 ± 0.04	6.63 ± 0.04	2.57 ± 0.02	2.18 ± 0.02
1800	2.8 ± 0.1	0.018 ± 0.003	0.019 ± 0.003	0.470 ± 0.007	6.51 ± 0.08	5.22 ± 0.06	6.62 ± 0.06	2.57 ± 0.03	2.19 ± 0.03
Total	28.9 ± 0.8	0.023 ± 0.001	0.0220 ± 0.0006	0.478 ± 0.005	6.52 ± 0.05	5.24 ± 0.03	6.63 ± 0.04	2.57 ± 0.02	2.18 ± 0.02
ice-18b, olivine, 3.649 g, Stapafell									
900	16.0 ± 0.5	0.022 ± 0.001	0.021 ±	0.466 ± 0.006	6.49 ± 0.07	5.22 ± 0.05	6.60 ± 0.05	2.56 ± 0.02	2.17 ± 0.02
1800	0.8 ± 0.1	b.b. --	b.b. --	0.45 ± 0.02	6.4 ± 0.2	5.4 ± 0.2	6.6 ± 0.1	2.57 ± 0.09	2.13 ± 0.07
Total	16.8 ± 0.5	0.022 ± 0.001	0.021 ± 0.001	0.465 ± 0.006	6.49 ± 0.06	5.22 ± 0.04	6.60 ± 0.05	2.56 ± 0.02	2.16 ± 0.02
ice-18g2, glass, 3.704 g, Stapafell									
700	4.2 ± 0.1	0.019 ± 0.002	0.019 ± 0.003	0.476 ± 0.008	6.58 ± 0.08	5.32 ± 0.06	6.69 ± 0.06	2.58 ± 0.03	2.17 ± 0.03
1500	4.2 ± 0.1	0.022 ± 0.003	b.b.	0.466 ± 0.008	6.24 ± 0.08	5.22 ± 0.05	6.61 ± 0.06	2.55 ± 0.03	2.16 ± 0.03
Total	8.3 ± 0.2	0.021 ± 0.002	0.019 ± 0.003	0.471 ± 0.006	6.41 ± 0.06	5.27 ± 0.04	6.65 ± 0.04	2.57 ± 0.02	2.17 ± 0.02
ice-18g3, glass, 0.983 g, Stapfell									
crush	b.c. --	b.c. --	b.c. --	b.c. --	b.c. --	b.c. --	b.c. --	b.c. --	b.c. --
ice-19a, olivine, 5.341 g, Sulur									
900	72 ± 2	0.024 ± 0.001	0.0222 ± 0.0005	0.476 ± 0.006	6.55 ± 0.06	5.26 ± 0.04	6.66 ± 0.04	2.57 ± 0.02	2.18 ± 0.02
1800	59 ± 2	0.024 ± 0.001	0.0223 ± 0.0005	0.470 ± 0.005	6.48 ± 0.06	5.22 ± 0.04	6.62 ± 0.04	2.57 ± 0.02	2.19 ± 0.02
Total	130 ± 3	0.0242 ± 0.0007	0.0222 ± 0.0003	0.473 ± 0.004	6.51 ± 0.04	5.24 ± 0.03	6.64 ± 0.03	2.57 ± 0.01	2.18 ± 0.01
ice-19b, olivine, 5.1531 g, Sulur									
900	4.7 ± 0.2	b.c. --	b.c. --	b.c. --	b.c. --	b.c. --	b.c. --	b.c. --	b.c. --
1800	b.c. --	b.c. --	b.c. --	b.c. --	b.c. --	b.c. --	b.c. --	b.c. --	b.c. --
Total	4.7 ± 0.2	b.c. --	b.c. --	b.c. --	b.c. --	b.c. --	b.c. --	b.c. --	b.c. --
ice-23a, olivine, 5.06 g, Haleyjarbunga									
900	8.5 ± 0.3	0.023 ± 0.002	0.0210 ± 0.0014	0.476 ± 0.006	6.57 ± 0.065	5.28 ± 0.05	6.64 ± 0.05	2.55 ± 0.02	2.17 ± 0.03
1800	0.59 ± 0.06	b.b. --	b.b. --	b.b. --	b.b. --	b.b. --	b.b. --	b.b. --	b.b. --
Total	9.1 ± 0.3	0.023 ± 0.002	0.0210 ± 0.0014	0.476 ± 0.006	6.57 ± 0.065	5.28 ± 0.05	6.64 ± 0.05	2.55 ± 0.02	2.17 ± 0.03
ice-24 , olivine, 2.847 g, Hraunsvik/Hrolfsvik									
900	1.13 ± 0.08	b.b. --	b.b. --	0.48 ± 0.02	6.7 ± 0.3	5.0 ± 0.2	6.8 ± 0.3	2.7 ± 0.1	2.33 ± 0.10
1800	0.88 ± 0.07	b.b. --	b.b. --	0.54 ± 0.04	7.4 ± 0.5	6.0 ± 0.4	7.5 ± 0.5	2.9 ± 0.2	2.5 ± 0.2
Total	2.0 ± 0.1	b.b. --	b.b. --	0.51 ± 0.02	7.0 ± 0.3	5.4 ± 0.2	7.1 ± 0.3	2.8 ± 0.1	2.39 ± 0.09
ice-25, olivine, 4.912, g, Bleikholl									
900	13.0 ± 0.4	0.020 ± 0.001	0.021 ± 0.001	0.473 ± 0.006	6.53 ± 0.07	5.30 ± 0.05	6.66 ± 0.05	2.56 ± 0.02	2.20 ± 0.03
1800	2.17 ± 0.08	0.028 ± 0.004	0.023 ± 0.003	0.48 ± 0.01	6.42 ± 0.10	5.20 ± 0.08	6.55 ± 0.08	2.52 ± 0.04	2.13 ± 0.03
Total	15.1 ± 0.4	0.021 ± 0.001	0.021 ± 0.001	0.473 ± 0.005	6.52 ± 0.06	5.29 ± 0.04	6.64 ± 0.04	2.55 ± 0.02	2.19 ± 0.02

Comparison of xenon results with previous xenon measurements from Icelandic basalts

Although $^{129}Xe/^{130}Xe$ ratios that are higher than the atmospheric ratios have been found in this study as well as two previous studies of samples from Midfell, the maximum value of the $^{129}Xe/^{130}Xe$ ratios vary. The maximum $^{129}Xe/^{130}Xe$ ratio from this study, from sample *ice-9g1* (from Midfell) is equal to 6.66 ± 0.09, which is only 2.5% higher than the atmospheric ratio (6.496). Higher $^{129}Xe/^{130}Xe$ ratios from the same locality, but possibly different flow unit, were reported by Harrison et al. (1999) ($^{129}Xe/^{130}Xe$ up to 7.37, ~13.5% higher than the atmospheric ratio), and Trieloff et al. (2000) ($^{129}Xe/^{130}Xe$ up to 6.92 ± 0.08, 6.52% higher than the atmospheric ratio).

5.2.3 Summary

The noble gas isotopic results from this study show a wide range in $^{3}He/^{4}He$ isotopic ratios that overlap the range in ratios from previous studies. The $^{3}He/^{4}He$ ratios range from 12 to 30 Ra in well-shielded samples; a much wider range than was reported previously for Reykjanes Peninsula samples, that is, from 15 to 19 Ra (Burnard et al., 1994; Harrison et al., 1999; Trieloff et al., 2000). The $^{3}He/^{4}He$ ratios from partly shielded samples extend to values as low as 8.3 Ra, close to the average MORB ratio, and to as high as 75 Ra (total gas ratios). The neon isotopic ratios from well-shielded samples from this study predominantly lie close to the air-solar mixing line and the MORB trend. Neon isotopic ratios of the total gas released from partly-shielded olivine samples predominantly lie on a trend that is intermediate between the air-solar mixing line and the MORB trend. Neon results from previous studies (Harrison et al., 1999; Trieloff et al., 2000) also lie on trends that are between the air-solar mixing line and the MORB trend. The maximum $^{40}Ar/^{36}Ar$ ratio measured in this study (1229 ± 150) is lower than the maximum measured ratios in previous studies of 2200 ± 200 (Burnard et al., 1994), 6501 ± 311 (Harrison et al., 1999) and 4350 ± 93 (Trieloff et al., 2000). The krypton isotopic ratios from this study are indistinguishable from the atmospheric ratios at the one sigma uncertainty level. The xenon isotopic ratios from this study are generally indistinguishable the atmospheric ratios at the one sigma uncertainty level in all samples except sample *ice-9g*. The maximum value of the $^{129}Xe/^{130}Xe$ ratio in sample *ice-9g1* (from Midfell) is 2% higher than the atmospheric ratio. Higher ratios from the same locality, but possibly different flow unit, are reported by Harrison et al. (1999) ($^{129}Xe/^{130}Xe$ up to ~13.5% higher than the atmospheric ratio), and Trieloff et al. (2000) ($^{129}Xe/^{130}Xe$ up to 6.52% higher than the atmospheric ratio).

5.3 References

Burnard P. G., Stuart F. M., Turner G., and Oskarsson N. (1994) Air contamination of basaltic magma: Implications for high $^{3}He/^{4}He$ mantle Ar isotopic composition. *Journal of Geophysical Research* **99**, 17709-17715.

Condomines M., Gronvold K., Hooker P. J., Muehlenbachs K., O'Nions R. K., Oskarsson N., and Oxburgh E. R. (1983) Helium, oxygen, strontium and neodymium isotopic relationships in Icelandic volcanics. *Earth and Planetary Science Letters* **66**, 125-136.

Farley K. A. and Neroda E. (1998) Noble gases in the Earth's mantle. *Annual Review of Earth and Planetary Sciences* **26**, 189-218.

Harrison D., Burnard P., and Turner G. (1999) Noble gas behaviour and composition in the mantle: constraints from the Iceland plume. *Earth and Planetary Science Letters* **171**, 199-207.

Hilton D. R., Gronvold K., Macpherson C. G., and Castillo P. R. (1999) Extreme $^{3}He/^{4}He$ ratios in northwest Iceland: constraining the common component in mantle plumes. *Earth and Planetary Science Letters* **173**, 53-60.

Hilton D. R., Gronvold K., O'Nions R. K., and Oxburgh E. R. (1990) Regional distribution of ^{3}He anomalies in the Icelandic crust. *Chemical Geology* **88**, 53-67.

Hilton D. R., Gronvold K., Sveinbjornsdottir A. E., and Hammerschmidt K. (1998) Helium isotope evidence for off-axis degassing of the Icelandic hotspot. *Chemical Geology* **149**, 173-187.

Hiyagon H., Ozima M., Marty B., Zashu S., and Sakai H. (1992) Noble gases in submarine glasses from mid-oceanic ridges and Loihi seamount: constraints on the early history of the Earth. *Geochimica et Cosmochimica Acta* **56**, 1301-1316.

Honda M., McDougall I., and Patterson D. B. (1993a) Solar noble gases in the Earth: the systematics of helium-neon isotopes in mantle derived samples. *Lithos* **30**, 257-265.

Honda M., McDougall I., Patterson D. B., Doulgeris A., and Clague D. A. (1991) Possible solar noble gas component in Hawaiian basalts. *Nature* **349**, 149-151.

Honda M., McDougall I., Patterson D. B., Doulgeris A., and Clague D. A. (1993b) Noble gases in submarine pillow basalt glasses from Loihi and Kilauea, Hawaii: a solar component in the Earth. *Geochimica et Cosmochimica Acta* **57**, 859-874.

Honda M., Patterson D. B., McDougall I., and Falloon T. J. (1993c) Noble gases in submarine pillow basalt glasses from the Lau Basin. *Earth and Planetary Science Letters* **120**, 135-148.

Kurz M., Meyer P. S., and Sigurdsson H. (1985) Helium isotopic systematics within the neovolcanic zones of Iceland. *Earth and Planetary Science Letters* **74**, 291-305.

Lal D. (1991) Cosmic ray labelling of erosion surfaces: in situ nuclide production rates and erosion models. *Earth and Planetary Science Letters* **104**, 424-439.

Moreira M., Kunz J., and Allegre C. (1998) Rare gas systematics in popping rock: isotopic and elemental compositions in the upper mantle. *Science* **279**, 1178-1181.

Poreda R. and Radicati di Brozolo F. (1984) Neon isotope variations in Mid-Atlantic Ridge basalts. *Earth and Planetary Science Letters* **69**, 277-289.

Poreda R., Schilling J.-G., and Craig H. (1986) Helium and hydrogen isotopes in ocean-ridge basalts north and south of Iceland. *Earth and Planetary Science Letters* **78**, 1-17.

Sano Y., Urabe A., Wakita H., Chiba H., and Sakai H. (1985) Chemical and isotopic compositions of gases in geothermal fluids in Iceland. *Geochemical Journal* **19**, 135-148.

Sarda P., Staudacher T., and Allègre C. J. (1988) Neon isotopes in submarine basalts. *Earth and Planetary Science Letters* **91**, 73-88.

Schilling J.-G. (1973) Iceland mantle plume: geochemical evidence along Reykjanes Ridge. *Nature* **242**, 565-571.

Trieloff M., Kunz J., Clague D., Harrison D., and Allegre C. (2000) The nature of pristine noble gases in mantle plumes. *Science* **288**, 1036-1038.

Valbracht P. J., Staudacher T., Malahoff A., and Allègre C. J. (1997) Noble gas systematics of deep rift zones glasses from Loihi Seamount, Hawaii. *Earth and Planetary Science Letters* **150**, 399-411.

CHAPTER 6: NOBLE GAS ISOTOPIC RATIOS IN ICELANDIC BASALTS

6.1 Introduction

The new isotopic and elemental noble gas data from Icelandic basalts reported in this study (Chapter 5) show that $^{3}He/^{4}He$ ratios measured in glass separates and well-shielded olivine separates have a broader compositional range (12 – 30 Ra) than those measured previously in samples from the Reykjanes Peninsula (12 – 18 Ra). In comparison, the partly shielded olivine separates have $^{3}He/^{4}He$ ratios that range from 8 to 75 Ra. It is possible that some of the partly shielded samples contain a component of cosmogenic ^{3}He, as will be shown in the next section. The range of helium isotopic ratios in well-shielded samples suggests that the mantle source of Reykjanes Peninsula basalts is likely to be heterogeneous and includes a noble gas source with relatively high $^{3}He/^{4}He$ ratios (at least 30 Ra) that is more primitive than the sources of basalts studied in previous investigations.

Like the helium isotopic ratios measured in Reykjanes Peninsula basalts from this study, the neon end-member isotopic ratios are also heterogeneous. Combined with the neon compositions from previous investigations (see Chapter 5), the results from this study suggest that Reykjanes Peninsula basalts originate from sources with neon end-member compositions ranging from solar-like to mid-ocean ridge basalt (MORB)-like compositions. Although near-solar neon isotopic ratios from samples along the Reykjanes Ridge to the south of Iceland have previously been reported by Poreda and Radicati di Brozolo (1984) (Chapter 5), the significance of these results was not discussed. The present study confirms the existence of solar-like neon isotopic ratios in mantle–derived samples, and evaluates the significance of these results. As will be shown in this chapter, the neon isotopic ratios obtained from this study are significant to our understanding of the nature of the Icelandic plume source and the degree of stirring in the mantle. When the neon isotopic ratios are compared with helium, argon and xenon isotopic ratios, they may also provide a means to understand the processes that lead to the isotopic heterogeneity found in Reykjanes Peninsula basalts.

This chapter is divided into three sections. In the first section, the noble gas isotopic ratios from the partly-shielded samples that may have cosmogenic components

of ^{3}He and ^{21}Ne, will be evaluated to determine whether they provide meaningful information about mantle noble gas compositions. In the second section, the means by which solar neon isotopic ratios may have been preserved in the mantle and core are discussed and evaluated. In the third section, a possible explanation is given for the variation in observed helium, neon, argon and xenon isotopic ratios in Icelandic basalts.

6.2 Cosmogenic versus mantle-derived ^{3}He and ^{21}Ne in partly-shielded samples

Cosmogenic isotopes are produced when material such as olivine is exposed to cosmic rays at or near the Earth's surface. These cosmogenic isotopes are released along with mantle-derived gases when samples are analysed by step-heating. Addition of cosmogenic isotopes increases the $^{3}He/^{4}He$ and $^{21}Ne/^{22}Ne$ ratios relative to the original mantle compositions in the samples (see Chapter 2). This is because the cosmogenic $^{21}Ne/^{22}Ne$ end-member ratio (0.94) (Lugmair et al., 1976) is much higher than even the maximum $^{21}Ne/^{22}Ne$ ratio found in mantle-derived samples (MORB $^{21}Ne/^{22}Ne$ extrapolated end-member ratio = 0.075, (e.g., Sarda et al., 1988)), so that addition of cosmogenic ^{21}Ne causes the $^{21}Ne/^{22}Ne$ isotopic ratio to be systematically shifted to higher values in the neon three-isotope plot. The mantle and atmospheric $^{20}Ne/^{22}Ne$ ratios are both decreased by addition of cosmogenic isotopes because their end-member ratios (13.8 and 9.8, respectively) are higher than the cosmogenic $^{20}Ne/^{22}Ne$ end-member ratio (0.84) (Lugmair et al., 1976). Addition of cosmogenic ^{3}He increases the $^{3}He/^{4}He$ ratio in material such as olivine because the concentration of mantle-derived ^{3}He in olivine is relatively low, so that relatively small additions of cosmogenic ^{3}He can produce large changes in the $^{3}He/^{4}He$ ratio. In contrast, the concentration of mantle-derived ^{4}He in olivine is several orders of magnitude higher than that of ^{3}He (e.g., for an ocean island basalt (OIB)-type $^{3}He/^{4}He$ ratio of 4×10^{-5} = 29 Ra), and addition of cosmogenic ^{4}He produced in terrestrial samples (Lal, 1988) does not appreciably change the measured $^{3}He/^{4}He$ ratio.

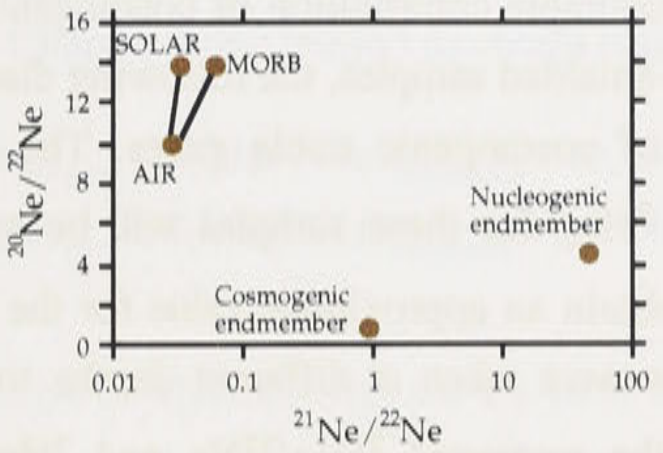

Figure 6-1. Neon three-isotope plot, showing the neon isotopic compositions of the air, solar, and MORB end-members compared with the values of the cosmogenic (Lugmair et al., 1976) and nucleogenic (Yatsevich and Honda, 1997) end-member compositions.

The near-solar neon isotopic ratios measured in some Icelandic samples in this study are expected to be associated with near-solar $^{3}He/^{4}He$ ratios. The solar $^{3}He/^{4}He$ ratio is not accurately known, but should lie within the range of the ratios measured in meteorites of 100 Ra (the so-called "planetary" ratio) (Reynolds et al., 1978) and the present-day solar wind of 326 Ra (Anders and Grevesse, 1989; Benkert et al., 1993). One of the Icelandic samples from this study has a $^{3}He/^{4}He$ ratio of 180 ± 20 Ra (individual gas extraction from step-heating, the total ratio is 75 ± 7 Ra), much higher than the maximum ratio reported in previous studies of mantle-derived samples from Iceland (ca. 40 Ra) (Hilton et al., 1999) (see Chapter 5). In light of the measured near-solar neon isotopic ratios in some of the Icelandic samples from this study, it is important to evaluate the highest measured $^{3}He/^{4}He$ ratios to determine whether they are cosmogenic or solar in origin.

6.2.1 Estimation of $^{21}Ne_C$ and $^{3}He_C$ concentrations

The object of the following evaluation of noble gas compositions is not to rigorously determine the cosmogenic exposure ages of the partly-shielded samples. Instead, the object is to determine how much cosmogenic helium and neon might be added to mantle-derived helium and neon, and if necessary, to correct the measured ratios to obtain the approximate mantle noble gas isotopic ratios. The samples for this study were collected with the objective of determining mantle isotopic ratios, but in some localities, well-shielded samples could not be collected, and partly-shielded samples were obtained. In three localities (localities of samples *ice-1, -2 and -4*), samples are known to have been collected from the surface, but were not collected by the author so the original degree of shielding from cosmic rays is unknown. In three other localities (*ice-12, -16, -25*), samples were obtained from small caves, eroding cliffs, or beneath in-situ boulders

to minimize the potential exposure to cosmic rays. Because there is some ambiguity as to whether there is a measurable contribution of cosmogenic noble gases to the mantle noble gases in the partly-shielded samples, the following discussion seeks to estimate the maximum contribution of cosmogenic noble gases. The estimated concentrations of cosmogenic $^{21}Ne_C$ and $^{3}He_C$ for these samples will be used to correct the measured $^{3}He/^{4}He$ ratios so as to obtain an approximate value for the initial mantle $^{3}He/^{4}He$ ratio. In two localities, samples were taken at different depths to determine what differences would be produced in the measured $^{21}Ne/^{22}Ne$ and $^{3}He/^{4}He$ ratios in samples that experienced different shielding conditions (samples *ice-10.1, -10.2, -11.1* and *–11.2*). The relative differences in the $^{21}Ne/^{22}Ne$ and $^{3}He/^{4}He$ ratios from these samples can be used to estimate the relative exposure ages of the flow surfaces.

$^{21}Ne_C$

Mantle-derived samples have three components of neon: the atmospheric, nucleogenic, and solar components, that can be deconvolved using the three neon isotopes (^{20}Ne, ^{21}Ne, and ^{22}Ne) (Honda et al., 1993a). Samples that have been exposed to cosmic rays and contain cosmogenic ^{21}Ne ($^{21}Ne_C$) have four components (equation 6-1), which cannot be deconvolved using three variables. Because $^{21}Ne_C$ cannot be distinguished from the other components of ^{21}Ne, it is not possible to subtract the $^{21}Ne_C$ to determine the initial mantle neon isotopic composition.

$$^{21}Ne/^{22}Ne_{Measured} = (^{21}Ne_C + ^{21}Ne_{solar} + ^{21}Ne^* + ^{21}Ne_{Air})/(^{22}Ne_{solar} + ^{22}Ne_{Air}) \quad (6\text{-}1)$$

Although $^{21}Ne_C$ cannot be deconvolved from the other three components of ^{21}Ne, it is possible to estimate the amount of $^{21}Ne_C$ that may be present in the sample if the initial mantle $^{21}Ne/^{22}Ne$ ratio is known.

The initial mantle $^{21}Ne/^{22}Ne$ of the Icelandic samples is not well constrained because the end-member $^{21}Ne/^{22}Ne$ ratios measured in this study and in previous studies (see Chapter 5, Figures 5-9 and 5-10) are heterogeneous. However, it is possible to estimate the *maximum* contributions of $^{21}Ne_C$ by assuming that the initial neon isotopic ratios lay on the air-solar mixing line. The most solar-like (i.e., un-nucleogenic) neon isotopic compositions in Icelandic basalts lie on or near the air-solar mixing line, making the solar neon isotopic composition a reasonable end-member to determine the maximum amount of $^{21}Ne_C$ that could be present in the Icelandic basalts from this study. The calculated amount of $^{21}Ne_C$ would of course be lower if the samples were assumed to initially lie on the L-K trend or the MORB trend (see Chapter 5, Fig. 5-9). Here, I will assume that the initial composition lay on the air-solar mixing line, meaning that initially,

the sample contained no nucleogenic ^{21}Ne. This allows $^{21}Ne_C$ to be substituted for $^{21}Ne^*$ in equation (2-9) (see Chapter 2 and below) to obtain equation (6-2).

$$(^{i}Ne/^{22}Ne)_{observed} = k(^{i}Ne/^{22}Ne)_{solar} + l(^{i}Ne/^{22}Ne)_{nucleogenic} + m(^{i}Ne/^{22}Ne)_{atmosphere} \quad (2\text{-}9)$$

$$(^{i}Ne/^{22}Ne)_{observed} = k(^{i}Ne/^{22}Ne)_{solar} + l(^{i}Ne/^{22}Ne)_{cosmogenic} + m(^{i}Ne/^{22}Ne)_{atmosphere} \quad (6\text{-}2)$$

In equations (2-9) and (6-2), $^{i}Ne = ^{20}Ne$ or ^{21}Ne, $k + l + m = 1$ and each represents the fractional contribution of a given end-member to the reference isotope ^{22}Ne (Honda et al., 1993a). The $^{20}Ne/^{22}Ne$ and $^{21}Ne/^{22}Ne$ isotopic ratios of the endmembers are: atmosphere (9.8, 0.029) (Eberhardt et al., 1965), solar (13.8, 0.0328) (Benkert et al., 1993), nucleogenic (48.0 and 4.47) (Yatsevich and Honda, 1997) and cosmogenic (0.94 and 0.84) (Lugmair et al., 1976). The calculated amount of $^{21}Ne^*$ from equation (2-9) using the nucleogenic end-member ratios is equivalent to the amount of $^{21}Ne_C$ calculated from equation (6-2) using the cosmogenic end-member ratios because the measured $^{21}Ne/^{22}Ne$ ratios in Icelandic basalts are much lower than either the nucleogenic or the cosmogenic end-member ratios. For example, using the neon data from sample *ice-4*, the calculated amount of $^{21}Ne_C$ from equation (6-2) based on the cosmogenic end-member ratios is $2.1 \pm 0.4 \times 10^{-14}$ cm^3STP/g. The calculated amount of $^{21}Ne^*$ from equation (2-5) using the nucleogenic end-member ratios is similar and equal to $2.1 \pm 0.5 \times 10^{-14}$ cm^3STP/g.

^3He_C

Using the cosmogenic $^{3}He/^{21}Ne$ production ratio in olivine (equation 6-3) (Marti and Craig, 1987), the calculated $^{21}Ne_C$ concentration obtained above can be used to estimate the maximum amount of cosmogenic ^{3}He in the sample. The estimated amount of ^3He_C can be subtracted from the measured ^{3}He to estimate the minimum mantle $^{3}He/^{4}He$ ratio for the sample using equation (6-4).

$$^3He_C = (^{21}Ne_C \times 2.1) \quad (6\text{-}3)$$

$$(^3He/^4He)_{Corrected} = [(^3He_{Measured} - {}^3He_{C\text{-}Max})/^4He_{Measured}] \quad (6\text{-}4)$$

Estimated exposure age

Although the exposure age of the samples is not of primary interest in this investigation, it is necessary to ensure that the time required to produce the estimated amount of ^3He_C does not exceed the estimated eruption ages for Reykjanes Peninsula basalts. The concentrations of ^3He_C in olivine in the Icelandic samples from this study are expected to be relatively small because the samples are relatively young. The production rate of ^3He_C, or $[^3He_C]_{PR}$, may be determined from Equation (2-1) (see Chapter 2) and used to estimate the exposure age of the sample:

$$[^3He_C]_{PR}\ (cm^3STP/g\ year) = H \times [1.68 - (0.0637 \times CR) + (9.99 \times 10^{-4} \times CR^2)] \qquad (2\text{-}1)$$

where $H = 3.7 \times 10^{-18}$ cm^3STP/g year and CR = 1 gigavolt for Icelandic latitudes (CR is Cut-off rigidity, see Chapter 2) (Kurz et al., 1990). The value of $[^3He_C]_{PR}$ needs to be adjusted to account for the effective depth of the sample below the Earth's surface, which is determined using a rock density of 3 g/cm^3, and the measured depth from the surface (Table 6-1). Previous studies have shown that for samples collected at high elevations, it is necessary to correct the $[^3He_C]_{PR}$ for elevation effects, since the $[^3He_C]_{PR}$ increases by a factor of two for every 1000 m above sea level (see Chapter 2). However, the elevation correction is neglected here because samples from this study were obtained from elevations of less than 300 meters above sea level (Table 4-1), meaning that the $[^3He_C]_{PR}$ would increase by less than a factor of two. For a sample at the surface, the $[^3He_C]_{PR}$ is equal to 5.9×10^{-18} cm^3STP/g year (Table 6-1). The calculated amount of ^3He_C (equation 6-3), divided by the $[^3He_C]_{PR}$, gives the exposure age.

Erosion Rate

Another factor that needs to be considered when determining the ^3He production rate is whether the present-day depth from the surface is representative of the depth since the basalt was erupted. In some localities (*ice-12, -16, -25*), samples were deliberately obtained from caves, eroding cliffs or in-situ outcrops on small volcanic cones where surrounding rocks were rolling downslope so as to minimize the contributions of cosomogenic isotopes. In such localities, the former eruptive surface has been lowered by erosion, but the initial depth from the surface is unconstrained. In these cases, the cosmogenic production rate based on the present-day depth from the surface to the sample is likely to be higher than the time-integrated production rate that accounts for the effects of erosion. Use of the higher estimated cosmogenic production rate would lead to a calculated exposure age that is much younger than the true exposure age.

Table 6-1. Estimated contributions of cosmogenic ^{3}He and ^{21}Ne to measured isotopic ratios

partly shielded olivine	^{4}He ($x10^{-9}$)	^{22}Ne ($x10^{-12}$)	$^{21}Ne/^{22}Ne$	$^{21}Ne_C$ ($x10^{-14}$)	$^{3}He_C$ ($x10^{-14}$)	depth cm	$[^{3}He_C]$ ($x10^{-18}$), cm^3STP/g yr	$^{3}He/^{4}He$ Ra	$^{3}He_{Meas}$ ($x10^{-13}$) cm^3STP/g	Corr. $^{3}He/^{4}He$	Expos. age, ka	Est. Eruption Age, ka, source
ice-1a	3.7 ± 0.2	n/a ± n/a	n/a ± n/a	n/a ± n/a	n/a	1	5.9	9.6 ± 0.6	0.5	n/a	n/a	10 – 13a
ice-1b	5.0 ± 0.3	1.45 ± 0.05	0.0320 ± 0.0005	0.3 ± 0.1	0.7	1	5.9	21 ± 2	1.5	20.0	1	10 – 13a
ice-2.1a	3.0 ± 0.1	4.4 ± 0.2	0.0312 ± 0.0005	0.5 ± 0.2	1.0	1	5.9	75 ± 7	3.1	72.6	2	10 – 13a
ice-2.2a	1.6 ± 0.1	4.2 ± 0.1	0.0306 ± 0.0004	0.6 ± 0.2	1.2	1	5.9	15 ± 1	0.3	9.4	2	10 – 13a
ice-2.2b	3.0 ± 0.1	0.92 ± 0.04	0.0335 ± 0.0008	0.4 ± 0.1	0.7	1	5.9	8.3 ± 0.8	0.3	6.5	1	10 – 13a
ice-4	0.5 ± 0.0	1.77 ± 0.08	0.0412 ± 0.0013	2.1 ± 0.5	4.3	1	5.9	56 ± 7	0.4	0.0	7	12 –13b
ice-10.1 (sfce)	3.4 ± 0.2	2.3 ± 0.1	0.0300 ± 0.0006	0.2 ± 0.3	0.4	5-10	5.4	18 ± 2	0.9	17.2	1	12 – 13b
ice-10.2	6.1 ± 0.3	1.90 ± 0.09	0.0294 ± 0.0005	0.1 ± 0.1	0.1	100	0.9	17 ± 1	1.5	16.9	1	12 – 13b
ice-11.1 (sfce)	3.1 ± 0.2	1.5 ± 0.1	0.0327 ± 0.0011	0.5 ± 0.3	1.0	1	5.9	19 ± 2	0.8	16.8	2	12 – 13b
ice-11.2	7.3 ± 0.4	1.09 ± 0.05	0.0301 ± 0.0005	0.1 ± 0.1	0.2	30	3.4	17 ± 1	1.7	16.8	1	12 – 13b
ice-12.2 (sfce)	1.3 ± 0.1	9.9 ± 0.4	0.0301 ± 0.0003	1 ± 8	2.2	1	5.9	24 ± 2	0.4	11.8	4	12 – 13b
ice-16	13.0 ± 0.7	4.0 ± 0.2	0.0321 ± 0.0004	1.0 ± 0.3	2.2	50	2.3	19 ± 2	3.5	17.8	9	5 – 7b
ice-25	11.3 ± 0.7	6.0 ± 0.2	0.0312 ± 0.0004	1.2 ± 1.1	2.6	60	1.9	16 ± 1	2.5	14.3	14	43c

Column 1: partly shielded samples. Columns 2-4: measured data. Columns 5-6: $^{21}Ne_C$ and $^{3}He_C$ concentrations. Column 7: Depth of sample below surface. Column 8: calculated cosmogenic ^{3}He production rate (see text) at depth in column 7. Columns 9, 10: measured $^{3}He/^{4}He$ ratio and ^{3}He concentration. Column 11: Corrected $^{3}He/^{4}He$ ratio using equation 6-4. Column 12: Exposure age based on calculated cosmogenic ^{3}He in column 6 and production rate in column 8. Column 13: Independent estimates of eruption ages from data sources shown: a (Tronnes, 1990); b. Haukur Johannesson, Pers. Comm.; c. Ingvar Sigurdsson, Pers. Comm.

Measured versus corrected $^{3}He/^{4}He$ ratios in partly-shielded samples

The difference between the measured and corrected $^{3}He/^{4}He$ ratios from these Icelandic samples provides an estimate of the amount of cosmogenic ^{3}He in the samples. The $^{3}He/^{4}He$ ratios shown in Column 11 of Table 6-1 are corrected for possible contributions of cosmogenic ^{3}He (equations 6-2 to 6-4). Only samples *ice-2.1a*, *-4* and *-12.2* have relatively high measured $^{3}He/^{4}He$ total gas ratios (75, 56, 24 Ra) compared with those of most other Reykjanes Peninsula samples (8 - 20 Ra) (see Figures 5-2 and 5-8). In two of these samples, *ice-4* and *ice-12.2*, there is a significant difference between the measured and corrected $^{3}He/^{4}He$ ratios. In sample *ice-12.2*, the measured ratio is 24 Ra, about two times higher than the corrected $^{3}He/^{4}He$ ratio (12 Ra), but both ratios are within the range observed in other Reykjanes Peninsula samples. The corrected $^{3}He/^{4}He$ ratio in sample *ice-4* is zero, which shows that the assumption that the initial $^{21}Ne/^{22}Ne$ ratio lay on the air-solar mixing line is incorrect for this sample, and has caused the amount of $^{21}Ne_C$ to be overestimated. Use of a lower $^{21}Ne/^{22}Ne$ end-member neon isotopic ratio as the initial ratio would yield a corrected $^{3}He/^{4}He$ ratio more similar to the ratios in other Reykjanes Peninsula basalts, but there are no constraints on how low the initial $^{21}Ne/^{22}Ne$ ratio should be. In the third sample, *ice-2.1a*, will be discussed further in the next section.

In most of the remaining samples (*ice-1b, -2.2b, -10.1, -10.2, -11.1, -11.2, -16,* and *-25*) the corrected $^{3}He/^{4}He$ ratios are not more than ~3 Ra lower than the measured ratios. Also, for most of the partly-shielded samples (ice-*10.1, -10.2, -11.1, -11.2, -16,* and *-25*), the calculated exposure ages (1 to 14 ka, Table 6-1, Column 12) are younger than, or similar to, the estimated eruption ages (5 to 13 ka, 43 ka, Table 6-1, column 13). In general, even if the samples are as young as 10 ka, the calculated cosmogenic exposure age should accurately express the exposure history of the samples. The relatively young calculated exposure ages compared with the estimated eruption ages of these Icelandic basalts is probably caused by overestimating the production rate of $^{3}He_C$ and $^{21}Ne_C$, which may be the result of not accounting for erosion of the flow surface. In any case, the small differences between the corrected and observed $^{3}He/^{4}He$ ratios in samples *ice-1b, -2.2b, -10.1, -10.2, -11.1, -11.2, -16,* and *-25* suggests that $^{3}He_C$ consititutes only a minor amount of the total ^{3}He, and that the measured ratios in these samples may regarded as being not more than 3 Ra higher than the mantle $^{3}He/^{4}He$ ratios.

Samples that were collected from the same locality, but at different depths (*ice - 10.1, -10.2,* from Maelifell, and *-11.1, -11.2,* from Sandfell) should have different $^{3}He/^{4}He$ ratios if the flows are relatively old. The samples that were collected from the surface (*ice-10.1* and *-11.1*) appear to have slightly higher $^{3}He/^{4}He$ ratios (18 ± 2 and

19 ± 2 Ra) than *ice-10.2* and *ice -11.2* (17 ± 1 Ra, 100 cm below surface and 17 ± 1 Ra, 30 cm below surface, respectively), but these differences are not significant at the one sigma uncertainty level. The corrected $^{3}He/^{4}He$ ratios for the shielded samples *ice-10.2* and *–11.2* are the same as both the measured ratios and the ratios from the surface samples *ice-10.1* and *11.1* at the one sigma uncertainty level. This suggests that the contributions of cosmogenic ^{3}He and ^{21}Ne to the measured $^{3}He/^{4}He$ and $^{21}Ne/^{22}Ne$ ratios in the surface samples are small. This further implies that the flow surfaces in localities of these samples have not been exposed to cosmic rays for prolonged time periods, meaning that these particular flows are likely to be relatively young.

Sample ice-2.1a: mantle-derived or cosmogenic $^{3}He/^{4}He$?

It is important to evaluate in detail whether the highest measured $^{3}He/^{4}He$ ratios in this study are cosmogenic or mantle-derived in origin. Sample *ice-2* was not collected by the author. It was obtained from the present-day flow surface, but the degree of erosion is not known. The rock sample from which the olivine was separated for *ice-2.1a* was collected at the same locality but possibly from a different part of the flow than sample *ice-2.2* (replicates *ice-2.2a* and *ice-2.2b*, Chapter 4, Table 4-1). It is therefore possible that the sample from which *ice-2.1a* was obtained has experienced different shielding conditions from cosmic rays compared with the sample from which *ice-2.2a* and *-2.2b* were obtained. However, owing to the lack of information about the shielding conditions from cosmic rays for these samples, it is impossible to directly calculate the expected contributions of cosmogenic ^{3}He and ^{21}Ne to the samples.

The total gas ratios for sample *ice-2.1a* are: $^{21}Ne/^{22}Ne = 0.0312 \pm 0.0005$ and $^{3}He/^{4}He = 75 \pm 7$ Ra (Table 6-1). The $^{3}He/^{4}He$ ratios from individual gas extractions range from 29 Ra (1800°C) to 181 Ra (900°C) (Table 5.1). Assuming surface exposure conditions (Table 6-1), the corrected $^{3}He/^{4}He$ total gas ratio is 73 Ra (equation 6-3) (Table 6-1). This corrected $^{3}He/^{4}He$ ratio is similar to the measured ratio (75 Ra), and is much higher than any previously measured mantle $^{3}He/^{4}He$ ratios in Icelandic samples (Table 5-2). The calculated exposure time for sample *ice-2.1a* is equal to

$$^{3}He_{C}/[^{3}He]_{PR} = [(1 \times 10^{-14}\ cm^{3}STP/g)/(6 \times 10^{-18}\ cm^{3}STP/g\ year)] = \sim 2\ ka$$

(Table 6-1). This estimated exposure time is well below the minimum estimated eruption ages of 10 ka for the Sandfell volcanoes in the Hengill system (Tronnes, 1990) from which this sample was derived. It appears that there is only a minor contribution of cosmogenic ^{3}He in sample *ice-2.1a*, suggesting that the high total gas $^{3}He/^{4}He$ ratio of 75 ± 7 Ra may represent a mantle-derived composition.

In comparison, the measured $^{3}He/^{4}He$ ratios for *ice-2.2a* and *ice-2.2b* are significantly lower (16 and 8 Ra, respectively) than *ice-2.1a*. The corrected $^{3}He/^{4}He$ ratios for *ice-2.2a* and *ice-2.2b* are 10 and 6 Ra, respectively (Table 6-1), and notably, fall within the range of $^{3}He/^{4}He$ ratios measured in well-shielded olivine separates from the Reykjanes Peninsula (see Chapter 5). Because the high $^{3}He/^{4}He$ ratio observed in *ice-2.1a* was not also found in *ice-2.2a* and *–2.2b*, the intriguing results from sample *ice-2.1a* will not be discussed further here. Clearly, further studies on the samples from this locality should be undertaken.

6.2.2 *Summary and conclusions regarding cosmogenic versus mantle-derived components of ^{3}He and ^{21}Ne*

This evaluation of the helium and neon isotopic ratios of the partly-shielded samples suggests that in most samples (excluding *ice–1a (unconstrained), -4, -2.2a, -12.2*), cosmogenic isotopes, where present, constitute only a minor component of the observed $^{3}He/^{4}He$ and $^{21}Ne/^{22}Ne$ ratios. In most of the partly shielded samples the corrected $^{3}He/^{4}He$ ratios are not more than ~3 Ra lower than the measured ratios. In those partly shielded samples that have corrected $^{3}He/^{4}He$ ratios much lower than the measured $^{3}He/^{4}He$ ratios (*ice-4, -2.2a, -12.2)* a significant component of cosmogenic $^{21}Ne_C$ may be present. However, in sample *ice-4,* the assumption that all the excess ^{21}Ne is $^{21}Ne_C$ may lead to an overestimate of the $^{21}Ne_C$ and $^{3}He_C$ concentrations. This overestimate results in a "corrected" $^{3}He/^{4}He$ ratio that is lower than the atmospheric ratio. Sample *ice-2.1a* presents a unique problem in that although the high $^{3}He/^{4}He$ ratio of 75 ± 7 Ra appears to be mantle-derived, this result cannot be authenticated, because the $^{3}He/^{4}He$ ratios in *ice-2.2a* and *–2.2b* are much lower and are similar to the ratios in other Reykjanes Peninsula samples. The discussion of mantle-derived helium and neon isotopic compositions in the following sections will focus on the well-shielded samples, and on those in which contributions from cosmogenic nuclides are very small.

6.3 Preservation of near-solar neon isotopic ratios

This section addresses the possible processes by which near-solar neon isotopic ratios are preserved in Icelandic basalts. The observed neon isotopic ratios from Icelandic basalts lying on or near the air-solar mixing line imply that a primordial solar component trapped within the Earth has remained relatively unchanged over the past 4.5 Ga. Preservation of solar isotopic neon ratios in the silicate mantle is unexpected because the production of time integrated $^{21}Ne^{*}$ in the mantle, from the Wetherill

reactions (Wetherill, 1954) might be expected to increase the $^{21}Ne/^{22}Ne$ ratio to a value well above the primordial solar ratio (Honda et al., 1993a). The measured neon isotopic ratio will be indistinguishable from the solar neon isotopic ratio if the concentration of solar neon is relatively high compared with that of time integrated $^{21}Ne^*$, owing to either a high solar neon concentration or a very low U + Th concentration in the neon source region. Near-solar neon isotopic ratios may result from: (1) preservation of a primitive mantle component with a Ne_{solar} concentration that is sufficiently high such that it overwhelms the amount of $^{21}Ne^*$ produced by decay of U and Th (i.e., a mantle source with a high $[Ne_{solar}]/[U + Th]$ ratio); or (2) the extraction of solar noble gases from the Earth's outer core, which is assumed to have a very low U and Th content such that the production of $^{21}Ne^*$ over the age of the Earth is negligible.

6.3.1 Ratio of solar to nucleogenic neon in the MORB and Iceland mantle sources

To evaluate whether the solar neon isotopic ratios are preserved in a part of the Icelandic plume source mantle that has a high $[Ne_{solar}]/[U + Th]$ ratio, it is convenient to compare the composition of the Icelandic plume source with that of the MORB source, which is known to have been largely degassed, and is therefore expected to have a comparatively low $[Ne_{solar}]/[U + Th]$ ratio. The relative degree of degassing of solar gases from the Icelandic plume source and the MORB source mantle can be obtained by calculating the ratio of solar to nucleogenic neon in basalts from the two sources. The neon isotopic ratio of the mantle is a mixture of the preserved initial solar neon $(^{21}Ne/^{22}Ne)_{solar}$ and the nucleogenic neon $(^{21}Ne^*/^{22}Ne^*)$ produced in the mantle over the Earth's history; it can be calculated using equation (6-5):

$$(^{21}Ne/^{22}Ne)_{mantle} = (^{21}Ne_{solar} + {}^{21}Ne^*)/(^{22}Ne_{solar} + {}^{22}Ne^*) \quad (6\text{-}5)$$

The amount of $^{21}Ne^*$ that needs to be added to the solar $^{21}Ne/^{22}Ne$ ratio to produce the observed $^{21}Ne/^{22}Ne$ ratio in the MORB source can be calculated using a simplified version of equation (6-5). The addition of $^{22}Ne^*$ has little effect on the observed ratio because the $(^{21}Ne/^{22}Ne)_{solar}$ ratio (0.0328) is orders of magnitude lower than the nucleogenic $^{21}Ne^*/^{22}Ne^*$ production ratio of 48 (Yatsevich and Honda, 1997) so that changes in the $^{21}Ne/^{22}Ne$ ratio are almost entirely caused by addition of $^{21}Ne^*$. Consequently, $^{22}Ne^*$ may be neglected so that the right hand side of the equation is approximated by $(^{21}Ne_{solar} + {}^{21}Ne^*) / (^{22}Ne_{solar})$. Equation (6-6) may then be solved for $^{21}Ne^*/^{22}Ne_{solar}$ as follows (Honda et al., 1993b):

$$^{21}Ne^*/^{22}Ne_{solar} = (^{21}Ne/^{22}Ne)_{mantle} - (^{21}Ne/^{22}Ne)_{solar} \quad (6\text{-}6)$$

Using a MORB $^{21}Ne/^{22}Ne$ end-member ratio of 0.0744 (Sarda et al., 1988) (the extrapolated value of the $^{21}Ne/^{22}Ne$ ratio at a solar $^{20}Ne/^{22}Ne$ ratio of 13.8 ± 0.1 (Benkert et al., 1993)) and a solar $^{21}Ne/^{22}Ne$ ratio of 0.0328 ± 0.0005 (Benkert et al., 1993), equation (6-6) yields $^{21}Ne^*/^{22}Ne_{solar} \approx 0.042$.

The ratio of solar to nucleogenic neon in the Icelandic plume source is expected to be higher than in the MORB source, because the measured Iceland neon isotopic ratios of some samples lie within experimental error of the air-solar mixing line. To obtain the mantle $^{21}Ne/^{22}Ne$ ratio from the measured ratios, the component of atmospheric neon must first be subtracted from the measured value by extrapolating the $(^{21}Ne/^{22}Ne)_{measured}$ ratio to the $(^{20}Ne/^{22}Ne)_{solar}$ ratio of 13.8. For example, the measured neon ratios for sample *ice-9g2* lie near the air-solar mixing line, with a $^{21}Ne/^{22}Ne$ ratio of 0.0304 ± 0.0005 (1.7% uncertainty) and a $^{20}Ne/^{22}Ne$ ratio of 10.74 ± 0.13 (1.2 % uncertainty) (Table 5-1). At a $^{20}Ne/^{22}Ne$ ratio of 13.8, the extrapolated $^{21}Ne/^{22}Ne$ ratio is about 0.035. The uncertainties in the extrapolated $^{21}Ne/^{22}Ne$ ratio are obtained by extrapolating the maximum and minimum $^{21}Ne/^{22}Ne$ ratios (0.0299 and 0.0309, respectively, prior to extrapolation), obtained from the measured uncertainties, along a line from the atmospheric ratio to the solar $^{21}Ne/^{22}Ne$ ratio. Following extrapolation, the maximum $^{21}Ne/^{22}Ne$ ratio is estimated to be 0.0375 and the minimum is 0.0328. Because the Icelandic mantle source region must contain some U and Th, it should contain some nucleogenic neon. The value of 0.0375 constrains the maximum proportion of nucleogenic neon that is likely to be present in the Icelandic plume source region. The results from other Icelandic samples with neon ratios near the air-solar mixing line would yield similar average neon ratios, but owing to their larger uncertainties they place poorer constraints on the maximum and minimum values of the $^{21}Ne/^{22}Ne$ ratio in the plume source.

From equation (6-6), the estimated maximum $^{21}Ne^*/^{22}Ne_{solar}$ ratio for the Icelandic plume is 0.0047. This is a measure of the $^{21}Ne^*$ required to shift the $^{21}Ne/^{22}Ne$ ratio from the solar to the maximum permitted ratio of 0.0375. The relative concentrations of solar neon in the Icelandic plume source and the MORB source can be obtained from the ratio of $(^{21}Ne^*/^{22}Ne_{solar})_{MORB}/(^{21}Ne^*/^{22}Ne_{solar})_{Iceland}$ and is equal to 9 (0.042/0.0047). This shows that the proportion of solar neon in the Icelandic plume source is at least 9 times greater than in the MORB source, provided that the uranium and thorium contents in the MORB and the Icelandic plume sources are similar.

Is the Icelandic mantle plume source solar neon-enriched or (U + Th)-depleted?

The higher $^{22}Ne_{solar}/^{21}Ne^*$ ratios in the Iceland plume source relative to the MORB source may be caused by a lower U + Th concentration in the Icelandic plume source region, a higher relative solar neon concentration, or both. Differences in the U + Th concentrations in the MORB and Icelandic plume sources alone are unlikely to explain the higher $^{22}Ne_{solar}/^{21}Ne^*$ ratio in the Iceland plume source for the following reason. Neodymium and strontium isotopic systematics for MORBs (e.g., Hofmann, 1997) and Icelandic basalts (Hemond et al., 1993) show evidence of time-integrated depletion of incompatible elements in both source regions relative to the primitive mantle composition, but the MORB source is more depleted than the Icelandic source. Uranium and thorium, which are typical incompatible elements, are therefore expected to be more depleted in the MORB source than the Icelandic source. If the higher $^{22}Ne_{solar}/^{21}Ne^*$ ratios in Icelandic basalts relative to MORBs are due to differences in U + Th concentrations, the Icelandic plume source would need to be even more depleted in U + Th than the MORB source. Considering that most Icelandic basalts have experienced less time integrated depletion in incompatible elements than MORB, this possibility appears unlikely.

Preservation of primitive undegassed mantle

The MORB source has a $^{40}Ar/^{36}Ar$ ratio of at least 40,000 (Allègre et al., 1986/87; Burnard et al., 1997; Moreira et al., 1998), markedly higher than the atmospheric value of 295. This difference requires at least the upper part of the Earth's mantle to have undergone a massive degassing event early in its history, before a significant amount of ^{40}K (half-life = 1.25×10^9 annum) had decayed to ^{40}Ar (Hart et al., 1985). The upper mantle is estimated to have lost much of its ^{36}Ar in the first 1 Ga of Earth history (Turner, 1989) and is likely also to have lost a similarly large amount of its primordial solar neon during this time. Following the early massive degassing event, ^{40}Ar continued to be produced in the mantle by the decay of ^{40}K (e.g., Turner, 1989). A major question that remains is whether this early degassing event also caused extensive degassing of the lower mantle (cf. Davies, 1999; O'Nions and Tolstikhin, 1994; Phipps Morgan, 1998; Porcelli and Wasserburg, 1995).

Given that at least the upper mantle has undergone a massive early degassing event, followed by continuous degassing, a key question is whether some primitive undegassed mantle could be preserved in the mantle over the age of the Earth. Continuous degassing occurs via partial melting of the mantle and creates a strongly degassed mantle component that is later recycled and stirred back into the mantle by convection. The result is a hybrid mantle comprised of two end-member components: a

strongly degassed recycled component (Allègre and Turcotte, 1986) and a much less degassed original primitive mantle component (Becker et al., 1999; Phipps Morgan, 1998). Because partial melting of the mantle is confined to the low pressure zone at the top of the mantle, only a small fraction of the previously undegassed mantle can degas at a given time. Furthermore, the material entering the zone of melting will be a random mixture of primitive undegassed mantle and degassed mantle. Consequently, although the fraction of primitive undegassed mantle will decrease with time, the modern mantle can be expected to contain a small but finite amount of primitive undegassed material (Davies, 1984 and references therein). The scale of these undegassed mantle domains will decrease with time as they are continually thinned by stirring in the mantle.

The concept that primitive, unmelted domains may exist in the modern mantle is controversial. Primitive mantle is expected to be characterised by chondritic abundances of refractory lithophile trace elements, ε_{Nd} and ε_{Sr} values of zero, and lead isotopes that lie on the geochron (e.g., Hofmann, 1997). If material with this composition exists in the modern mantle, no evidence for it has been found in the thousands of OIB and MORB samples that have been analysed for radiogenic isotopes. The strontium, neodymium and lead isotopic data therefore appear to preclude the possibility that zones of primitive undegassed mantle exist on a scale equal to or greater than the zone of melting sampled by basalts. Radiogenic isotope results, however, do not preclude the possibility that regions of primitive undegassed mantle exist within the Icelandic plume source region, provided that the scale of these primitive mantle domains is small compared with the total volume of mantle processed to produce the erupted basalts. If the concentrations of Nd, Sr, and Pb in the primitive mantle component are of the same order as in the degassed mantle component, the isotopic compositions of the erupted basalts will lie on mixing arrays between the various isotopic mantle end-members that are sampled by the plume. Radiogenic isotope results will not necessarily provide a definitive test for the presence or absence of a primitive, undegassed mantle component under these circumstances.

The concentration of solar neon contained in relatively primitive undegassed mantle that remains in the lower mantle is likely to be greater than the concentration of solar neon in the upper mantle source of MORBs. One reason is that partial melting occurs in the low pressure region of the upper mantle, so that the degassed mantle residue from partial melting is more likely to be stirred into the adjacent upper mantle than it is into the more distant lower mantle. A second factor is that the viscosity of the mantle increases with pressure, and is believed to be about a factor of thirty higher in the lower mantle than it is in the upper mantle (Gurnis and Davies, 1986a). Stirring of degassed mantle with the undegassed mantle therefore is expected to take longer in the lower mantle than in the upper mantle. Because the Iceland plume source region contains at least nine times more solar neon than the MORB source, it is unlikely to originate within the upper mantle. In comparison, the Hawaiian plume source, with a mantle end-

member $^{21}Ne/^{22}Ne$ ratio of 0.0400 (Honda et al., 1993b), has a fraction of solar neon that is only about (0.042/0.0072) ~6 times greater than the MORB source (equation 6-6) and about (0.0072/0.0047) half the amount in the Icelandic plume source. Clearly, the concentration of solar neon in mantle plumes is heterogeneous, which is not unexpected if solar neon is stored in the viscous, poorly stirred lower mantle. Seismic studies have found evidence of a column of hot mantle extending from below Iceland well into the lower mantle (e.g., Bijwaard, 1999 and references therein), and it is possible that the Iceland plume originates from the thermal boundary layer that is believed to overlie the core (Griffiths and Campbell, 1990).

6.3.2 *The core as a source of solar neon in the Icelandic plume*

An alternative, speculative possibility is that the Icelandic plume obtained its helium, and by inference, solar neon, from the core, as discussed by Macpherson et al. (1998). One complicating factor in this hypothesis is that there is no known mechanism by which noble gases may have been incorporated into the core and subsequently released into the mantle. Owing to the low solubility of noble gases in metals (Becker and Pepin, 1984; Matsuda et al., 1993), during equilibrium melting and segregation of molten iron-nickel phase from the silicate mantle to form the core, the gases would be expected to partition preferentially into the silicate mantle (Matsuda et al., 1993). However, if non-equilibrium partitioning of noble gases occurs between the metal and silicate phases (Matsuda et al., 1993), it is possible that solar neon might be incorporated into the core. Because U and Th are unlikely to dissolve in Fe at any pressure and are not believed to be major constituents in the core (Ringwood, 1979), the core is a potential source where pure solar neon isotopic ratios could be preserved. However, as there are no experimental data for helium and neon to support this mechanism, or that proposed by Macpherson et al. (1998), for incorporating helium and neon into the core, any suggestion that neon has been stored in the core remains highly speculative.

6.3.3 *Conclusions regarding preservation of near-solar neon isotopic ratios*

The neon isotopic ratios measured on some Icelandic samples are among the most primitive reported so far from terrestrial mantle-derived samples. These neon data suggest that a small amount of primitive, undegassed material is present in the lower mantle source of the Icelandic plume, which contains much more solar neon than the upper mantle MORB source. The amount of solar neon in mantle plumes appears to be variable because the Hawaiian plume has a proportion of solar neon that is less than that

in the Icelandic plume (assuming that the U and Th contents in these reservoirs are similar).

The solar-like neon isotopic ratios in some Icelandic basalts have important implications for mantle convection models because they suggest that the mantle is highly heterogeneous in terms of noble gas concentrations. The Icelandic plume is unlikely to originate from the upper mantle, which is well-mixed and has a less solar-like $^{21}Ne/^{22}Ne$ ratio than the solar end-member in the Icelandic plume. The neon and helium characteristics of the Iceland plume are most consistent with a plume source deep in the lower mantle, a conclusion consistent with recent seismic studies of Iceland (Helmberger et al., 1998). The alternative possibility, that noble gases are stored in the outer core, is considered highly speculative.

The near-solar neon isotopic ratios are expected to be coupled with near-solar helium isotopic ratios, but this is not observed. Instead, the solar-like neon isotopic ratios are associated with lower $^{3}He/^{4}He$ ratios of 15 to ~30 Ra, interpreted to indicate decoupling of helium and neon during the generation and eruption of the magmas.

6.4 Decoupling neon and helium isotopic ratios

The near-solar neon isotopic ratios observed in some Icelandic basalts are expected to be coupled with measured $^{3}He/^{4}He$ ratios close to the solar ratio. This is because coupled production of ^{4}He and $^{21}Ne^{*}$, related to the decay of uranium and thorium, produces systematic changes in the $^{3}He/^{4}He$ and $^{21}Ne/^{22}Ne$ ratios in the mantle (Honda et al., 1993a) (see Chapter 2). As mentioned previously, the solar $^{3}He/^{4}He$ ratio is expected to lie in the range of the "planetary" ratios in meteorites and the ratio measured in the solar wind (100 and 320 Ra, respectively, see Chapter 2). Both ratios are much higher than the observed ratios of 15 – 30 Ra in the well-shielded samples that have solar neon isotopic ratios. Because the observed $^{3}He/^{4}He$ ratios in most samples from this study are much lower than the expected range of possible solar $^{3}He/^{4}He$ ratios, it appears necessary to infer that the neon and helium isotopic ratios are decoupled. Decoupling is also suggested by the compositions of the Icelandic samples from this study that have MORB-like neon isotopic ratios, which might be expected to have MORB-like $^{3}He/^{4}He$ ratios near 8.5 Ra, but instead have higher observed $^{3}He/^{4}He$ ratios from 12 to 20 Ra. However, the sense of decoupling in these samples is the opposite to that observed in the samples with solar neon isotopic ratios which have $^{3}He/^{4}He$ ratios between 15 and 30 Ra. Likewise, the results reported by Trieloff et al. (2000) show neon ratios that lie on a slightly steeper trend than the Loihi-Kilauea line in the neon three-isotope plot (Chapter 5). These neon ratios are predicted to be coupled with $^{3}He/^{4}He$

ratios greater than or equal to the Loihi ratio of ~30 Ra, but are instead lower, and between 17 –18 Ra. The decoupled helium and neon isotopic ratios in the results from this study and that of Trieloff et al. (2000) are in contrast to the seemingly coupled ratios reported by Harrison et al. (1999) (see Chapter 5).

6.4.1 Mixing solar helium and neon isotopic components from the Icelandic plume with MORB-derived helium and neon

The preceding discussion in section 6.3.1 suggests that noble gas isotopic heterogeneity is expected in the Icelandic plume source if the bodies of primitive, undegassed material exist on a relatively small scale within a matrix of less primitive mantle. However, shallow-level processes may also contribute to noble gas heterogeneity. Experiments to simulate the behaviour of plumes suggest that when plumes rise vertically from the core mantle boundary, entrainment of surrounding material occurs predominantly at the base of the lower mantle (Campbell, 1998, and references therein). However, when there are large-scale systematic motions in the surroundings such as a superimposed horizontal shear flow or convective overturning, as might be driven by the movement of tectonic plates, the plume conduit will be bent in the direction of horizontal flow (Griffiths and Turner, 1998, and references therein). A consequence of the tilting of plume conduits is enhanced entrainment of surrounding material as it is heated in a boundary layer around the rising plume tail and is drawn into it. Such entrainment has been investigated experimentally for a plume rising beneath a spreading ridge and show that the plume is spread laterally by the moving plates (Feigner and Richards, 1995). The behaviour of the model plume corresponds reasonably well with the isotopically "enriched" signature of the Icelandic plume over a great distance along the Mid-Atlantic Ridge (Griffiths and Turner, 1998; Schilling, 1973; Schilling, 1991). A MORB component has previously been suggested as a possible end-member that mixes with the Icelandic plume magmas in the source of Reykjanes Peninsula (Iceland) basalts on the basis of lead, strontium and neodymium isotopic data (Merz and Haase, 1997) (see Chapter 4). Mixing between plume and MORB magmatic components could also occur in magma chambers within the Icelandic crust near spreading ridges, such as along the Reykjanes Peninsula or the northern NVZ, and may be expected to lead to heterogeneous noble gas isotopic compositions in erupted basalts on a local scale.

Comparison of the helium and neon isotopic ratios from this study with those from previous studies shows that the mantle source of Icelandic basalts is quite heterogeneous. Mixing between plume and MORB-derived helium is implied by: (1) the increase in $^{3}He/^{4}He$ ratios in MORBs approaching Iceland from the north and south (Poreda et al., 1986) (see Chapter 5); (2) the increase in $^{3}He/^{4}He$ ratios along the

northern neovolcanic zone of Iceland, from MORB-like values of 8 Ra at northernmost locality near the coast, to higher values of 20 Ra near the center of Iceland (Breddam et al., 2000); and (3) the range in $^3He/^4He$ ratios of Reykjanes Peninsula samples from MORB-like $^3He/^4He$ ratios of 8.3 Ra (sample *ice-2.2b*) to higher ratios of at least 30 Ra (*ice-9a*). The gradient in $^3He/^4He$ ratios along the Mid Atlantic Ridge near Iceland, and along neovolcanic zones in Iceland, may suggest that the observed noble gas heterogeneity may arise in part from mixing plume and MORB-derived noble gases at relatively shallow levels in the mantle and/or in Icelandic crustal magma chambers.

The neon data appear to suggest that there are at least two mantle neon isotopic end-members, MORB-like and solar-like (Fig. 5-9). The neon isotopic compositions from the present study that have solar- and MORB-like neon ratios may represent the most- and least- "primitive" noble gas end-members, respectively, in this environment (Figs. 5-8, 5-9). These end-members may have mixed together to produce a range of intermediate neon isotopic ratios in Icelandic basalts. Compositions intermediate between the solar and MORB neon end-member compositions, such as those reported by Harrison et al. (1999) and Trieloff et al. (2000) (Fig. 5-4), may be expected in some localities where mixing between these end-members has occurred. Mixing solar-like helium and neon in the Icelandic plume with MORB-derived noble gas components may provide an explanation for the observed range of helium and neon end-member isotopic ratios in Reykjanes Peninsula basalts.

Mixing model

If mixing between plume and MORB-derived noble gases is the explanation for the observed range in helium and neon isotopic ratios in Icelandic basalts from the Reykjanes Peninsula, a model devised to describe such mixing should be able to explain (1) the apparently decoupled helium and neon isotopic ratios from this study (that include the samples with MORB-like neon isotopic ratios and those with solar-like neon isotopic ratios) and in the study by Trieloff et al. (2000) as well as (2) the nearly coupled helium and neon isotopic ratios reported in Harrison et al. (1999) (see Chapter 5, section 5.1.1). The equations that will follow describe mixing noble gases between a plume end-member that has a solar-like neon isotopic composition and a MORB end-member that has a neon isotopic ratio equal to the end-member MORB composition, as is suggested by the some of the neon compositions measured in this study (Figure 5-10). As such, the equations describe binary mixing between noble gases in the plume and MORB end-members. Although it is possible that other noble gas components are present, it will be shown that a two component model adequately describes the entire range in helium and neon isotopic compositions in Icelandic basalts.

End-member compositions: helium and neon

The plume end-member $^{3}He/^{4}He$ ratio is not well constrained. Based on the measured solar-like neon isotopic ratios, it is inferred that the $^{3}He/^{4}He$ ratio of the plume end-member should be close to the solar ratio. The solar $^{3}He/^{4}He$ ratio has been described in the literature as having a value as high as 320 Ra (the ratio in the solar wind) (Geiss et al., 1972) but may be as low as 100 Ra (the value measured in meteorites) (Anders and Grevesse, 1989) (see Chapter 2). These values define the maximum ratios that might be expected for the end-member $^{3}He/^{4}He$ ratio in the Icelandic plume. Much lower $^{3}He/^{4}He$ ratios are actually observed in most OIBs, including Icelandic basalts. Because the measured $^{3}He/^{4}He$ ratios in Icelandic basalts are much lower than the range of possible ratios for the solar end-member, the actual choice of 320 Ra or 100 Ra does not affect the interpretations that will be made from the data. This analysis of the data seeks to describe only the relative differences in the contributions of noble gases from the plume and MORB end-members in a mixture of gases, and the absolute values are not important here. Hence, a conservative estimate for the $^{3}He/^{4}He$ ratio of the solar end-member of 100 Ra will be used here, but similar conclusions could be drawn using higher ratios.

The maximum ratio and near-solar $^{21}Ne/^{22}Ne$ ratios (0.0328 - 0.0375) (see section 6.3.1 for an explanation of the maximum and minimum $^{21}Ne/^{22}Ne$ ratios used here) (Fig. 6-2), and the MORB end-member is known to have relatively low average $^{3}He/^{4}He$ ratios near 8.5 Ra and a relatively high end-member $^{21}Ne/^{22}Ne$ ratio (~0.075) (Sarda et al., 1988) compared with the solar ratio.

The compositions of some Icelandic samples from this study that have near-solar neon isotopic ratios and helium isotopic ratios of 20 - 30 Ra can be produced by binary mixing if the helium in the mixture is dominated by the MORB component (which has a low $^{3}He/^{4}He$ ratio of 8.5 Ra), but the neon in the mixture is dominated by a plume component that has a near-solar $^{21}Ne/^{22}Ne$ ratio. The relative proportions of helium and neon from the plume and MORB end-members in the mixture are described by the parameter $R^{P,M}_{He,Ne}$, which is the ratio of two ratios: the $^{22}Ne_S/^{3}He$ ratio (where the subscript "S" refers to "solar) in the plume divided by the $^{22}Ne_S/^{3}He$ ratio in MORB (equation 6-7),

$$R = \left[\frac{\left({}^{22}Ne_s / {}^{3}He \right)_P}{\left({}^{22}Ne_s / {}^{3}He \right)_M} \right] \qquad (6\text{-}7)$$

where "P" stands for plume and "M" for MORB.

The actual variation in the $^{22}Ne_s/^3He$ ratios in OIBs and MORBs was shown previously in Figure 2-20G (shown instead as $^3He/^{22}Ne_s$ ratios). There is a very large range in $^{22}Ne_s/^3He$ in oceanic basalt samples, with the $^{22}Ne_s/^3He$ ratios in MORBs generally lower than the ratio in OIBs (a detailed explanation of elemental ratios will be provided in Chapter 7). Mixing between OIB and MORB gases with fractionated $^{22}Ne_s/^3He$ ratios may produce a large range in $R^{P,M}_{He,Ne}$. In other words, varying $R^{P,M}_{He,Ne}$ relates to the relative degree of fractionation of the $^{22}Ne_s/^3He$ ratios in the MORB and plume end-member components. If $R^{P,M}_{He,Ne}$ has a relatively low value (e.g., 0.1), then the neon in the mixture is dominated by the MORB component in the denominator, and the neon isotopic composition of the mixture will be more similar to the MORB end-member than to the plume end-member, but the $^3He/^4He$ ratio will be higher than the MORB ratio. Conversely, if $R^{P,M}_{He,Ne}$ is relatively high (e.g., 5), then the mixture will have a neon isotopic composition that is dominated by the plume end-member composition, but the helium isotopic ratio will be lower than the plume end-member ratio owing to a contribution of helium from the MORB end-member. The equations below will show how varying the $R^{P,M}_{He,Ne}$ value changes the isotopic compositions in the mixture. The decoupled helium and neon isotopic ratios observed in the Icelandic samples will be explained as caused by mixing end-member plume and MORB compositions with a range of $R^{P,M}_{He,Ne}$ values.

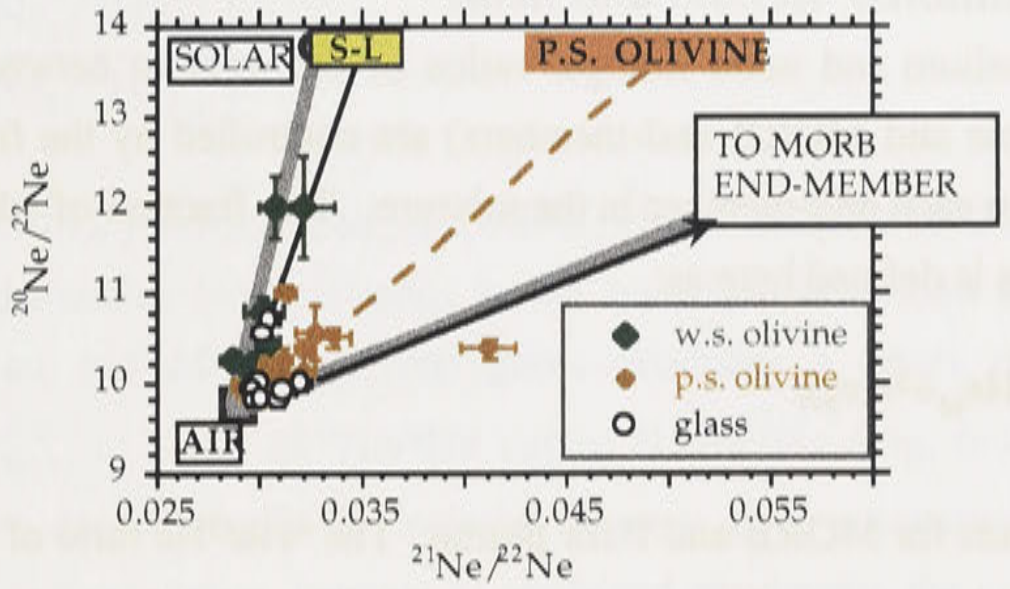

Figure 6-2. Neon three-isotope plot (see Fig. 5-10), showing the end-member $^{21}Ne/^{22}Ne$ ratios that will be used to model the Icelandic data from this study. The data shown from this study are total gas ratios, and the trends are formed by data from numerous samples. The size of the rectangle shows the range in extrapolated end-member $^{21}Ne/^{22}Ne$ ratios for each trend including the uncertainties, and was obtained in the same manner as described previously in this chapter. The $^{21}Ne/^{22}Ne$ end-member ratios are between 0.0328 and 0.0375 for trend S-L (solar-like), approximately equal to 0.075 for trend M-L (MORB-like), and between 0.038 and 0.055 for trend P.S. (Partly-Shielded olivine).

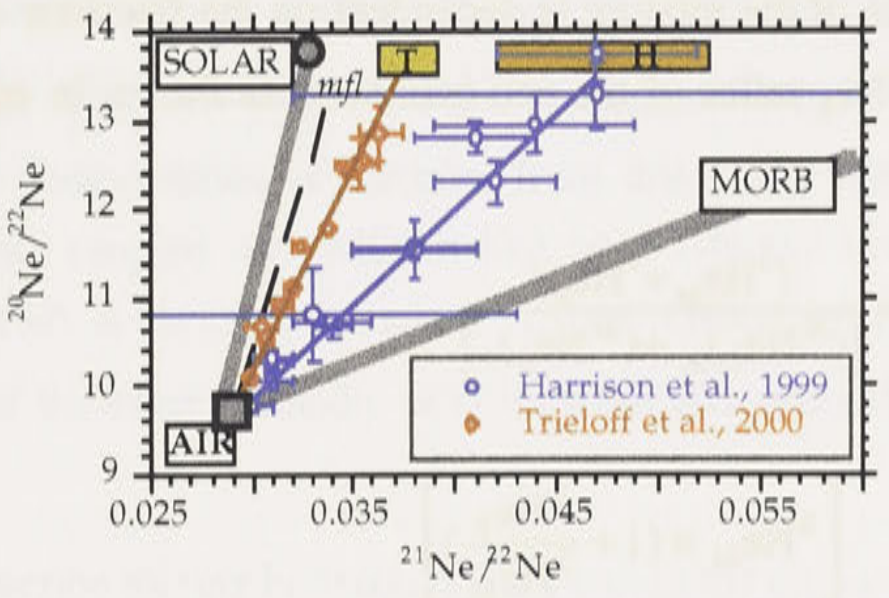

Figure 6-3. Neon three isotope plot showing end-member $^{21}Ne/^{22}Ne$ ratios for step-wise crushing data from Icelandic samples reported by Trieloff et al. (2000) and Harrison et al. (1999) (see Figure 5-4). Note that two samples were analysed for each study, and that the samples for both studies were obtained from Midfell (see Chapter 4). The end-member $^{21}Ne/^{22}Ne$ ratio for trend T (Trieloff et al., 2000) is between 0.036 and 0.039, and that for trend H (Harrison et al., 1999) is between 0.042 and 0.052.

Mixing equations: helium and neon

The helium and neon isotopic ratios of the mixture between two end-members (e.g., the plume and MORB end-members) are controlled by the fractions (f) of helium and neon from each end-member in the mixture. The fraction of MORB-derived helium in the mixture is defined here as:

$$f_M = {}^3He_M/({}^3He_M+{}^3He_P), \tag{6-8}$$

where M stands for MORB and P for plume. The $^4He/^3He$ ratio of the mixture can then be written as:

$$(^4He/^3He)_{MIX} = (^4He/^3He)_M \times f_M + (^4He/^3He)_P \times (1- f_M) \tag{6-9}$$

Similarly, the fraction of MORB-derived neon in the mixture can be defined as:

$$F_M = (^{22}Ne_S)_M/[(^{22}Ne_S)_M + (^{22}Ne_S)_P] \tag{6-10}$$

so that the $^{21}Ne/^{22}Ne$ ratio of the mixture is described by equation (6-11):

$$(^{21}Ne/^{22}Ne)_{MIX} = (^{21}Ne/^{22}Ne)_M \times F_M + (1- F_M) \times (^{21}Ne/^{22}Ne)_P \tag{6-11}$$

The $^3He/ Ne_S$ ratio of the mixture is dependent on the fractions of helium and neon and the relative $^3He/ Ne_S$ ratios of the end-members, as shown in equations (6-12) and (6-13):

$$(^3He/^{22}Ne_S)_{MIX} = \frac{(^3He_M+^3He_P)}{[(^{22}Ne_S)_M+(^{22}Ne_S)_P]} \tag{6-12}$$

$$= \frac{\left[{}^3He_M \times (1+\frac{{}^3He_P}{{}^3He_M})\right]}{\left[{}^{22}Ne_M \times (1+\frac{(^{22}Ne_s)_P}{(^{22}Ne_s)_M})\right]}$$

$$= (^3He/^{22}Ne_S)_M \times (1/f_M)/(1/ F_M)$$

$$= (^3He/^{22}Ne_S)_M \times F_M /f_M$$

$$= \left(\frac{^3He}{^{22}Ne_S}\right)_M \times \frac{1}{\left[f_M+(1-f_M)\times\left[\frac{\left(^{22}Ne_S/^3He\right)_P}{\left(^{22}Ne_S/^3He\right)_M}\right]\right]} \tag{6-13}$$

$$\text{where } R^{P,M}_{He,Ne} = \left[\frac{\left({}^{22}Ne_S / {}^{3}He \right)_P}{\left({}^{22}Ne_S / {}^{3}He \right)_M} \right] \qquad (6\text{-}7)$$

Model results: mixing plume- and MORB-derived helium and neon

Using the end-member isotopic ratios in the equations described above, mixing between plume-derived and MORB-derived gases produces a series of curves for different values of $R^{P,M}_{He,Ne}$ in a plot of $^{3}He/^{4}He$ versus $^{21}Ne/^{22}Ne$ (Fig. 6-4). The $R^{P,M}_{He,Ne}$ values are intended to describe only the *relative* degrees of fractionation required to produce the observed isotopic ratios, because as explained previously, the composition of the solar end-member helium isotopic ratio is not well constrained. Because sample *ice-9*, from this study and the samples analyzed by Harrison et al. (1999) and Trieloff et al. (2000) are from the same quarry, their helium and neon isotopic compositions are evaluated to determine whether they have been produced by a mixture of the plume and MORB end-member components with the same isotopic ratios, but with different $R^{P,M}_{He,Ne}$.

A mixture of plume and MORB-derived gases with an $R^{P,M}_{He,Ne}$ value of at least 5 (Fig. 6-4) may explain the results from this study, represented by the square labelled "S-L" (which stands for "Solar-Like" as described previously in this chapter) in Figure 6-4 and those reported by Trieloff et al. (2000) (labelled "T"). In comparison, the results from Harrison et al.(1999), shown as a rectangle labelled "H" in Figure 6-4, may be produced by lower $R^{P,M}_{He,Ne}$ values near 1-2. Still lower $R^{P,M}_{He,Ne}$ values near 0.03 to 0.1 are required to explain the compositions of samples from this study with $^{3}He/^{4}He$ ratios from 12 to 20 Ra that are coupled with MORB-like neon isotopic ratios (box labelled "M-L" in Fig. 6-4). This is the opposite sense of fractionation needed to explain the isotopic compositions of the other Icelandic samples from this study that require $R^{P,M}_{He,Ne}$ values of near 5.

The model to describe mixing between noble gases in the plume and MORB end-members with different $R^{P,M}_{He,Ne}$ values appears to explain all the results from this study, as well as those reported by Harrison et al. (1999) and Trieloff et al. (2000). Such a large range in $R^{P,M}_{He,Ne}$ values (0.03 to 5) requires a significant range of fractionated $^{22}Ne_S/^{3}He$ ratios in the plume and/or MORB end-members (see Fig. 2-20). The degree of fractionation of the $^{22}Ne_S/^{3}He$ ratios in the plume and MORB end-members is a very important topic, but discussion of this topic is deferred to Chapter 7 because the elemental ratios in Icelandic basalts are complex and require a great deal of background explanation.

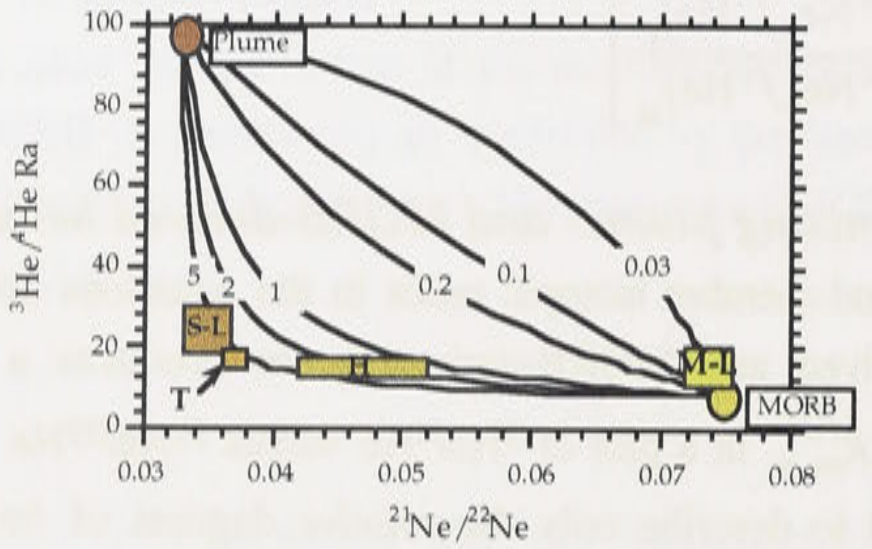

A

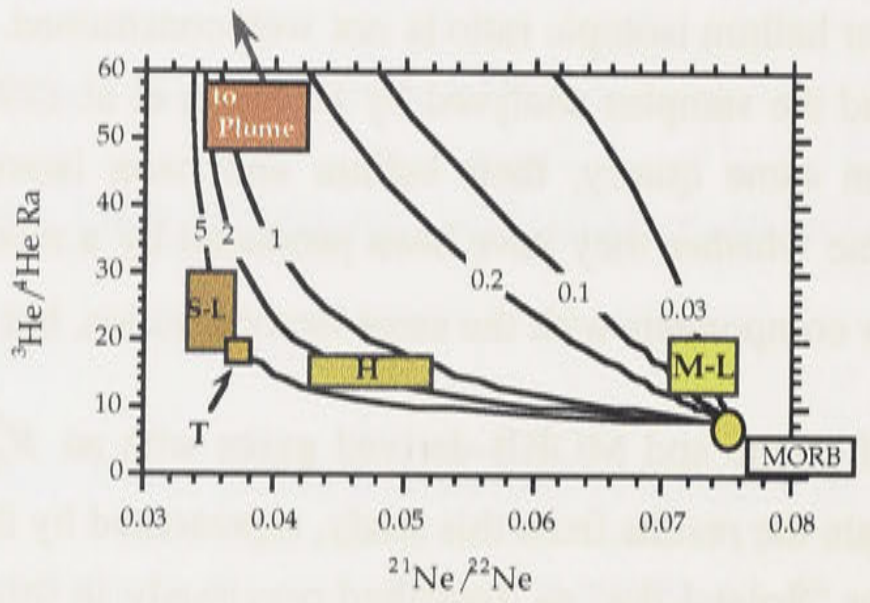

B

Figure 6-4A and B (blow-up of figure in A). Plots of ^{3}He/^{4}He versus ^{21}Ne/^{22}Ne showing mixing curves between the plume and MORB end-members (circles) that pass through the end-member ratios from this study and previous noble gas studies of Icelandic basalts (rectangles). The "Plume" end-member has a ^{3}He/^{4}He ratio of 100 Ra and a solar ^{21}Ne/^{22}Ne ratio (see text), and the MORB end-member has a ^{3}He/^{4}He ratio of 8.5 Ra and an end-member ^{21}Ne/^{22}Ne ratio of 0.075. Calculated mixing curves show the compositions that would be produced by mixtures of noble gases from the plume and MORB end-members with $R^{P,M}_{He,Ne}$ values of 5, 2, 1, 0.2, 0.1 and 0.03. Some of these curves intersect the rectangles labelled *S-L*, *T*, *H*, and *M-L* (see Figs. 6-2 and 6-3). (1) **S-L** = "Solar-Like", samples from this study with neon isotopic ratios near the air-solar mixing line (^{21}Ne/^{22}Ne ratios in the range of 0.0328 – 0.0375, ^{3}He/^{4}He from 17 – 30 Ra); (2) **M-L** = "MORB-like" samples from this study with neon isotopic ratios near the MORB trend, but relatively high ^{3}He/^{4}He ratios (end-member ^{21}Ne/^{22}Ne = ~0.070 – 0.075, ^{3}He/^{4}He ratios from 12 - 20 Ra); (3) **H** = Harrison et al., (1999), (^{21}Ne/^{22}Ne ratios = 0.042 – 0.052 and ^{3}He/^{4}He ratios from 15 - 18 Ra); (4) **T** = Trieloff et al. (2000), (^{21}Ne/^{22}Ne ratios = 0.036 – 0.038, and ^{3}He/^{4}He = 17 - 18 Ra). These plots show that the decoupled helium and neon isotopic ratios can be produced by mixing noble gases derived from the plume and MORB end-members using a range of $R^{P,M}_{He,Ne}$ values. A curve with an $R^{P,M}_{He,Ne}$ of 5 passes through both end-member *S-L* and end-member *T*, but a lower $R^{P,M}_{He,Ne}$ of 1 to 2 is needed to explain end-member *H*. Still lower values of $R^{P,M}_{He,Ne}$ near 0.03 best explain the composition of end-member *M-L*.

Summary

A mixture of plume and MORB-derived noble gases with an $R^{P,M}_{He,Ne}$ value of approximately 5 best describes the results from this study with near-solar neon isotopic ratios and the results reported by Trieloff et al. (2000). The results of Harrison et al. (1999) are best described by lower values of $R^{P,M}_{He,Ne}$ in the range of 1 to 2. Still lower $R^{P,M}_{He,Ne}$ values near 0.1 to 0.03 are needed to explain the data from this study with MORB-like neon isotopic ratios. Mixing between noble gases from the plume and MORB end-members provides one possible explanation for the observed variation in helium and neon isotopic ratios in samples that were obtained from the same quarry (but possibly different flow units) including sample *ice-9*, from this study, and samples from Harrison et al. (1999) and Trieloff et al. (2000). The range in $R^{P,M}_{He,Ne}$ values required to explain the range in helium and neon isotopic ratios requires fractionated $^{22}Ne_S/^{3}He$ ratios in the end-member plume and/or MORB component, as will be discussed in Chapter 7.

6.4.2 Mixing plume- and MORB-derived neon and argon

Given that the decoupled helium and neon isotopic ratios may be explained satisfactorily by mixing between gases derived from the Icelandic plume and MORB, it is necessary to show that the argon isotopic ratios are also consistent with this process. By comparing the helium, neon and argon isotopic ratios, it is possible to show that part of the variation in $^{40}Ar/^{36}Ar$ ratios in Icelandic basalts may be caused by mixing between plume and MORB-derived argon.

Neon and argon isotopic ratios in mantle-derived samples may be compared in both plots of $^{20}Ne/^{22}Ne$ versus $^{40}Ar/^{36}Ar$ (Fig. 6-5) and $^{21}Ne/^{22}Ne$ versus $^{40}Ar/^{36}Ar$ (Fig. 6-6). The plot of $^{20}Ne/^{22}Ne$ versus $^{40}Ar/^{36}Ar$ (Fig. 6-5) shows three main trends (I, II and III) that intersect the atmospheric composition. Trend I is defined by the data from this study, comprised of individual gas extractions released by step-heating, including the olivine data with near-solar neon isotopic ratios; trend II is defined by step-wise crushing data reported by Harrison et al. (1999) and Trieloff et al. (2000), plus some of the data from this study (note that the end-member compositions of the data that lie along trend II are also intermediate between the plume and MORB end-member compositions in plots that include helium and neon isotopic ratios in Figures 6-2, 6-3, 6-4); and trend III is defined by data from the MORB popping rock (Moreira et al., 1998). The end-member isotopic compositions of trend III is the MORB end-member composition.

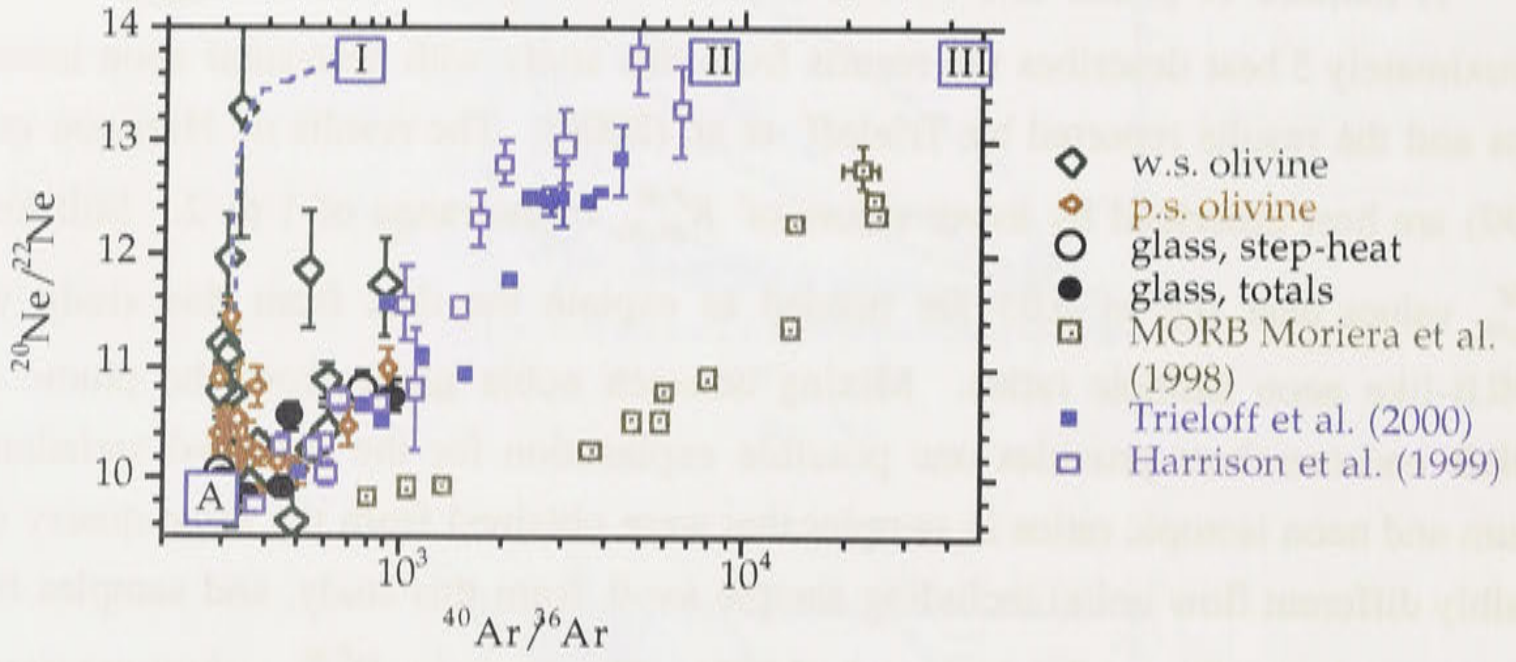

Figure 6-5. $^{20}Ne/^{22}Ne$ versus $^{40}Ar/^{36}Ar$ plot showing Icelandic data from this study and those of Harrison et al. (1999) and Trieloff et al. (2000), as well as data from the MORB popping rock (Moreira et al., 1998). The trends formed by the data converge at the atmospheric ratio, labelled "A." Some of the olivine data from this study lie on a near-vertical trend, with a range of $^{20}Ne/^{22}Ne$ ratios from atmospheric to 13.2 ± 1 and relatively low $^{40}Ar/^{36}Ar$ ratios (trend I). Note that the end-member $^{40}Ar/^{36}Ar$ ratio of trend I cannot be determined from this plot because at high $^{20}Ne/^{22}Ne$ ratios there may not be a linear relationship between neon and argon isotopic ratios (indicated by dashed line for trend I). Most of the remaining data from this study form a trend with a shallower slope, similar to that formed by the data from Harrison et al., (1999) and Trieloff et al. (2000) (trend II). The data from Harrison et al. (1999) have a maximum $^{40}Ar/^{36}Ar$ ratio near 7000 and a maximum $^{21}Ne/^{22}Ne$ ratio near the solar ratio. The MORB data define trend III, with an end-member $^{40}Ar/^{36}Ar$ ratio near 40,000. The data that define these three trends are not necessarily related to the data that define the solar-like and MORB-like trends in the neon three-isotope plot, because samples with a range of different $^{21}Ne/^{22}Ne$ end-member ratios lie on trend II.

In Figure 6-6 (a plot of $^{21}Ne/^{22}Ne$ versus $^{40}Ar/^{36}Ar$), only two of the main trends are visible: trend II and trend III. Trend I is not clearly visible in this plot because the data from this study that defined trend I in Figure 6-5 overlap the data forming trends II and III. Interestingly, the data reported by Trieloff et al. (2000) do not lie on trend II, as they do in Figure 6-5, but instead lie on trend III, defined by the MORB data. Although the neon and argon data from Trieloff et al. (2000) appear to have been produced by mixing between MORB-like and atmospheric gases in Figure 6-6, this is not the case. As shown in Figure 6-3, the data reported by Trieloff et al. (2000) define a mixing trend with atmospheric neon that is distinct from the MORB trend, and the end-member $^{21}Ne/^{22}Ne$ ratio (~0.038) is distinct from MORB end-member ratio (0.075). Thus, the neon data reported by Trieloff et al. (2000) clearly cannot be explained as being

produced by mixing between a MORB end-member neon isotopic composition with atmospheric gases (see also Fig. 6-5). The calculations below will show that the compositions of the data in Figures 6-5 and 6-6 are consistent with mixing between plume and MORB-derived gases, and that these mantle-derived gases subsequently mix with atmospheric gases.

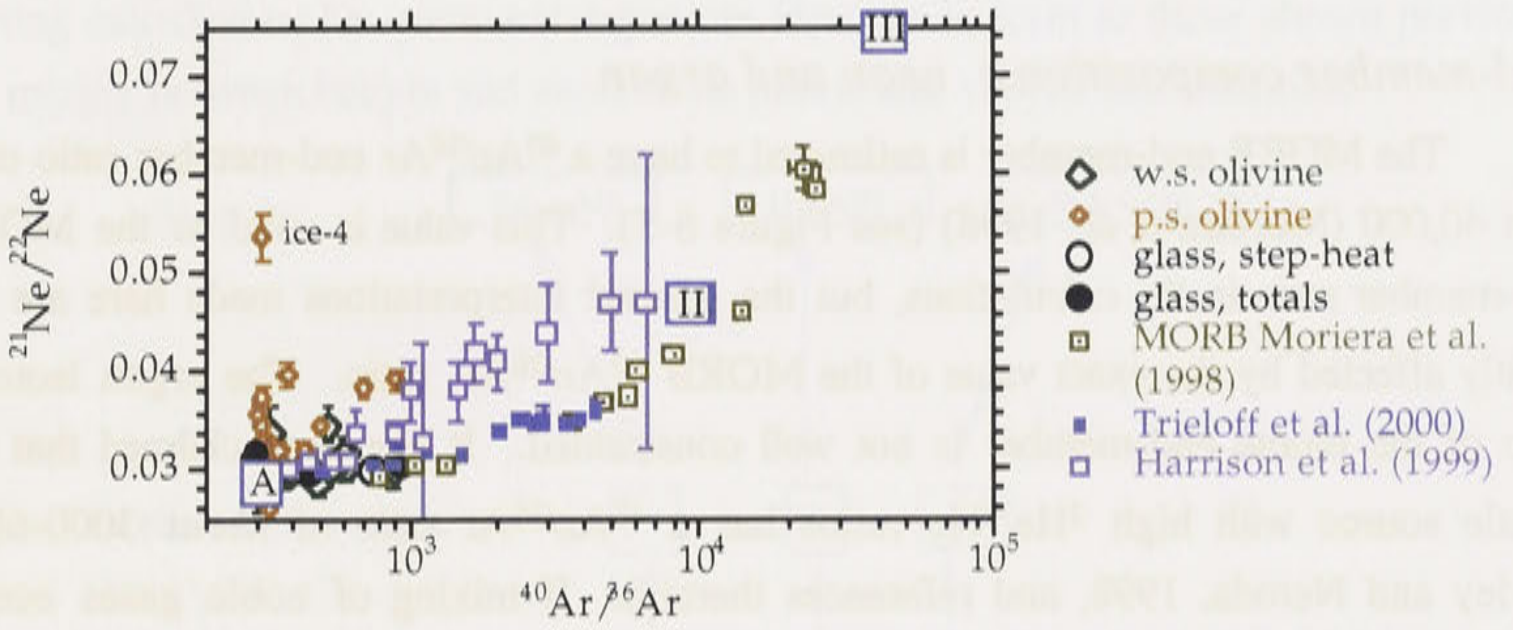

Figure 6-6. $^{21}Ne/^{22}Ne$ versus $^{40}Ar/^{36}Ar$ plot showing data from the same sources as in Figure 6-5, above. The atmospheric ratio is the square labelled "A." Most of the data from well-shielded (w.s.) olivine from this study overlap the data from Harrison et al. (1999) that lie along trend II so that trend I is not visible in this plot. Interestingly, (unlike in Figure 6-5) the data from Trieloff et al. (2000) do not lie on trend II, but instead lie on trend III, defined by the MORB data. It appears from this plot that the data reported by Trieloff et al. (2000) could be explained by mixing between air and MORB end-members. This is not the case: the data reported by Trieloff et al. (2000) *cannot* be explained as being produced by mixing between a MORB end-member neon isotopic composition with atmospheric gases because the end-member $^{21}Ne/^{22}Ne$ ratio is distinct from the MORB end-member ratio (Figure 6-5 and see text for explanation).

Summary

The data that define trend II have neon and argon isotopic mantle end-member compositions that lie between those of trend I and trend III in Figure 6-5. This allows the neon and argon isotopic compositions of trend II to be modelled as the product of mixing between the noble gas mantle end-members for trends I and III.

Mixing calculations

Calculations similar to those shown above to describe mixing between plume and MORB-derived helium and neon are used below to describe mixing between neon and argon. These mixing calculations use the variations in the measured $^{21}Ne/^{22}Ne$ ratio to

model the data because the $^{20}Ne/^{22}Ne$ ratios are assumed to be equal to the solar ratio of 13.8 in the plume and MORB end-members. Subsequent to mixing between the plume and MORB noble gas end-members, a second stage of mixing between mantle-derived and atmospheric noble gases is suggested by trends that intersect the atmospheric composition in plots of $^{20}Ne/^{22}Ne$ versus $^{40}Ar/^{36}Ar$ (Fig. 6-5) and $^{21}Ne/^{22}Ne$ versus $^{40}Ar/^{36}Ar$ (Fig. 6-6).

End-member compositions: neon and argon

The MORB end-member is estimated to have a $^{40}Ar/^{36}Ar$ end-member ratio of at least 40,000 (Moreira et al., 1998) (see Figure 6-5). This value is used as the MORB end-member ratio in the calculations, but the general interpretations made here are not greatly affected by the exact value of the MORB $^{40}Ar/^{36}Ar$ ratio. The argon isotopic ratio of the plume end-member is not well constrained. It has been claimed that the mantle source with high $^{3}He/^{4}He$ ratios has a $^{40}Ar/^{36}Ar$ ratio of about 3000-6000 (Farley and Neroda, 1998, and references therein). If mixing of noble gases occurs between the plume and MORB end-member components, the maximum $^{40}Ar/^{36}Ar$ ratio in Icelandic samples from this study (approximately 1000) may be comprised of plume-derived argon $(^{40}Ar/^{36}Ar)_P$, MORB-derived argon $(^{40}Ar/^{36}Ar)_{MORB}$, and atmospheric argon $(^{40}Ar/^{36}Ar)_{AIR}$. Hence, the $^{40}Ar/^{36}Ar$ mantle end-member composition of Icelandic basalts cannot be accurately determined from the measured ratios. It can, however, be estimated if the $^{22}Ne/^{36}Ar$ ratio of the mantle is known. Data reported by Moreira et al. (1998) for the MORB popping rock suggest that at an end-member solar $^{20}Ne/^{22}Ne$ ratio of 13.8, the $^{22}Ne/^{36}Ar_{Mantle}$ ratio is 0.096. For an Icelandic plume (P) end-member $^{21}Ne/^{22}Ne$ ratio of 0.03515 ± 0.0024 (total range of 0.0328 to 0.0375), and a $^{21}Ne^*/^{40}Ar^*$ production ratio of 6.36×10^{-8} (see Chapter 2), the range in the $^{40}Ar/^{36}Ar$ ratio of the Icelandic plume source may be obtained using equation (6-14):

$$\left(^{40}Ar/^{36}Ar\right)_P = (^{40}Ar/^{36}Ar)_{initial} + \frac{\left(\left(^{21}Ne/^{22}Ne\right)_P - \left(^{21}Ne/^{22}Ne\right)_{solar}\right) \times \left(^{22}Ne_S/^{36}Ar\right)_{mantle}}{\left(^{21}Ne^*/^{40}Ar^*\right)_{production}} \qquad (6\text{-}14)$$

Because the $^{40}Ar/^{36}Ar$ ratio is based on the amount of $^{21}Ne^*$, the $^{40}Ar/^{36}Ar$ ratio of the Icelandic plume source is predicted to approach the estimated initial $^{40}Ar/^{36}Ar$ ratio in the Earth (less than 1 for either the solar or the meteoritic ratio, see Chapter 2, Table 2-5) for a $^{21}Ne/^{22}Ne$ ratio near the solar ratio of 0.0328. The maximum end-member $^{40}Ar/^{36}Ar$ ratio of 7100 is estimated for the maximum extrapolated $^{21}Ne/^{22}Ne$ ratio of 0.0375. A

lower $^{40}Ar/^{36}Ar$ of ~3500 is predicted if the mantle plume source $^{21}Ne/^{22}Ne$ ratio is equal to the median extrapolated ratio of 0.03515. This $^{40}Ar/^{36}Ar$ of 3500 will be used as composition of the plume end-member. Use of a somewhat lower or higher $^{40}Ar/^{36}Ar$ would not change the general interpretations made here. The plume and MORB end-member compositions will be used to generate a series of mixing curves by varying $R^{P,M}_{Ne,Ar}$, where $R^{P,M}_{Ne,Ar} = (^{36}Ar/^{22}Ne_S)_P/(^{36}Ar/^{22}Ne_S)_{MORB}$. The equations used for the mixing calculations for neon and argon are identical in form to those shown previously for mixing between helium and neon in the plume and MORB end-members.

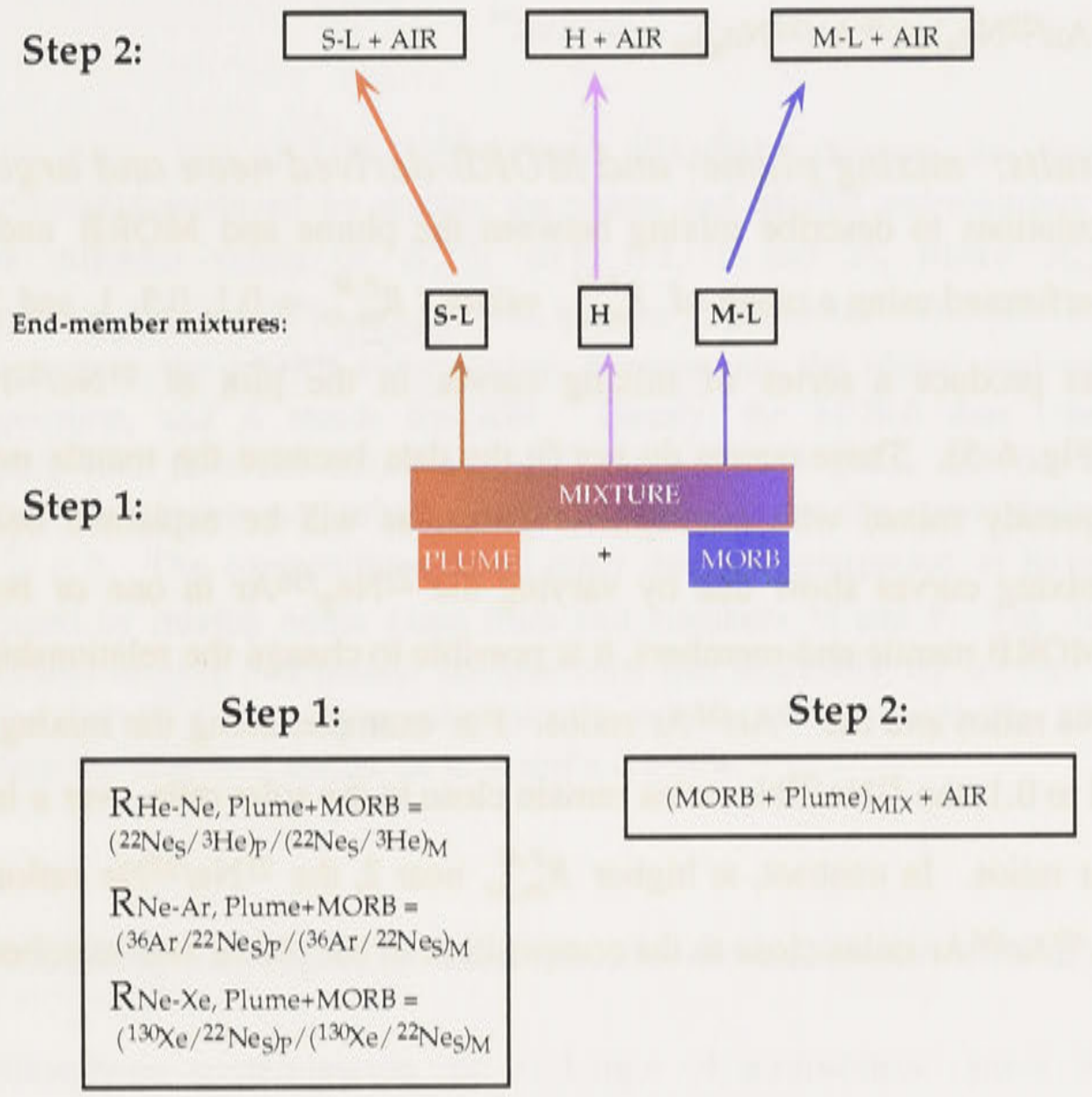

Figure 6-7. Diagram showing the postulated stages of mixing between the plume and MORB noble gases (step 1), followed by mixing between atmospheric noble gases and end-member mixtures S-L (solar-like), H (Harrison) and M-L (MORB-like composition). Addition of atmospheric noble gases is shown as a separate stage from mixing mantle noble gases for simplicity, though it is possible that these processes do not occur in two distinct stages in nature. The ratio $R^{P,M}_{He,Ne}$ is used in the equations describing mixing between plume (P) and MORB (M)-derived helium and neon, $R^{P,M}_{Ne,Ar}$ is used in the mixing equations for plume and MORB-derived neon and argon, etc. The subscript "MIX" indicates a mixture of plume and MORB-derived gases represented by end-members S-L, H or M-L.

Mixing Equations: neon and argon

$$g_M = (^{22}Ne_S)_M/[(^{22}Ne_S)_M+(^{22}Ne_S)_P], \quad (6\text{-}15)$$

$$(^{21}Ne/^{22}Ne)_{MIX} = (^{21}Ne/^{22}Ne)_M \times g + (^{21}Ne/^{22}Ne)_P \times (1-g_M) \quad (6\text{-}16)$$

$$G_M = {}^{36}Ar_M/({}^{36}Ar_M+{}^{36}Ar_P) \quad (6\text{-}17)$$

$$(^{40}Ar/^{36}Ar)_{MIX} = (^{40}Ar/^{36}Ar)_M \times G_M + (1-G_M) \times (^{40}Ar/^{36}Ar)_P \quad (6\text{-}18)$$

$$(^{22}Ne/^{36}Ar)_{MIX} = [(^{22}Ne_S)_M+(^{22}Ne_S)_P]/({}^{36}Ar_M + {}^{36}Ar_P) \quad (6\text{-}19)$$

$$(^{22}Ne/^{36}Ar)_{MIX} = (^{22}Ne_S/^{36}Ar)_M \times 1/[g_M + (1-g_M) \times (^{36}Ar/^{22}Ne_S)_P/(^{36}Ar/^{22}Ne_S)_M] \quad (6\text{-}20)$$

$$R^{P,M}_{Ne,Ar} = (^{36}Ar/^{22}Ne_S)_P/(^{36}Ar/^{22}Ne_S)_M \quad (6\text{-}21)$$

Model Results: mixing plume- and MORB-derived neon and argon

Calculations to describe mixing between the plume and MORB end-members have been performed using a range of $R^{P,M}_{Ne,Ar}$ values ($R^{P,M}_{Ne,Ar}$ = 0.1, 0.5, 1, and 2). These $R^{P,M}_{Ne,Ar}$ values produce a series of mixing curves in the plot of $^{21}Ne/^{22}Ne$ versus $^{40}Ar/^{36}Ar$ (Fig. 6-5). These curves do not fit the data because the mantle noble gases have subsequently mixed with atmospheric gases, as will be explained below. The calculated mixing curves show that by varying the $^{22}Ne_S/^{36}Ar$ in one or both of the plume and MORB mantle end-members, it is possible to change the relationship between the $^{21}Ne/^{22}Ne$ ratios and the $^{40}Ar/^{36}Ar$ ratios. For example, along the mixing curve for $R^{P,M}_{Ne,Ar}$ equal to 0.1, the $^{21}Ne/^{22}Ne$ ratios remain close to the solar ratio over a large range of $^{40}Ar/^{36}Ar$ ratios. In contrast, at higher $R^{P,M}_{Ne,Ar}$ near 2, the $^{21}Ne/^{22}Ne$ ratios are only solar-like at $^{40}Ar/^{36}Ar$ ratios close to the composition of the plume end-member.

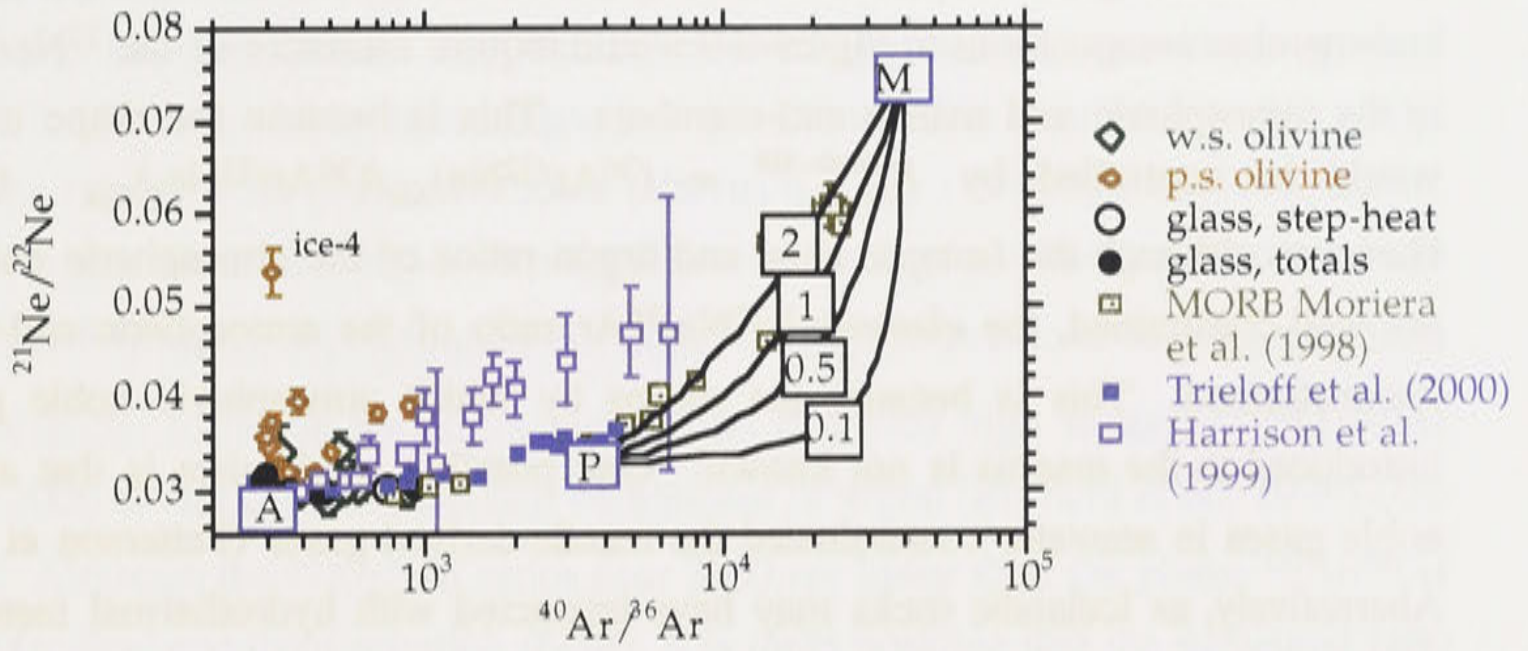

Figure 6-8. Plot of $^{21}Ne/^{22}Ne$ versus $^{40}Ar/^{36}Ar$ showing the range of compositions produced by mixing the plume and MORB end-members for a range different values of $R^{P,M}_{Ne,Ar}$ (0.1, 0.5, 1 and 2), where $R^{P,M}_{Ne,Ar} = (^{36}Ar/^{22}Ne_S)_P/(^{36}Ar/^{22}Ne_S)_{MORB}$. See text for explanation. The box labelled M represents the MORB end-member, P represents the plume end-member composition, and A stands for AIR. Clearly, the MORB data from the popping rock have not mixed with the plume-derived gases, and the MORB data define a curve that only by coincidence lies near the curve defined by $R^{P,M}_{Ne,Ar} = 2$. The compositions of all other data are interpreted to have been produced by mixing noble gases from end-members M and P. The data are postulated to have had mantle compositions that originally lay on one of the mixing curves, and to have subsequently mixed with atmospheric gases to produce the observed trends, as is described below.

6.4.3 *Mixing atmospheric and mantle-derived neon and argon*

Atmospheric contamination, or exchange of atmospheric gases with mantle-derived gases, is observed in all noble gas data (except helium data) from mantle-derived samples. The observed noble gas isotopic compositions of these samples define apparent mixing trajectories that pass through the atmospheric composition (Farley and Neroda, 1998). Figure 6-9 is schematic diagram showing how a mantle noble gas component with a composition that lies on a curve with a given $R^{P,M}_{Ne,Ar}$ may mix with the atmospheric end-member. It is easy to imagine how, for a given mantle end-member in Figure 6-9, the addition of atmospheric neon and argon could produce the observed trends in the data shown in Figure 6-8. In Icelandic basalts, the initial $^{40}Ar/^{36}Ar$ ratio of a mantle end-member produced by mixing between plume and MORB-derived gases is unconstrained. However, using the data from Harrison et al. (1999) as an example, a mantle component with an end-member $^{21}Ne/^{22}Ne$ ratio of ~0.047 may have lain on the curve with $R^{P,M}_{Ne,Ar}$ equal to 0.1. Addition of noble gases with atmospheric isotopic ratios would then produce the observed trend in the data shown in Figure 6-8.

Calculating the shape of the mixing curves between the mantle and atmospheric end-member compositions in Figure 6-9 would require estimates of the $^{22}Ne/^{36}Ar$ ratios in the atmospheric and mantle end-members. This is because the shape of the curve would be controlled by $R_{Ne,Ar}^{Mantle,AIR} = (^{36}Ar/^{22}Ne)_{AIR}/(^{36}Ar/^{22}Ne_S)_{MIX}$ (Fig. 6-7). However, although the *isotopic* neon and argon ratios of the atmospheric end-members are well-constrained, the *elemental* $^{22}Ne/^{36}Ar$ ratio of the atmospheric end-member is unconstrained. This is because the means by which atmospheric noble gases were introduced to the magma is not known. One possible mechanism is that atmospheric noble gases in seawater contaminated the mantle-derived gases (Patterson et al., 1990). Alternatively, as Icelandic rocks may have interacted with hydrothermal meteoric water that is present in pores and fractures within the Icelandic crust (Hemond et al., 1993), atmospheric noble gases may have been introduced into the magma via interaction with hydrothermal meteoric water. Atmospheric gases may also have been introduced to the lava during eruption. The $^{22}Ne/^{36}Ar$ ratio of the atmospheric end-member would be different for each of these three cases. Although interesting, the process by which mantle noble gases mix with the gases from the atmosphere is considered to be of secondary importance here, as the main aim of the modelling is to show that Icelandic basalts in this study may contain mixtures of gases from the MORB and Icelandic plume end-members.

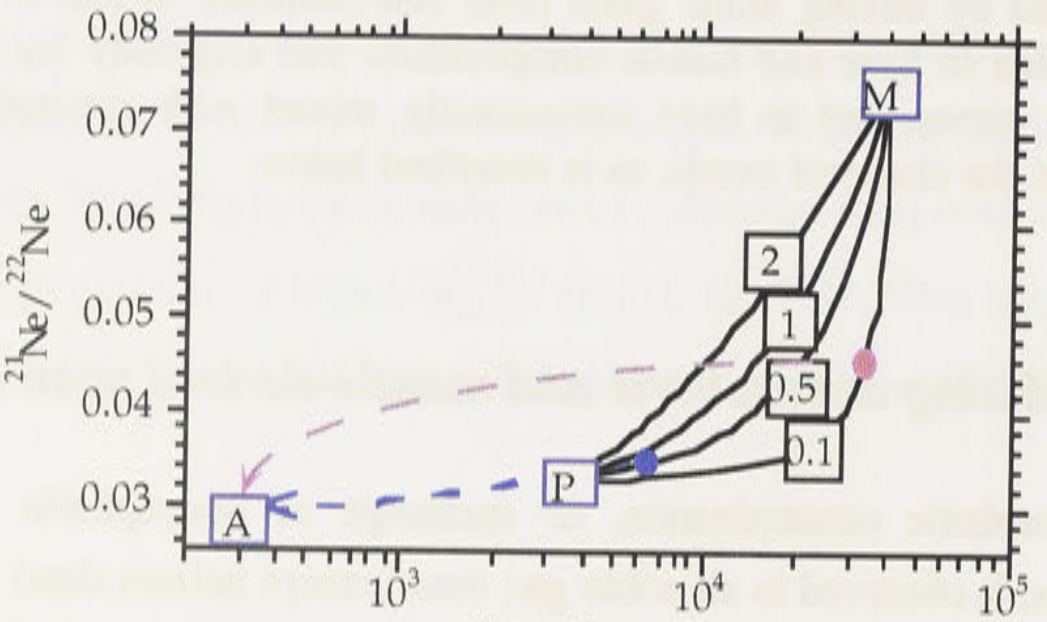

Figure 6-9. $^{21}Ne/^{22}Ne$ versus $^{40}Ar/^{36}Ar$ plot with (1) calculated mixing curves between P and M end-members, as shown in Fig. 6-8 (solid curves), and (2) schematic mixing curves between mantle mixtures and atmospheric end-member compositions (dashed curves). Mixing between the plume and MORB end-members produces an intermediate noble gas composition lying on one of the solid curves that are defined by different values of $R_{Ne,Ar}^{P,M}$. This gas with an intermediate composition then mixes with gases that have atmospheric isotopic ratios to produce the observed trends in the data in Figure 6-8. Mantle noble gas mixtures with $R_{Ne,Ar}^{P,M}$ near 0.1 may have a wide range in $^{40}Ar/^{36}Ar$ ratios at near-solar $^{21}Ne/^{22}Ne$ ratios, and subsequent addition of atmospheric noble gases with different $R_{Ne,Ar}^{Mantle,AIR}$ may cause the data to lie along trends such as that defined by the data from Trieloff et al. (2000) that intersect the atmospheric composition in Figure 6-8.

Summary and discussion

Mixing between plume and MORB-derived gases may provide a general explanation for the range in neon and argon isotopic ratios in the results from this study, as well as the results from previous studies (Harrison et al., 1999; Trieloff et al., 2000). The model suggests that samples with solar-like neon isotopic ratios may have a large range of $^{40}Ar/^{36}Ar$ ratios, depending on the values of $R^{P,M}_{Ne,Ar}$. Previous investigators have suggested that the Icelandic basaltic samples with relatively high measured $^{40}Ar/^{36}Ar$ ratios near 2000 do not contain a MORB component of argon (Burnard et al., 1994) (see Chapter 5). Although the $^{40}Ar/^{36}Ar$ ratios near 2000 are lower than the plume $^{40}Ar/^{36}Ar$ ratio of 3500 calculated from equation (6-14), it is quite possible that the measured ratio represents a mixture of plume-derived, MORB-derived and atmospheric argon (Figure 6-9). The postulated mixing between plume and MORB noble gas end-members appears to explain the decoupled helium and neon isotopic ratios. The observed $^{40}Ar/^{36}Ar$ ratios may also reasonably be explained as the product of mixing between these end-members, followed by addition of atmospheric argon, as is explained further below.

6.4.4 Mixing plume- and MORB-derived helium and argon

The models shown above describe mixing between the plume and MORB end-members for helium and neon, as well as neon and argon. It follows that the model should also apply to mixing between helium and argon. Figure 6-10 shows the helium and argon data from this study, as well as data reported by Burnard et al. (1994), Harrison et al. (1999) and Trieloff et al. (2000). The data reported by Harrison et al. (1999) span a large range of $^{40}Ar/^{36}Ar$ ratios from near-atmospheric values to 7000 at near-constant $^{3}He/^{4}He$ ratios from 15.6 to 18.4 Ra. Data reported by Trieloff et al. (2000) have a maximum $^{40}Ar/^{36}Ar$ ratio of 4350 and near-constant $^{3}He/^{4}He$ ratios of 17 to 18 Ra. Data reported by Burnard et al. (1994) have a slightly lower range of $^{3}He/^{4}He$ ratios from 12.8 to 16.8 Ra and maximum $^{40}Ar/^{36}Ar$ ratios of near 2000. The data from this study have the largest range of $^{3}He/^{4}He$ ratios (12 - 30 Ra), but the range in $^{40}Ar/^{36}Ar$ ratios is relatively small, with a maximum ratio near 1000.

Using the same compositions for the plume and MORB end-members as in previous calculations, mixing curves are shown for $R^{P,M}_{He,Ne}$= 5 and $R^{P,M}_{Ne,Ar}$ = 0.1, 0.2, 1, 2 (Fig. 6-10). These mixing curves suggest that the range in $^{40}Ar/^{36}Ar$ ratios observed Icelandic basalts may be produced by three end-member mixing, that is, between plume-derived, MORB-derived and atmospheric argon. The mantle helium and argon isotopic compositions are interpreted to have initially lain on mixing curves between the plume and MORB end-members in Figure 6-10. Subsequent addition of atmospheric argon is

then postulated to cause the $^{40}Ar/^{36}Ar$ ratio to decrease towards the atmospheric ratio. In contrast, the $^{3}He/^{4}He$ ratios remain constant owing to the relatively low abundance of helium in the atmosphere (5 ppm, Ozima and Podosek, (1983)). The measured $^{40}Ar/^{36}Ar$ ratio that is associated with a given $^{3}He/^{4}He$ ratio in Icelandic basalts is here interpreted to depend principally on two factors. The first is the initial mantle ratio, which may depend on the $R^{P,M}_{He,Ne}$ and $R^{P,M}_{Ne,Ar}$ values of the mixtures of plume and MORB noble gas end-members. The second is the amount of atmospheric contamination of the sample. Contrary to previous interpretations (Burnard et al., 1994), the presence of a plume-derived component of helium as indicated by the $^{3}He/^{4}He$ ratios in Icelandic samples does not necessarily require that the mantle argon is entirely plume-derived. Both the measured helium and the measured argon ratios may contain MORB-derived components. A component of MORB-derived argon may contribute to the relatively high $^{40}Ar/^{36}Ar$ ratios in Icelandic basalts.

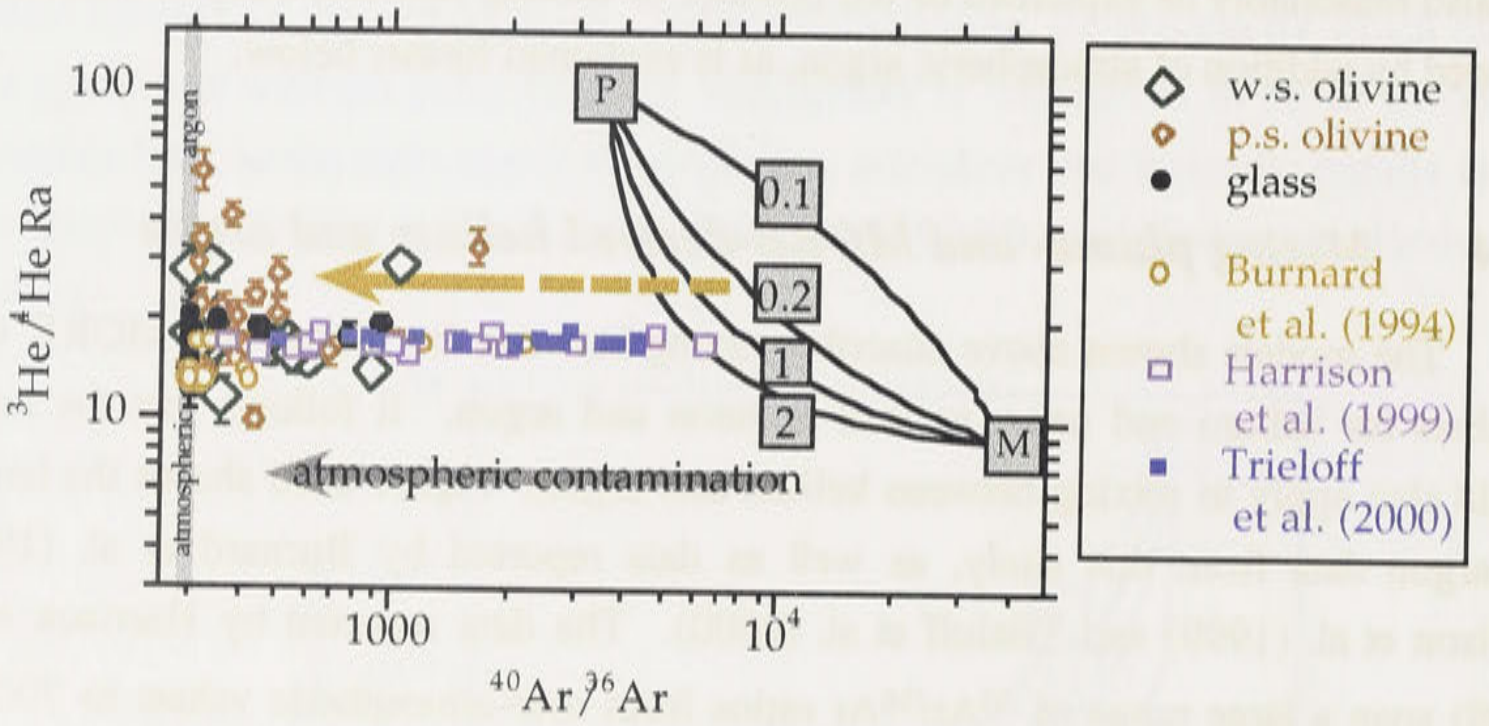

Figure 6-10. Plot of $^{3}He/^{4}He$ versus $^{40}Ar/^{36}Ar$ showing both calculated mixing curves and the data from this study, and those of Burnard et al. (1994), Harrison et al. (1999) and Trieloff et al. (2000). The data reported by Harrison et al. (1999) span a large range of $^{40}Ar/^{36}Ar$ ratios from near-atmospheric values to 7000 at near-constant $^{3}He/^{4}He$ ratios from 15.6 to 18.4 Ra. Data reported by Trieloff et al. (2000) have $^{40}Ar/^{36}Ar$ ratios of up to 4350 at $^{3}He/^{4}He$ ratios from 17 to 18 Ra. Data reported by Burnard et al. (1994) have maximum $^{40}Ar/^{36}Ar$ ratios of near 2000 and $^{3}He/^{4}He$ ratios of 12.8 to 16.8 Ra. The data from this study have the largest range of $^{3}He/^{4}He$ ratios (10 – 30 Ra), and the smallest range in $^{40}Ar/^{36}Ar$ ratios, with a maximum ratio near 1000. The calculated mixing curves are shown for $R^{P,M}_{He,Ne}$= 5 (see Fig. 6-4) for a range of $R^{P,M}_{Ne,Ar}$ values (solid lines) (0.1, 0.2, 1, 2). Note that slightly different curves would be produced for $R^{P,M}_{He,Ne}$= 1 to 2 values that fit the helium and neon isotopic data from Harrison et al. (1999). The relatively large range in $^{40}Ar/^{36}Ar$ ratios over much smaller ranges in $^{3}He/^{4}He$ ratios from this and previous studies is interpreted to arise from addition of atmospheric argon to mantle noble gases that initially had compositions that lay along one of the mixing curves.

6.4.5 *Plume- versus MORB-derived xenon*

The preceding models and discussion suggest that mixing between plume and MORB-derived noble gases may explain the range in helium, neon and argon isotopic ratios in Reykjanes Peninsula basalts from this study, as well as those of Harrison et al. (1999) and Trieloff et al. (2000). The following discussion seeks to evaluate whether xenon isotopic ratios may also be explained by the same process.

Relatively high $^{129}Xe/^{130}Xe$ and $^{136}Xe/^{130}Xe$ ratios (compared with the atmospheric ratios) observed in mantle-derived samples from MORBs and OIBs (Chapter 2) may be attributed to decay of ^{129}I and ^{238}U (and possibly ^{244}Pu), respectively. One general possible interpretation of the relatively high $^{129}Xe/^{130}Xe$ ratios in mantle-derived samples is that the mantle source has been highly degassed of primordial ^{130}Xe (and the other isotopes of xenon) prior to the decay of all ^{129}I to $^{129}Xe^*$ (see Chapter 2). This interpretation is consistent with observed relatively high $^{129}Xe/^{130}Xe$ ratios in the MORB popping rock, combined with other supporting evidence for loss of primordial gases from the MORB source (Chapter 2). Recently, relatively high $^{129}Xe/^{130}Xe$ and $^{136}Xe/^{130}Xe$ ratios have also been found in Icelandic basalts (Harrison et al., 1999; Trieloff et al., 2000) (Figure 6-11). This may suggest that the $^{129}I/^{130}Xe$, $^{244}Pu/^{130}Xe$ and $^{238}U/^{130}Xe$ ratios in the mantle source of the Icelandic plume were relatively high. Alternatively, the observed ratios in Icelandic basalts may have been produced by contamination of plume-derived xenon by MORB-derived xenon, when in fact the $^{129}I/^{130}Xe$, $^{244}Pu/^{130}Xe$ and $^{238}U/^{130}Xe$ ratios in the Icleandic plume source were relatively low (see Chapter 2, (Trieloff et al., 2000 and references therein).

The Icelandic sample from this study (*ice-9g*) that was used to define the mantle end-member near-solar neon isotopic ratios in the Icelandic plume source (section 6.3.1) is also the only sample from this study that has $^{129}Xe/^{130}Xe$ and $^{136}Xe/^{130}Xe$ ratios higher than the atmospheric ratios (Figure 6-11 and Chapter 5). Other samples from the same locality as *ice-9g* have less solar-like neon end-member isotopic ratios, and also have much higher $^{129}Xe/^{130}Xe$ and $^{136}Xe/^{130}Xe$ ratios (Figure 6-11) (Harrison et al., 1999; Trieloff et al., 2000). As described above, these relatively high $^{129}Xe/^{130}Xe$ and $^{136}Xe/^{130}Xe$ ratios may imply early degassing of primordial ^{130}Xe (as well as the other isotopes of xenon) from the mantle material currently residing in the Icelandic plume source, prior to production of all the $^{129}Xe^*$ from decay of ^{129}I. However, degassing of primordial ^{130}Xe from the mantle component that preserves near-solar neon isotopic ratios appears difficult to reconcile with the postulated primitive, undegassed mantle component in the Icelandic plume source (Section 6.3.1.2). The following discussion evaluates the possible origin of the $^{129}Xe/^{130}Xe$ and $^{136}Xe/^{130}Xe$ ratios in sample *ice-9g*

to determine whether they can be reconciled with the near-solar neon isotopic ratios in the same sample.

Mantle xenon isotopic ratios

All mantle-derived samples that have non-atmospheric $^{129}Xe/^{130}Xe$ and $^{136}Xe/^{130}Xe$ ratios lie along the same trend as the MORB data (Farley and Neroda, 1998) (Fig. 5-16 and 6-11). The relatively high $^{129}Xe/^{130}Xe$ and $^{136}Xe/^{130}Xe$ ratios from OIBs, MORBs, diamonds, and CO_2 well gases could mean that the entire mantle has elevated ratios. It is not possible to determine the whether the relatively high $^{129}Xe/^{130}Xe$ and $^{136}Xe/^{130}Xe$ ratios in Icelandic basalts are the product of mixing MORB and plume-derived xenon using only xenon isotopic ratios. The possible presence of plume- and MORB-derived components of xenon in Icelandic samples may be further evaluated by comparison of xenon isotopic ratios with other noble gas isotopic ratios.

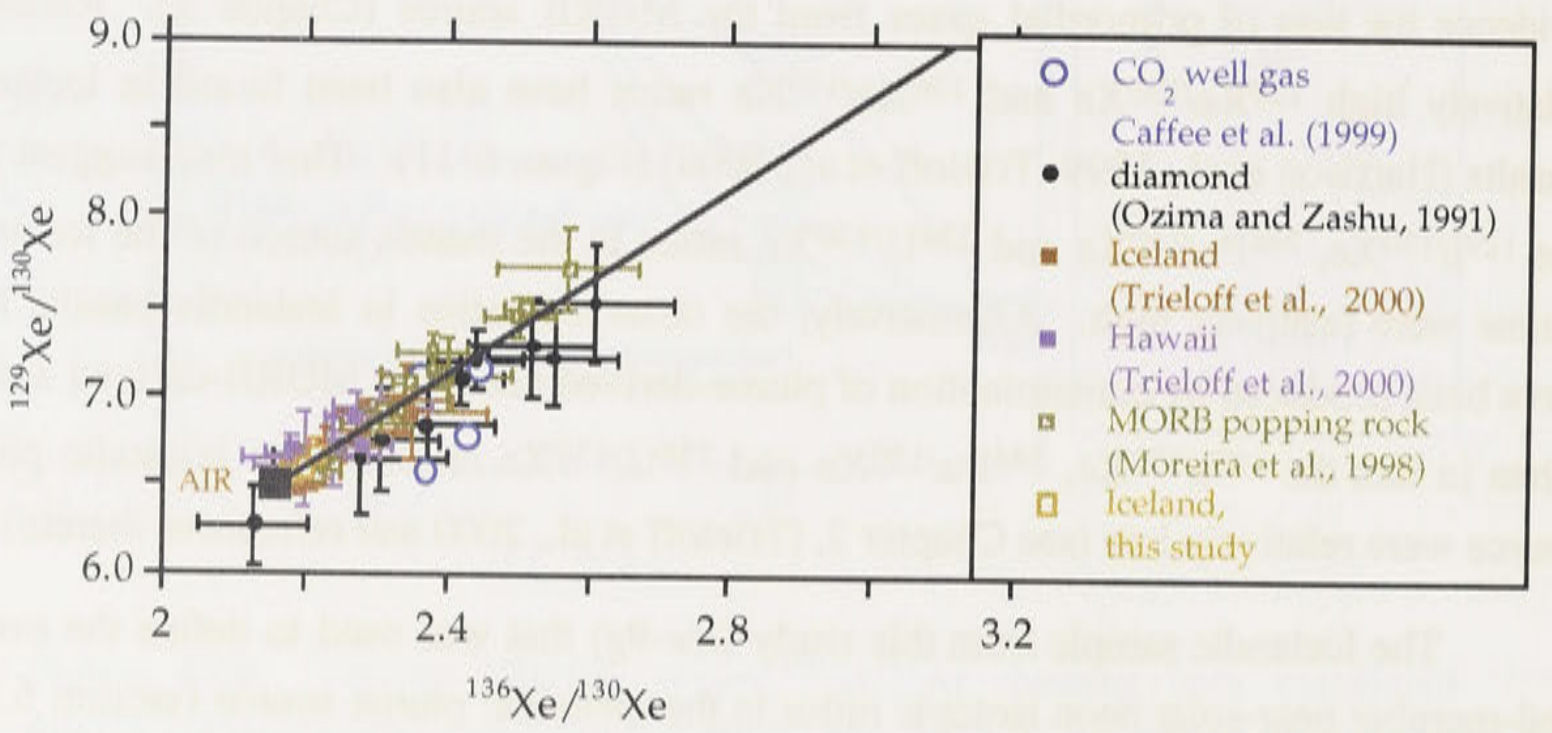

Figure 6-11. $^{129}Xe/^{130}Xe$ versus $^{136}Xe/^{130}Xe$, showing the data from a variety of sources (see legend), including the Icelandic data from this study (*ice-9g1* and *ice-9g2*). All the xenon data lie on the same linear trend that intersects the atmospheric composition. Data sources: (Caffee et al., 1999; Moreira et al., 1998; Ozima and Zashu, 1991; Trieloff et al., 2000).

Origin of elevated $^{129}Xe/^{130}Xe$ and $^{136}Xe/^{130}Xe$ ratios in Icelandic basalts

A plume-derived component of xenon

Although the MORB and Icelandic data lie on the same trend that intersects the atmospheric $^{129}Xe/^{130}Xe$ and $^{136}Xe/^{130}Xe$ ratios (Fig. 6-11), it is fairly obvious from

the preceding discussion that the Icelandic noble gases contain a plume-derived component and cannot be explained solely by mixing between MORB-derived and atmospheric gases. First, the $^{3}He/^{4}He$ ratios of the Icelandic data indicate the presence of a plume component because they do not all lie close to the MORB ratio of 8.5 Ra in Figures 6-13A ($^{3}He/^{4}He$ versus $^{129}Xe/^{130}Xe$) and B ($^{3}He/^{4}He$ versus $^{136}Xe/^{130}Xe$), but instead range from 16 to 20 Ra in these samples. Second, the neon isotopic compositions of Icelandic data from this study, and those of Harrison et al. (1999) and Trieloff et al. (2000) (Figs. 5-4, 5-9), clearly define unique neon isotopic end-member compositions that are distinct from the MORB end-member composition. Thus, because the Icelandic neon data are unlikely to have been produced solely by addition of atmospheric noble gases to a MORB-like noble gas component, it is also unlikely that the xenon isotopic ratios are purely the product of mixing between atmospheric and MORB-derived xenon.

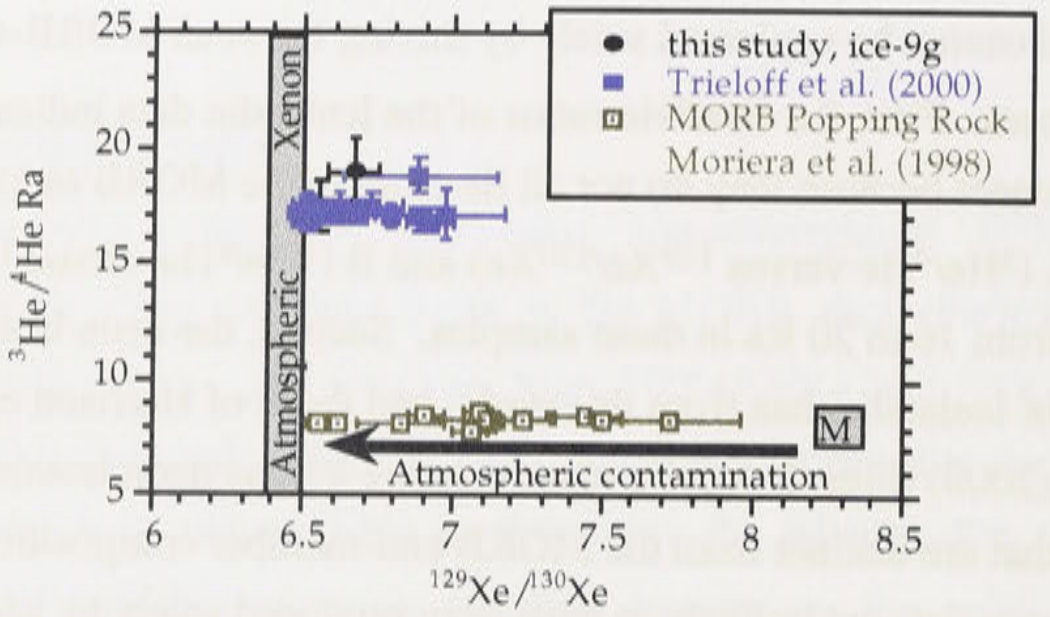

A

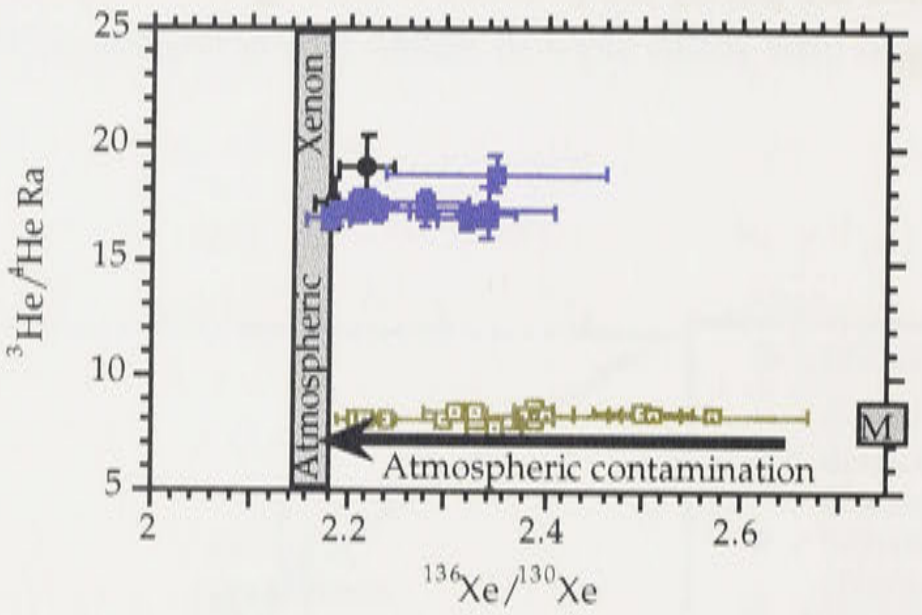

B

Figure 6-12A, plot of ^{3}He/^{4}He Ra versus ^{129}Xe/^{130}Xe, and **Figure 6-12B**, ^{3}He/^{4}He Ra versus ^{136}Xe/^{130}Xe, showing Icelandic data from this study (*ice-9g*), that of Trieloff et al. (2000) and MORB data from the MORB popping rock reported by Moriera et al. (1998). These diagrams are similar to the ^{3}He/^{4}He versus ^{40}Ar/^{36}Ar plot (Figure 6-10). The Icelandic data with relatively high xenon isotopic ratios have higher ^{3}He/^{4}He ratios (16-20 Ra) than MORBs (8.5 Ra) (shown as M in this plot). This means that the Icelandic noble gas data cannot be explained solely by addition of atmospheric noble gases to a MORB-like end-member. A plume-derived component of xenon may therefore be present.

Neon and xenon ratios

To evaluate the possible origin of the relatively high ^{129}Xe/^{130}Xe and ^{136}Xe/^{130}Xe ratios in mantle-derived samples from Iceland, it is useful to compare these ratios to the maximum ratios in MORBs, because the MORB source is likely to have been highly degassed of primordial noble gas isotopes. The upper mantle MORB-source end-member xenon isotopic ratios may be estimated by comparing the ^{129}Xe/^{130}Xe and ^{136}Xe/^{130}Xe ratios with the ^{20}Ne/^{22}Ne ratios from the MORB popping rock. Because the MORB popping rock has unfractionated elemental ratios compared

with the mantle primordial and production ratios (e.g., Moreira et al., 1998), a linear correlation exists between neon and xenon (Figs. 6-13A and 6-13B). The maximum $^{129}Xe/^{130}Xe$ ratio in the upper mantle is ~8.2, and the maximum $^{136}Xe/^{130}Xe$ ratio is ~2.75 if it is assumed that end-member $^{20}Ne/^{22}Ne$ ratio in the mantle is equal to the solar ratio of 13.8 (Moreira et al., 1998).

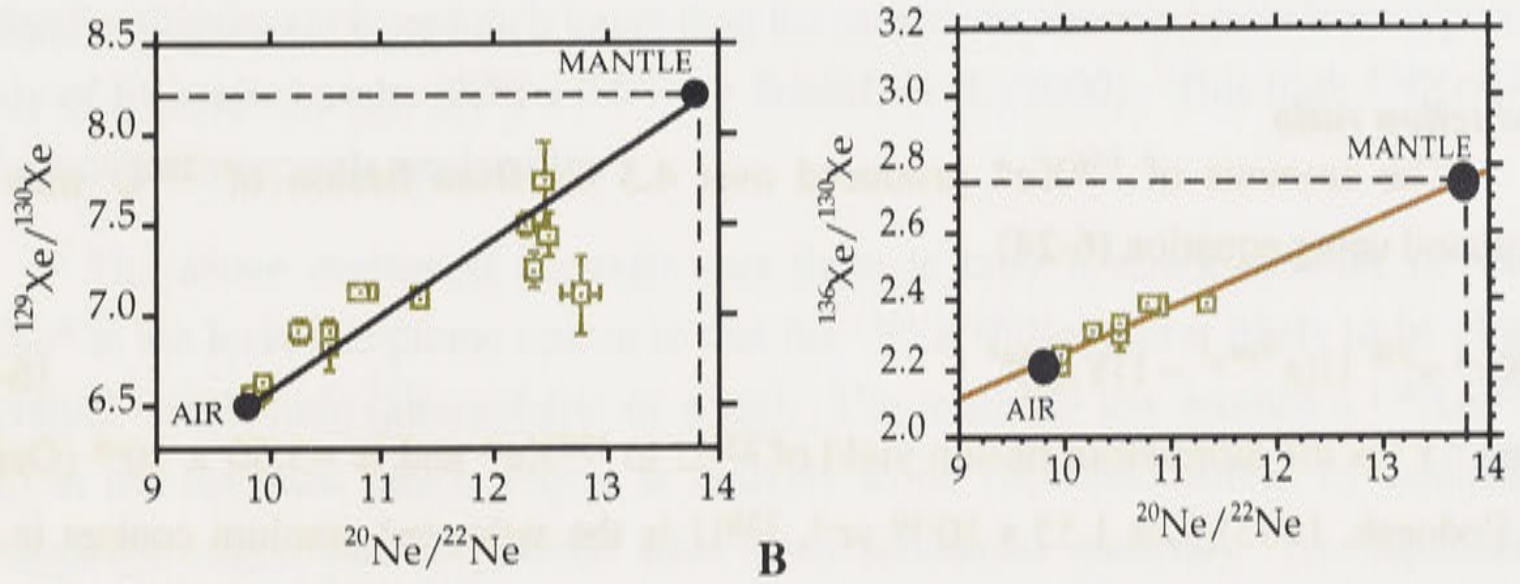

Figures 6-13A and **6-13B**. Xenon and neon isotopic data from the MORB popping rock (Moreira et al., 1998). These plots suggest that the mantle has a maximum $^{129}Xe/^{130}Xe$ ratio of ~8.2 and $^{136}Xe/^{130}Xe$ ratio of ~2.75 at a $^{20}Ne/^{22}Ne$ ratio of 13.8 (solar ratio).

Estimated $^{129}Xe^*/^{130}Xe$ and $^{136}Xe^*/^{130}Xe$ in the Icelandic plume source

To further evaluate the origin of relatively high $^{129}Xe/^{130}Xe$ and $^{136}Xe/^{130}Xe$ ratios in some Icelandic basalts (Figure 6-11), it is necessary to estimate the value of these ratios in the Icelandic plume source. In a previous section, the mantle $^{22}Ne/^{36}Ar$ ratio and the $^{40}Ar^*/^{21}Ne^*$ production ratio were used to estimate the $^{40}Ar/^{36}Ar$ ratio in the Icelandic plume source using equation (6-14). A similar equation (6-22) cannot be used to calculate the initial the $^{129}Xe/^{130}Xe$ ratio of the Icelandic plume end-member. Unlike the K/U ratio of the silicate Earth (12700) which is reasonably well known and is used to estimate the mantle $^{40}Ar^*/^{21}Ne^*$ production ratio, there are no good estimates of the $(U + Th)/^{129}I$ ratio that can be used to estimate the mantle $^{21}Ne^*/^{129}Xe^*$ production ratio.

$$(^{129}Xe^*/^{130}Xe)_P = \left[\left(\left(\frac{^{21}Ne}{^{22}Ne} \right)_P - \left(\frac{^{21}Ne}{^{22}Ne} \right)_{solar} \right) \times \frac{^{22}Ne}{^{130}Xe_{Mantle}} \right] \Big/ \left(\frac{^{21}Ne^*}{^{129}Xe^*} \right)_{production} \quad (6\text{-}22)$$

In contrast, it may be possible to estimate the production of $^{136}Xe^*$ from fission of ^{238}U to obtain the $^{136}Xe^*/^{130}Xe$ ratio in the Icelandic plume source (equation 6-23). There has been some debate over whether decay of ^{238}U or ^{244}Pu produces the majority of $^{136}Xe^*$ in the mantle (see Chapter 2). The following calculations to estimate the Icelandic plume source $^{136}Xe/^{130}Xe$ ratio will make the simplifying assumption that all

$^{136}Xe^*$ is derived entirely from decay of ^{238}U. The calculations assume that no fission products were lost following their production in the mantle, owing to being stored in a relatively primitive, undegassed mantle component.

$$(^{136}Xe^*/^{130}Xe)_P = \left[\left(\left(\frac{^{21}Ne}{^{22}Ne} \right)_P - \left(\frac{^{21}Ne}{^{22}Ne} \right)_{solar} \right) \times \frac{^{22}Ne}{^{130}Xe_{Mantle}} \right] \Big/ \left(\frac{^{21}Ne^*}{^{136}Xe^*} \right)_{production} \quad (6\text{-}23)$$

Production ratio

The amounts of $^{136}Xe^*$ produced over 4.5 Ga from fission of ^{238}U may be calculated using equation (6-24)

$$^{136}Xe^* = {}^{238}U(e^{\lambda_{238_U} t} - 1)Y^{^{136}Xe^*}_{^{238}U} \quad (6\text{-}24)$$

where "Y" is the atom/atom fission yield of ^{238}U to $^{136}Xe^*$ and is ~3.50 x 10^{-8} (Ozima and Podosek, 1983), λ is 1.55 x 10^{-10} yr^{-1}, ^{238}U is the estimated uranium content in the primitive mantle of 1 x 10^{41} atoms based on a uranium content of 20 ppb. The calculated concentration of $^{136}Xe^*$ in the mantle from equation (6-24) is 6.58 x 10^{-14} cm^3/g. The concentration of $^{21}Ne^*$ produced over 4.5 Ga in the mantle is 1.45 x 10^{-12} cm^3STP/g (Yatsevich and Honda, 1997). From these values, the $^{21}Ne^*/^{136}Xe^*_{^{238}U}$ production ratio is estimated to be 22.

End-member elemental and isotopic ratios

The $^{22}Ne/^{130}Xe$ ratio in the entire mantle is assumed to be equal to the ratio in the MORB popping rock (162) because, as discussed by Moreira et al. (1998), the elemental ratios of different noble gases (including $^{22}Ne/^{130}Xe$) in the upper and lower mantles should be equal as long as no elemental fractionation occurred during outgassing of the upper mantle. The end-member $^{21}Ne/^{22}Ne$ ratio in the Icelandic plume source is estimated to be 0.035 (the estimated maximum and miniumum values of the $^{21}Ne/^{22}Ne$ ratio in the plume source are 0.033 to 0.038 including the uncertainties), which is the same value used previously to calculate the $^{40}Ar/^{36}Ar$ ratio in the Icelandic plume source (see equation 6-14).

^{238}U-derived $^{136}Xe^*$

The results of the calculation give a $^{136}Xe^*/^{130}Xe$ ratio of 0.016 in the Icelandic plume source (equation 6-23). This value (0.016) plus the initial $^{136}Xe/^{130}Xe$ ratio in the mantle would give the Icelandic plume source ratio (i.e., $(^{136}Xe/^{130}Xe)_{plume\ source} = [(^{136}Xe/^{130}Xe)_{initial} + (^{136}Xe^*/^{130}Xe)_{4.5Ga}]$). Inspection of Figure 6-11 shows that the $^{136}Xe/^{130}Xe$ ratios in mantle-derived samples from MORBs range from 2.18 (the atmospheric ratio) to 2.6. Although the $^{136}Xe/^{130}Xe$ ratio in the Icelandic plume source

is not known, addition of the calculated $^{136}Xe^*/^{130}Xe$ ratio (0.016) to either the solar $^{136}Xe/^{130}Xe$ ratio (1.66) or the atmospheric $^{136}Xe/^{130}Xe$ ratio (2.176) give $^{136}Xe/^{130}Xe$ ratios that are slightly lower than (1.68) or similar to (2.19) the maximum observed $^{136}Xe/^{130}Xe$ ratio from this study (2.22 ± 0.03 in *ice-9g*). Thus, addition of fission $^{136}Xe^*$ produced by decay of ^{238}U may not greatly increase the $^{136}Xe/^{130}Xe$ ratio in Icelandic plume-source from the initial ratio. These calculated $^{136}Xe/^{130}Xe$ ratios for the Icelandic plume source are much lower than the maximum observed ratio from a previous study of Icelandic basalts (2.32 ± 0.03) by Trieloff et al. (2000). This high $^{136}Xe/^{130}Xe$ ratio requires a separate explanation.

The above evaluation suggests that there is only a minor amount of excess $^{136}Xe^*$ in the Icelandic plume source so that the $^{136}Xe/^{130}Xe$ ratio is likely to be close to the initial mantle ratio (atmospheric or solar). The relatively low estimated $^{136}Xe/^{130}Xe$ ratio in the Icelandic plume source is unlikely to be explained solely by addition of atmospheric argon into the plume source via subducted material. As explained in Chapters 3, owing to the higher viscosity in the lower mantle, stirring of the mantle by convection should be more rapid in the upper mantle than in the lower mantle. If atmospheric xenon is carried into the mantle by subducted material, the upper mantle is likely to be more contaminated than the lower mantle. The relatively low estimated $^{136}Xe/^{130}Xe$ ratio may instead be related to a relatively low $U/^{130}Xe$ ratio in the primitive undegassed component in the Icelandic plume source compared with that in the MORB source (see Chapter 2). The relatively high $^{136}Xe/^{130}Xe$ ratios reported in a previous study of Icelandic basalts (Trieloff et al., 2000) may be explained if plume-derived xenon, that has relatively low $^{136}Xe/^{130}Xe$ ratios, is overwhelmed by mixing with MORB-derived xenon, that has much higher $^{136}Xe/^{130}Xe$ ratios.

Summary

The noble gas data from this study were evaluated to determine whether the near-solar neon isotopic ratios that are associated with $^{136}Xe/^{130}Xe$ ratios slightly higher than the atmospheric ratio (by up to 2%) could be explained by either: (1) mixing plume-derived xenon with MORB-derived xenon; or (2) production of fission of $^{136}Xe^*$ in the Icelandic plume source. The above evaluation shows that the $^{136}Xe^*/^{130}Xe$ ratio in the Icelandic plume source (0.016) is likely to be relatively small. Although the initial $^{136}Xe/^{130}Xe$ ratio in the plume source is not known, addition of this $^{136}Xe^*/^{130}Xe$ to either the atmospheric or the solar $^{136}Xe/^{130}Xe$ ratio would not increase the total $^{136}Xe/^{130}Xe$ ratio in the Icelandic plume source to values above the maximum measured $^{136}Xe/^{130}Xe$ ratio in *ice-9g* (2.22 ± 0.03). This measured $^{136}Xe/^{130}Xe$ is unlikely to preserve the mantle ratio owing to addition of atmospheric argon close to the time of eruption. Thus, although an estimated $^{136}Xe/^{130}Xe$ ratio for the Icelandic plume source (~2.19) is close to the measured ratio in *ice-9g*, the original $^{136}Xe/^{130}Xe$ ratio in *ice-9g* is

likely to have been higher. The $^{136}Xe/^{130}Xe$ ratio in *ice-9g*, as well as the much higher $^{136}Xe/^{130}Xe$ ratios reported by Trieloff et al. (2000), may be explained if plume-derived xenon, with a relatively low $^{136}Xe/^{130}Xe$ ratio, was overwhelmed by mixing with MORB-derived xenon, with relatively a high $^{136}Xe/^{130}Xe$ ratio. Addition of atmospheric xenon close to the time of eruption is then likely to have decreased the mantle-ratio to the observed values. Binary mixing between plume and MORB-derived noble gases may provide a reasonable explanation for the observed helium, neon, argon and xenon isotopic ratios in this study, and in previous studies of Icelandic basalts.

6.5 Overall conclusions for Chapter 6

The solar neon isotopic ratios observed in some Icelandic samples from this study suggest that primitive, undegassed material may be present in the lower mantle source of the Icelandic plume. The existence of primitive neon isotopic ratios preserved in these Icelandic basalts and in samples from the adjacent Mid-Atlantic Ridge (Poreda and Radicati di Brozolo, 1984), but not in mantle-derived samples from other localities, suggests that the mantle has highly heterogeneous ratios of primitive noble gases to parent radioactive isotopes (e.g., U, Th, ^{40}K). This study proposes that high $Ne_{solar}/[U+Th]$ ratios are preserved in relatively small bodies of primitive undegassed mantle in the Icelandic plume source. Thus, solar-like $^{3}He/^{4}He$ ratios, and relatively low $^{40}Ar/^{36}Ar$ ratios compared with those in MORBs, may also be expected in these mantle bodies. However, the measured solar neon isotopic ratios are associated with $^{3}He/^{4}He$ ratios that are much lower than the solar ratio, implying that the helium and neon isotopic ratios are decoupled.

Some noble gas isotopic heterogeneity is expected in the Icelandic plume source if the bodies of primitive, undegassed material exist on a relatively small scale within a matrix of less primitive mantle. Additional noble gas heterogeneity may be produced by mixing between noble gases from the plume and MORB end-members in the shallow upper mantle beneath the Icelandic crust. The gradients in $^{3}He/^{4}He$ ratios within the neo-volcanic zones in Iceland and in MORBs along the Reykjanes Ridge (Chapter 5) suggest that entrainment of MORB melts may be responsible for the local variation in $^{3}He/^{4}He$ ratios. Such entrainment of MORB material is predicted by geophysical models to describe plume behaviour beneath spreading ridges.

The decoupled helium and neon isotopic ratios in Icelandic samples from this study may be explained by mixing between plume-derived and MORB-derived noble gases if the elemental He/Ne ratios in the two end-members are fractionated relative to each other. Such mixing between plume and MORB noble gas end-members may also

be expected to produce systematic compositional variations in $^{40}Ar/^{36}Ar$, $^{129}Xe/^{130}Xe$ and $^{136}Xe/^{130}Xe$ ratios in Icelandic basalts. Subsequent contamination by atmospheric components of the noble gases (excluding helium) may explain the observed variation in $^{21}Ne/^{22}Ne$, $^{40}Ar/^{36}Ar$, $^{129}Xe/^{130}Xe$ and $^{136}Xe/^{130}Xe$ isotopic compositions reported in Icelandic basalts in this study, as well as those reported by Harrison et al. (1999) and Trieloff et al. (2000). Binary mixing of noble gases between the Icelandic plume and MORB end-members provides a reasonable explanation for the range in noble gas isotopic ratios in Icelandic basalts, though additional complexity may exist because the Icelandic plume end-member is likely to be heterogeneous.

6.6 References

Allègre C. J., Staudacher T., and Sarda P. (1986/87) Rare gas systematics: formation of the atmosphere, evolution and structure of the Earth's mantle. *Earth and Planetary Science Letters* **81**, 127-150.

Allègre C. J. and Turcotte D. L. (1986) Implications of a two-component marble cake mantle. *Nature* **323**, 123-127.

Anders E. and Grevesse N. (1989) Abundances of the elements: meteoritic and solar. *Geochimica et Cosmochimica Acta* **53**, 197-214.

Becker R. H. and Pepin R. O. (1984) Solar composition noble gases in the Washington County iron meteorite. *Earth and Planetary Science Letters* **70**, 1-10.

Becker T. W., Kellogg J. B., and O'Connell R. J. (1999) Thermal constraints on the survival of primitive blobs in the lower mantle. *Earth and Planetary Science Letters* **171**, 351-365.

Benkert J.-P., Baur H., Signer P., and Wieler R. (1993) He, Ne, and Ar from the solar wind and solar energetic particles in lunar ilmenites and pyroxenes. *Journal of Geophysical Research* **98**, 13147-13162.

Bijwaard H. (1999) Tomographic evidence for a narrow whole mantle plume below Iceland. *Earth and Planetary Science Letters* **166**, 121-126.

Breddam K., Kurz M. D., and Storey M. (2000) Mapping out the conduit of the Iceland plume with helium isotopes. *Earth and Planetary Science Letters* **176**, 45-55.

Burnard P., Graham D., and Turner G. (1997) Vesicle-specific noble gas analyses of "popping rock": implications for primordial noble gases in Earth. *Science* **276**, 568-571.

Burnard P. G., Stuart F. M., Turner G., and Oskarsson N. (1994) Air contamination of basaltic magma: implications for high $^{3}He/^{4}He$ mantle Ar isotopic composition. *Journal of Geophysical Research* **99**, 17709-17715.

Caffee M. W., Hudson G. B., Velsko C., Huss G. R., Alexander E. C., Jr., and Chivas A. R. (1999) Primordial noble gases from Earth's mantle: identification of a primitive volatile component. *Science* **285**, 2115-2118.

Campbell I. H. (1998) The mantle's chemical structure: insights from the melting products of mantle plumes. In *The Earth's Mantle: composition, structure, and evolution* (ed. I. Jackson), pp. 566. Cambridge University Press. Melbourne.

Davies G. F. (1984) Geophysical and isotopic constraints on mantle convection: an interim synthesis. *Journal of Geophysical Research* **89**, 6017-6040.

Davies G. F. (1999) Geophysically constrained mantle mass flows and the ^{40}Ar budget: a degassed lower mantle? *Earth and Planetary Science Letters* **166**, 149-162.

Eberhardt P., Eugster O., and Marti K. (1965) A redetermination of the isotopic composition of atmospheric neon. *Zeitschrift fur Naturforschung* **20a**, 623-624.

Farley K. A. and Neroda E. (1998) Noble gases in the Earth's mantle. *Annual Review of Earth and Planetary Sciences* **26**, 189-218.

Feigner M. A. and Richards M. A. (1995) Plume-ridge and plume-plate interactions. *Earth and Planetary Science Letters* **129**, 171-182.

Geiss J., Buehler F., Cerutti H., Eberhardt P., and Filleaux C. H. (1972) Solar wind composition experiments. In *Apollo 16 Preliminary Scientific Report*, Vol. SP-315, pp. 14.1-14.10. NASA.

Griffiths R. W. and Campbell I. H. (1990) Stirring and structure in mantle starting plumes. *Earth and Planetary Science Letters* **99**, 66-78.

Griffiths R. W. and Turner J. S. (1998) Understanding mantle dynamics through mathematical models and laboratory experiments. In *The Earth's Mantle: composition, structure and evolution* (ed. I. Jackson), pp. 566. Cambridge University Press. Melbourne.

Gurnis M. and Davies G. F. (1986a) The effect of depth-dependent viscosity on convective mixing in the mantle and the possible survival of primitive mantle. *Geophysical Research Letters* **13**, 541-544.

Harrison D., Burnard P., and Turner G. (1999) Noble gas behaviour and composition in the mantle: constraints from the Iceland plume. *Earth and Planetary Science Letters* **171**, 199-207.

Hart R., Hogan L., and Dymond J. (1985) The closed-system approximation for evolution of argon and helium in the mantle, crust and atmosphere. *Chemical Geology (Isotope Geosciences)* **52**, 45-73.

Helmberger D. V., Wen L., and Ding X. (1998) Seismic evidence that the source of the Iceland hotspot lies at the core-mantle boundary. *Nature* **396**, 251-255.

Hemond C., Arndt N. T., Lichtenstein U., and Hofmann A. (1993) The heterogeneous Iceland Plume: Nd-Sr-O isotopes and trace element constraints. *Journal of Geophysical Research* **98**, 15850-16833.

Hilton D. R., Gronvold K., Macpherson C. G., and Castillo P. R. (1999) Extreme $^{3}He/^{4}He$ ratios in northwest Iceland: constraining the common component in mantle plumes. *Earth and Planetary Science Letters* **173**, 53-60.

Hofmann A. W. (1997) Mantle geochemistry: the message from ocean volcanism. *Nature* **385**, 219-229.

Honda M., McDougall I., and Patterson D. B. (1993a) Solar noble gases in the Earth: the systematics of helium-neon isotopes in mantle derived samples. *Lithos* **30**, 257-265.

Honda M., McDougall I., Patterson D. B., Doulgeris A., and Clague D. A. (1993b) Noble gases in submarine pillow basalt glasses from Loihi and Kilauea, Hawaii: a solar component in the Earth. *Geochimica et Cosmochimica Acta* **57**, 859-874.

Kurz M. D., Colodner D., Trull T. W., Moore R. B., and O'Brien K. (1990) Cosmic ray exposure dating with in situ produced cosmogenic ^{3}He: results from young Hawaii lava flows. *Earth and Planetary Science Letters* **97**, 177-189.

Lal D. (1988) In situ-produced cosmogenic isotopes in terrestrial rocks. *Annual Reviews in Earth and Planetary Sciences* **16**, 355-388.

Lugmair G. W., Marti K., Kurz J. P., and Scheinin N. B. (1976) History and genesis of lunar troctolite 76535 or: how old is old? *Proceedings of the Lunar Planetary Science Conference*, 2009-2033.

Macpherson C. G., Hilton D. R., Sinton J. M., Poreda R. J., and Craig H. (1998) High $^{3}He/^{4}He$ ratios in the Manus backarc basin: implications for mantle mixing and the origin of plumes in the western Pacific Ocean. *Geology* **26**, 1007-1010.

Marti K. and Craig H. (1987) Cosmic-ray-produced neon and helium in the summit lavas of Maui. *Nature* **325**, 335-337.

Matsuda J., Sudo M., Ozima M., Ito K., Ohtaka O., and Ito E. (1993) Noble gas partitioning between metal and silicate under high pressures. *Science* **259**, 788-790.

Merz D. F. and Haase K. M. (1997) The radiogenic isotope composition of the high-latitude North Atlantic mantle. *Geology* **25**, 411-414.

Moreira M., Kunz J., and Allegre C. (1998) Rare gas systematics in popping rock: isotopic and elemental compositions in the upper mantle. *Science* **279**, 1178-1181.

O'Nions R. K. and Tolstikhin I. N. (1994) Behaviour and residence times of lithophile and rare gas tracers in the upper mantle. *Earth and Planetary Science Letters* **124**, 131-138.

Ozima M. and Podosek F. A. (1983) *Noble Gas Geochemistry*. Cambridge University Press, Cambridge. pp 367.

Ozima M. and Zashu S. (1991) Noble gas state of the ancient mantle as deduced from noble gases in coated diamonds. *Earth and Planetary Science Letters* **105**, 13-27.

Patterson D. B., Honda M., and McDougall I. (1990) Atmospheric contamination: a possible source for heavy noble gases in basalts from Loihi seamount, Hawaii. *Geophysical Research Letters* **17**, 705-708.

Phipps Morgan J. (1998) Thermal and rare gas evolution of the mantle. *Chemical Geology* **145**, 431-445.

Porcelli D. and Wasserburg G. J. (1995) A unified model for terrestrial rare gases. In *Volatiles in the Earth and Solar system* (ed. K. A. Farley), pp. 56-69. American Institute of Physics. New York.

Poreda R. and Radicati di Brozolo F. (1984) Neon isotope variations in Mid-Atlantic Ridge basalts. *Earth and Planetary Science Letters* **69**, 277-289.

Poreda R., Schilling J.-G., and Craig H. (1986) Helium and hydrogen isotopes in ocean-ridge basalts north and south of Iceland. *Earth and Planetary Science Letters* **78**, 1-17.

Reynolds J. H., Frick U., Niel J. M., and Phinney D. L. (1978) Rare-gas-rich separates from carbonaceous chondrites. *Geochimica et Cosmochimica Acta* **42**, 1775-1797.

Ringwood A. E. (1979) *Origin of the Earth and Moon*. Springer-Verlag, New York. pp 295.

Sarda P., Staudacher T., and Allègre C. J. (1988) Neon isotopes in submarine basalts. *Earth and Planetary Science Letters* **91**, 73-88.

Schilling J.-G. (1973) Iceland mantle plume: geochemical evidence along Reykjanes Ridge. *Nature* **242**, 565-571.

Schilling J.-G. (1991) Fluxes and excess temperatures of mantle plumes inferred from their interaction with migrating mid-ocean ridges. *Nature* **352**, 397-403.

Trieloff M., Kunz J., Clague D., Harrison D., and Allegre C. (2000) The nature of pristine noble gases in mantle plumes. *Science* **288**, 1036-1038.

Tronnes R. G. (1990) Basaltic melt evolution of the Hengill volcanic system, SW Iceland, and evidence for clinopyroxene assimilation in primitive tholeiitic magmas. *Journal of Geophysical Research* **95**, 15,893-15,910.

Turner G. (1989) The outgassing history of the Earth's atmosphere. *Journal of the Geological Society of London* **146**, 147-154.

Wetherill G. W. (1954) Variations in the isotopic abundances of neon and argon extracted from radioactive minerals. *Physical Science Review* **96**, 679-683.

Yatsevich I. and Honda M. (1997) Production of nucleogenic neon in the Earth from natural radioactive decay. *Journal of Geophysical Research* **102**, 10281-10288.

CHAPTER 7: NOBLE GAS ELEMENTAL ABUNDANCE RATIOS IN ICELANDIC BASALTS

7.1 Introduction

The majority of mantle noble gas studies focus on isotopic ratios in mantle-derived samples because they are not readily fractionated during partial melting or by diffusion. Thus, these samples provide information about the compositions of the mantle source reservoirs from which the magmas were derived (e.g., the MORB source). In contrast, owing to the differences in atomic radii and masses of the gases, elemental ratios of the noble gases are highly susceptible to fractionation during partial melting, fractional crystallization, bubble formation and diffusion-related processes (Honda and Patterson, 1999). This makes the elemental ratios of noble gases potentially useful for obtaining information about the effect of melt generation and differentiation on noble gas abundances in both magmatic liquids and residual solids (Carroll and Draper, 1994), and thus on the nature of the mantle source regions, as well as on processes that have occurred during the transit of magma to the surface.

One application of elemental ratios to understanding mantle processes showed that the mean primordial $^{3}He/^{22}Ne_{s}$ ratios of basaltic glass samples from OIBs (6 ± 1), and MORBs (10 ± 2) are elevated relative to the solar $^{3}He/^{22}Ne_{s}$ ratio of 3.8 by approximately factors of 2 and 3, respectively. The gross average of all $^{3}He/^{22}Ne_{s}$ ratios in all mantle-derived samples is 8 ± 3 (Honda and McDougall, 1998) (see Table 2-8). The elemental fractionation between helium and neon in OIBs and MORBs from the presumed initial solar composition was interpreted to be caused by solubility controlled degassing at an early stage in the Earth's evolution from a magma ocean (Honda and McDougall, 1998). The processes that cause elemental fractionation are unlikely to have caused isotopic fractionation, and the mantle end-member neon isotopic ratios are expected to be close to the solar composition (see Chapter 6).

In a separate study by Moreira et al. (1998), the mantle $^{3}He/^{22}Ne_{s}$ ratio of the MORB popping rock (7.3) was found to be higher than the solar ratio (3.8). In contrast, the $^{3}He/^{36}Ar$ ratio of the popping rock (0.7) is much lower than the solar $^{3}He/^{36}Ar$ ratio (12.9, calculated from the solar ratios: $^{3}He/^{22}Ne_{s}$ x $^{22}Ne_{s}/^{36}Ar$ = 3.8 x 3.4, values from

Geiss et al. (1972) and Pepin (1998)). Owing to the higher relative solubility of helium than both neon and argon in melt (Lux, 1987), the $^{3}He/^{22}Ne_{s}$ and the $^{3}He/^{36}Ar$ ratios of the residual melt should both be higher than the initial ratio in the melt following solubility controlled degassing from the magma ocean (see Chapter 2). Other processes may have been involved in producing the observed relatively low $^{3}He/^{36}Ar$ ratio in the MORB popping rock, assuming that the Earth's primitive material had a relatively unfractionated solar $^{3}He/^{36}Ar$ abundance ratio. These examples show that understanding the variety of processes that produce fractionated elemental ratios in the mantle may ultimately be used to help understand the accretion and degassing history of the Earth.

The elemental abundance ratios in Icelandic samples to be presented in this chapter may have been produced by unique processes that are related to the location of Iceland astride an active spreading ridge. As shown in Figure 7-1, mixing between plume and MORB-derived melts may occur in mantle regions below the Icelandic crust owing to entrainment of MORB-derived melts by the laterally-spreading Icelandic plume (see Chapters 3 and 6). As the plume and MORB magmas ascend to shallow levels near the base of the Icelandic crust, noble gas elemental fractionation may occur in the magma by processes related to the ascent and degassing of the magma. Mixing between plume and MORB-derived noble gases with a range of different elemental ratios (see Chapter 2, Figure 2-20) may produce a range of noble gas isotopic ratios (see Chapter 6). Dikes may sample different parts of the hybrid plume + MORB mixture and inject these magmas into crustal magma chambers (see Chapter 4). During intrusion of these dikes through the crust, additional elemental fractionation processes, such as diffusion, solubility controlled fractionation, and crystal-melt fractionation, may occur. As is suggested in the schematic cross-section of Iceland and the adjacent Mid-Atlantic Ridge in Figure 7-1, mixing between hybrid magmatic components may occur within Icelandic crustal magma chambers and produce additional heterogeneity in elemental and isotopic ratios of Icelandic basalts.

In Chapter 6, binary mixing between MORB- and plume-derived noble gases was proposed as a possible means by which to explain the decoupled helium and neon isotopic ratios in Icelandic basalts. A range of $R^{P,M}_{He,Ne}$ values was needed to explain the large range in observed helium and neon isotopic ratios. The large range in $R^{P,M}_{He,Ne}$ values requires that the $^{3}He/^{22}Ne_{s}$ ratios in the plume and/or MORB end-members also had a range of values. The $^{3}He/^{22}Ne_{s}$ ratios in the mixture of elementally fractionated plume and MORB end-members should be intermediate between these end-members and lie within the range of compositions observed in OIBs and MORBs. In most cases, the observed $^{3}He/^{22}Ne_{s}$ ratios in Icelandic basalts are unlikely to preserve the $^{3}He/^{22}Ne_{s}$ ratio of the plume + MORB mixture owing to subsequent elemental fractionation processes that may have occurred during ascent of the magma. However, in cases where Icelandic samples have elemental ratios that lie within the range observed in OIBs and

MORBs, there may not have been significant elemental fractionation following mixing. In such cases, it is possible to evaluate whether the $R^{P,M}_{He,Ne}$ values that were proposed in Chapter 6 to explain the decoupled helium and neon isotopic ratios are reasonable. For the remaining Icelandic samples, it is possible to show that following the postulated binary mixing, systematic fractionation processes produced the observed elemental ratios.

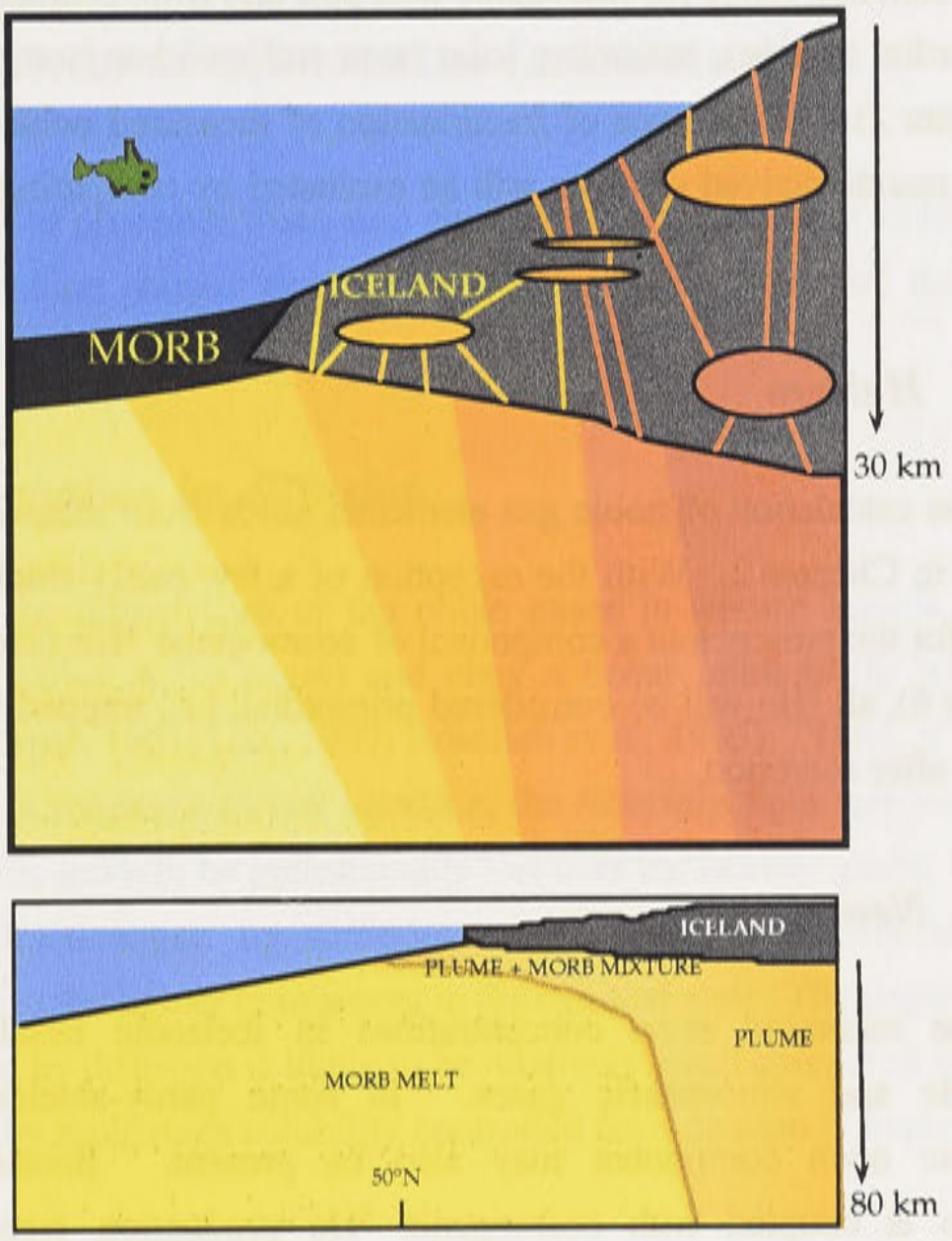

Figure 7-1. Schematic cross sections showing how the Icelandic plume melts may mix with MORB melts along the Reykjanes Peninsula (Iceland) and Reykjanes Ridge (Mid-Atlantic Ridge) (see chapter 4). Not to scale. The upper figure is an expanded version of the lower figure, and the range of colors shows the possible gradients in chemical composition that arise from entrainment of MORB melts (yellow) into the Icelandic plume (red). Such entrainment may explain the range in helium and lead isotopic compositions observed in Reykjanes Ridge (MORB) basalts described in Chapters 4 and 5. The dikes (thin lines) that feed the crustal magma chambers (ellipses) and eruptions along the Reykjanes Peninsula (Iceland) may tap different parts of this heterogeneous mixture of plume and MORB melts, giving rise to a range of isotopic and elemental ratios in the magma chambers. Additional elemental fractionation (but not isotopic fractionation) may occur as the magmas ascend via dikes to the surface.

7.2 Reference mantle ratios, and calculating elemental abundances from measured data

The initial noble gas elemental ratios in the mantle may be estimated from the mantle production ratios for radiogenic isotopes, and from estimates of the solar ratio for the primordial isotopes, assuming solar neon end-member isotopic ratios in the mantle (see Chapter 2). The degree of fractionation of measured noble gas elemental ratios in Icelandic mantle-derived samples will be evaluated by comparing them with these initial ratios.

7.2.1 Helium

The calculation of noble gas elemental ratios from measured isotopic ratios was explained in Chapter 2. With the exception of a few partly-shielded samples that show evidence for the presence of a component of cosmogenic ^{3}He (see discussion below and in Chapter 6), all ^{3}He will be considered primordial, i.e., trapped within the Earth during or shortly after accretion.

7.2.2 Neon

The measured neon concentrations in Icelandic basalts include primordial, nucleogenic and atmospheric gases. In some partly-shielded olivine samples, a cosmogenic neon component may also be present. Because cosmogenic ^{21}Ne production is coupled with cosmogenic ^{3}He production (see Chapters 2 and 6), cosmogenic components produce different trends in elemental abundance plots than those that are produced by the coupled radiogenic and nucleogenic components, ^{4}He and $^{21}Ne^{*}$. In gases released from step-heated olivine, addition of a cosmogenic component of ^{21}Ne ($^{21}Ne_C$) lowers the mantle $^{4}He/^{21}Ne^{*}$ ratio ($^{4}He/(^{21}Ne^{*} + {}^{21}Ne_C)$), and addition of ^{3}He ($^{3}He_C$) elevates the mantle $^{3}He/^{22}Ne_s$ ratio (($^{3}He_{Mantle} + {}^{3}He_C)/^{22}Ne_s$). Measured elemental ratios in Icelandic basalts that may contain significant amounts of $^{3}He_C$ and $^{21}Ne_C$ (e.g., sample *ice-4*, see chapter 6) are labeled in the elemental abundance plots that will be shown in subsequent sections. Because there is little difference in the calculated concentrations of excess ^{21}Ne whether the cosmogenic or nucleogenic end-members are used (see Chapter 6), the nucleogenic end-member will be used here, assuming that no cosmogenic neon is present. To obtain the mantle elemental ratios, the atmospheric components must be subtracted. The equation and end-member compositions used to calculate the concentrations of $^{21}Ne^{*}$ and $^{22}Ne_s$ were described in Chapter 2 (equation 2-2) and in Chapter 6.

7.2.3 Argon

The calculation of the radiogenic component of ^{40}Ar in mantle-derived samples, $^{40}Ar^*$, was described in Chapter 2 (equation 2-11).

7.3 Mechanisms of elemental fractionation

Descriptions of processes that cause elemental fractionation of noble gases in the melt, gas and crystalline phases were given in Chapter 2. Some of these points are briefly summarized here.

7.3.1 Fractionation by diffusion

In general, the diffusivities of the noble gases in silicate liquids increase with decreasing atomic radius, r, (or mass) and obey a linear relationship with $1/r^2$ (Hart, 1984; Kurz and Jenkins, 1981; Lux, 1987; Roselieb et al., 1995). Thus, if gas loss from a magma occurs at a magma/wallrock interface, the relatively light gas will be supplied faster to the interface, and will be preferentially lost over the heavier gases. Under certain conditions, mass fractionation by diffusion may cause enrichment of the heavier component relative to the lighter component in the residual melt. The degree of elemental fractionation caused by diffusion is likely to be relatively small compared with that which could be produced by multistage solubility controlled fractionation (Chapter 2).

7.3.2 Solubility controlled fractionation

The calculated trends that would be produced by multistage solubility controlled fractionation during bubble formation were shown in Chapter 2. These trends will be compared with the trends formed by the Icelandic data in this chapter.

7.3.3 Partitioning of noble gases between crystals and melt

Noble gas elemental ratios in melt and crystalline phases may be fractionated during crystallization or during melting. The elemental ratios in the crystalline (in this study, olivine) and melt phases following crystallization are likely to be dependent in part on the manner in which the gases are incorporated in the olivine. Gases may be incorporated in (1) fluid inclusions or (2) point defects in the olivine lattice (Carroll and Draper, 1994). Estimating the degree of elemental fractionation that would be produced by crystal-melt fractionation requires knowledge of crystal-melt partition coefficients. Experimental determinations of noble gas crystal-melt partition coefficients (Carroll and

Draper, 1994) have yielded a wide range of values, making it difficult to calculate the expected degree of fractionation that would be produced in the residual melt by this process.

7.4 Results: Icelandic elemental abundance ratios

The elemental abundance data from olivine and glass separates from Icelandic basalts are shown in Figure 7-2A-H and are compared with data from previous studies (Honda and Patterson, 1999) in Figure 7-3A-H. The Icelandic elemental abundance data presented from this study do not include the results with uncertainties >50% of observed ratio, nor do they include those that were not completely melted during step-heating experiments (Appendix 3). The olivine separates obtained from samples that were well-shielded from cosmic rays are distinguished from those that were only partly shielded (Chapter 6). Because the uncertainties in different elemental abundance ratios vary, not all samples appear in all plots. For example, some samples that have near-solar $^{21}Ne/^{22}Ne$ ratios have little $^{21}Ne^*$, resulting in large uncertainties in the amount of $^{21}Ne^*$. These samples do not appear in plots including $^{4}He/^{21}Ne^*$ or $^{21}Ne^*/^{40}Ar^*$ ratios. However, nearly all samples have a relatively large component of $^{40}Ar^*$, so most samples appear in plots of $^{4}He/^{40}Ar^*$.

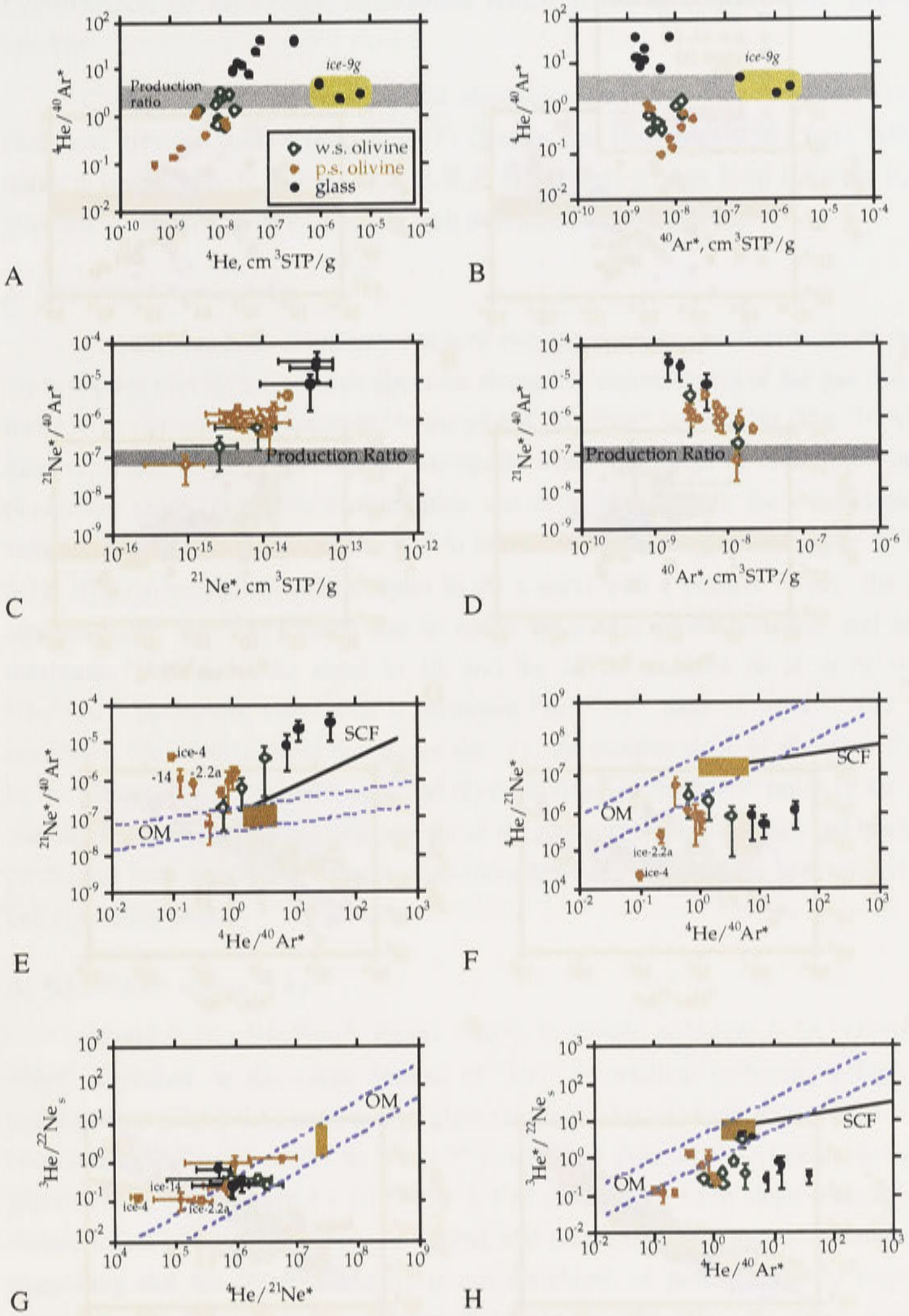

Figure 7-2A-H. Elemental abundance ratios measured in Icelandic samples from this study. "w.s. olivine" is well-shielded olivine; "p.s. olivine" is partly-shielded olivine, and "glass" represents basaltic glass samples. The grey bands in Figures A-D and the orange rectangles in Figures E-H represent the possible range of the mantle primordial and/or production ratios (see Chapter 2). The lines "SCF" are calculated solubility controlled fractionation trends. The lines labelled "OM" show the range in compositions of the majority of OIB and MORB data.

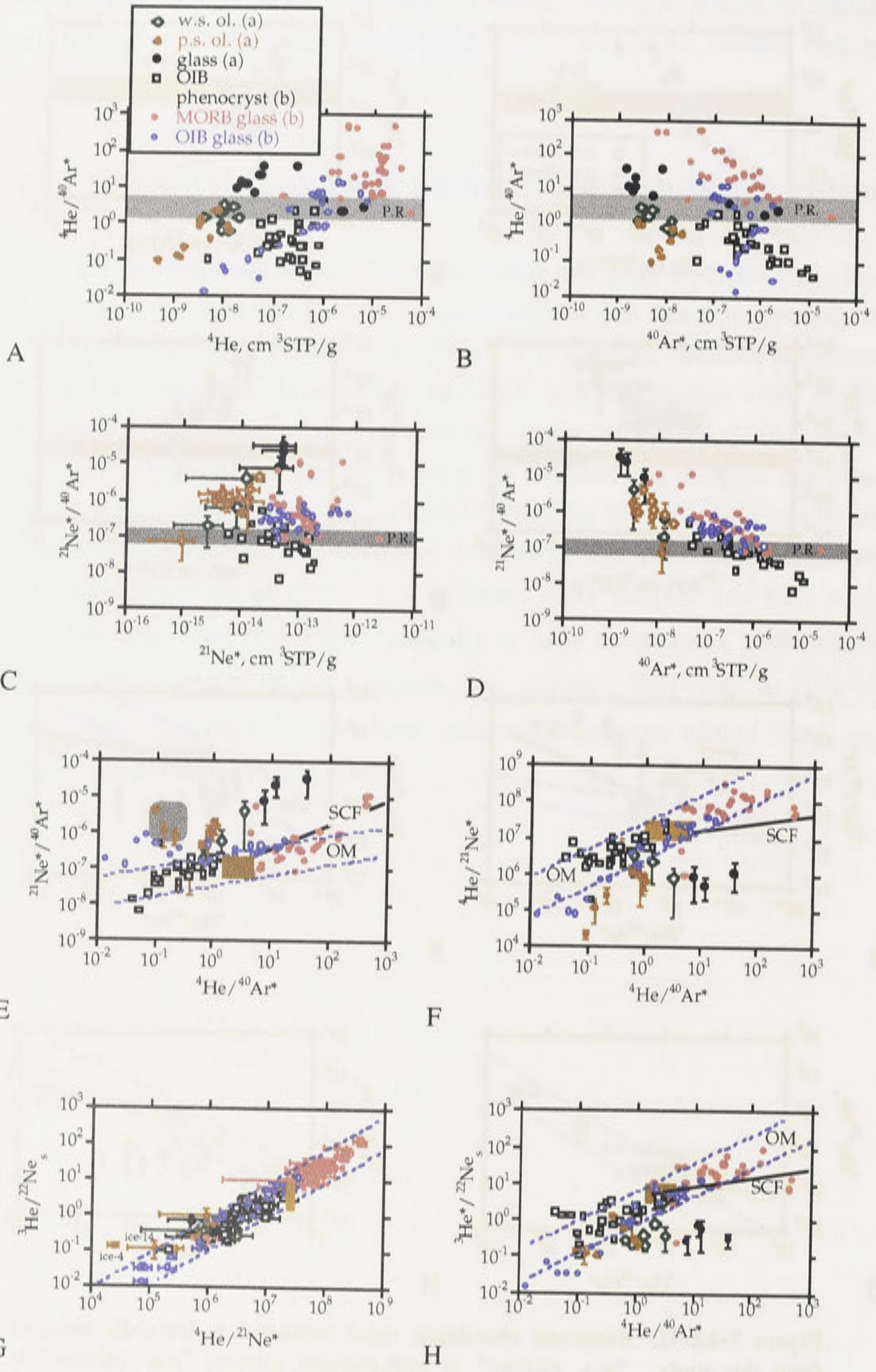

Figure 7-3. Plots of elemental abundance ratios (a) from Icelandic basalts from this study and (b) from previous studies of MORB glasses, OIB glasses and OIB phenocrysts (data sources as in Fig. 2-20). The symbols used for the data from the present study are the same as those used in Figure 7-2A-H. "ol." stands for olivine.

Comparison of noble gas elemental ratios from this study and previous studies

Composite plots of the elemental abundance data show that the data from this study and previous studies (Fig. 7-3A-F) (Honda and Patterson, 1999) form different trends in several plots (e.g., Fig. 7-3A, C, E, F, H). However, data from Icelandic basalts also share some important similarities with data from previous studies.

A. $^4He/^{40}Ar^*$ versus ^4He

Plots of elemental abundance ratios of two gases versus the abundance of one of the two gases provide information about the changes in concentration of the gas that may result from elemental fractionation. In the plot of $^4He/^{40}Ar^*$ versus ^4He (Fig. 7-2A), the three replicates of the glass sample, *ice-9g,* lie within the range of $^4He/^{40}Ar^*$ mantle production ratios, at a ^4He concentration that is higher than all the other Icelandic samples from this study, from 9 x 10^{-7} to 6.2 x 10^{-6} cm^3STP/g (see Chapter 5, Table 5-1). The remaining Icelandic samples lie on a trend with a positive slope: the glass separates have $^4He/^{40}Ar^*$ ratios that lie above the mantle production ratio and have a maximum $^4He/^{40}Ar^*$ ratio equal to 40, and the olivine samples lie at or below the $^4He/^{40}Ar^*$ production ratio, with a minimum $^4He/^{40}Ar^*$ ratio of ~0.1. The most significant observations from this figure are: (1) the positive slope of the trend formed by the majority of the Icelandic data, and (2) the division in $^4He/^{40}Ar^*$ ratios of the glass and olivine separates, to values that are above the production ratio for glass, and below the production ratio for olivine, reflecting partitioning of the noble gases between the melt and crystalline phases.

B. $^4He/^{40}Ar^*$ versus $^{40}Ar^*$

Figure 7-2B ($^4He/^{40}Ar^*$ versus $^{40}Ar^*$) is similar to Figure 7-2A, except that $^{40}Ar^*$ is plotted on the x-axis instead of ^4He. In addition to having a high ^4He concentration (Fig. 7-2A), replicates of glass sample *ice-9g* also have much higher $^{40}Ar^*$ concentrations (from 2 x 10^{-7} to 2 x 10^{-6} cm^3STP/g) than other Icelandic olivine and glass samples ($^{40}Ar^*$ from 2 x 10^{-10} to 2 x 10^{-8} cm^3STP/g). The slope formed by the Icelandic data in this plot is close to vertical, and there may be a slightly negative slope, suggesting that the $^4He/^{40}Ar^*$ ratio is not correlated, or perhaps slightly negatively correlated, with $^{40}Ar^*$, whereas in Figure 7-2A, the $^4He/^{40}Ar^*$ ratio is clearly positively correlated with ^4He.

Comparison with data in Honda and Patterson (1999)

In Figures 7-3A and B, ($^4He/^{40}Ar^*$ versus ^4He, and $^4He/^{40}Ar^*$ versus $^{40}Ar^*$, respectively) the OIB and MORB data define trends that are parallel to those formed by the Icelandic data from this study, but most Icelandic data lie at lower gas concentrations

(^{4}He or ^{40}Ar* cm^{3}STP/g) for a given ^{4}He/^{40}Ar* ratio than the OIB and MORB data. The exception to this generalization is glass sample *ice-9g*, whose three replicates (*ice-9g1, -g2, -g3*) have gas concentrations that are similar to those found in the OIBs and MORBs. The MORB popping rock (point labelled "P.R." for popping rock) has higher gas concentrations compared with the other MORB data.

C. ^{21}Ne/^{40}Ar* versus ^{21}Ne*

The Icelandic data have ^{21}Ne/^{40}Ar* ratios that range from values equal to the mantle production ratio (2 x 10^{-7}) to those that are more than two orders of magnitude higher (3 x 10^{-5}) than the mantle production ratio (Fig. 7-2C). The data lie on a positive slope, showing increasing ^{21}Ne*/^{40}Ar* ratios with increasing ^{21}Ne* concentration. The glass separates have higher ^{21}Ne/^{40}Ar* ratios and higher ^{21}Ne* concentrations than the olivine separates. What is most interesting about this plot is that, unlike the plot of ^{4}He/^{40}Ar* versus ^{4}He, where the olivine data lie below the mantle production ratio, and the glass data above the production ratio, here, both the olivine and the glass separates have ^{21}Ne/^{40}Ar* ratios that are greater than or equal to the production ratio.

Comparison with data in Honda and Patterson (1999)

In Figure (7-3C), the MORB and OIB glass data have ratios that are above the ^{21}Ne/^{40}Ar* mantle production ratio, and most of the phenocryst data have ^{21}Ne/^{40}Ar* ratios that are below the mantle production ratio. The maximum ^{21}Ne/^{40}Ar* ratios in MORB glasses are similar to the maximum ratios in Icelandic glass separates. However, unlike the Icelandic data, the MORB and OIB data do not define a clear trend in this plot.

D. ^{21}Ne*/^{40}Ar* versus ^{40}Ar*

This plot (Fig. 7-2D) is similar to Figure 7-2C (^{21}Ne*/^{40}Ar* versus ^{21}Ne*), except in this plot, ^{40}Ar* is shown on the x-axis. The slope in this plot is negative, the opposite of the slope in Figure 7-2C. The trends in Figures 7-2C and D are similar to those in Figures 7-2A and B (the plots of ^{4}He/^{40}Ar* versus ^{4}He and ^{4}He/^{40}Ar* versus ^{40}Ar*): when ^{4}He/^{40}Ar* and ^{21}Ne*/^{40}Ar* are plotted against ^{4}He and ^{21}Ne*, respectively, the slopes are positive, but when plotted against ^{40}Ar*, the slopes are negative.

Comparison with data in Honda and Patterson (1999)

Like the Icelandic data, the MORB and OIB data also appear to define a trend with a negative slope in Figure 7-3D (^{21}Ne*/^{40}Ar* versus ^{40}Ar*). As stated above for Figure 7-3C, the main difference between the MORB and OIB data and the Icelandic data is that, unlike the Icelandic olivine ^{21}Ne/^{40}Ar* ratios, which lie at values greater than

or equal to the production ratio, the OIB phenocryst data have compositions that are generally less than or equal to the mantle production ratio.

E. $^{21}Ne^*/^{40}Ar^*$ versus $^{4}He/^{40}Ar^*$

Most of the Icelandic data (excluding samples *ice-2.2a, -4, and –14*) define a linear trend in this plot (Fig. 7-2E). The trend formed by the Icelandic data does not intersect the field defining the range of the mantle production ratio (orange box). On both axes, the data extend to values well above the values of the mantle production ratio, as described for Figures 7-2A and 7-2C. At a $^{21}Ne/^{40}Ar^*$ ratio near the mantle production ratio of 2×10^{-7}, the data have $^{4}He/^{40}Ar^*$ ratios (approximately. 0.5) that are lower than the mantle production ratio (1.4 to 4.8). Most of the Icelandic data lie on a trend that is similar to the SCF trend. The data points that lie off the linear trend are from partly-shielded samples that may have a component of cosmogenic $^{21}Ne^*$ and will not be discussed further here

Comparison with data in Honda and Patterson (1999)

In Figure 7-3E, unlike the Icelandic data, the MORB and OIB data from previous studies appear to lie on a trend that intersects the mantle production ratio. The OIB glass data do not lie on a trend that is parallel to the SCF trend, but instead lie on a near-horizontal trend, and have a wide range of $^{4}He/^{40}Ar^*$ ratios at nearly constant $^{21}Ne^*/^{40}Ar^*$ ratios.

F. $^{4}He/^{21}Ne^*$ versus $^{4}He/^{40}Ar^*$

In this plot (Fig. 7-2F) the data lie below the $^{4}He/^{21}Ne^*$ production ratio, and have $^{4}He/^{21}Ne^*$ ratios from 4×10^{-5} to 3×10^{-6}. Most of the data form a roughly horizontal trend that is sub-parallel to the solubility controlled fractionation trend, with $^{4}He/^{40}Ar^*$ ratios from 0.4 to 40. Three samples lie at relatively low $^{4}He/^{21}Ne^*$ ratios, and may contain a cosmogenic component of $^{21}Ne^*$ (see Fig. 7-2E).

Comparison with data in Honda and Patterson (1999)

In Figure 7-3F, the majority of the OIB and MORB glass data lie within a range of compositions that do not overlap the Icelandic data.

G. $^{3}He/^{22}Ne^*$ versus $^{4}He/^{21}Ne^*$

In a plot of $(^{3}He/^{22}Ne_s)$ versus $(^{4}He/^{21}Ne^*)$, the data should show the same behaviour on both axes (Fig. 7-2G). The $(^{3}He/^{22}Ne_s)$ and $(^{4}He/^{21}Ne^*)$ ratios of the Icelandic data lie on or near the trend defined by the OIB and MORB data, at values that are below the mantle primordial/production ratios.

Comparison with data in Honda and Patterson (1999)

In Figure 7-3G, all OIB and MORB data lie on the same trend. Most OIB phenocryst and OIB glass data lie at values that are below the primordial/production ratios, and most MORB glass data have ratios that are greater than or equal to the mantle primordial/production ratios.

H. $^{3}He/^{22}Ne(s)$ versus $^{4}He/^{40}Ar^{*}$

Like in Figure 7-2F, in Figure 7-2H, the Icelandic data lie well below the primordial mantle $^{3}He/^{22}Ne_{s}$ ratio, on a roughly horizontal trend, with near-constant $^{3}He/^{22}Ne_{s}$ ratios over a range of $^{4}He/^{40}Ar^{*}$ ratios. The trend formed by the data is roughly parallel to the solubility controlled fractionation trend.

Summary

The Icelandic elemental abundance ratios show some similarities to, but also some important differences from the OIB and MORB data. Specifically, the trends formed by the Icelandic data do not pass through the primordial and production ratios in plots that include neon. Instead, in plots that include elemental ratios with neon in the numerator or the denominator, the data are fractionated relative to the mantle primordial/production ratios in a sense that would suggest neon addition. Elemental fractionation between neon and argon has caused the $^{21}Ne^{*}/^{40}Ar^{*}$ ratios of the Icelandic data to lie well above the production ratio in some samples (Figs. 7-2C, E). Fractionation between helium and neon has caused the $^{3}He/^{22}Ne_{s}$ ratios to lie well below the mantle primordial ratio for all samples except the glass separates from *ice-9g* (Fig. 7-2H). There is also a large degree of fractionation of the $^{4}He/^{40}Ar^{*}$ ratio in the Icelandic data that is positively correlated with the ^{4}He concentration and negatively correlated with the $^{40}Ar^{*}$ concentration. In comparison, the $^{21}Ne/^{40}Ar^{*}$ ratio is positively correlated with the $^{21}Ne^{*}$ concentration and negatively correlated with the $^{40}Ar^{*}$ concentration.

Unlike the Icelandic data, the main trends formed by the OIB and MORB data pass through the compositions of the mantle primordial/production ratios. There is relatively little fractionation of neon from argon in the OIB and MORB data, but where fractionation of Ne/Ar ratios is evident, it is in the same sense as the He/Ne and He/Ar fractionation. There are good correlations between the ^{4}He concentrations and $^{4}He/^{40}Ar^{*}$ ratios. Although there does appear to be a correlation between the $^{21}Ne/^{40}Ar^{*}$ ratios and the $^{40}Ar^{*}$ concentrations, there is little correlation between the $^{21}Ne/^{40}Ar^{*}$ ratios and the $^{21}Ne^{*}$ concentrations. Owing to the differences between the Icelandic data and the OIB and MORB data described by Honda and Patterson (1999), different and/or additional processes are required to explain the Icelandic data.

7.5 Discussion

Owing to the possibly complex nature of the mixing and fractionation processes controlling the noble gas isotopic and elemental ratios in Icelandic basalts, it is necessary to develop a model with which to evaluate the data. One model is that the elemental ratios in Icelandic basalts were produced first by mixing between elementally fractionated plume and MORB-derived gases, with elemental ratios within the range of those observed in mantle-derived samples (Fig. 7-3). Hence, the elemental ratios in most Icelandic basalts from this study will be explained as resulting from two main processes: (1) mixing between elementally fractionated plume and MORB-derived gases, and (2) subsequent elemental fractionation processes that occurred during magmatic ascent through the Icelandic crust. In one sample from this study (*ice-9g*), the processes described in Part II do not appear to have occurred. The noble gas elemental composition of this sample will be evaluated to determine whether it can be explained by binary mixing.

7.5.1 Part I: Mixing plume- and MORB-derived noble gases: elemental abundance ratios

As shown in Chapter 2, OIBs and MORBs have a range of $^{3}He/^{4}He$ and end-member $^{21}Ne/^{22}Ne$ ratios. The different *isotopic* ratios of OIBs and MORBs have been used to infer that they arise from different source reservoirs. Despite their origins in different source reservoirs, the *elemental* ratios measured in MORBs and OIBs worldwide lie on broadly similar trends (Figs. 7-3A-H). Like the helium and neon (end-member) isotopic ratios measured in OIBs and MORBs worldwide, the Icelandic basalts from this study have a wide range in helium and neon isotopic compositions, yet lie on similar trends in the elemental ratio plots. This shows that samples with very different isotopic ratios may lie on the same trend in plots of elemental ratios.

When noble gases with different isotopic ratios and different elemental ratios from the plume (P) and MORB (M) end-members are mixed together, the isotopic and the elemental ratios in the mixture should have a range in compositions that lie between the end-member compositions. In Chapter 6, to produce the range of helium, neon and argon isotopic compositions in Icelandic basalts by binary mixing, a large range in $R^{P,M}_{He,Ne}$ and $R^{P,M}_{Ne,Ar}$ was required, where:

$$R^{P,M}_{He,Ne} = \left[\frac{\left({}^{22}Ne_S / {}^{3}He \right)_P}{\left({}^{22}Ne_S / {}^{3}He \right)_M} \right] \tag{6-7}$$

$$R^{P,M}_{Ne,Ar} = \left[\frac{\left({}^{36}Ar / {}^{22}Ne_S \right)_P}{\left({}^{36}Ar / {}^{22}Ne_S \right)_M} \right] \tag{6-21}$$

The actual end-member elemental ratios (e.g., $^{3}He/^{22}Ne_{s}$, $^{22}Ne/^{36}Ar$) in the plume and MORB end-members at the time of mixing are not known. The calculated elemental ratios in the OIB and MORB end-members needed to produce the required $R^{P,M}_{He,Ne}$ value will be compared with the elemental ratios observed in OIBs and MORBs.

Calculated trends

Equations

The equations presented in Chapter 6 and additional equations given below will be used to calculate the $(^{3}He/^{22}Ne_{s})_{MIX}$ (equation 6-13), $(^{22}Ne/^{36}Ar)_{MIX}$ (equation 6-20) and $(^{4}He/^{40}Ar^{*})_{MIX}$ (equation 7-1) elemental ratios that would be produced by mixing noble gases from the plume (P) and MORB (M) end-members. The isotopic compositions used in equation (7-1) are calculated using the same plume and MORB end-member compositions and equations that were given in Chapter 6, e.g., $(^{4}He/^{3}He)_{MIX}$ is calculated from equation (6-9) and $(^{40}Ar/^{36}Ar)_{MIX}$ is from equation (6-18).

$$f_{M} = {}^{3}He_{M}/({}^{3}He_{M}+{}^{3}He_{P}), \tag{6-8}$$

$$(^{4}He/^{3}He)_{MIX} = (^{4}He/^{3}He)_{M} \times f_{M} + (^{4}He/^{3}He)_{P} \times (1- f_{M}) \tag{6-9}$$

$$\left(\frac{^{3}He}{^{22}Ne_{S}}\right)_{MIX} = \left(\frac{^{3}He}{^{22}Ne_{S}}\right)_{M} \times 1 \Big/ \left(f_{M} + (1-f_{M}) \times \frac{(^{22}Ne_{S}/^{3}He)_{P}}{(^{22}Ne_{S}/^{3}He)_{M}}\right) \tag{6-13}$$

$$g_{M} = (^{22}Ne_{s})_{M}/[(^{22}Ne_{s})_{M}+(^{22}Ne_{s})_{P}], \tag{6-15}$$

$$\left(\frac{^{22}Ne_{S}}{^{36}Ar}\right)_{MIX} = \left(\frac{^{22}Ne_{S}}{^{36}Ar}\right)_{M} \times 1 \Big/ \left(g_{M} + (1-g_{M}) \times \frac{(^{36}Ar/^{22}Ne_{S})_{P}}{(^{36}Ar/^{22}Ne_{S})_{M}}\right) \tag{6-20}$$

$$G_{M} = {}^{36}Ar_{M}/({}^{36}Ar_{M}+{}^{36}Ar_{P}) \tag{6-17}$$

$$\left(\frac{^{40}Ar}{^{36}Ar}\right)_{MIX} = \left(\frac{^{40}Ar}{^{36}Ar}\right)_{M} \times G_{M} + (1-G_{M}) \times \left(\frac{^{40}Ar}{^{36}Ar}\right)_{P} \tag{6-18}$$

$$\left(\frac{^4He}{^{40}Ar^*}\right)_{MIX} = \left(\frac{^3He}{^{22}Ne_S}\right)_{MIX} \times \left(\frac{^4He}{^3He}\right)_{MIX} \times \left(\frac{^{22}Ne_S}{^{36}Ar}\right)_{MIX} \times 1\Big/\left(\frac{^{40}Ar}{^{36}Ar}\right)_{MIX} \quad (7\text{-}1)$$

Sample ice-9g

One of the most interesting samples from this study is sample *ice-9g* because it has near-solar neon isotopic ratios with relatively small uncertainties (see Chapter 6), $^3He/^{22}Ne_s$ and $^4He/^{40}Ar^*$ ratios that are within the range of those observed in OIBs and MORBs, and relatively high gas concentrations similar to those observed in OIBs and MORBs (compare Figures 7-2A and 7-2B with Figures 7-3A and 7-3B). As explained previously, the noble gas elemental ratios produced by mixing elementally fractionated OIB and MORB end-members should lie within the observed range of compositions in OIBs and MORBs. This sugests that *ice-9g* has not experienced significant elemental fractionation following the postulated plume + MORB mixing. As was explained in Chapter 6, the decoupled neon and helium *isotopic* ratios in *ice-9g* require a plume + MORB mixture with an $R^{P,M}_{He,Ne}$ value of near 5. The following discussion is intended to show that the observed *elemental* ratios in sample *ice-9g* are consistent with mixing between MORB and plume end-members in which the elemental ratios in at least one of the two end-members is fractionated. As mentioned previously, in most Icelandic samples from this study, the measured $^3He/^{22}Ne_s$ ratio may not be representative of the $^3He/^{22}Ne_s$ ratio of the postulated plume + MORB mixture because additional elemental fractionation may have occurred after mixing and prior to eruption.

The observed $^3He/^{22}Ne_s$ and $^4He/^{40}Ar^*$ ratios in *ice-9g* are assumed to be close to the values in the original plume + MORB mixture because (unlike in most Icelandic samples from this study) they lie within the range of compositions observed in OIBs and MORBs. Using the observed values in *ice-9g* for $(^3He/^{22}Ne)_{MIX}$ and $(^4He/^{40}Ar^*)_{MIX}$ in equation (6-13) and (7-1), it is possible to calculate the $^3He/^{22}Ne_s$ ratio in the MORB end-member that is required to produce the observed elemental ratios in *ice-9g*. To produce the observed $^3He/^{22}Ne_s$ ratio in a mixture with an $R^{P,M}_{He,Ne}$ value of near 5, the plume end-member should have a relatively unfractionated $^3He/^{22}Ne_s$ ratio near 5, and MORB end-member a relatively high $^3He/^{22}Ne_s$ ratio (~25) compared with the primordial mantle ratio. This value (~25) is well within the range of observed $^3He/^{22}Ne_s$ ratios in MORBs (up to 100) (Fig. 7-3H). The $R^{P,M}_{Ne,Ar}$ value is not well constrained, but for a value of 1.6, the $^{22}Ne_s/^{36}Ar$ ratios in the MORB and plume end-members (0.3 and 0.19 respectively) are relatively unfractionated compared with the presumed initial mantle ratio (0.1).

As expected, the calculated mixing curve between the plume and MORB end-members intersects the composition of sample *ice-9g* (*ice-9g1* and *–9g2*), the glass samples that lie in the yellow ellipse in Figure 7-4. The calculation suggests that the primordial $^{3}He/^{22}Ne_s$ ratio in sample *ice-9g* is consistent with binary mixing between a relatively unfractionated plume end-member with a $^{3}He/^{22}Ne_s$ ratio near 5, and MORB end-member with a fractionated $^{3}He/^{22}Ne_s$ ratio near 25. This MORB end-member $^{3}He/^{22}Ne_s$ ratio is consistent with the observed sense of fractionation in MORBs, which have $^{3}He/^{22}Ne_s$ ratios as high as 100 (Fig. 7-3H).

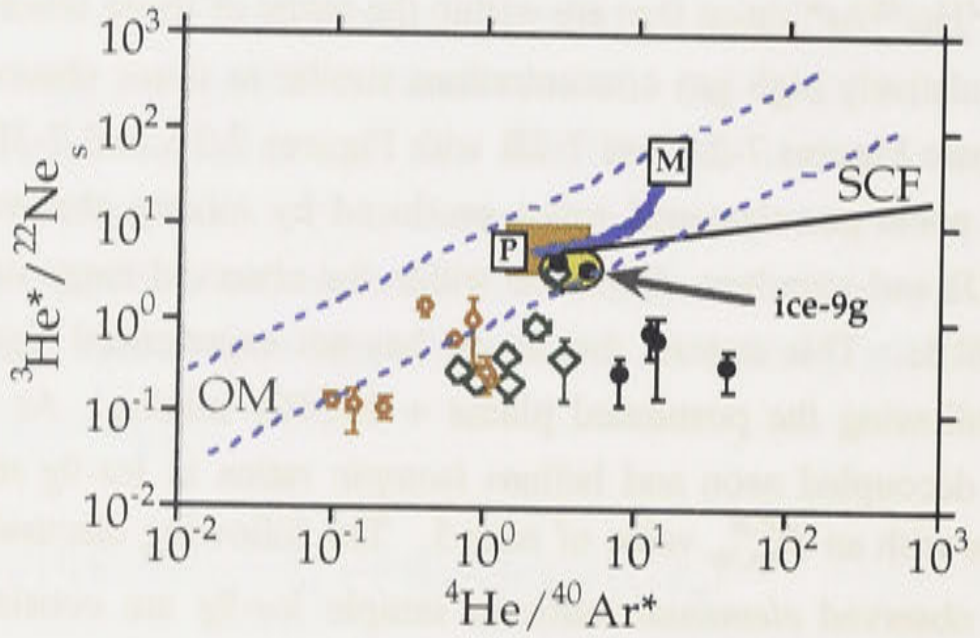

Figure 7-4. A plot of $^{3}He/^{22}Ne_s$ versus $^{4}He/^{40}Ar^{*}$ showing a mixing curve between the plume (P) and MORB (M) end-members. The curve between P and M passes through the primordial/production ratios in the mantle (orange box), and close to the compositions of *ice-9g1* and *–g2*, the two glass samples that lie within the yellow ellipse. The decoupled helium and neon isotopic ratios, as well as the measured elemental ratios in *ice-9g* may be produced by mixing between noble gases from the plume and MORB end-members. The field between the dashed lines labelled"OM" represents the range of compositions observed in the majority of OIBs and MORB data. Symbols for the Icelandic data are as shown in Figure 7-2A. SCF stands for solubility controlled fractionation (see Chapter 2).

7.5.2 Part II: Evaluation of possible elemental fractionation mechanisms in Icelandic basalts

As was discussed in Chapter 6, the noble gas isotopic compositions of *all* the samples from this study are postulated to have been produced by binary mixing between elementally fractionated MORB and plume end-member components. Binary mixing between plume and MORB noble gas end-members should produce elemental ratios in the mixture that lie between the elemental ratios in the end-members. However, in contrast to sample *ice-9g* described above, the majority of the Icelandic samples from this

study have elemental ratios that lie outside of the range of those observed in MORBs and OIBs worldwide, i.e., the elemental ratios do not lie between the compositions of the postulated end-members. Because the noble gas elemental ratios of Icelandic basalts lie outside the fields defined by OIB and MORB data, additional fractionation mechanisms are postulated to explain their compositions. This means that the Icelandic data are unlikely to be explained by the single stage elemental fractionation process that was used by Honda and Patterson (1999) to explain the compositions in OIBs and MORBs (see Chapter 2). This additional elemental fractionation is postulated to have occurred following binary mixing (see Part I) and during ascent of magma through dikes in the Icelandic crust (Fig. 7-1). The following discussion of the elemental fractionation processes that may produce the observed elemental ratios in Icelandic basalts will be general owing to the limited experimental constraints on elemental fractionation processes. This general analysis will show that the noble gas elemental ratios in Icelandic samples from this study were produced by systematic fractionation processes. There are at least two general scenarios that may have occurred to produce the observed trends in the Icelandic data (Figs. 7-2A-H): (1) neon addition, and (2) multistage elemental fractionation. These two possible scenarios are shown schematically in Figures 7-5A-H and 7-6A-H and will be explained in detail in the following sections.

Apparent neon enrichment

The Icelandic data from this study appear to suggest that neon has been enriched, and helium lost, relative to $^{40}Ar^*$. Neon enrichment is suggested because the majority of the data from this study have: (1) He/Ne ratios that are below the $^{3}He/^{22}Ne_s$ primordial ratio and the $^{4}He/^{21}Ne^*$ production ratio (Fig. 7-2H, F); as well as (2) $^{21}Ne^*/^{40}Ar^*$ ratios that are greater than (by more than two orders of magnitude) or equal to the production ratio (Fig. 7-2C). In addition, some of the data that have $^{21}Ne/^{40}Ar^*$ ratios equal to the production ratio also have $^{4}He/^{40}Ar^*$ ratios lower than the production ratio (Fig. 7-2E). This means that neon has been enriched relative to argon, but helium has been lost relative to argon. Because the $^{3}He/^{22}Ne_s$ and the $^{4}He/^{21}Ne^*$ ratios are also below the production ratio in Figure 7-2H, the implication is that $^{21}Ne^*$ and $^{22}Ne_s$ have been enriched relative to helium.

Although addition of neon relative to helium and argon appears to provide a simple explanation for the data, neon enrichment cannot be explained by the known mechanisms of elemental fractionation, including diffusion, crystal-melt fractionation and solubility controlled fractionation. In any of these processes, if the relatively light element is fractionated from the relatively heavy element so that the $^{3}He/^{22}Ne_s$ ratios are below the primordial ratio, the $^{21}Ne^*/^{40}Ar^*$ ratios should also lie below the production ratio.

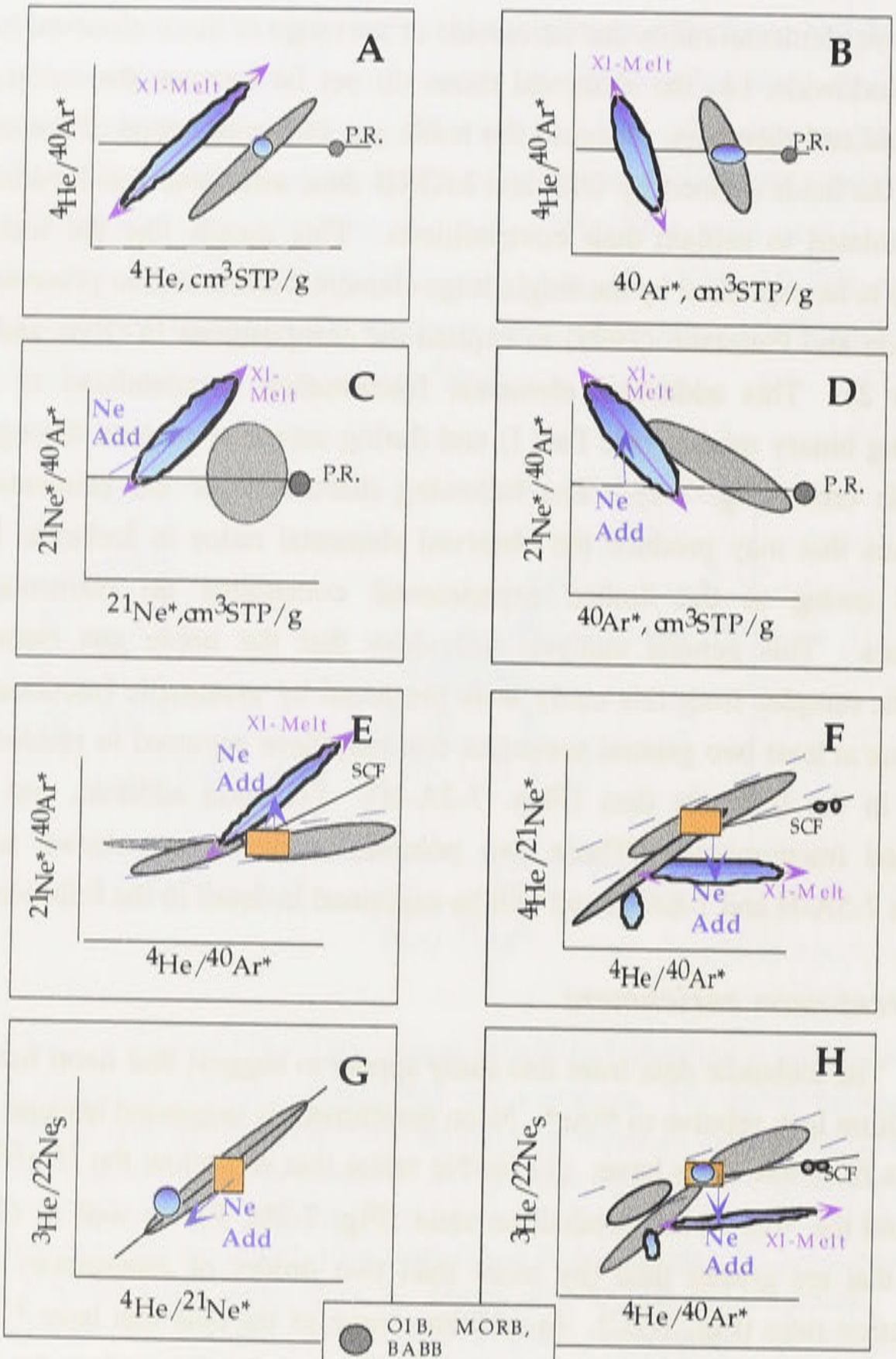

Figure 7-5A-H. Schematic representations of data from this study that were shown in Figures 7-2A-H (in blue) and the data from Honda and Patterson (1999, and references therein) (in gray) that are shown in Figures 7-3A-H. "Xl-melt" stands for crystal-melt fractionation (here, crystal-melt fractionation is not intended to specify how the gases are contained in olivine), "SCF" is solubility controlled fractionation. The production/primordial mantle ratios are shown as orange rectangles or horizontal lines, as in previous figures. The relatively low He/Ne ratios and relatively high Ne/Ar ratios appear to be caused by addition of neon. An additional fractionation process between olivine and melt (Xl-melt fractionation) is needed such that the elemental ratios in the glass are higher than the ratios in the olivine.

Multistage elemental fractionation

Preferential helium loss

The apparent neon enrichment described above may be explained by a multistage process that involves: (1) preferential helium loss, (2) solubility controlled fractionation by bubble formation, and (3) crystal-melt fractionation. This three-stage process may provide a self-consistent means to explain the elemental ratios in Icelandic basalts. This multi-stage process seems more reasonable than relative neon enrichment by a single-stage process because it does not involve addition of gases, but instead only involves fractionation of gases to produce the observed trends.

The physical mechanism that controls preferential helium loss is not well understood. A previous study of elemental ratios in OIB and MORB samples suggested that there is a mass-threshold process whereby helium, which has been preferentially excluded- or extracted from crystallizing oceanic crust, contaminates outgassed magmas (Honda and Patterson, 1999). The mechanism that causes preferential helium loss could be related to a mass threshold process, such as was described by Honda and Patterson (1999).

Solubility controlled fractionation

Solubility controlled fractionation by bubble formation was not considered to be a major process that produced the observed trends in the elemental ratios measured in samples from OIB and MORBs (Fig. 7-3A-H) (Honda and Patterson, 1999) (see Chapter 2). Although solubility controlled fractionation is unlikely to have produced the observed trends in elemental ratios from OIBs and MORB samples, the Icelandic data appear to have experienced additional stages of fractionation that may have included solubility controlled fractionation.

Solubility controlled fractionation provides a mechanism to enrich the residual melt in the light isotopes of the noble gases (see Chapter 2). Although solubility controlled fractionation would produce a large degree of fractionation in the $^{4}He/^{40}Ar^{*}$ ratios, it would cause only relatively minor fractionation of the $^{4}He/^{21}Ne^{*}$ ratios (see Chapter 2). This means that in plots of $^{4}He/^{21}Ne^{*}$ versus $^{4}He/^{40}Ar^{*}$ (Fig. 7-2F) and $^{3}He/^{22}Ne_{s}$ versus $^{4}He/^{40}Ar^{*}$ (Fig. 7-2H), solubility controlled fractionation would cause the elemental compositions to lie along a nearly horizontal trajectory. Thus, following the stage of preferential helium loss, solubility controlled fractionation provides a mechanism to explain how the $^{4}He/^{40}Ar$ ratios were increased so that the data lie off the observed trend formed by the OIB and MORB data. The proposed stages of helium loss and solubility controlled fractionation are not only consistent with the $^{4}He/^{40}Ar^{*}$ ratios, but also with all the Icelandic data shown in Figures 7-3A-H (as shown schematically in Figs. 7-5A-H).

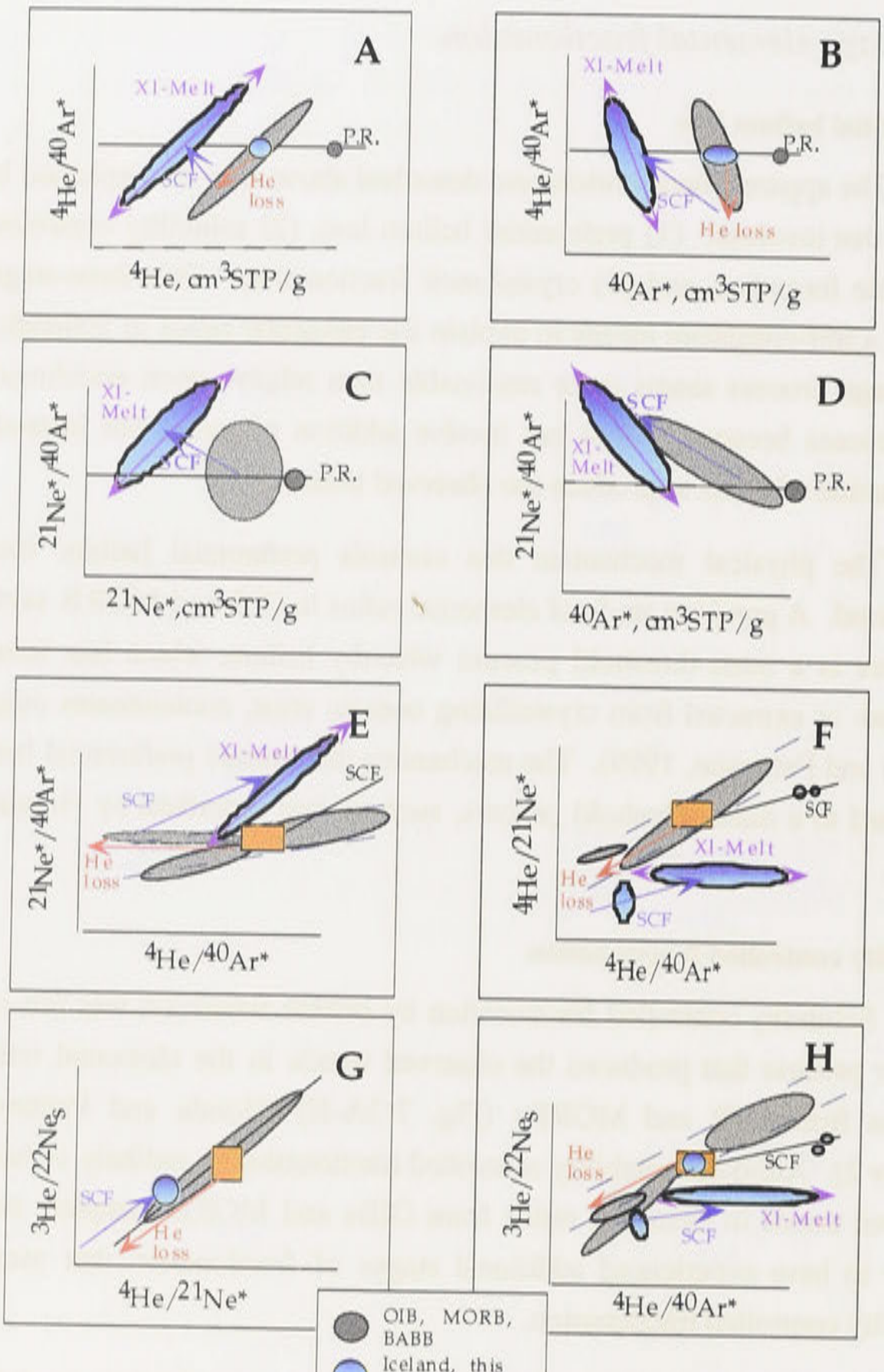

Figure 7-6A-H. A schematic diagram illustrating a possible multistage elemental fractionation process to explain the elemental ratios of Icelandic basalts (see Figure 7-5A-H for explanation of symbols). The first stage involves preferential helium loss to decrease the $^3He/^{22}Ne_s$, $^4He/^{21}Ne^*$ and $^4He/^{40}Ar^*$ ratios to values below the primordial or production ratios. Subsequent solubility controlled fractionation then increases the He/Ne and Ne/Ar ratios to higher values. Finally, the noble gas compositions are fractionated between the crystals and melt, so that elemental ratios in the melt are higher than those in the olivine.

Crystal-melt fractionation

Solubility controlled fractionation may provide an explanation for why the $^{21}Ne/^{40}Ar^*$ ratios are elevated to values above the production ratio in Figure 7-2C. However, an additional process is also needed to explain why the $^{4}He/^{40}Ar^*$ and $^{21}Ne^*/^{40}Ar^*$ ratios in the basaltic glass separates are consistently higher than the $^{4}He/^{40}Ar^*$ and $^{21}Ne^*/^{40}Ar^*$ ratios in the olivine separates (Figures 7-2A-D).

The explanation for the low $^{4}He/^{40}Ar^*$ and $^{21}Ne^*/^{40}Ar^*$ ratios in olivine compared with the glass is likely to relate to: (1) how the gases are incorporated into olivine; and/or (2) the relative compatabilities of noble gases in the melt compared with olivine. There is insufficient information to further evaluate the possible means by which noble gases may be elementally fractionated between olivine and melt phases.

Summary

The above evaluation shows that the observed elemental ratios in Icelandic basalts can be explained by systematic fractionation processes. One seemingly unlikely possible scenario to explain the data involves neon enrichment by a single-stage process (Fig. 7-5A-H). A major problem with this scenario is that there are no known processes by which neon could be enriched relative to argon without also enriching helium. A second, more likely possible explanation for the elemental ratios in Icelandic samples from this study is that they were produced by a three stage process (Figs. 7-6A-H) that involves: (1) preferential helium loss relative to neon; (2) solubility controlled fractionation between melt and vesicles to increase the He/Ne and Ne/Ar ratios; and (3) crystal-melt fractionation to produce the higher $^{4}He/^{40}Ar^*$ and $^{21}Ne/^{40}Ar^*$ ratios in the glass than the olivine. In nature, helium loss, bubble formation and olivine crystallization processes may be concurrent and occur as the magmas ascend through the crust and intrude into magma chambers and sills. These postulated explanations are not unique, and other processes may also have produced the observed elemental ratios in Icelandic basalts.

Comparison of elemental fractionation processes in Icelandic basalts with other mantle-derived samples

The postulated stages of fractionation (preferential helium loss, solubility controlled fractionation and crystal-melt fractionation) that may provide an explanation for the Icelandic data do not appear to explain the OIB and MORB data. This is in part because unlike the Icelandic data, the MORB and OIB data lie on a trend that intersects the mantle primordial/production ratios. The observed elemental ratios in the majority of the Icelandic samples may differ from those in OIBs and MORBs owing to processes that fractionated the noble gases during intrusion of magmas into the Icelandic crust.

7.6 Conclusions

The decoupled helium and neon *isotopic* ratios shown in Chapter 6 were explained as having been produced by binary mixing between noble gases from the Icelandic plume and MORB end-members. The *elemental* ratios in Icelandic basalts have also been evaluated to determine whether they are consistent with having been produced by binary mixing between the OIB and MORB end-members. The elemental ratios of one sample from this study lie in the range of those observed in OIBs and MORBs and are consistent with binary mixing between a plume component with a relatively unfractionated $^{3}He/^{22}Ne_{s}$ ratio near 5 and a MORB component that has a relatively high $^{3}He/^{22}Ne_{s}$ ratio of near 25. This relatively high $^{3}He/^{22}Ne_{s}$ ratio (25) is consistent with the observed ratios in MORBs worldwide, which have $^{3}He/^{22}Ne_{s}$ ratios of up to 100, much higher than the range of solar or primordial mantle ratios (3.8 to 8, respecively). The postulated mixing between MORB and OIB noble gas components may occur in the shallow upper mantle beneath the Icelandic crust, or within deep magma chambers in the Icelandic crust. Following the postulated mixing between the Icelandic plume and MORB noble gas end-members, the noble gases in the majority of Icelandic samples from this study may have been further fractionated by processes including preferential helium loss, solubility controlled fractionation, and crystal-melt fractionation as the magma ascended via dikes to the surface. Other alternative fractionation processes or sequences of events may account for the observed elemental ratios in Icelandic basalts but there are insufficient constraints to further evaluate these possibilities.

The postulated three-stage process to explain the elemental ratios in Icelandic basalts (preferential helium loss, solubility controlled fractionation between melt and bubbles, and crystal-melt fractionation) differs from the single-stage fractionation mass-threshold processes used to explain the data presented by Honda and Patterson (1999) for oceanic basalt samples. This is simply because although the Icelandic data are similar to the MORB and OIB data in some respects, they are also different in several important ways from these data. The multistage elemental fractionation processes that are proposed to explain the elemental ratios in the majority of the Icelandic samples may not occur in other OIB localities owing to differences in the tectonic settings, as well as in the structure of dikes and magma chambers in the Icelandic crust compared with other localities. The most important conclusion to be drawn from this analysis is that the observed noble gas elemental ratios in Icelandic basalts do not preclude binary mixing between noble gases in the Icelandic plume and MORB end-members.

7.7 References

Carroll M. R. and Draper D. S. (1994) Noble gases as trace elements in magmatic processes. *Chemical Geology* 117, 37-56.

Geiss J., Buehler F., Cerutti H., Eberhardt P., and Filleaux C. H. (1972) Solar wind composition experiments. In *Apollo 16 Preliminary Scientific Report*, Vol. SP-315, pp. 14.1-14.10. NASA.

Hart S. R. (1984) He diffusion in olivine. *Earth and Planetary Science Letters* 70, 297-302.

Honda M. and McDougall I. (1998) Primordial helium and neon in the Earth - a speculation on early degassing. *Geophysical Research Letters* 25, 1951-1954.

Honda M. and Patterson D. B. (1999) Systematic elemental fractionation of mantle-derived helium, neon and argon in MORB glasses. *Geochimica et Cosmochimica Acta* 63, 2863-2874.

Kurz M. and Jenkins W. J. (1981) The distribution of helium in oceanic basalt glasses. *Earth and Planetary Science Letters* 53, 41-54.

Lux G. (1987) The behaviour of noble gases in silicate liquids: solution, diffusion, bubbles and surface effects, with applications to natural samples. *Geochimica et Cosmochimica Acta* 51, 1549-1560.

Moreira M., Kunz J., and Allegre C. (1998) Rare gas systematics in popping rock: isotopic and elemental compositions in the upper mantle. *Science* 279, 1178-1181.

Pepin R. O. (1998) Isotopic evidence for a solar argon component in the Earth's mantle. *Nature* 394, 664-667.

Roselieb K., Rammensee W., Buttner H., and Rosenhauer M. (1995) Diffusion of noble gases in melts of the system SiO_2-$NaAlSi_2O_6$. *Chemical Geology* 120, 1-13.

CHAPTER 8: SYNTHESIS

This chapter summarizes the results, observations, major findings and conclusions from Chapters 2 through 7. As this chapter is intended to provide a broad, general overview of the results of this study, it does not include cited references or specific values unless necessary.

The overview of noble gas geochemistry in Chapter 2 showed that the Earth is likely to contain components of primordial solar noble gases that have been augmented by radiogenic and nucleogenic gases produced over time in the Earth. The noble gas isotopic compositions of mantle-derived samples from MORBs differ from the compositions measured in OIB samples in some important respects. In particular, the helium and neon end-member isotopic compositions of mantle-derived samples from MORBs are relatively homogeneous. In contrast, the neon isotopic ratios measured in samples from different OIBs (e.g., Tahiti, Reunion, Hawaii, Samoa) range from ratios that are relatively close to the solar ratio (e.g., Hawaiian basalts), to less primitive, MORB-like ratios (e.g., Tahiti). However, although neon end-member ratios of mantle-derived samples from different OIB localities have a large range in compositions, they are relatively homogeneous in different samples from the same OIB locality.

Insights into the degree of mantle degassing, and perhaps the timing of mantle degassing, may be obtained from argon and xenon isotopic ratios, respectively. Arguments based on argon mass balance suggest that a mantle mass equivalent to one half to two thirds of the mass of the mantle is likely to have been largely degassed of primordial noble gases. Subsequent decay of ^{40}K to ^{40}Ar has produced the relatively high $^{40}Ar/^{36}Ar$ ratios in MORBs. Additional insights into mantle degassing may be inferred from xenon isotopic ratios. Some MORB samples have relatively high $^{129}Xe/^{130}Xe$ and $^{136}Xe/^{130}Xe$ ratios compared with atmospheric ratios. This was interpreted as indicating that the mantle was degassed of primordial isotopes of xenon prior to decay of all the short-lived extinct nuclides, ^{129}I and possibly ^{244}Pu, in the mantle. The relatively high $^{129}Xe/^{130}Xe$ ratios were used to infer that most (80%) of the gas release from the mantle occurred early (in the first 50 Ma) of Earth history. Until recently, it appeared that the $^{129}Xe/^{130}Xe$ and $^{136}Xe/^{130}Xe$ ratios of most OIBs, excluding Samoa, were similar to the atmospheric ratio. These atmosphere-like ratios were interpreted to suggest that, unlike the MORB source, the OIB source had not been largely degassed of the primordial isotopes of xenon prior to decay of ^{129}I and possibly

^{244}Pu. However, recent analyses of Hawaiian and Icelandic basalts suggest that other OIBs besides Samoa may also have ^{129}Xe/^{130}Xe and ^{136}Xe/^{130}Xe ratios that are significantly higher than the atmospheric ratios. These ratios could be interpreted as indicating that, like the MORB source, the OIB source has also been at least partly degassed of primordial isotopes of xenon prior to the decay of all the ^{129}I and ^{244}Pu in the mantle, but other interpretations are possible.

Although isotopic ratios measured in OIBs and MORBs may provide some insights into the compositions of their mantle source regions, the noble gas elemental ratios (e.g., ^{4}He/^{40}Ar*, ^{21}Ne*/^{40}Ar*) in mantle-derived samples from OIBs and MORBs do not appear to preserve the compositions in their respective source reservoirs. Noble gas elemental ratios from MORBs and OIBs have a broad range in compositions that indicate that the noble gases have been elementally fractionated. Despite their origins from different source reservoirs deduced from the isotopic ratio, the elemental ratios measured in MORBs and OIBs worldwide lie on broadly similar trends. The range in elemental ratios observed in MORBs and OIBs has been interpreted as resulting from a mass-threshold process involving preferential exclusion of helium from crystallizing oceanic crust.

Chapter 3 summarizes some of the arguments for and against layered- and whole-mantle convection. Layered mantle models postulate that the upper mantle is degassed and depleted in incompatible elements, whereas the lower mantle is relatively unmelted and undegassed. Such layered mantle models are based in part on observations of the relative helium and heat fluxes from the Earth. The helium flux out of oceanic areas is lower than that which would be predicted based on the heat flux. This was interpreted to suggest that helium is trapped in a relatively undegassed lower mantle. A boundary layer between the lower and upper mantles through which heat could be transferred more readily than helium was proposed to explain the discrepancy in helium and heat fluxes. However, if the lower mantle is relatively undegassed, it should be relatively unmelted and therefore relatively chemically homogeneous. This implies that trace element ratios (e.g., Nb/U, Nb/Th) and lead isotopic ratios should preserve some evidence for the derivation of OIBs from melting of primitive mantle. However, as there is little or no direct evidence of an original primitive mantle composition in most OIBs, the layered mantle paradigm does not appear to adequately explain the geochemical observations.

In contrast, in a whole mantle convection regime, the lower mantle is likely to have experienced differing degrees of melt extraction and mixing. It is therefore likely to be heterogeneous in terms of neodymium, strontium and lead isotopic ratios, as well as noble gas isotopic compositions. The expected heterogeneous isotopic compositions are consistent with the observed isotopic compositions in mantle-derived samples from

OIBs. However, if the entire mantle is stirred by convection, some explanation is required for: (1) how relatively solar-like noble gas isotopic compositions are preserved in some OIBs; (2) the apparent discrepancy between helium and heat fluxes from the Earth; and (3) argon mass balance arguments that suggest that a large fraction of the lower mantle is relatively undegassed. These considerations may relate to the rate of mantle convection.

The rate of mantle convection is one of the factors that controls the extent to which the mantle has been stirred. The rate of mantle convection is likely to have decreased as the mantle has cooled over the 4.5 billion years of Earth history. It has been suggested that at the *current* rate of convection, the entire mantle will take at least 5 billion years to make one complete overturn. Such a slow mantle convection rate may provide a means to explain the argon mass balance arguments if the radiogenic ^{40}Ar ($^{40}Ar^*$) is stored in a portion of the mantle that has not been melted and degassed since the time that the $^{40}Ar^*$ was produced by radioactive decay. In this way, the $^{40}Ar^*$ need not be stored in an undegassed lower mantle. The rate of stirring in the mantle may also be influenced by the increasing viscosity of the mantle with depth. A relatively high viscosity in the lower mantle compared with that in the upper mantle may help to preserve chemical heterogeneity in the lower mantle. Although numerical models that are based on viscosity-dependent rates of convection in the mantle have not yet been able to reproduce the observed $^3He/^4He$ ratios in OIBs, the models may need to incorporate factors such as extraction of uranium and thorium from the mantle to the crust, or to consider that the mantle bodies that contain noble gases with relatively high $^3He/^4He$ ratios are relatively small.

Chapter 4 discusses the Icelandic regional geologic setting, the general petrography of Reykjanes Peninsula (Iceland) basalts, and the geochemistry of Reykjanes Peninsula and Reykjanes Ridge (MORB) basalts. The position of the Icelandic plume along a major spreading ridge, the Mid-Atlantic Ridge, may influence the isotopic compositions of Icelandic basalts. This is because as the plume flattens against the base of the lithosphere, geophysical models suggest that the plume moves laterally along with the diverging plates, which causes MORB material to be entrained into the plume. The geophysical model may be further evaluated by comparison of geochemical compositions of Icelandic and MORB samples. Because the lead, strontium and neodymium isotopic ratios of Icelandic basalts from the Reykjanes Peninsula overlap normal MORB compositions, MORB melts may be a possible end-member that mixes with the Icelandic plume. Noble gases from MORB melts may therefore also contribute to the noble gas isotopic compositions of basalts erupted on the Reykjanes Peninsula, Iceland.

In addition to isotopic ratios, trace element ratios also provide insights into the compositions of mantle sources sampled by the Icelandic plume. Icelandic data from this study and a previous study show that the incompatible element ratios such as Nb/U, Nb/Th and Ce/Pb of Icelandic basalts are more heterogeneous than those measured in other OIBs (e.g., Hawaiian basalts). Icelandic basalts have a large range in Nb/U ratios, with a minimum value close to 50, and a maximum ratio of near 100. In comparison, most OIBs and MORBs have Nb/U ratios of near 50 (47 ± 10). Icelandic Nb/Th and Ce/Pb ratios also show a much larger range of compositions than those in OIBs and MORBs. However, the Th/U ratios in Icelandic basalts, OIBs and MORBs have a relatively narrow range in compositions between 3.2 and 2.6, respectively.

The relatively homogenous Nb/U, Nb/Th and Ce/Pb ratios in OIBs and MORBs have previously been used to argue that OIBs cannot be derived from melting of primitive mantle. Instead, following extraction of continental crust, the OIB and MORB sources are postulated to have been well-mixed to produce the relatively homogeneous incompatible element ratios. In contrast to these previous interpretations based on samples from other localities, the mantle source sampled by the Icelandic plume does not appear to be homogeneous in terms of Nb/U, Nb/Th and Ce/Pb ratios. An previously calculated estimate for the Nb/U ratio of the MORB source following extraction of the continental crust is ~150. The maximum Nb/U ratio measured in this study of Icelandic basalts is near 100. This suggests that following extraction of the continental crust from the original presumably primitive mantle, the mantle source of Icelandic plumes was not well-mixed.

Chapter 5 summarizes the results of previous noble gas investigations and presents the new helium, neon, argon, krypton and xenon isotopic results from this study. The maximum helium isotopic ratios from well-shielded olivine separates (29 ± 3) in this study are close to the maximum observed in Loihi basalts (ca. 30 Ra), but are lower than the maximum ratio observed in previous studies of Icelandic basalts (37 ± 2 Ra). Some of the neon isotopic ratios in Icelandic samples from this study lie within one sigma uncertainty of the air-solar mixing line, and are the most solar-like described thus far in terrestrial samples, including those measured in previous noble gas investigations of Icelandic samples. Previous studies of Icelandic basalts reported different neon end-member isotopic ratios from samples obtained from the same locality. One neon end-member is similar to the Loihi neon end-member isotopic compostion, and the second is in-between the Loihi and MORB end-member isotopic compositions. The highest $^{40}Ar/^{36}Ar$ isotopic ratio (1667 ± 365) from this study is lower than the maximum ratios measured previously in Icelandic basalts (6500 ± 310). The relatively high maximum $^{40}Ar/^{36}Ar$ ratio measured previously in Icelandic basalts of near 6500 is similar to the maximum ratio measured in Hawaiian basalts (6300 ± 360). Krypton isotopic ratios

measured in this study are close to the atmospheric ratios at the one sigma uncertainty level. Xenon isotopic ratios in this study are close to the atmospheric ratios in all but one sample. This sample has $^{129}Xe/^{130}Xe$ and $^{136}Xe/^{130}Xe$ ratios that are significantly higher than the atmospheric ratio (at the one sigma uncertainty level), but the ratios are relatively low compared with those measured in previous studies of Icelandic basalts. The maximum $^{129}Xe/^{130}Xe$ and $^{136}Xe/^{130}Xe$ ratios measured in previous studies of Icelandic basalts are similar to the maximum ratios measured in Hawaiian basalts, but are lower than the maximum ratios measured in MORBs.

Chapter 6 has three parts. Section 1 shows that the helium and neon isotopic ratios of most of the partly-shielded olivine separates have relatively minor concentrations of cosmogenic ^{3}He and ^{21}Ne. This means that most of the partly-shielded olivine separates are likely to preserve meaningful information about the helium and neon isotopic compositions in their mantle sources.

Section 2 discusses the significance of the measured near-solar neon isotopic ratios in some of the Icelandic basalts from this study. Two possible means of preserving near-solar neon isotopic ratios are described. The first is where the source of near-solar neon isotopic ratios resides in the mantle. This mantle source is interpreted to have relatively high $[Ne_{solar}]/[U+Th]$ ratio that is at least nine times higher than the ratio in the MORB source. This estimate assumes that the U and Th contents of the MORB and the Icelandic plume sources are similar. Owing to the highly incompatible nature of helium and neon during mantle melting, a mantle source that has a high Ne/[U+Th] ratio is likely to be relatively unmelted and undegassed. A relatively unmelted region of the mantle is inferred to have a composition that is close to the postulated primitive mantle composition. The near-solar neon isotopic component in some Icelandic basalts may therefore originate from a primitive, undegassed mantle component in the Icelandic plume source. It is alternatively possible that the near-solar neon was derived from the Earth's core, but this scenario is considered highly speculative owing to the lack of experimental evidence to show that noble gases could be stored in iron-nickel alloys under the pressure and temperature conditions that exist at the core.

Section 3 explains that the near-solar neon isotopic ratios are expected to be coupled with near-solar helium isotopic ratios. Contrary to expectations, the helium isotopic ratios measured in Icelandic basalts are much lower than the possible range of solar $^{3}He/^{4}He$ ratios (100 to 320 Ra). Binary mixing between MORB-derived and plume-derived noble gases is postulated as a possible explanation for the decoupled helium and neon isotopic ratios in Icelandic basalts. The range in helium and neon isotopic ratios is interpreted to result from mixing between plume and MORB noble gas end-members in which the He/Ne elemental ratios in one or both end-members are fractionated relative to the initial mantle primordial and mantle production ratios. The

proposed binary mixing model is evaluated by calculating the expected compositions that would be produced by mixtures of plume and MORB-derived: (1) neon and argon; and (2) helium and argon isotopic ratios. The xenon isotopic ratios in Icelandic basalts are also evaluated by comparison with helium and neon isotopic ratios. The contribution of fission ^{136}Xe from ^{238}U to the observed $^{136}Xe/^{130}Xe$ ratio in the Icelandic plume source is estimated to be small compared with the high values of the $^{136}Xe/^{130}Xe$ ratios measured in Icelandic basalts from previous studies. This suggests that the plume-derived xenon may have been overwhelmed by addition of MORB-derived xenon with higher $^{136}Xe/^{130}Xe$ ratios. Although it is possible that some noble gas heterogeneity arises from the Icelandic plume source itself, and that other noble gas end-members besides the MORB end-member mix with the Icelandic plume, the MORB end-member provides the simplest explanation for the observed data. It is concluded that binary mixing between plume and MORB-derived noble gases is a reasonable explanation for the range in helium, neon, argon and xenon isotopic ratios in Icelandic basalts.

As was discussed in Chapter 7, the degree of fractionation of noble gas elemental ratios provides a means to understand the scale and nature of fractionation processes that may occur during magmatic ascent and intrusion of magma in the Icelandic crust. Comparison of the postulated processes that control noble gas elemental fractionation in Icelandic basalts with those postulated to explain the elemental ratios from OIBs and MORBs worldwide may help elucidate the differences in the eruptive mechanisms of Icelandic basalts compared with other localities. In addition, development of a hypothetical sequence of binary mixing and elemental fractionation events helps to evaluate whether the elemental ratios in Icelandic basalts may reasonably be reconciled with the proposed binary mixing model proposed in Chapter 6.

The elemental ratios in Icelandic basalts share some similarities, but also some important differences from the OIB and MORB data. One sample from this study that has OIB-like elemental ratios is consistent with binary mixing between a plume component, with a relatively unfractionated $^{3}He/^{22}Ne_{s}$ ratio of near 5, and a MORB component that has a relatively high ratio of near 25. This high $^{3}He/^{22}Ne_{s}$ ratio (25) is well within the observed range in MORBs worldwide. The postulated mixing between MORB and OIB noble gas components may occur in the shallow upper mantle beneath the Icelandic crust, or within deep magma chambers in the Icelandic crust.

The remaining Icelandic samples from this study have lower gas concentrations, and elemental ratios that lie on different trends, than observed in mantle-derived samples from OIBs and MORBs. Following the postulated mixing between the Icelandic plume and MORB noble gas end-members, the noble gases in the majority of Icelandic samples from this study may have been further fractionated by processes including preferential helium loss, solubility controlled fractionation, and crystal-melt fractionation as the

magma ascended via dikes to the surface. Other alternative fractionation processes or sequences of events could account for the observed elemental ratios in Icelandic basalts.

The postulated three-stage process to explain the elemental ratios in Icelandic basalts (preferential helium loss, solubility controlled fractionation between melt and bubbles, and crystal-melt fractionation) differs from the single-stage fractionation mass-threshold processes used to explain the data presented by Honda and Patterson (1999) for oceanic basalt samples. The additional elemental fractionation processes that are proposed to explain the majority of the Icelandic elemental ratios may relate to differences in the structure of the Icelandic crust compared with other localities.

In conclusion, the near-solar neon isotopic ratios measured in some Icelandic samples from this study are postulated to originate from a primitive, undegassed component in the Icelandic plume source. The range in noble gas isotopic ratios observed in Icelandic basalts is consistent with mixing a primitive noble gas mantle end-member with MORB-derived gases.

APPENDIX 1: SAMPLE LOCATIONS AND PETROGRAPHIC DESCRIPTIONS

A1.1 Sample locations

The locations of all samples collected for this study are shown in Table A-1 and in Figure A1-1. Samples that were used in this study are highlighted in bold type in Table A1-1. For samples in which the rock type is listed as "thol.," or tholeiitic basalt in Table A1-1, a basaltic glass sample was collected. Samples *ice-1-8* were collected by I. Sigurdsson, and the remaining samples were collected by the author.

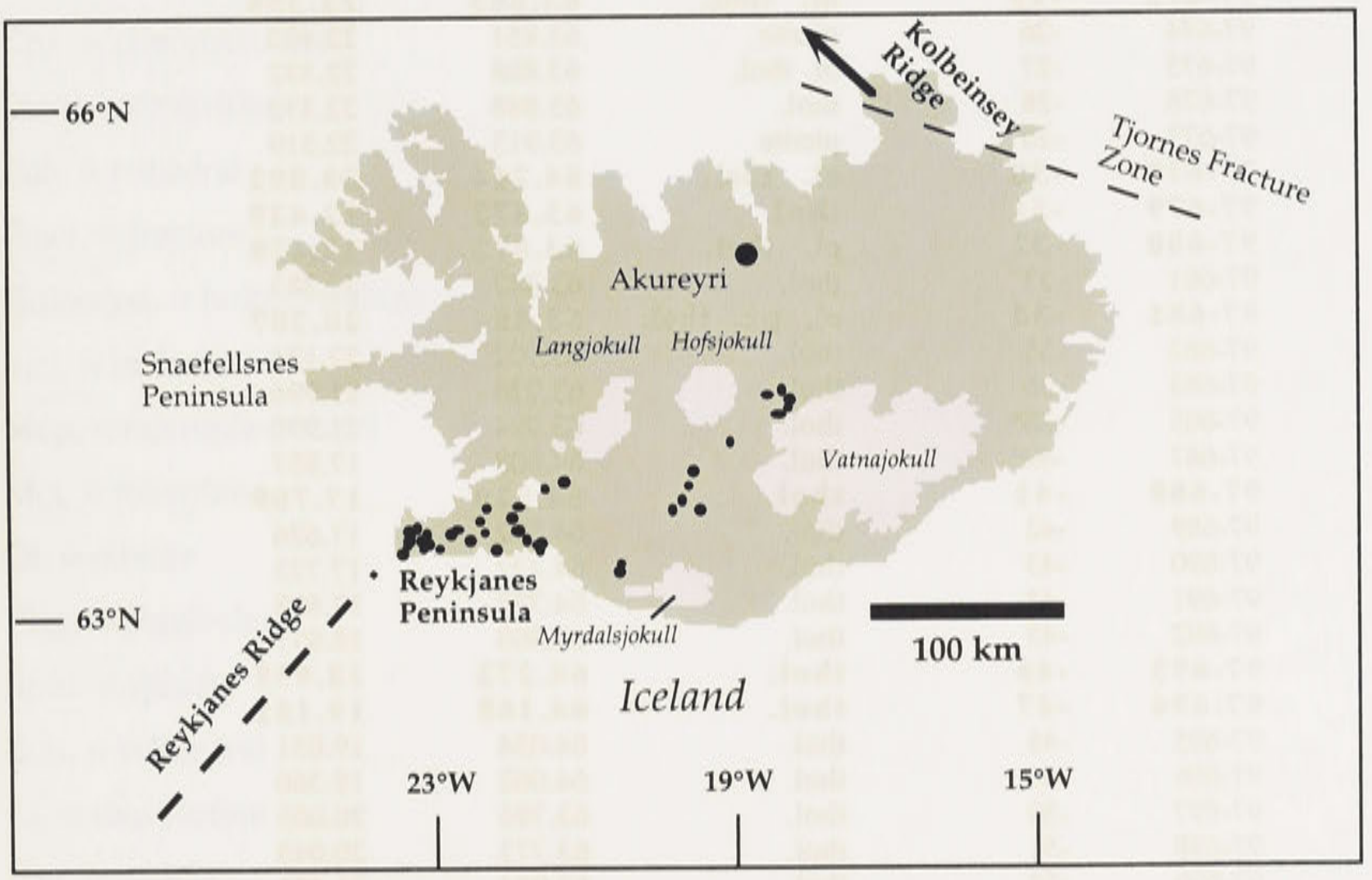

Figure A1-1. Map of Iceland, showing the locations of all samples collected for this study. A sub-set of these samples was actually used in this study, as shown in Chapter 4 and Table A1-1.

Table A1-1. Sample localities in Iceland

ANU#	Sample no., ice	Rock type	Latitude, °N	Longitude, °W
96-0743	**-1**	**picrite**	**64.176**	**21.057**
96-744	**-2**	**picrite**	**64.110**	**21.199**
96-745	**-3**	**picrite**	**63.910**	**21.481**
96-746	**-4**	**picrite**	**63.815**	**22.670**
96-747	-5	picrite	63.851	22.402
96-748	-6	picrite	63.912	21.918
96-749	-7	picrite	63.928	21.431
96-750	-8	picrite	63.867	21.688
97-657	**-9**	**picrite**	**64.176**	**21.057**
97-658	**-10**	**picrite**	**64.104**	**21.202**
97-659	**-11**	**picrite**	**64.110**	**21.199**
97-660	**-12**	**picrite**	**63.912**	**21.918**
97-661	-13	picrite	63.928	21.431
97-662	**-14**	**picrite**	**63.910**	**21.481**
97-663	-15	ol. thol.	63.846	21.670
97-664	**-16**	**ol. thol.**	**63.857**	**22.005**
97-665	-17	ol. thol.	64.003	21.900
97-666	**-18**	**ol. thol.**	**63.905**	**22.534**
97-667	**-19**	**ol. thol.**	**63.900**	**22.550**
97-668	-20	ol. thol.	63.879	22.553
97-669	-21	ol. thol.	63.857	22.590
97-670	-22	ol. thol.	63.870	22.572
97-671	**-23**	**picrite**	**63.815**	**22.670**
97-672	**-24**	**ol. xenolith**	**63.849**	**22.362**
97-673	**-25**	**ol. thol.**	**63.863**	**22.356**
97-674	-26	picrite	63.851	22.402
97-675	-27	ol. thol.	63.888	22.332
97-676	-28	thol.	63.888	22.332
97-677	-29	picrite	63.913	22.319
97-678	**-30**	**ol. thol.**	**64.214**	**20.892**
97-679	**-31**	**thol.**	**63.872**	**22.429**
97-680	**-32**	**ol. thol.**	**63.872**	**22.429**
97-681	-33	thol.	63.847	22.383
97-681	**-34**	**ol. px. thol.**	**63.854**	**20.307**
97-682	-35	thol.	63.902	22.124
97-683	-36	thol.	63.924	21.996
97-685	-38*	thol.	63.924	21.996
97-687	-40*	thol.	64.808	17.937
97-688	**-41**	**thol.**	**64.820**	**17.709**
97-689	-42	thol.	64.802	17.626
97-690	-43	thol.	64.732	17.723
97-691	-44	thol.	64.777	17.688
97-692	-45	thol.	64.303	18.977
97-693	**-46**	**thol.**	**64.272**	**18.995**
97-694	**-47**	**thol.**	**64.168**	**19.151**
97-695	-48	thol.	64.034	19.051
97-696	-49	thol.	64.062	19.366
97-697	-50	thol.	63.786	20.005
97-698	-51	thol.	63.772	20.043
97-699	-52	thol.	63.954	21.471
97-700	-53	thol.	63.991	21.461
97-701	**-54**	**thol.**	**64.011**	**21.470**
97-702	**-55**	**thol.**	**64.037**	**22.416**

*indicates that the previous sample was discarded. ol. = olivine, thol. = tholeiitic basalt. Samples used in this study are highlighted in bold type.

A1.2 Petrographic descriptions

The following petrographic descriptions of Icelandic basaltic samples were primarily used to evaluate the suitability of the phenocryst phases for noble gas analyses, and are not intended to provide a detailed petrographic description of the samples. Detailed petrographic descriptions of basalts from the Reykjanes Peninsula, Iceland may be found in the literature (see references cited in Chapter 4). All modes given below in Table A1-2 are based on visual estimates. Clinopyroxene is generally not sufficiently abundant to appear in a single thin section, but is listed in Table A1-2 if it was found during mineral separation. Thin sections were not available for samples *ice-1* through *–4* and *–47* through *–55*.

A list of abbreviations that will be used in the following descriptions is provided below:

Abd. = abundant

Alt. = altered

Anh. = anhedral

Cpx. = clinopyroxene

Devit. = devitrified

Euh. = euhedral

Fract. = fracture

Holocryst. = holocrystalline

Incl. = inclusion

Mcp. = microphenocryst

Mct. = microlite

Ol. = olivine

Plag. = plagioclase

Spin. = spinel

Sub. = subhedral

t.s. = thin section

Ves. = vesicle

Table A1-2. Petrographic descriptions of Icelandic samples used in this study

Locality	Sample No.	% olivine	Incl. in ol.	Cpx.	Plag.	Groundmass	%Ves.	Alt.
Midfell	ice-1					no t.s.		
Sandfell/ Hengill	ice-2.1, -2.2					no t.s.		
Burfell i olfusi	ice-3					no t.s.		
Haleyjar-bunga	ice-4					no t.s.		
Midfell	ice-9	25, euh-sub	spin, raremelt	1-2%		plag. met., spin.	10	none
Maelifell	ice-10.1, -10.2	35, sub	spin, melt	abd		plag met, ol. mcp.	rare	none
Sandfell/ Hengill	ice-11.1, -11.2	30-40, euh-sub	glass, spin, fluid	1%		plag met., ol. mcp.	20	none
Asar	ice-12.1, -12.2	15, sub	spin, melt, fluid	1%		plag met., w/ ol mcp..	1-2	none
Burfell i olfusi	ice-14	15, euh–sub	spin	<1%		plag met., euh ol mcp.	25-30	in ol. fract.
Eldborg	ice-16	5-10, euh.	spin, rare glass	2-3%		plag met., ol mcp.	40	
Stapafell	ice-18	10, euh	spin			plag met.,	15	none
Sulur	ice-19	15-20, euh-sub	spin, devit. melt		x	plag met.	40	none
Haleyarbunga	ice-23a	50, sub	spin, fluid, melt	1%	x	plag met.	<5	in fract.
Hraunsvik/ Hrolfsvik	ice-24 (xenolith)	50, anh.	rare spin, melt	1%	x	holocryst.		none
Bleikholl	ice-25	5, euh-sub	spin		w/ ol.	v. fine grained	10	none
~Landamnna-hellir	ice-30	5-10, sub	no vis. incl.			plag met., ol mcp.	5	none
~Svartsen-gisfell	ice-32.1, -32.2	5-10, euh-sub	no vis. incl.			plag met.	5	none
SW of Skala-Maelifell	ice-34	5, euh-sub	plag, melt, spin	abd	x	plag met.	10	none
Sigalda	ice-47	aphyric				no t.s.		
Lambafell	ice-54	aphyric				no t.s.		
Kongsgil	ice-55	1-2			x	no t.s.		

APPENDIX 2: MAJOR AND TRACE ELEMENT ANALYTICAL METHODS

A2.1 Major Elements

Icelandic natural basaltic glass samples from the Reykjanes Peninsula (n = 6) and Central Iceland (n = 2) were hand-picked to ensure freshness and then mounted in epoxy. The mounts were trimmed to expose the fresh glass surface, then diamond polished, and cleaned with methanol. Electron microprobe analyses of the glass samples were performed using EDS on a Cameca Camebax electron microprobe at the ANU with an operating voltage of 15 keV in raster mode over an area of 12.5 μm^2. The major element compositions of natural glass samples were measured in part to determine their CaO content because calcium is used as an internal standard for data acquired using laser-ablation inductively coupled plasma mass spectrometer (LA-ICPMS) analyses of trace elements (see section A2.2). When analysing rock samples for trace element compositions, it is standard to first melt the rock samples in order to homogenize the microphenocryst phases. However, for these analyses, the microphenocryst phases (olivine and plagioclase) were not homogenized by first melting the whole rock sample. Instead, multiple analyses of different glass chips from the sample were performed to obtain an average glass composition.

The major element compositions measured in this study are shown in Table A2-1 and Figure A2-1, and are compared with whole rock data (homogenized glass samples) from Reykjanes Peninsula tholeiites and picrites reported by Hemond et al. (1993). The major element compositions of the samples from this study lie within or close to the fields defined by the data from Hemond et al. (1993). For example, the glasses from this study have MgO contents between ~6 and 10 wt.% that are within the range of compositions reported by Hemond et al. (1993) (Fig. A2-1 D), and similarly, the CaO contents from this study overlap those reported by Hemond et al. (1993).

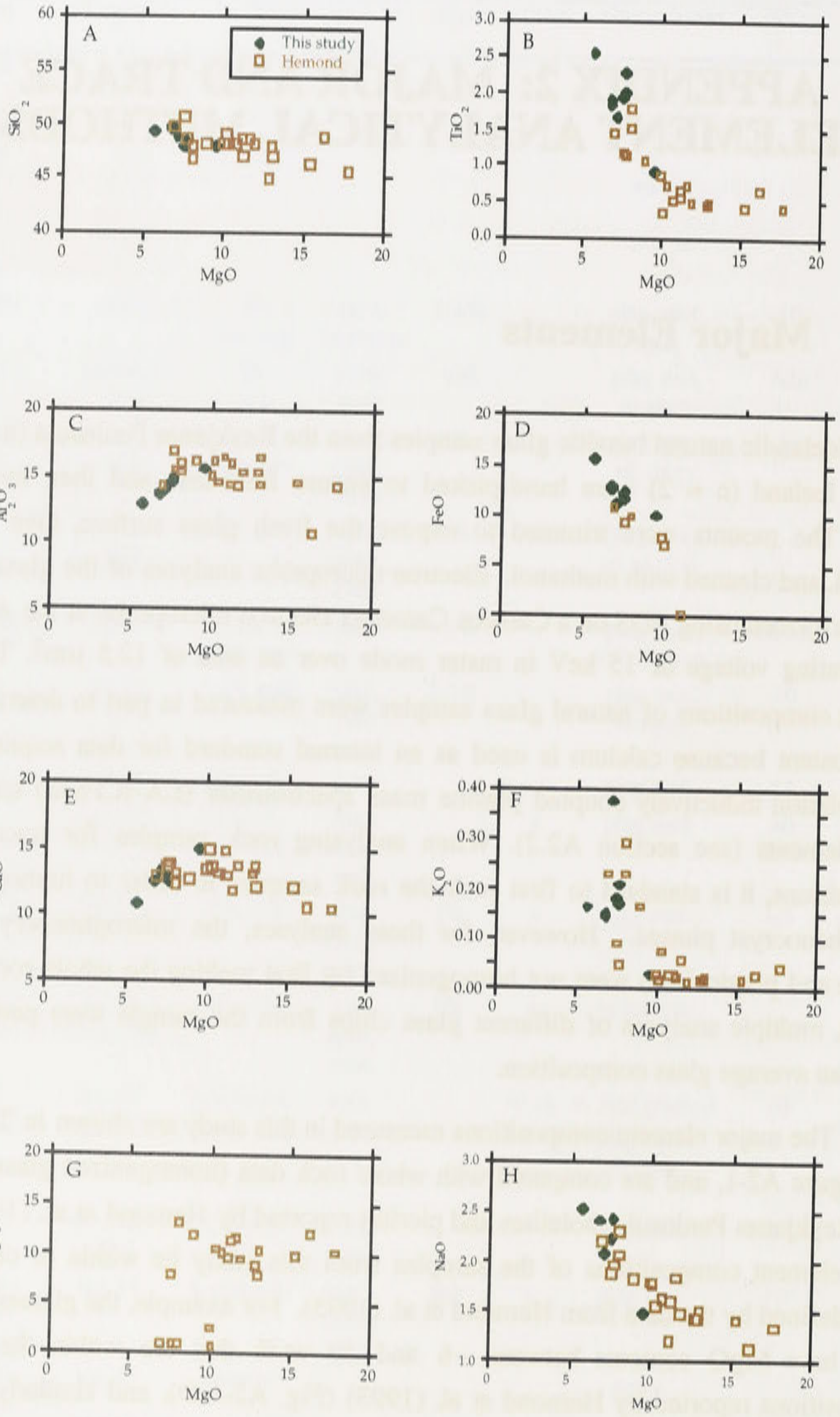

Figure A2-1 A-H. Major element compositions (in weight percent oxide) of Icelandic basalts from this study (green) and Hemond et al. (1993) (red). Note that Fe is reported as FeO from this study, but Hemond et al. (1993) report both FeO (D) and Fe_2O_3 (G). The data from this study lie on the same trends as tholeiitic basalts and picrites from Hemond et al. (1993). Although the analyses are of natural glasses, their compositions overlap those measured previously on whole rock samples.

Table A2-1. Major element composition of natural glass samples, Iceland

wt.% oxide	ice-9 (N=7)	ice-18 (N=5)	ice-32c (N=8)	ice-41 (N=4)	ice-46 (N=2)	ice-47 (N=2)	ice-54 (N=4)	ice-55 (N=4)
SiO_2	48.0	48.3	47.9	49.2	49.5	49.6	48.8	47.9
±	0.3	0.1	0.1	0.4	0.1	0.1	0.2	0.2
TiO_2	0.91	2.00	2.27	2.55	1.906	1.836	1.7	1.94
±	0.02	0.04	0.03	0.02	0.002	0.004	0.5	0.04
Al_2O_3	15.6	14.88	14.8	12.90	13.66	13.71	14.0	14.60
±	0.1	0.07	0.1	0.07	0.04	0.01	0.1	0.06
Cr_2O_3	0.13	0.14	0.09	<0.08	<0.08	0.080	0.10	0.12
±	0.01	0.03	0.01	0.01	0.01	0.001	0.01	0.03
FeO	10.0	11.6	12.4	15.6	12.7	12.89	11.21	12.07
±	0.1	0.2	0.1	0.1	0.1	0.01	0.09	0.06
MnO	0.10	0.12	0.15	0.13	0.12	0.16	0.10	0.08
±	0.02	0.04	0.01	0.05	0.02	0.00	0.01	0.00
MgO	9.5	7.58	7.59	5.62	6.73	6.77	7.1	7.4
±	0.1	0.08	0.09	0.05	0.03	0.06	0.1	0.1
CaO	15.0	12.99	12.55	10.80	12.48	12.51	13.22	12.85
±	0.1	0.07	0.06	0.09	0.06	0.05	0.06	0.06
Na_2O	1.48	2.24	2.42	2.5	2.41	2.41	2.1	2.2
±	0.05	0.03	0.04	0.4	0.05	0.01	0.3	0.1
K_2O	0.03	0.21	0.17	0.16	0.150	0.15	0.38	0.180
±	0.02	0.02	0.01	0.01	0.004	0.00	0.01	0.004
Total	100.7	100.0	100.2	99.5	99.6	99.98	98	99.2
±	0.5	0.3	0.4	0.3	0.1	0.27	1	0.4

A2.2 Trace Elements

At least three separate glass chips from each of the eight natural glass samples described above were analysed for trace element abundances, including Nb, Th and U. Analyses were performed using the pulsed ArF eximer laser ablation inductively coupled plasma mass spectrometer (ELA-ICP-MS) at the ANU described by Eggins et al. (1997). The ELA-ICP-MS was operated under the following conditions: repetition rate = 6 Hz; pulse energy = 100 mJ; spot size = 100 μm, ablation time = 60 seconds. Standards (BCR, BGD) were routinely measured before and following each 6 to 9 measurements of the unknowns. The ^{43}Ca peak was used as an internal standard to correct for differences in ablation yield and temporal variations in instrument signal intensity (drift) (Eggins et al., 1997; Sylvester and Ghaderi, 1997). The data reduction was performed according to methods described by Eggins et al. (1997). Uncertainties in

the concentration of elements due to variations in concentration in the different glass fragments from each sample were larger than those from other corrections including drift, so the former (larger) uncertainties are reported. Other details of ICP-MS analyses are the same as those described by Sylvester et al. (1997). The results of the ICP-MS analyses are shown in Chapter 4.

A2.3 References

Eggins S. M., Woodhead J. D., Kinsely L. P. J., Mortimer G. E., Sylvester P., McCulloch M. T., Hergt J. M., and Handler M. R. (1997) A simple method for the precise determination of >= 40 trace elements in geological samples by ICPMS using enriched isotope internal standardisation. *Chemical Geology* **134**, 311-326.

Hemond C., Arndt N. T., Lichtenstein U., and Hofmann A. (1993) The heterogeneous Iceland Plume: Nd-Sr-O isotopes and trace element constraints. *Journal of Geophysical Research* **98**, 16833-15850.

Sylvester P. J. and Ghaderi M. (1997) Trace element analysis of scheelite by excimer laser ablation-inductively coupled plasma-mass spectrometry (ELA-ICP-MS) using a synthetic silicate glass standard. *Chemical Geology* **141**, 49-65.

APPENDIX 3: NOBLE GAS ANALYTICAL METHODS

A3.1 Sample extraction, separation and cleaning

A3.1.1 Sample extraction

To obtain olivine and pyroxene separates from the basaltic matrix, basaltic samples weighing up to 2 kg were coarsely crushed in a steel jaw-crusher. The rock fragments were then sieved using sieve sizes of (a) > 2.34 mm (b) 2.34 mm > x > 1mm, (c) 1 mm > x > 420 microns and (d) <420 microns. The grain size fraction that yielded the largest number of relatively matrix-free phenocrysts was chosen for analysis. This was usually the 2.34 > x > 1mm fraction or the 1 mm > x > 420 micron fraction.

To obtain glass separates, the vitreous, glassy rind was chiseled to remove it from the non-vitreous basaltic portion of the sample. The glass was then crushed to a smaller size using a mortar and pestle in order to further separate the glassy from the non-glassy portions. The glass was then sieved using the same sieve size fractions as described above. The grain-size fraction with the largest chunks of fresh vitreous glass was selected for analysis.

A3.1.2 Mineral separation

Olivine and pyroxene concentrates were obtained by first using a magnetic separator to separate the majority of basaltic matrix material from the phenocrysts. Further separation of basaltic matrix and of olivine from pyroxene (where present) was accomplished using heavy liquid gravimetry with methylene iodide (CH_2I_2, which has a specific gravity of 3.32 g/cm^3). A second stage of magnetic separation was used to further purify the olivine or pyroxene separates.

A3.1.3 Sample cleaning procedure

The mineral separates were first rinsed once in acetone to remove the methylene iodide. Then, olivine and pyroxene separates were placed in a 7% HF solution in an ultrasonic bath for 10 minutes to remove any surface oxidation or particulate matter from

the outside of the grains. The samples were then immersed in HCl for a duration of at least 30 seconds for the 420 micron < x < 1 mm fraction, and up to 4 minutes for the 1 mm < x < 2.39 mm fraction. The samples were then rinsed in acetone in the ultrasonic bath for half an hour. This process was repeated at least twice. The samples were then immersed in ethanol or methanol for 20 minutes in the ultrasonic bath. This process was repeated at least once. Finally, the samples were rinsed in deionized water in the ultrasonic bath for at least half an hour. This process was repeated at least once. Samples were then dried in beakers in a clean oven for at least 5 hours. Samples were stored in vials cleaned with acetone or ethanol.

Basaltic glass samples were cleaned using the same procedure as above for the olivine separates, except without the rinses in HF and HCl because the acids etch the glass surface, making it difficult to identify oxidized grains.

Any remaining impurities in the olivine, glass and pyroxene separates were removed by hand-picking under a binocular microscope, with particular attention given to alteration and compound olivine/basalt grains. Olivine grains that contained glass inclusions were retained. The mineral separates used for analyses typically comprised 3 to 6 grams of olivine.

Glass separates were obtained by hand-picking of coarsely crushed fragments under a binocular microscope. Glass fragments with oxidation or discoloration were discarded, as were fragments that contained visible olivine phenocrysts. Some olivine microphenocrysts may have been present in the glass.

A3.2 Noble gas analyses

A3.2.1 Equipment

The following descriptions of the noble gas analytical system are summarized from Honda et al. (1993) and Patterson (1992). The noble gas analytical system at the Research School of Earth Sciences, Australian National University, consists of two main parts, the main sample gas handling system (3100 cm^3) and a VG5400 noble gas mass spectrometer (1500 cm^3). The main gas handling system has four major sections: (1) gas extraction; (2) gas purification; (3) the cryogenic charcoal trap; and (4) the standard gas pipette system (Figure A3-1). A quadropole gas analyser (AMETEK M200) is also fitted to the system and is sometimes used to analyse the abundances of CO_2, H_2O and other non-noble gas species.

Main gas handling system

Gas extraction. Gases are extracted from samples via step-heating in a furnace or by crushing under vacuum. (i) The furnace consists of a tantalum crucible and connecting tubes. The tantalum crucible is radiatively heated with a resistive tantalum element housed in a separately pumped vacuum chamber. The furnace is heated via a surrounding heating element made of tantalum sheeting. The heating element is surrounded by radiation shields that are also made of tantalum. To protect the crucible from corrosion by alloying and reacting with the samples, a disposable molybdenum liner was placed in the crucible and samples were heated inside the liner. (ii) The crushing apparatus consists of a tungsten carbide piston with a nickel guide that can be raised and dropped at a rate of approximately 300 strokes/minute by a magnetic field induced in a series of three coils attached to the outside of the vessel (Matsumoto, 1997). Prior to crushing the sample, the crushing vessel was degassed by operating the crusher without a sample for about 30 minutes. The sample and the crusher were then baked under the same conditions as in the stepheating experiments. Procedural blanks were determined by operating the crusher without the samples.

Gas purification. Gases are purified in the section of the line between valves V2 and V10 (Figure A3-1). Purification is achieved using two bulk getters (BG1 and BG2) containing a zirconium alloy, three SAES (R) getters (SAES1, 2 and 3; Milan Italy), a titanium filament flash getter and two activated charcoal traps (CF1 and CF3). To remove active species, the gases were first exposed to BG1, then exposed to BG2 at 300°C. The bulk getters were subsequently brought to room temperature by cooling with compressed air. The gases were then exposed to the SAES getters, one kept at room temperature to absorb hydrogen, and the other operated at approximately 250°C to getter other active gases. This was followed by exposure to a freshly deposited film of titanium from the Ti flash getter and another SAES getter held at room temperature. As a final step in the cleaning process, the tungsten filament of the ionsisation gauge (G1) was kept hot under floating mode (where there is no potential between grid and anode of the gauge) in order to break down high-order hydrocarbons.

Cryogenic charcoal trap. A cryogenic charcoal trap was used to separate the noble gases prior to analysis. In the first set of experiments (see Table A2-1), the cryogenic charcoal trap had a configuration as follows. The cooling head of a double-stage helium expansion refrigerator (model 22, CTI Cryogenics) was brought into contact with the charcoal trap, which consists of two isolated stainless steel chambers. One of these chambers is filled with activated charcoal for the adsorption of noble gases in the extraction system. The second chamber is external to the ultra-high vacuum system and can be used for rapid cooling of the trap by flushing with liquid nitrogen. For temperatures above 60°C, which are necessary to release xenon from the charcoal trap, the helium refrigerator head was physically separated from the trap. In the second set of

experiments, a new cryogenic charcoal head was installed. This cryogenic charcoal assembly had a knife edge-type contact between the charcoal canister and the refrigerator head. This cryogenic assembly collected all noble gases below 30 Kelvin (Honda, 1997).

Two different procedures were used during the course of the experiments in this study owing to the change in the configuration of the cryogenic charcoal trap. In the first set of experiments, which includes the samples with run numbers 2359-2504 (Table A3-1), all the gases including helium were adsorbed onto the charcoal trap at temperatures below 20 K. By means of a heater coil wound around the outside of the trap, the temperature was incrementally increased to successively desorb the noble gases so that they were released into the gas line for analysis. The charcoal trap was heated to 125 K to release helium and neon into the gas extraction line. The gas was expanded into the sections of the gas extraction line between V5 and V12 (Figure A3-1). The gas was split into two fractions (4:1 by volume) by closing the valve between the mass spectrometer and sample handling line. Neon was analysed first (the volume of gas from V9 to V12 was used to analyse neon), then helium (after pumping away the volume of gas between V9 to V12, the second aliquot of gas was expanded from V5 to V12 and was then inlet into the mass spectrometer, and the volume from V9 to V12 was used for helium analysis). Argon (190 K), krypton (250 K)) and xenon (320 K) were then released into the gas line for analysis.

In the second set of analyses (from run 02679 onwards, Table A3-1), the configuration of the charcoal head was changed. Only neon, argon krypton and xenon were adsorbed onto the charcoal trap (minimum T = 35 K), and helium remained in the gas lines. This helium was analysed, and neon was released at 100 K after helium had been pumped away. Argon (190 K), krypton (230 K) and xenon (320 K) were then released successively from the charcoal trap into the gas line for analysis. During baking, the charcoal trap is heated to 523 K (250 °C).

Table A3-1. Samples analysed prior to, and following, a change in cryogenic charcoal trap configuration

Run numbers	Date	all gases adsorbed onto charcoal trap
02359-52	28 Nov 1996	ice-4
02370-73	17 Dec 1996	-1a
02389-94	21 Jan 1997	-2.1a
02405-06	5 Feb 1997	-2.1 crush
02411-27	10 Feb 1997	-2.2a
02429-34	28 Feb 1997	-3a
02448-59	27 Mar 1997	-2.2b
02470-75	18 Apr 1997	-3b
02499-02504	9 May 1997	-1b
		helium not adsorbed onto charcoal
02679-82	1 Dec 97	-11.1
02690-93	9 Dec 97	-10.1
02702-03;06-07	6 Jan 98	-9a
02714-19	15 Jan 98	-9b
02732-35	26 Jan 98	-9c
02786-89	11 Mar 98	-12.1
02805-10	23 Mar 98	-30
02811-12	26 Mar 98	-9d
02817-20	2 Apr 98	-9g1
02828-29	16 Apr 98	-9g2
02832-33	18 Apr 98	-14
02853-56	30 Apr 98	-25
02859-60	7 May 98	-54g
02865-68	17 May 98	-16
02888-91	25 May 98	-32.1
02894-95	28 May 98	-55g
02913-16	4 June 98	18a (discarded)
02919-20	8 June 98	-18g1 (discarded)
02930-33	15 June 98	-34
02936-37	18 June 98	-18g3
02946-49	28 June 98	-19a
02952-53	1 July 98	-47g
02959-62	7 July 98	-32.2g1
02965-68	10 July 98	-18g3p (discarded)
02974-76	16 July 98	-9g2p (discarded)
02979-82	21 July 98	-55 gp (discarded)
02987-88	27 July 98	-32.2g2
03019	18 Aug 98	-2d (nupro crush) (below blank)
03031-34	28 Aug 98	-18b
03039-42	1 Sep 98	-18g2
03049-52	8 Sep 98	-12.2
03059-64	14 Sep 98	-10.2
03075-76	24 Sep 98	-34PX
03082-85	28 Sep 98	-24
03090-93	2 Oct 98	-11.2
03098-03101	14 Oct 98	-19b
03106-09	20 Oct 98	-23a
03114-15	29 Oct 98	-9g3

C. **Standard gas pipette system.** Two noble gas pipettes that are attached to the sample system (Fig. A3-1) were used to deliver aliquots of known volume of standard gases to calibrate instrumental sensitivity and mass discrimination. The Heavy Gas Pipette was prepared from air collected in Canberra. Active gases were removed using hot titanium bulk getters. The amounts of ^{20}Ne, ^{40}Ar, ^{84}Kr and ^{132}Xe in one aliquot of the Heavy Gas pipette are 2.7×10^{-9}, 1.5×10^{-6}, 1.1×10^{-10}, and 3.8×10^{-12} cm^3STP, respectively. These amounts are based on Boyle's Law after correction for barometric pressure, temperature and relative humidity when the standard gases were collected. The Yellowstone Pipette contains He and Ne collected from the Mud Volcano area of Yellowstone National Park, Montana, U.S.A. One aliquot of Yellowstone gas contains 1.9×10^{-7} cm^3STP of ^4He. The Yellowstone pipette is used as the primary standard for determining the He mass discrimination factor.

Figure A3-1, following page. Schematic outline of the RSES, ANU noble gas facility, showing the arrangement of the vacuum components. QMS – quadrupole mass spectrometer, MECH PUMP – mechanical roughing pump, SORP PUMP – sorption pump activated by immersion in liquid nitrogen, PG – Pirani vacuum gauge, IG – ionisation vacuum gauge, BG – titanium and zirconium foil bulk getters, CF – charcoal finger, (NO) normally open valve, (NC) normally closed valve.

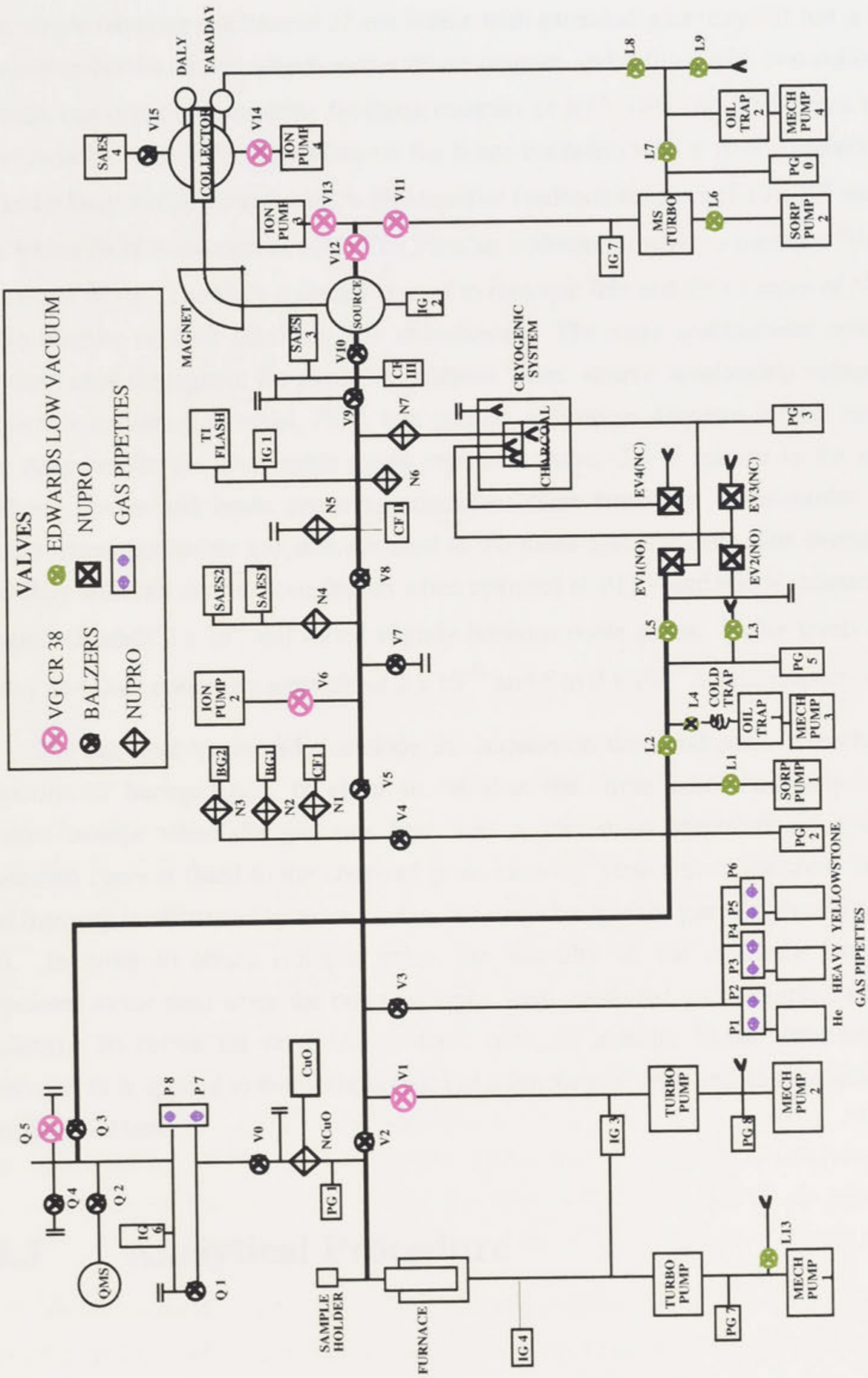
VALVES
VG CR 38
BALZERS
NUPRO
EDWARDS LOW VACUUM
NUPRO
GAS PIPETTES
DALY
FARADAY
COLLECTOR
MAGNET
SOURCE
CRYOGENIC SYSTEM
CHARCOAL
TI FLASH
SAES 1
SAES2
SAES 3
SAES 4
ION PUMP 2
ION PUMP 3
ION PUMP 4
MS TURBO
SORP PUMP 1
SORP PUMP 2
OIL TRAP 1
OIL TRAP 2
MECH PUMP 1
MECH PUMP 2
MECH PUMP 4
COLD TRAP
TURBO PUMP
TURBO PUMP
SAMPLE HOLDER
FURNACE
QMS
CuO
NCuO
CF I
CF II
CF III
EV1(NO)
EV2(NO)
EV3(NC)
EV4(NC)
He
HEAVY YELLOWSTONE GAS PIPETTES

Noble gas mass spectrometer

Gases were analysed using a VG5400 mass spectrometer. This is a magnetic sector, single focusing machine of 27 cm radius with extended geometry. It has a Nier-type electron bombardment source with a source magnet, and is fitted with two collectors: a Faraday cup collector (amplifier feedback resistors of 10^{10}, 10^{11} and 10^{12} ohms which can be switched externally depending on the beam intensity) with a fixed resolution of 230; and a Daly multiplier collector, with amplifier feedback resistors of 10^{7}, 10^{8} and 10^{9} ohms with a fixed resolution of 600. The Faraday collector is used to measure ^{4}He and the isotopes of Ar. The Daly collector is used to measure ^{3}He and the isotopes of Ne, Kr and Xe because of their relatively low abundances. The mass spectrometer operating conditions used throughout the period of analyses were: source accelerating voltage, 4.5 kV; electron ionisation potential, 75 V; trap current, 400 micro Amperes for He and 200 micro Amperes for the other noble gases; repeller voltage, -3.4 V relative to the source chamber. Focus and beam centering conditions were tuned up to maximise beam intensity when each noble gas was admitted to the mass spectrometer. The overall gain of the Daly collector and photomultiplier when operated at 10 kV and 960 V, respectively, was approximately 2×10^{6}, and varied slightly between noble gases. Noise levels of the Faraday and Daly collectors were about 2×10^{-16} and 6 to 9×10^{-19} Amps, respectively.

The data that are recorded include the acquisition time and peak intensity after subtraction of background. In order to calculate the "time zero" intensity of the reference isotope when the gas was first inlet to the mass spectrometer, a double exponential curve is fitted to the observed peak intensity versus time spectrum and the initial intensity is calculated by extrapolating the curve back to the gas inlet time (i.e., time zero). In order to obtain isotopic ratios, the intensity of the reference isotope is interpolated to the time when the other isotopes were measured and isotopic ratios are calculated. To obtain the time zero isotopic ratio, an average, linear, exponential or polynomial fit is applied to the isotopic ratios as a function of time, and extrapolated back to the gas inlet time.

A3.3 Analytical Procedure

A3.3.1 Sample loading, baking and outgassing prior to analysis

Between 3 and 6 grams of sample were split into aliquots of about 0.8 grams each and were individually wrapped in tin foil that had been previously rinsed in acetone

and dried in an oven. For the run numbers between 02349 – 02504, up to three samples were loaded, but it was found that the samples did not melt thoroughly (samples *ice-1a, -2.1a, -2.2b, -10.2 and -11.2* did not melt completely) so that in subsequent runs (run numbers > 02679), only one sample was loaded into the sample turret (a carousel with ten holes in it that is attached to the top of the extraction furnace). Samples were sequentially introduced into the furnace by rotating the carousel to align the hole with the cylindrical furnace and allowing the foil balls to drop. A new molybdenum liner was installed within the tantalum crucible each time the vacuum was broken to change samples. The samples were baked at about 150°C, whereas the remaining all-metal extraction and purification system was baked at 250°C for at least 36 hours. After baking the noble gas extraction system and prior to running blanks, the furnace (tantalum tube and molybdenum liner), was outgassed at 1850°C for up to one hour.

A3.3.2 Gas extraction

Gases were extracted from the samples by step-heating or crushing them under vacuum. The analytical blanks for these procedures are described below.

Blanks

Step-heating experiments

Samples were step-heated because previous studies have shown that atmospheric gases are mainly released in the low temperature steps (≤ 900 °C), and mantle components in the high temperature steps (> 900°C). Prior to sample analysis, the following procedure was used. After baking the noble gas extraction system and prior to running blanks, the furnace (tantalum tube and molybdenum liner), was outgassed at 1850°C for up to one hour. Blanks run at 1800°C were applied to both 1800°C and 900°C sample runs. Using the 1800°C blank for the 900°C step did not result in a significant difference in the isotopic ratios of the samples following blank corrections. The range in the size of 1800°C blanks prior to olivine runs are as follows: $^{4}He = 4 \times 10^{-12}$ to 8×10^{-10} cm^3STP; $^{20}Ne = 2 \times 10^{-12}$ to 6×10^{-11} cm^3STP; $^{40}Ar = 2 \times 10^{-11}$ to 8×10^{-8} cm^3STP; ^{84}Kr 2×10^{-13} to 3×10^{-11} cm^3STP; $^{132}Xe = 1.2 \times 10^{-14}$ to 5.3×10^{-13} cm^3STP (Table A3-2). Because the gas concentrations in glasses are substantially higher than in olivine, less time was spent outgassing the furnace prior to glass runs than prior to olivine runs. Blanks prior to step-heating glasses were run at 1600°C and are within the same range as the 1800°C blanks.

In most blank measurements, the ^{3}He beam was below detection levels so the $^{3}He/^{4}He$ ratio was assumed to be isotopically atmospheric ($^{3}He/^{4}He = 1.4 \times 10^{-6}$). The neon isotopic ratios of the blanks varied depending on the abundance of gas (see Data Filtering section). The large observed range in the neon isotopic ratios are likely to be analytical artefacts and atmospheric neon isotopic ratios were also assumed for the neon

blank corrections. Similar behaviour to that seen for neon was also observed in the blank ratios for argon, krypton and xenon ratios.

Crushing experiments

Crushing experiments are useful to assess the difference between gases trapped in inclusions or vesicles versus those in the matrix of glasses or minerals, particularly where a cosmogenic component may be present in the matrix. The crusher was run for 5 minutes at 300 strokes/minute for both samples and blanks. The range in blanks for the crushing experiments are: $^{4}He = 2 \times 10^{-11}$ to 8×10^{-10} cm^3STP; $^{20}Ne = 4 \times 10^{-12}$ to 6×10^{-11} cm^3STP; $^{40}Ar = 1 \times 10^{-8}$ to 4×10^{-8}; $^{84}Kr = 5 \times 10^{-13}$ to 1.1×10^{-12}; $^{132}Xe = 3 \times 10^{-14}$ to 8×10^{-14} (Table A3-2). Following crushing, the sample chamber of the crusher was heated to 100°C in order to drive off re-adsorbed gases from the freshly exposed sample surface. After the gas extraction, the sample was recovered and sieved; the crushed sample yield was taken as the fraction less than <150 μm, which was typically about 50% of the total sample mass loaded.

Table A3-2. Measured analytical banks

Blank Run no.	For sample ice-	Blank T°C	^{4}He, cm^{3}STP ($1x10^{-11}$)	^{20}Ne, cm^{3}STP ($1 x 10^{-11}$)	Daly, ^{36}Ar, cm^{3}STP, ($1x10^{-11}$)	Faraday, ^{40}Ar cm^{3}STP, ($1x10^{-8}$)	^{84}Kr, cm^{3}STP, ($1x10^{-12}$)	^{132}Xe, cm^{3}STP, ($1x10^{-14}$)
2347	-4	1800	5.8	0.7	2.5	2.5	5.4	6.9
2366	-1a	1800	9.5	1.2	5.0	5.0	5.1	8.9
2368	-1a	900	n.a.	0.4	0.8	0.8	0.6	1.6
2387	-2.1a	1800	12.2	0.8	8.2	0.8	2.1	3.0
2407	-2.2a	1800	3.8	0.4	1.0	1.0	0.7	1.8
2409	-2.2a	900	0.5	0.4	0.4	0.4	0.5	1.6
2428	-3a	1800	6.0	0.4	n.a.	4.0	4.1	17.3
2446	-2.2b	1800	9.3	0.2	0.8	0.7	1.2	2.1
2466	-3b	1800	4.9	1.0	0.1	0.6	13.6	5.7
2468	-3b	900	7.9	0.4	0.3	0.3	29.6	4.2
2495	-1b	1800	6.4	0.4	0.6	0.6	3.8	8.1
2497	-1b	900	8.7	0.4	0.6	0.6	0.6	n.a.
2677	-11.1	1800	2.1	1.0	0.5	0.5	2.5	18.4
2688	-10.1	1800	1.0	0.9	1.1	1.0	5.2	18.9
2700	-9a	1800	3.7	3.5	8.0	8.3	5.1	
2712	-9b	1800	0.6	2.8	2.4	2.3	11.2	29.1
2730	-9c	1800	3.3	1.1	1.3	1.2	7.2	10.9
2785	-12.1	1800	6.8	2.2	1.2	1.1	0.2	1.2
2803	-30	1800	2.1	1.3	0.7	0.6	1.4	2.1
2815	-9g1	1600	3.0	2.6	2.6	2.4	9.0	10.2
2826	-9g2	crush	3.9	0.8	1.1	1.0	0.9	2.9
2830	-14	1800	3.8	1.0	1.5	1.3	0.2	2.1
2849	-54g	crush	28.6	2.7	0.0	2.1	0.4	7.6
2851	-25	1800	3.2	1.4	1.3	1.2	3.9	7.6
2863	-16	1800	4.6	1.7	1.2	1.1	4.0	5.1
2886	-32.1a	1800	2.5	1.6	0.6	0.6	1.6	4.3
2892	-55g	crush	2.2	0.9	1.7	1.5	1.2	3.7
2917	-18g1	crush	14.1	2.0	1.6	1.4	2.0	3.7
2928	-34	1800	26.5	2.0	1.3	1.1	2.4	4.8
2934	-18g3	crush	70.3	2.5	2.3	1.9	5.6	6.1
2944	-19a	1800	5.9	0.8	0.5	0.4	1.7	5.1
2950	-47 g	crush	6.4	1.1	1.2	1.1	2.1	5.3
2957	-32.2g1	1800	4.4	0.9	0.8	0.8	3.6	6.0
2985	-32.2g2	crush	7.7	0.4	1.3	1.1	0.5	4.3
3029	-18b	1800	3.3	0.6	0.6	0.5	1.3	20.8
3037	-18g2	1800	8.8	0.8	0.7	0.6	1.8	4.3
3047	-12.2	1800	1.7	0.5	0.8	0.7	1.7	4.3
3057	-10.2	1800	1.4	0.7	0.8	0.8	1.5	5.4
3073	-34PX	crush	5.4	1.0	1.2	1.1	3.0	4.5
3080	-24	1800	1.4	0.5	1.2	1.0	2.5	6.6
3088	-11.2	1800	1.0	0.8	1.9	1.7	1.6	4.0
3096	-19b	1800	0.8	0.5	0.5	0.8	4.7	21.6
3104	-23a	1800	0.4	0.5	n.a.	0.002	9.9	17.7
3112	-9g3	crush	16.0	0.8	0.02	1.0	3.1	5.6

A3.3.3 Corrections to the measured data

Interference corrections

The resolution of the Daly collector on the VG5400 mass spectrometer is 600, hence corrections are needed for interferences from peaks that require resolution greater than 600 for separation. In particular, corrections need to be made for $^{40}Ar^{++}$ and $H_2{}^{18}O^+$ on ^{20}Ne; CH_2CO^{++} on ^{21}Ne, and $CO_2{}^{++}$ on ^{22}Ne. For example, to determine the interferences of $^{40}Ar^{++}$ and $H_2{}^{18}O^+$ on the ^{20}Ne peak, the ratio of double to single-charged ^{40}Ar (i.e., $^{40}Ar^{++}/^{40}Ar^+$) and heavy to light water ($H_2{}^{18}O^+/H_2{}^{16}O^+$) produced in the mass spectrometer were determined. During measurement of the neon isotopes, the $^{40}Ar^+$ and H_2O^{16+} peaks were monitored, and the size of the $^{40}Ar^{++}$ and $H_2{}^{18}O^+$ interferences on the ^{20}Ne peak were calculated from the $^{40}Ar^{++}/^{40}Ar^+$ and $H_2{}^{18}O^+/H_2{}^{16}O^+$ ratios, respectively. A similar process was followed to determine interferences to the ^{22}Ne peak by $CO_2{}^{++}$ by determining the $CO_2{}^{++}/CO_2{}^+$ ratio and monitoring of the $CO_2{}^+$ peak. On average, the contributions of the $^{40}Ar^{++}$, $H_2{}^{18}O^+$, $CHCO^{++}$ and $CO_2{}^{++}$ interferences in the samples from this study were equal to 1.3%, 0.1%, 0.5% and 3%, respectively.

Sensitivities and mass discrimination

The sensitivities and mass discrimination corrections for the noble gases were calibrated at regular intervals, normally at the end of an analytical suite immediately prior to breaking the vacuum to change samples. This was accomplished by analysing aliquots of known volume and isotopic composition form the standard gas pipettes. Helium was calibrated using the Yellowstone (YS) Pipette, and the heavier gases were calibrated using the Heavy Gas pipette. The mass discrimination factor is defined as the isotopic ratio of the standard divided by the measured isotopic ratio of the standard. The mass discrimination factors for helium and neon as applied to each analytical run are listed in Table A3-3. These values changed with time; the mass discrimination factor for the $^3He/^4He$ ranged from 2.0 ± 0.2 to 1.7 ± 0.1; $^{21}Ne/^{20}Ne$ from 1.018 ± 0.007 to 0.995 ± 0.005 and $^{22}Ne/^{20}Ne$ from 1.028 ± 0.008 to 1.021 ± 0.008. The helium sensitivity increased from 1.33×10^{-5} A/cm^{3}STP to ca. 3×10^{-5} A/cm^{3}STP when helium was no longer adsorbed onto the charcoal trap (Table A3-1). In contrast, the mass discrimination factors and sensitivities for the isotopes of argon, krypton and xenon remained relatively constant over a long time period, as shown in Table A3-4 for n = 52 analyses of the heavy gas pipette.

Neon isotope analysis

Possible pressure effects on the neon mass discrimination factors were examined by measuring neon isotopic ratios in air neon stored in a gas pipette (one aliquot contains

2.7×10^{-9} cm^3STP of ^{20}Ne) by expansion to reduce the amounts analyzed by two orders of magnitude. The neon mass discrimination factors were constant (within ~1 %) over this pressure range. Thus, no corrections for pressure effects needed to be applied to neon isotope ratios measured on gases released from the samples in this study.

Table A3-3. Helium and neon sensitivities and mass discrimination factors

Sample ice-	YS Pipette Number	$^3He/^4He$ Disc. factor	Helium sensitivity A/cm^3STP $1x10^{-5}$	Heavy Gas Pipette Number	$^{21}Ne/^{22}Ne$ Disc. factor	$^{22}Ne/^{20}Ne$ Disc. factor	Neon sensitivity A/cm^3STP $1x10^{-5}$
-4	342-362	2.03 ± 0.23	1.33 ± 0.13	362-369	1.018 ± 0.007	1.027 ± 0.008	5.3 ± 0.2
-1a	342-362	"	"	362-369	"	"	"
-2.1a	342-362	"	"	362-369	"	"	"
-2.1cr	342-362	"	"	362-369	"	"	"
-2.2a	342-362	"	"	362-369	"	"	"
-3a	342-362	"	"	362-369	"	"	"
-2.2b	342-362	"	"	362-369	"	"	"
-3b	342-362	"	"	362-369	"	"	"
-1b	342-362	"	"	362-369	"	"	"
-11.1	404-421	1.95 ± 0.23	3.40 ± 0.20	386-404	1.012 ± 0.005	1.024 ± 0.012	4.7 ± 0.9
-10.1	404-421	"	"	386-404	"	"	"
-9a	404-421	"	"	386-404	"		"
-9b	422-430	1.25 ± 0.08	3.36 ± 0.33	386-404	"	"	"
-9c	422-430	"	"	386-404	"	"	"
-12.1	422-430	"	"	386-404	"	"	"
-30	431-436	1.24 ± 0.09	3.52 ± 0.08	386-404	"	"	"
-9d	431-436	"	"	386-404	"	"	"
-9g1	431-436	"	"	386-404	"	"	"
-9g2	431-436	"	"	386-404	"	"	"
-14	431-436	"	"	386-404	"	"	"
-25	443-449	1.9 ± 0.16	3.68 ± 0.17	386-404	"	"	"
-54	443-449	"	"	386-404	"	"	"
-16	443-449	"	"	405-420	0.995 ± 0.005	1.021 ± 0.008	5.5 ± 0.5
-32.1	451-469	1.71 ± 0.21	3.52 ± 0.17	405-420	"	"	"
-55g	451-469	"	"	405-420	"	"	"
-18g3	451-469	"	"	405-420	"	"	"
-34	451-469	"	"	405-420	"	"	"
-19a	451-469	"	"	405-420	"	"	"
-47g	451-469	"	"	405-420	"	"	"
-32.2g1	451-469	"	"	405-420	"	"	"
-32.2g2	451-469	"	"	405-420	"	"	"
-2d	451-469	"	"	405-420	"	"	"
-18b	451-469	"	"	405-420	"	"	"
-18g2	451-469	"	"	405-420	"	"	"
-12.2	451-469	"	"	405-420	"	"	"
-10.2	470-481	1.71 ± 0.14	3.52 ± 0.20	405-420	"	"	"
-34px	470-481	"	"	405-420	"	"	"
-24	470-481	"	"	405-420	"	"	"
-11.2	470-481	"	"	405-420	"	"	"
-19b	470-481	"	"	405-420	"	"	"
-23a	470-481	"	"	405-420	"	"	"
-9g3	470-481	"	"	405-420	"	"	"

Table A3-4. Argon, krypton and xenon sensitivities and mass discrimination factors

ratio	pipette numbers	Run number	Discrimination factor		Sensitivity ($1x10^{-5}$)
Argon	361-369	2336- 2505			
$^{36}Ar/^{40}Ar$			1.015	± 0.003	17 ± 2
$^{38}Ar/^{40}Ar$			1.005	± 0.002	
$^{38}Ar/^{36}Ar$ Daly			1.007	± 0.003	
	378-403	2528-2839			
$^{36}Ar/^{40}Ar$			1.016	± 0.005	22 ± 3
$^{38}Ar/^{40}Ar$			1.007	± 0.004	
$^{38}Ar/^{36}Ar$ Daly			0.997	± 0.008	
	404-420	2844-3119			
$^{36}Ar/^{40}Ar$			1.016	± 0.003	25 ± 2
$^{38}Ar/^{40}Ar$			1.007	± 0.002	
$^{38}Ar/^{36}Ar$ Daly			0.996	± 0.004	
Krypton	361-369	2336- 2505			
$^{80}Kr/^{84}Kr$			0.967	± 0.011	16 ± 2
$^{82}Kr/^{84}Kr$			0.981	± 0.003	
$^{83}Kr/^{84}Kr$			0.991	± 0.003	
$^{86}Kr/^{84}Kr$			1.015	± 0.001	
	378-403	2528-2839			
$^{80}Kr/^{84}Kr$			0.978	± 0.007	13 ± 3
$^{82}Kr/^{84}Kr$			0.990	± 0.003	
$^{83}Kr/^{84}Kr$			0.995	± 0.002	
$^{86}Kr/^{84}Kr$			1.008	± 0.004	
	404-420	2844-3119			
$^{80}Kr/^{84}Kr$			0.979	± 0.004	18 ± 1
$^{82}Kr/^{84}Kr$			0.988	± 0.003	
$^{83}Kr/^{84}Kr$			0.996	± 0.002	
$^{86}Kr/^{84}Kr$			1.010	± 0.002	
Xenon	361-369	2336-2505			
$^{124}Xe/^{132}Xe$			0.958	± 0.055	43 ± 1
$^{126}Xe/^{132}Xe$			1.008	± 0.048	
$^{128}Xe/^{132}Xe$			0.979	± 0.016	
$^{129}Xe/^{132}Xe$			0.987	± 0.014	
$^{130}Xe/^{132}Xe$			0.987	± 0.017	
$^{131}Xe/^{132}Xe$			0.989	± 0.010	
$^{134}Xe/^{132}Xe$			0.999	± 0.006	
$^{136}Xe/^{132}Xe$			1.008	± 0.007	
	378-403	2528-2839			
$^{124}Xe/^{132}Xe$			0.994	± 0.041	43 ± 1
$^{126}Xe/^{132}Xe$			1.024	± 0.063	
$^{128}Xe/^{132}Xe$			0.989	± 0.008	
$^{129}Xe/^{132}Xe$			0.994	± 0.005	
$^{130}Xe/^{132}Xe$			0.994	± 0.005	
$^{131}Xe/^{132}Xe$			0.991	± 0.003	
$^{134}Xe/^{132}Xe$			1.002	± 0.004	
$^{136}Xe/^{132}Xe$			1.004	± 0.005	
	404-420	2844-3119			
$^{124}Xe/^{132}Xe$			0.965	± 0.049	39 ± 1
$^{126}Xe/^{132}Xe$			0.988	± 0.054	
$^{128}Xe/^{132}Xe$			0.991	± 0.006	
$^{129}Xe/^{132}Xe$			0.993	± 0.003	
$^{130}Xe/^{132}Xe$			0.993	± 0.005	
$^{131}Xe/^{132}Xe$			0.997	± 0.005	
$^{134}Xe/^{132}Xe$			1.002	± 0.005	
$^{136}Xe/^{132}Xe$			1.007	± 0.005	

Data filtering

The helium and neon abundances measured in the gas released from the samples are well above the detection limits calculated from the sensitivity and collector noise of the mass spectrometer (detection limits: helium = 3×10^{-14} cm^3STP; neon = 2×10^{-14} cm^3STP; argon = 1×10^{-12} cm^3STP; krypton = 6×10^{-15} cm^3STP; xenon = 2×10^{-15} cm^3STP). The quality of the data was further evaluated by plotting the isotopic ratio versus the absolute abundance of gas in the samples prior to blank correction. Samples with helium amounts below 3×10^{-9} cm^3STP ^4He, and 7×10^{-14} cm^3STP ^3He were discarded because there was a change in the measured $^3He/^4He$ ratios from relatively constant values above these gas amounts, but a marked increase at lower amounts. This relates to an increase in the uncertainties of the measurements at low gas amounts. The neon data were filtered to discard samples with measured amounts of ^{22}Ne (e.g., before blank subtraction) below 1.5×10^{-12} cm^3STP, and ^{21}Ne amounts below 8×10^{-14} cm^3STP, because the isotopic ratios were unreasonably scattered below these gas amounts. The argon, krypton and xenon data were filtered in a similar fashion to the helium and neon data. The values below which data were discarded (listed as "b.c." or below cut-off in Tables 5-1 and 5-2), for argon, krypton and xenon are: $^{36}Ar = 3 \times 10^{-11}$ cm^3STP, $^{84}Kr = 5 \times 10^{-12}$ cm^3STP, and $^{130}Xe = 5 \times 10^{-14}$ cm^3STP, respectively.

Blank Corrections

Following interference corrections, correction for mass discrimination and data filtering, the noble gas data were blank-corrected using the measured blank values in Table A3-2. The blank volumes are expressed as a fraction of the total sample gas volume in Table A3-5. A 10% uncertainty was assigned to all blanks. The blank level expressed as a fraction of the total gas released is shown in Table A3-5. Helium constituted 0.001% to 2%, neon 0.2 to 14%, argon 0.3 to 80%, krypton 2 to 47% and xenon 0.1 to 40% of the total gas released.

Table A3-5. Total gas released from Icelandic samples, and blank level as fraction of total gas.

Blank Run no.	For sample no. -ice	^{4}He cm^3STP $1x10^{-9}$	fraction blank	^{20}Ne, cm^3STP $1x10^{-12}$	fraction blank	^{40}Ar cm^3STP $1x10^{-8}$	fraction blank	^{84}Kr cm^3STP $1x10^{-11}$	fraction blank	^{132}Xe cm^3STP $1x10^{-13}$	fraction blank
2366	-1a	19	0.0051	66	0.18	6.07	0.452	2.7	0.19	21	0.043
2495	-1b	28	0.0023	64	0.06	14.59	0.040	2.6	0.15	169	0.005
2387	-2.1a	13	0.0094	215	0.04	19.19	0.040	7.1	0.03	46	0.007
2407	-2.2a	10	0.0039	266	0.02	68.56	0.014	13.0	0.01	126	0.001
2446	-2.2b	19	0.0050	62	0.03	2.05	0.254	1.0	0.11	97	0.002
2428	-3a	b.c.	–	128	0.03	6.86	0.368	b.b.	–	b.b.	--
2466	-3b	b.c.	–	49	0.20	3.18	0.159	b.b.	–	b.c.	--
2347	-4	2	0.0376	65	0.11	14.08	0.151	3.1	0.18	32	0.022
2700	-9a	44	0.0008	159	0.22	31.43	0.209	b.b.	–	14	0.382
2712	-9b	48	0.0001	79	0.35	1.17	0.663	b.b.	–	7	0.397
2730	-9c	33	0.001	b.c.	–	1.13	0.514	b.b.	–	b.c.	--
9999	-9d	b.c.	–	b.c.	–	b.c.	–	b.c.	–	b.c.	--
2815	-9g1	1890	$1x10^{-5}$	758	0.03	53.54	0.043	3.6	0.25	33	0.031
2826	-9g2	3649	$1x10^{-5}$	1145	0.01	310.86	0.003	3.1	0.03	11	0.027
3112	-9g3	1712	0.0001	2434	0.003	325.44	0.003	8.1	0.04	24	0.023
2688	-10.1	20	0.0005	142	0.06	1.17	0.460	1.5	0.35	36	0.053
3057	-10.2	29	0.0005	94	0.07	1.73	0.316	0.8	0.18	32	0.017
2677	-11.1	12	0.0018	70.1	0.14	1.77	0.220	b.c.	–	23	0.081
3088	-11.2	41	0.0002	69	0.12	0.42	0.803	0.3	0.47	b.c.	--
2785	-12.1	b.c.	–	287	0.08	4.00	0.216	0.1	0.16	b.c.	--
3047	-12.2	6	0.0026	503	0.01	5.33	0.116	2.7	0.06	114	0.004
2830	-14	3	0.0112	116	0.09	2.50	0.342	b.c.	–	b.c.	--
2863	-16	70	0.0007	241	0.07	3.67	0.231	1.1	0.37	104	0.005
3029	-18b	35	0.0009	676	0.01	1.63	0.235	0.9	0.15	43	0.049
3037	-18g2	194	0.0046	3279	0.002	9.17	0.061	2.7	0.07	21	0.021
2934	-18g3	62	0.0129	750	0.03	8.43	0.184	b.c.	–	b.c.	--
2944	-19a	59	0.0010	713	0.01	43.51	0.009	8.7	0.02	462	0.001
3096	-19b	75	0.0001	98.6	0.05	b.c.		b.c	–	b.c.	--
3104	-23a	b.c.	–	144	0.03	0.64	0.56	1.5	0.64	32	0.055
3080	-24	b.c.	–	b.c.	–	1.78	0.360	b.c.	–	5	0.140
2851	-25	56	0.0006	308	0.05	2.62	0.314	1.2	0.32	50	0.015
2803	-30	43	0.0005	216	0.06	2.67	0.184	0.6	0.22	7	0.032
2886	-32.1a	94	0.0003	971	0.02	3.49	0.147	0.7	0.23	24	0.018
2957	-32.2g1	120	0.0004	2409	0.004	48.93	0.016	6.8	0.05	24	0.025
2985	-32.2g2	18	0.0043	363	0.01	25.15	0.042	1.0	0.05	b.c.	--
2928	-34	14	0.0189	141	0.14	2.56	0.300	b.c.	–	b.c.	--
3073	-34PX	b.c.	–	b.b.	–	4.99	0.181	b.c.	–	b.c.	--
2950	-47 g	270	0.0002	660	0.02	4.50	0.196	b.c.	–	b.c.	--
2849	-54g	18	0.0156	275	0.10	19.10	0.099	0.8	0.05	b.c.	--
2892	-55g	22	0.0010	171	0.05	18.86	0.074	1.0	0.12	b.c.	--

A3.4 Error propagation

For the interference corrections, blank subtractions and reference isotope changes, algorithms were used to keep track of correlated errors in isotopic ratios (Honda et al., 1993). To demonstrate how errors associated with such corrections are propagated, neon

data obtained from *ice-9g2* are used in the following example. The measured and unprocessed $^{21}Ne/^{20}Ne$ and $^{22}Ne/^{20}Ne$ ratios (reference isotope: ^{20}Ne) were 0.002787 ± 0.000027 (± 0.9%) and 0.092165 ± 0.000068 (± 0.07%), respectively ($^{20}Ne/^{22}Ne$ = 10.85; $^{21}Ne/^{22}Ne$ = 0.0302). The quoted errors are one standard deviation, which include uncertainties in regression calculation of time-zero extrapolation to gas inlet time. The fractions from (1) CO_2^{++}, (2) CH_2CO^{++}, (3) $^{40}Ar^{++}$ and (4) $H_2{}^{18}O^+$ subtracted from the measured amounts of the neon isotopes in *ice-9g2* were: (1) $4.5 \times 10^{-3} \pm 0.5 \times 10^{-3}$; (2) $1.8 \times 10^{-4} \pm 0.4 \times 10^{-4}$; (3) $1.4 \times 10^{-3} \pm 0.3 \times 10^{-3}$; and (4) $1.1 \times 10^{-4} \pm 0.4 \times 10^{-4}$, respectively. After the corrections for interferences and mass discrimination (uncertainties determined by repeated analysis of the air neon from the gas pipette), the $^{21}Ne/^{20}Ne$ and $^{22}Ne/^{20}Ne$ ratios were 0.002826 ± 0.000032 (1.1%) and 0.0937 ± 0.0011 (1.2%) (for reference isotope $^{20}Ne = 1.96 \pm 0.09 \times 10^{-9}$ cm^3STP/g, $^{20}Ne/^{22}Ne$ = 10.67 and $^{21}Ne/^{22}Ne$ = 0.0302). The amount of ^{20}Ne in the blank was 7.86×10^{-12} cm^3STP (± 10%) and atmospheric isotopic ratios were used for blank subtraction. After the blank correction the $^{22}Ne/^{20}Ne$ ratio was equal to 0.0931 ± 0.0011 and $^{21}Ne/^{20}Ne$ = 0.002829 ± 0.000031; for reference isotope $^{20}Ne = 1.94 \pm 0.09 \times 10^{-9}$ cm^3STP/g, the $^{20}Ne/^{22}Ne$ and $^{21}Ne/^{22}Ne$ ratios are 10.74 ± 0.07 and 0.0304 ± 0.0005, as listed in Table 5-1. In addition to the standard corrections for mass interferences, the ^{20}Ne peak was scanned for possible interferences from $H^{19}F$ associated with cleaning the samples in HF. Although the $^{40}Ar^{++}$ peak could be seen as a small flat peak overlapping part of the ^{20}Ne peak, there was no evidence for interference from HF. Mass 19 was also scanned for possible evidence of F, but no peak was visible.

A3.5 Interferences on ^{36}Ar and ^{38}Ar for measurements performed on the Daly collector

The signal to background ratio for the measurements of the $^{38}Ar/^{36}Ar$ ratio on the Faraday are larger than those measured on the Daly collector. This means that measurements on the Daly collector are more susceptible to problems caused by small interference peaks from hydrocarbons that may be present in the system. During field-mass scans, small interference peaks (in the range of 0.1 volt for a scan performed for run number 02977) were seen on the ^{36}Ar peak (probably W^{3+} or $W4^+$), and on the ^{38}Ar peak (possibly $^{12}C_3H_2$). These interference peaks were not removed even when the gas was pumped out of the mass spectrometer during the field-mass scan. When the ratio of ^{38}Ar to $^{12}C_3H_2$ is relatively small, there is a chance that the $^{12}C_3H_2$ peak is measured instead of the ^{38}Ar peak. The small interference peaks on mass ^{38}Ar are probably the

explanation for why the $^{38}Ar/^{36}Ar$ ratios measured on the Daly collector are systematically higher than those measured on the Faraday for a given amount of ^{36}Ar (compare Figures A3-2 and A3-3). Owing to these problems with interference peaks, the $^{38}Ar/^{36}Ar$ ratios were not used in this study, and the data are instead only shown in Table A3-6.

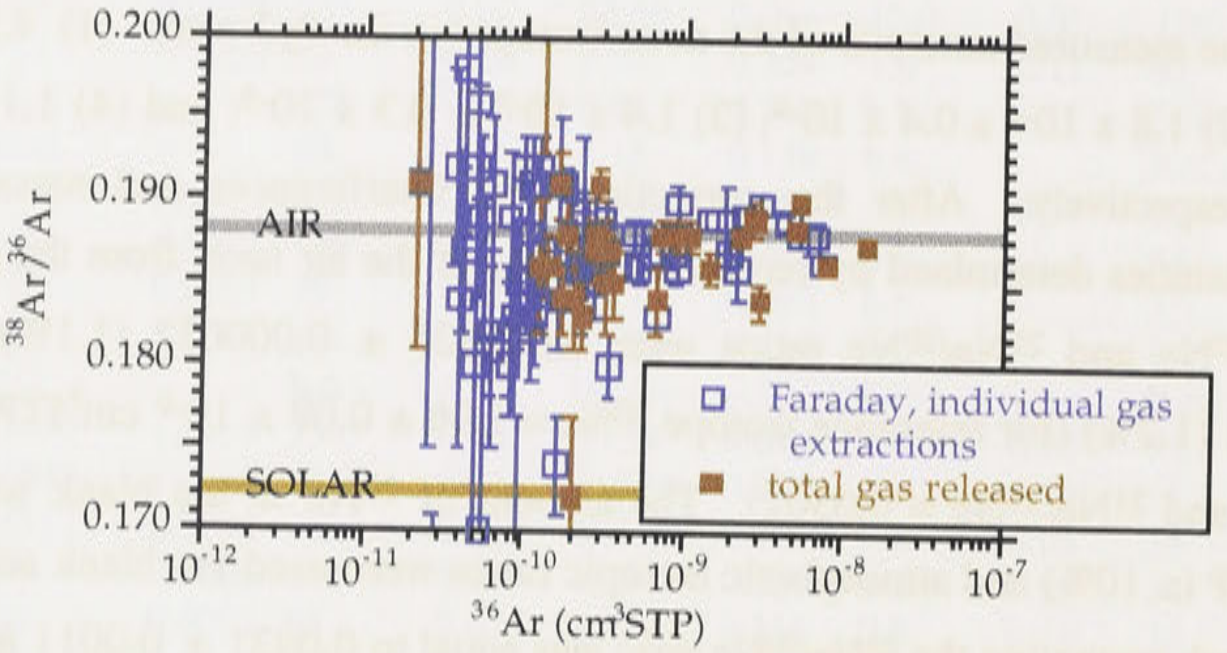

Figure A3-2. $^{38}Ar/^{36}Ar$ versus ^{36}Ar (cm^3STP) of individual gas extractions and total gas released measured on the Faraday collector. At ^{36}Ar volumes of less than 4×10^{-9} cm^3STP some of the $^{38}Ar/^{36}Ar$ ratios are above or below the atmospheric ratio by more than one sigma uncertainty. At lower gas volumes, the deviation of the $^{38}Ar/^{36}Ar$ ratio from the atmospheric ratio increases, as do the uncertainties.

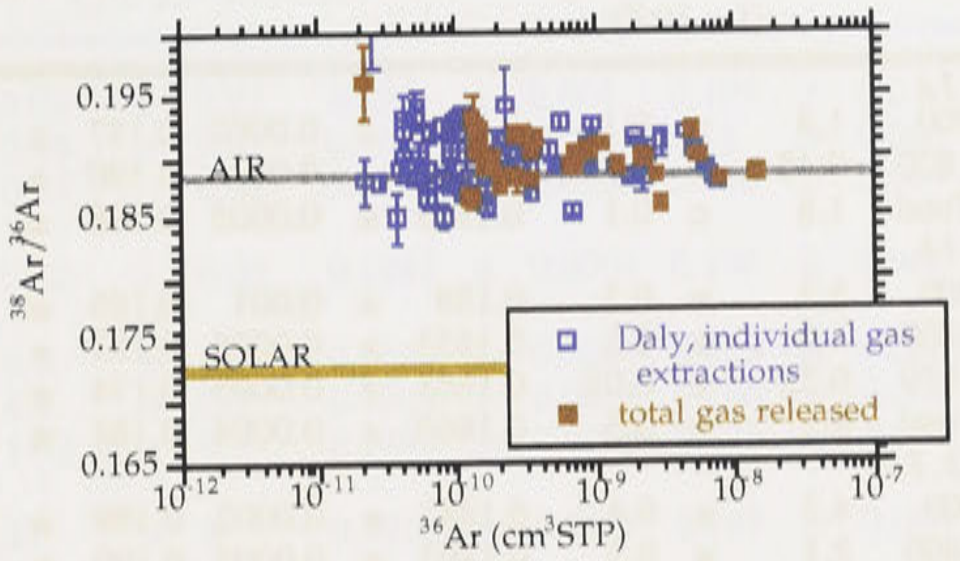

Figure A3-3. $^{38}Ar/^{36}Ar$ versus ^{36}Ar (cm^3STP/g) of individual gas extractions and total gas released measured on the Daly collector. Even at relatively high gas volumes of greater than 1×10^{-9} cm^3STP, the $^{38}Ar/^{36}Ar$ ratios are higher than the atmospheric ratio by more than one sigma uncertainty. At lower gas volumes of 4×10^{-10} cm^3STP some of the data lie below, and other data lie above, the $^{38}Ar/^{36}Ar$ ratio and are significantly different from the atmospheric ratio by more than one sigma uncertainty.

Table A3-6. Poor quality argon data measured on the Daly and Faraday collectors

T, °C	^{36}Ar cm^{3}STP/g (1×10^{-10})	$^{38}Ar/^{36}Ar$ Daly	$^{38}Ar/^{36}Ar$ Faraday
-1a			
900	1.4 ± 0.1	0.1898 ± 0.0002	0.187 ± 0.001
1800	0.45 ± 0.04	0.194 ± 0.003	0.190 ± 0.004
Total	1.8 ± 0.1	0.1903 ± 0.0005	0.188 ± 0.001
-1b			
900	3.2 ± 0.3	0.188 ± 0.001	0.186 ± 0.002
1800	1.0 ± 0.1	0.1853 ± 0.0005	0.183 ± 0.001
1850	0.25 ± 0.02	0.1865 ± 0.0005	0.174 ± 0.003
Total	4.5 ± 0.3	0.1860 ± 0.0004	0.184 ± 0.001
-2.1a			
900	4.3 ± 0.4	0.1882 ± 0.0002	0.189 ± 0.002
1800	2.1 ± 0.2	0.1893 ± 0.0005	0.190 ± 0.001
1850	b.c. –	b.c. ± –	b.c. –
Total	6.4 ± 0.5	0.1884 ± 0.0002	0.189 ± 0.001
-2.2a			
400	0.015 ± 0.003	b.b. –	b.b. –
700	10 ± 1	0.1890 ± 0.0002	0.188 ± 0.001
900	1.0 ± 0.1	0.1890 ± 0.0005	0.187 ± 0.001
1350	11 ± 1	0.1881 ± 0.0002	0.188 ± 0.001
1800	0.56 ± 0.09	0.1868 ± 0.0003	0.188 ± 0.001
1850	0.08 ± 0.08	0.1892 ± 0.0005	0.180 ± 0.01
1900	0.09 ± 0.08	0.190 ± 0.001	0.170 ± 0.02
Total	22.8 ± 1.5	0.1885 ± 0.0001	0.1876 ± 0.0004
-2.2b			
400	b.b. –	b.b. –	b.b. –
800	0.31 ± 0.03	0.1886 ± 0.0007	0.187 ± 0.002
870	b.b. –	b.b. –	b.b. –
1280	0.034 ± 0.005	b.b. –	b.b. –
1800	0.18 ± 0.02	0.1869 ± 0.0003	0.182 ± 0.003
1850	b.b. –	b.b. –	b.b. –
Total	0.53 ± 0.04	0.1880 ± 0.0004	0.185 ± 0.003
-3a			
900	0.8 ± 0.1	0.1891 ± 0.0005	0.188 ± 0.001
1800	1.0 ± 0.1	0.189 ± 0.001	0.18 ± 0.002
1850	0.12 ± 0.05	b.d. –	b.d. –
Total	2.0 ± 0.2	0.1891 ± 0.0007	0.184 ± 0.002
-3b			
900	0.33 ± 0.03	0.188 ± 0.001	0.169 ± 0.008
1800	0.31 ± 0.03	0.1873 ± 0.0004	0.183 ± 0.006
1850	0.10 ± 0.01	0.1877 ± 0.0006	0.151 ± 0.02
Total	0.73 ± 0.05	0.1875 ± 0.0005	0.172 ± 0.005
-4			
900	2.8 ± 0.3	0.1889 ± 0.0003	0.186 ± 0.001
1800	1.6 ± 0.2	0.1894 ± 0.0003	0.186 ± 0.001
1850	0.2 ± 0.1	0.1918 ± 0.0009	0.181 ± 0.006
Total	4.6 ± 0.4	0.1892 ± 0.0002	0.186 ± 0.001
-9a			
900	4.6 ± 0.3	0.190 ± 0.001	0.1892 ± 0.0006
1800	5.7 ± 0.4	0.191 ± 0.001	0.19 ± 0.0006
Total	10.3 ± 0.5	0.190 ± 0.000	0.19 ± 0.0004
-9b			
900	0.08 ± 0.02	0.193 ± 0.002	0.207 ± 0.02
1800	0.05 ± 0.01	0.204 ± 0.007	0.225 ± 0.05
1850	0.12 ± 0.02	0.189 ± 0.002	0.191 ± 0.004
Total	0.25 ± 0.03	0.193 ± 0.002	0.203 ± 0.01

T, °C	^{36}Ar cm^3STP/g (1×10^{-10})			$^{38}Ar/^{36}Ar$ Daly			$^{38}Ar/^{36}Ar$ Faraday		
-9c									
900	0.08	±	0.01	0.190	±	0.001	0.198	±	0.01
1800	0.16	±	0.01	0.185	±	0.001	0.18	±	0.003
Total	0.24	±	0.02	0.1866	±	0.0009	0.186	±	0.004
-9d									
crush	0.72	±	0.05	0.1882	±	0.0004	0.196	±	0.006
-9g1									
700	6.9	±	0.5	0.1889	±	0.0007	0.189	±	0.0006
1600	4.3	±	0.3	0.1903	±	0.0007	0.188	±	0.001
Total	11.2	±	0.5	0.1897	±	0.0005	0.188	±	0.0006
-9g2									
crush	33	±	2	0.1912	±	0.0002	0.187	±	0.001
-9g3									
crush	72	±	5	0.1904	±	0.0002	0.188	±	0.0007
-10.1									
900	0.20	±	0.02	0.191	±	0.001	0.22	±	0.01
1800	0.11	±	0.01	0.193	±	0.001	0.192	±	0.005
Total	0.31	±	0.02	0.192	±	0.001	0.214	±	0.007
-10.2									
900	0.31	±	0.02	0.1913	±	0.0007	0.191	±	0.001
1800	0.17	±	0.01	0.1927	±	0.0008	0.192	±	0.002
Total	0.49	±	0.02	0.1918	±	0.0006	0.191	±	0.001
-11.1									
900	0.22	±	0.02	0.1922	±	0.0008	0.189	±	0.004
1800	0.27	±	0.02	0.1873	±	0.0009	0.188	±	0.003
Total	0.49	±	0.02	0.1895	±	0.0006	0.188	±	0.002
-11.2									
900	b.b.		–	b.b.		–	b.b.		–
1800	0.04	±	0.01	0.196	±	0.003	0.191	±	0.01
Total	0.04	±	0.01	0.196	±	0.003	0.191	±	0.01
-12.1									
900	0.07	±	0.01	0.188	±	0.002	n.d.		–
1800	1.06	±	0.07	0.1906	±	0.0003	0.187	±	0.002
Total	1.12	±	0.07	0.1905	±	0.0003	0.187	±	0.002
-12b									
900	0.94	±	0.06	0.1903	±	0.0007	0.188	±	0.001
1800	0.49	±	0.03	0.1899	±	0.0007	0.188	±	0.002
Total	1.43	±	0.07	0.1901	±	0.0005	0.188	±	0.001
-14									
900	b.c.		–	b.c.		–	b.c.		–
1800	0.57	±	0.04	0.1897	±	0.0008	0.184	±	0.002
Total	0.57	±	0.04	0.1897	±	0.0008	0.184	±	0.002
-16									
900	0.22	±	0.02	0.190	±	0.001	0.183	±	0.003
1800	0.31	±	0.02	0.186	±	0.001	0.191	±	0.004
Total	0.53	±	0.03	0.188	±	0.001	0.188	±	0.002
-18b									
900	0.34	±	0.02	0.1882	±	0.0008	0.192	±	0.002
1800	0.113	±	0.009	0.1918	±	0.0011	0.187	±	0.005
Total	0.45	±	0.02	0.1891	±	0.0006	0.191	±	0.002
-18g2									
700	0.53	±	0.04	0.1900	±	0.0006	0.1893	±	0.0006
1500	2.5	±	0.2	0.1924	±	0.0007	0.188	±	0.001
Total	3.0	±	0.2	0.1908	±	0.0005	0.1879	±	0.0009
-18g3									
crush	2.8	±	0.2	0.1901	±	0.0003	0.185	±	0.002
-19a									
900	0.59	±	0.04	0.1907	±	0.0007	0.189	±	0.001
1800	14.1	±	0.9	0.1878	±	0.0006	0.1863	±	0.0004
Total	14.7	±	0.9	0.1879	±	0.0006	0.1864	±	0.0004

T, °C	^{36}Ar cm^3STP/g (1×10^{-10})	$^{38}Ar/^{36}Ar$ Daly	$^{38}Ar/^{36}Ar$ Faraday
-19b			
900	b.c. –	b.c. –	b.c. –
1800	b.c. –	b.c. –	b.c. –
Total	b.c. –	b.c. –	b.c. –
-23a			
900	b.b. –	b.b. –	b.b. –
1800	0.21 ± 0.01	n.d. –	n.d. –
Total	0.21 ± 0.01	n.d. –	n.d. –
-24			
900	0.13 ± 0.02	0.185 ± 0.002	0.192 ± 0.006
1800	0.36 ± 0.03	0.1924 ± 0.0009	0.184 ± 0.002
Total	0.49 ± 0.03	0.1904 ± 0.0008	0.186 ± 0.002
-25			
900	0.08 ± 0.01	0.189 ± 0.001	0.184 ± 0.009
1800	0.32 ± 0.02	0.187 ± 0.001	0.184 ± 0.003
Total	0.41 ± 0.02	0.1877 ± 0.0009	0.184 ± 0.003
-30			
900	0.18 ± 0.01	0.1900 ± 0.0008	0.185 ± 0.004
1800	0.16 ± 0.01	0.1880 ± 0.0009	0.182 ± 0.004
1850	0.120 ± 0.009	0.1867 ± 0.0010	0.182 ± 0.004
Total	0.46 ± 0.02	0.1884 ± 0.0005	0.183 ± 0.002
-32.1a			
900	0.26 ± 0.02	0.1911 ± 0.0007	0.187 ± 0.003
1800	0.46 ± 0.03	0.1913 ± 0.0007	0.184 ± 0.002
Total	0.72 ± 0.04	0.1912 ± 0.0005	0.185 ± 0.002
-32cg1			
700	14.5 ± 1	0.1919 ± 0.0006	0.1888 ± 0.0005
1500	1.8 ± 0.1	0.1926 ± 0.0007	0.188 ± 0.001
Total	16.3 ± 1	0.1920 ± 0.0006	0.1886 ± 0.0004
-32cg2			
crush	8.4 ± 0.6	0.1909 ± 0.0002	0.187 ± 0.001
-34			
900	0.15 ± 0.02	0.1939 ± 0.0012	0.189 ± 0.005
1800	0.62 ± 0.04	0.1910 ± 0.0008	0.186 ± 0.002
Total	0.77 ± 0.05	0.1916 ± 0.0007	0.187 ± 0.002
-34PX			
crush	1.6 ± 0.1	0.1934 ± 0.0004	0.191 ± 0.003
-47g			
crush	1.26 ± 0.09	0.1916 ± 0.0004	0.183 ± 0.003
-54g			
crush	6.4 ± 0.4	0.1892 ± 0.0002	0.186 ± 0.001
-55g			
crush	6.3 ± 0.4	0.1893 ± 0.0003	0.186 ± 0.001

b.b. is below blank, b.c. is below cut-off, and n.d. is not determined.

A3.6 References

Honda M. (1997) Research School of Earth Sciences Annual Report, pp. 154. Research School of Earth Sciences.

Honda M., McDougall I., Patterson D. B., Doulgeris A., and Clague D. A. (1993) Noble gases in submarine pillow basalt glasses from Loihi and Kilauea, Hawaii: a solar component in the Earth. *Geochimica et Cosmochimica Acta* **57**, 859-874.

Matsumoto T. (1997) Noble gas geochemistry of mantle-derived xenolliths from the newer volcanics, southeastern Australia. Ph.D. Dissertation, The Australian National University.

Patterson D. B. (1992) Noble gas geochemistry of selected basalts and basaltic andesites: New Zealand, Tonga-Kermadec and Vanuatu. Ph.D. dissertation, The Australian National University.